CONFIGURATION INTERACTION (SINGLES) STUDY OF GEOMETRIC AND ELECTRONIC PROPERTIES OF CONDUCTING POLYMERS

DEBANOND CHAKRABORTY

INFORMATION TO USERS

This manuscript has been reproduced from the microfilm master. UMI films the text directly from the original or copy submitted. Thus, some thesis and dissertation copies are in typewriter face, while others may be from any type of computer printer.

The quality of this reproduction is dependent upon the quality of the copy submitted. Broken or indistinct print, colored or poor quality illustrations and photographs, print bleedthrough, substandard margins, and improper alignment can adversely affect reproduction.

In the unlikely event that the author did not send UMI a complete manuscript and there are missing pages, these will be noted. Also, if unauthorized copyright material had to be removed, a note will indicate the deletion.

Oversize materials (e.g., maps, drawings, charts) are reproduced by sectioning the original, beginning at the upper left-hand corner and continuing from left to right in equal sections with small overlaps.

Photographs included in the original manuscript have been reproduced xerographically in this copy. Higher quality 6" x 9" black and white photographic prints are available for any photographs or illustrations appearing in this copy for an additional charge. Contact UMI directly to order.

Bell & Howell Information and Learning
300 North Zeeb Road, Ann Arbor, MI 48106-1346 USA
800-521-0600

Configuration Interaction (Singles) Study of Geometric and Electronic Properties of Conducting Polymers

by

©Debanond Chakraborty

A thesis submitted to the School of Graduate Studies
in partial fulfillment of the requirements for the degree of

Master of Science

Department of Physics and Physical Oceanography
Memorial University of Newfoundland

May 18, 2000

St. John's Newfoundland

Abstract

The nature of the geometric and electronic transitions taking place in π-conjugated oligo(thiophene)s, oligo(cyclopentadiene)s, oligo(fulvene)s and their cyano based derivatives are investigated using an *ab initio* approach, including correlation effects. Theoretical evidence based on excited state electronic studies of the most stable forms of thiophene and cyclopentadiene based oligomers show that the cyano-derivatives of these polymers possess smaller intrinsic band gaps than their parents. The geometries of these neutral five-membered ring oligomers have been optimized using the *ab initio* restricted Hartree-Fock method followed by the single configuration interaction (CIS) technique with 3-21G* basis set within the framework of Gaussian 94. It has been observed that the 3-21G* basis set describes the qualitative geometric and electronic features reliably. Single substitution of electrons in the lowest unoccupied molecular orbitals (conduction band) from the highest occupied molecular orbitals (valence band) shows good agreements with the experimentally observed excited state energies (where available) for the six molecular systems investigated in this study. Of these, the lowest was for the tetramer of poly-(dicyanomethylene cyclopentadithiophene) (1.63 eV), followed by poly-(dicyanomethylene cyclopentadifulvene) (2.34 eV) and poly-(dicyano-methylene cyclopentadicyclopentadiene) (2.57 eV). The molecular geometric modifications in going from the ground to the lowest excited state show particular trends towards a full aromatic benzoid like structure with almost equal bond lengths along the molecular backbone. The heteroatomic substitutions and the geometry relaxation phenomenon show an efficient approach to band gap control. The geometry relaxation phenomena occurring in the singlet and triplet states show more pronounced

and localized bond length alternations in the triplet states, confirming the more localized character of triplet states. Maximum planarity, weak interactions of the chain backbone with the bridging group, enhanced π character of the highest occupied and the lowest unoccupied molecular orbitals along with charge transfer phenomenon also contribute to band gap lowering. For these oligomers, the evolution of the lowest energy, singlet-triplet transitions with chain length ranging from one to eight rings, has also been investigated. The lowest three singlet and three triplet states are characterized with the oscillator strengths in the oligomers along with the lattice distortions taking place due to the $\pi - \pi^*$ transitions. The inclusion of electron correlation results in a significant reduction in the band gap and shows excellent agreement with the experimental results. The calculated transition energies are within 0.1−0.4 eV of the experimental results.

Dedicated to my parents

Acknowledgement

I would like to take this opportunity to extend my most sincere appreciation to my supervisor Dr. Jolanta B. Lagowski for her guidance, support, encouragement and precious suggestions throughout this research work and for her counting on my capabilities.

I also wish to thank the Departmental Faculty and staff for their valuable help and guidance during my student tenure at MUN. I am grateful to the chairman Dr. Michael Morrow, associate chair Dr. John deBruyn, Dr. John Whitehead and graduate administrator Ms. Daphne Corbett for their cooperation and help.

My gratitude also goes to the Memorial University of Newfoundland for awarding me a Graduate Scholarship and offering me Teaching assistantships.

I am thankful to the system administrators of the department Mr. Fred Perry and Mr. Chris Stevenson for their warm cooperation and computational support.

I would like to convey my appreciation to Mr. Paul Fardy and Mr. Gilbert Wong of the Department of Computing and Communications for their immense computational aide and assistance in the computational part of this work.

I would like to acknowledge the support from National Science and Engineering Research Council of Canada for their grants in this research.

Finally, I am thankful to my uncle Mr. Rajeeb Chakraborty whose encouragement and inspiration meant a lot to me. I also acknowledge here the cooperation of my friends Dr. David Facey-Crowther, Kaleem Momin, Kamrul Islam and Martin Kenward. Special thanks are extended to Ms. Dawn Michelle Shaw.

Contents

List of Figures

List of Tables

List of Abbreviations and Symbols

αT_2	α-bithiophene
AM1	Austin Model 1
CASSCF	Complete Active Space Self Consitent Field
CI	Configuration Interaction
CIS	Configuration Interaction Singles
CISD	Configuration Interaction Singles and Doubles
CP	Conjugated or Conducting Polymer
DFT	Density Functional Theory
$E_{cal.}/E_{tran.}/E_g$	Energy Gap or Band Gap
FMO	Frontier Molecular Orbital
HF	Hartree-Fock
HOMO	Highest Occupied Molecular Orbital
INDO	Intermediate Neglect of Differential Overlap
IP	Ionizing Potential
LCAO	Linear Combination of Atomic Orbitals
LUMO	Lowest Unoccupied Molecular Orbital
MNDO	Modified Neglect of Diatomic Overlap

continued over-leaf

List of Abbreviations and Symbols

MO	Molecular Orbital
MP2	Møller-Plesset Second Order Perturbation
MR-CI	Multi Reference Configuration Interaction
NMR	Nuclear Magnetic Resonance
PA	Polyacetylene
PAni	Polyanilyne
PCY	Polycyclopentadiene
PFV	Polyfulvene
PPY	Polypyrole
PT	Polythiophene
PCNCY	Poly-(dicyano-methylene cyclopentadicyclopentadiene)
PCNFV	Poly-(dicyanomethylene cyclopentadifulvene)
PCNTH	Poly-(dicyanomethylene cyclopentadithiophene)
QCISD	Quadratic Configuration Interaction, including Singles, Doubles
RHF	Restricted Hartree-Fock
SCF	Self-Consistent Field
VEH	Valence Effective Hamiltonian

Chapter 1

Introduction

1.1 Conjugated Polymers

We investigate the intrinsic ground and excited state geometric and electronic properties of conjugated oligomers (see Section 1.3 for details) using configuration interaction (CI), a qunatum mechanical method, to provide insights that can not be easily obtained from experiments alone. An important aspect of studying conducting oligomers is that they allow for a rational approach from molecule to bulk material. That is, the ultimate goal of this work is to understand and control the route from molecule to bulk material. This thesis focuses mostly on the first step in this aim, i.e., on studying the excited state properties of oligomers.

By using oligomers with an increasing number of monomer units, it is possible to evaluate the effect of conjugation length and estimate characteristics for more complex polymers. Conjugation of small molecules and their extension leads to polymeric materials with unique properties. Intensive investigations on conjugated polymers have been carried out mainly for two reasons: firstly, these materials are stable under normal conditions and are very flexible with respect to modifications

of their chemical structure; secondly, since they are very promising candidate for materials with high nonlinear optical properties, they can be used in a wide range of applications from optoelectronics to information-storage devices [1]. In Section 1.2 we summarize previous studies of small band gap conjugated polymers. In Section 1.3 we briefly discuss the goals and scopes of this thesis.

1.1.1 The Characteristics of Conjugated Polymers

The electronic structure of the chain of atoms or chemical groups along the backbone of the non-conjugated polymers consists of only σ-bands (likely with *localized* π-electronic levels) [2]. The large electron energy gap in the σ-system makes these polymers electrically insulating as well as transparent to visible light. On the other hand, the unique electronic features of the conjugated polymers lie in their inherent π-electrons, the wave functions of which are delocalized along their alternating single and double bonded backbone. The unique opto-electronic properties of these delocalized π-electron systems with respect to the conventional σ-systems are as follows: (i) Relatively small electronic band gap ($\sim$1 to 3.5 eV), making them available for low energy electronic excitations and semiconducting behaviour; (ii) Can be easily oxidized or reduced, usually through charge transfer with molecular dopants; (iii) Large carrier mobility, so that high electrical conductivities are possible; and (iv) The presence of charge carriers, which are neither free electrons nor holes, but quasi-particles, such as polarons, solitons etc. (see page 3 for definitions) may move relatively freely through the material [2].

Polyacetylene ($(CH)_x$) is the simplest conjugated polymer, consisting of weakly coupled chains of CH units forming a pseudo-one-dimensional lattice. Such a system

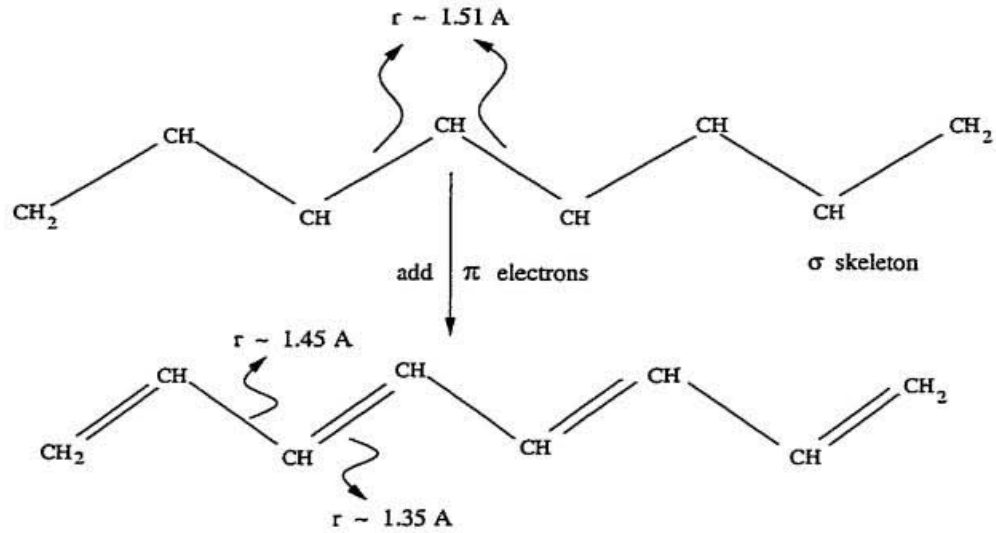

Figure 1.1: Schematic illustration of dimerization of octatetraene (C_8H_{10}) geometric structure due to the uneven distribution of the π electrons over the bonds [3].

with a partially filled π energy band structure is unstable with respect to a dimerization distortion, the Peierls instability [4], in which the adjacent CH groups move towards each other, forming alternating short (double) and long (single) bonds, thereby lowering the electronic energy of the system (see Fig. 1.1) by opening up a gap at the Fermi level [5]. The bond length alternation (δ_r), a common phenomenon in one-dimensional systems, which, depending upon the orientation of the bonds in the respective mesomers may be in phase L or in phase R. Hence after lattice distortion the resulting mesomers can be degenerate (e.g., *trans*-PA Fig. 1.2) or non-degenerate (e.g., PT, PPy, PPP, PAni). Because of this stabilizing deformation of the system, which destroys the degeneracy of orbitals, one ends up with a semiconductor, whereas the non distorted structure would have been a metal.

The intrinsic low dimensionality of linear polymer chains, and the general property of conjugated organic molecules that the geometric structure is dependent upon

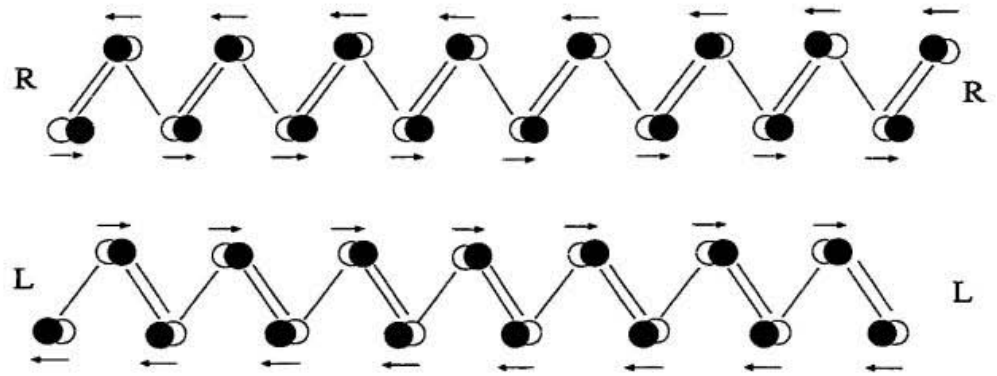

Figure 1.2: Two degenerate ground state structures of *trans*-PA $(CH)_x$.

the ionic state of the molecule (strong electron(hole)-lattice interactions), leads to the creation of unusual charge carrying species. These species, associated with other localized electronic states, manifest themselves through electronic processes (by photo excitation in the neutral system or charge transfer upon reduction, oxidation or protonation, i.e., doping, of the polymer chains), with energy levels within the otherwise forbidden electronic energy gap [6, 7, 8]. This is clarified in Fig. 1.3, where it is shown how an excess electron on a conjugated polymer chain leads to the formation of new electronic states within the energy gap. The idea of solitons in polyacetylene was first implicitly introduced by Pople and Walmsley [9] in 1962, who suggested that such defects could be made mobilized and, upon charging, could be made responsible for a high electrical conductivity. Generally, depending upon the symmetry of the ground state, the charge carrying species are charged polarons, spinless charged solitons, or spinless charged bipolarons [10, 6, 7, 8]. These species, solitons, polarons and bipolarons, represent the lowest energy eigenstates of the coupled electron(hole)-lattice systems [11], and are responsible for several unique electrical, magnetic and optical (even non-linear) properties of the conjugated poly-

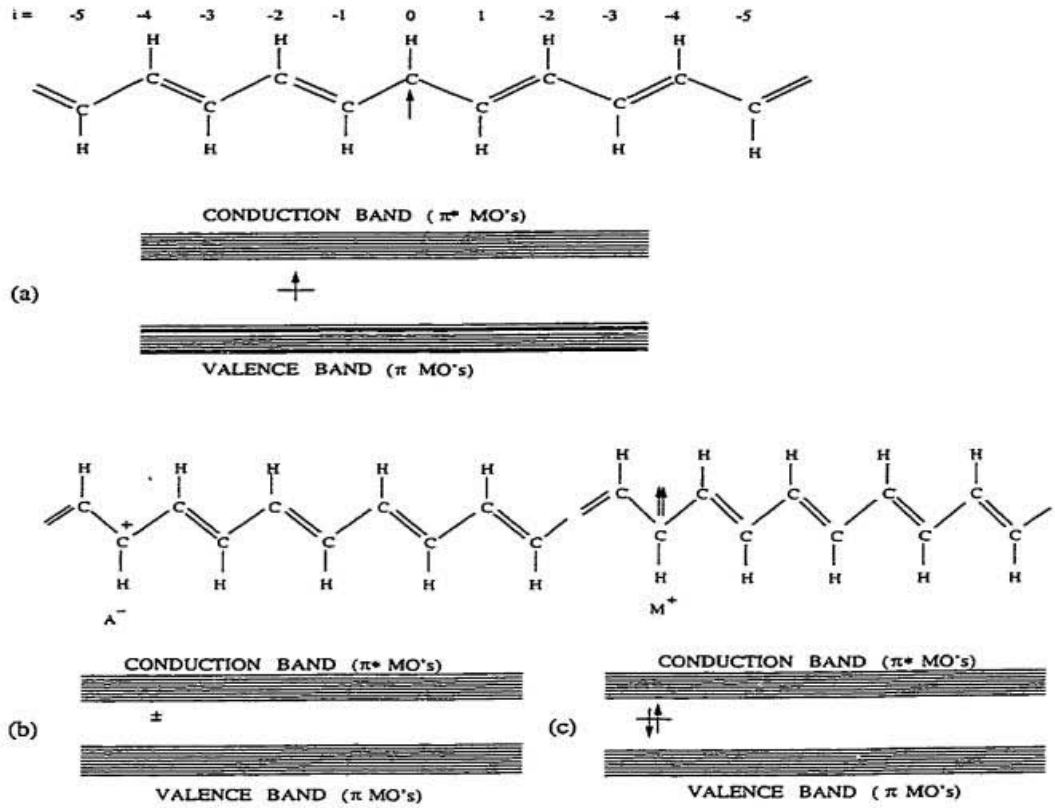

Figure 1.3: (a) Neutral, (b) positively charged, and (c) negatively charged solitons in *trans*-PA. Figure taken from ref. [5].

mers. The soliton is a localized, nonbonding state with its energetic location in the middle of the Peierls gap between the π and π^* bands (see Fig. 1.3). This nonbonding nature is exposed in its wave function - even in regions of high probability density there is a likelihood of finding the electron only on every second carbon atom, and zero at the carbon atom in between [12].

Conjugated cyclic polymers based on *cis*-polyacetylene (PA) backbone are found in two possible isomeric forms: aromatic (s-*cis* or *tran-cisoid*)and quinoid (s-*trans* or

cis-transoid)[1] which are non degenerate and exhibit different electronic properties. Heterocyclic polymers such as polythiophene (PT), polyfuran (PF), and polypyrrole (PPy) are known to possess aromatic forms in their ground states [13, 14]. Simple nonheterocyclic polymers like polyfulvene (PFV), poly(oxocyclopentadiene) (POPD), poly(thiocyclopentadiene) (PTPD) and poly(cyclopentadiene) (PCY) show strong preference for quinoid structures [15, 16, 17, 18]. In general the more stable isomer possesses a larger band gap than its counterpart.

Three routes towards the design and synthesis of low-band-gap organic polymers have been explored. The first is the construction of fully fused-ring hydrocarbon structures in order to obtain a system corresponding more or less to a one-dimensional graphite, e.g., polyacene-like systems [19, 20, 21, 22, 23] or polyperinaphthalene [24, 25]. The second is the modification of the geometric and/or electronic structure of known and well-characterized conjugated polymers like polythiophene and polypyrole that can be easily derivatized. In this context, the present investigation was performed to discover a compound in which the quinoid geometric form (possessing usually a higher total energy but a smaller band gap than that of an aromatic one) is favoured in which quinoid electronic contributions are stabilized in the ground state. Using this concept polyisothianaphthene (band gap ~1 eV), a polythiophene chain to which benzene rings are fused along the 3,4 positions of the thiophene units, has been synthesized [26, 27, 28, 29, 30, 31, 32, 33, 34]. This synthesis has been followed by studies on numerous compounds like poly(arene methines) [35, 36, 37, 38, 39, 40, 41]. A third and very exciting route was approached by Havinga *et al.* [42, 43] who introduced a regular alternation of conjugated donor

[1]The terms aromatic and quinoid should not be confused with the aromatic benzene structure.

and acceptor-like moieties with a low ionizing potential and large electron affinity along a conjugated chain, inducing a small band gap energy. The band gap is expected to be lowest for a combination in which the electro negativity difference between donor and acceptor moieties is highest [44]. This concept has already led to the synthesis of polysquaraines and polcroconaines (band gap ~0.5-eV) [42, 43] as well as that of poly(cyclopentadithiophene) derivatives [45, 46].

1.2 Summary of Previous Works

Investigation of conjugated organic polymers with small band gaps has considerably increased during the last couple of decades. A broad range of studies have shown that conjugated molecules and polymers constitute prototypes of systems whose chemical, geometric, and electronic structures are strongly interconnected. Any electronic process, be it a charge transfer upon doping or a charge excitation upon illumination, leads to very fast local geometry relaxations which in turn modify the original electronic structure significantly [47].

In order to put our work in proper context, we will review relevant previous work. The initial use of polymers for their electronic conducting properties dates back to the 60's [48]. Naarman and his group [49] synthesized a doped polyacetylene with a conductivity of 6×10^5 S cm^{-1} which is larger than that of copper. The existence of bond alternation in *trans*-polyacetylene was demonstrated by Fincher *et al.* [50]. The importance of the interconnection between chemical and electronic structure in this simplest conjugated molecule was established by the relationship of the magnitude of the bond alternation to the energy gap in its excitation spectrum

[10, 51, 52]. The interest reached its height in 1977 when Heeger and MacDiarmid [53] discovered that polyacetylene could undergo a 12 fold increase in conductivity upon charge-transfer oxidative doping.

Most of the previous work concerned (i) determination of the polymers' intrinsic electronic properties via the evaluation of important parameters like ionization potential, electron affinities, bandwidths, and band gaps [54, 55] and (ii) description of the geometric and electronic structural modifications taking place upon reaction with reducing or oxidizing agents, thereby characterizing the nature of the charge storage species formed upon doping, such as, solitons, polarons, and bipolarons [56, 10, 57, 58]. In addition, these early quantum-mechanical calculations were performed mostly at the semiempirical, *ab initio* Hartree-Fock level or at the simple Hückel level. The enhancement in computer power and the possibilities of application to larger systems and exploitation of more sophisticated quantum-chemical techniques including electron correlation effects like post-Hartree-Fock methods have enabled one to obtain the excited-state properties of larger conjugated polymers or their oligomers. This has by now been proven essential in providing a deeper understanding of, for instance, (i) the linear and nonlinear optical response of these systems, (ii) the characteristics of both singlet and triplet polaron-excitons, and (iii) the interactions of conjugated systems with metals [59].

The currently studied conjugated polymers for nonlinear optical applications include polyacetylene, polyarylenes, polyarylene vinylenes, polythiophene and their derivatives [60]. The electronic states of thiophene have been assigned by Palmer and coworkers [61] using optical absorption, near threshold electron energy-loss spectroscopy and *ab initio* multi-reference multi-root CI methods with several basis

sets. Colditz *et al.*, [62] have investigated the ground and excited electronic states of thiophene oligomers both theoretically and experimentally for 2-6 monomer units studying the vertical transition energies from the ground to the lowest excited singlet states using CI-singles. In their paper they have stressed on the single excitation configurations discarding the double excitations since with double excited configurations the state ordering was not consistent with the experimental results. In another multi configuration second order perturbation study, Andrés and his coworkers [63] have also rationalized the redundancy of doubly excited configurations for thiophene. Fagerström and Stafström [64] in their excited singlet-triplet state study used the semiempirical AM1 followed by INDO/CI methods, where they have accounted for electroluminescence in polythiophene as the phenomenon appears in light-emitting diode devices. They have also shown that the triplet states are very close in energy to the singlet states as an indication that spin-orbit coupling can play an important role in this system. Negri and Zgierski [65] have analyzed the vibronic structure of the lowest two valence excited states of fulvene by using different *ab initio* and semiempirical methods with different basis sets in order to obtain ground and excited electronic state geometries and force fields involved in the transitions. Another detailed ground and excited state study with the photochemical reactivity of fulvene was carried out by Dreyer and Klessinger [66]. In an earlier experimental gas phase study of fulvene [67], the authors have assigned several of the electronic and vibrational spectra. Harman *et al.* [68], in their UV study have shown that the absorption spectra of fulvene around 200 nm are not due to valence shell transitions but rather are Rydberg transitions (transitions into atomic orbitals of higher principal quantum numbers). Asmis and his coworkers

[69] have also studied the triplet and singlet excited states of fulvene in gas phase by electron-energy-loss spectroscopy, supporting the previous results. Nakano and his coworkers [70] have assigned the excitation spectra of cyclopentadiene in the range on 5-8 eV using CASSCF method with an accuracy of 0.27 eV with the experimental results. In a similar study of electronic structure of pyridine based polymers, Blatchford *et al.*, [71] have accounted for important issues like spatial symmetry breaking with related consequences.

Large molecules like the nucleic acid bases: thymine, cytosine, uracil in the ground and the lowest two singlet excited states were studied by Shukla and Mishra [72] using single configuration interaction. A better insight into the molecular orbital theory of excited states for simple organic molecules like ethylene, formaldehyde etc. could be found in a paper by Pople *et al.* [73]. H. O. Villar and his coworkers [74] in an *ab initio* Hartree-Fock calculation have established the need for electron correlation in order to correct the band gap calculated for the five-membered heterocycles: polythiophene, polyfurane, polypyrrole and polyselenophene starting from monomer through pentamer. In their study they have also shown that residual corrections of the band gaps could be achieved with the inclusion of larger basis sets. Salzner *et al.*, in their article [75] have presented excitation energies of 20 small and medium-sized π-systems estimated as one-electron energy differences at the HF and DFT levels with various combinations of exchange and correlation functionals. They have shown that inclusion of the exact HF exchange via the hybrid B3LYP, B3P86, and B3PW91 functionals leads to the HOMO-LUMO (Highest Occupied Molecular Orbital and Lowest Unoccupied Molecular Orbital) gap in good agreement with experimental excitation energies. S. Y. Hong and J. M. Song [76, 77, 78]

in their semiempirical studies on conjugated cyclic polymers have shown that the band gaps of the polymers mainly evolved from the bond-length alternations with a few exceptions. Lee and Kertesz [79] used semiempirical Hückel assorted with MNDO method to show the effects of nuclear relaxation and heteroatomic substitution on polythiophene and other molecules. They have demonstrated that energy gap is controlled not by aromatic vs. quinoid contributions, but by the geometric and heteroatomic effects on the frontier orbitals of the polymer. Beljonne *et al.*, [80] in their HF coupled with INDO/CI study demonstrated electronic excitation, relaxation energies and nonlinear optical properties of thiophene oligomers. Jean Roncali [81] has covered a wide perspective in his review specifically focused on synthesis, functionalization and application of poly(thiophenes). Lambert and Ferraris [45, 46] in their experimental study have designed an electroactive polymer with a lowered band gap from the monomer cyclopenta[2,1-b;3,4-b']dithiophen-4-one displaying a reduced HOMO-LUMO separation with E_g <1.5 eV.

The recent records on the state-of-the-art of the chemistry of conducting polymers and related materials can be obtained in the Proceedings of the 81st Nobel Symposium on Conducting Polymers [47], the book by Brédas and Silbey [82] and the book edited by Skotheim [83].

Conducting polymers are quasi crystalline because more than 50% of the total volume is amorphous. For structural studies crystallinity is essential. Depending on the way a polymer synthesized it can be either crystalline or amorphous. For example, electrochemically prepared PT is amorphous [84], but chemically prepared polymer is partly crystalline [85]. Due to the dominance of amorphous nature the X-ray determination of these polymers' structures are not available except for a few

cases [85, 86]. Hence, the amount of structural information that can be obtained from X-ray, neutron or electron diffraction of CPs is minimal. Scanning electron microscopy and scanning tunnelling microscopy are major sources of information regarding the morphology of surface regions of these compounds at mesoscopic scales. NMR was used to measure C–C bond lengths. Resonance Raman Spectroscopy is useful for measurement of conjugation lengths on the scale of 10 - 100 Å [87, 88]. Spectroscopic methods provide information about the energy gap. Photo-induced absorption, emission and luminescence spectra are widely used for determining the mid-gap states. For example, with soft X-ray photons both core and valence electrons can be studied. With UV and visible photo electron spectra only the valence electrons can be studied.

Theoretical calculations on the polymers and/or oligomers are performed at the *ab initio* or semiempirical levels. In case of conjugated systems the large number of atoms per unit cell requires an *ab initio* methodology for accurate structure determination. The most widely used techniques start from a single configuration-based Hartree-Fock self-consistent-field wave function [89] wherein the wave function Ψ_0 is a product of one-electron wave functions. These Ψ_0's are referred to as molecular spin orbitals, antisymmetrized with respect to interchange of electronic coordinates. The molecular spin orbitals are themselves expanded as a linear combination of atom-centred basis functions. While the *ab initio* Hartree-Fock approximation is remarkably successful in many cases, its treatment of the correlation between the motions of different electrons within a molecular system, especially those arising between electrons of opposite spin is inadequate. In most techniques, electron correlation effects are introduced by allowing the wave function to be a linear com-

bination of many electron configurations. The other configurations are produced by the replacements of occupied spin orbitals in Ψ_0 by virtual spin orbitals. The conceptually simple, configuration interaction (CI) is a straightforward and general approach for the treatment of electron correlation in atoms and molecules. The ideal CI calculation would be "full CI" (FCI) in which the full many-electron functions space of the appropriate spin and symmetry generated by the basis set is used in the wavefunction expansion [90, 91]. Such a calculation provides the most complete solution of the non-relativistic Schrödinger equation within that function space spanned by a given basis set, but is clearly not practical. Since the number of configuration state functions in FCI goes up exponentially with the size of the system it is computationally expensive. Therefore in most applications, especially for many-electron systems with large basis sets, it is necessary to truncate the CI expansion space in some way to make the calculations practical, leading to limited CI techniques. Accurate CI calculations are possible for only short chain molecules containing very few valence electrons. However, the short chain wavefunctions gradually evolve into localized excitons or delocalized band states as the chain length is increased, hence must have the same characteristics as their long chain counterparts. In an experimental study on chain length dependence of thiophene oligomers, Horowitz *et al.* [92] have found that short ($n \leq 8$) oligomers are better described in terms of molecular orbitals, whereas one electron model of conjugated polymers is more appropriate for longer chains, i.e., for $n = 12$ and the polymer (n = number of monomer units).

The most widely used treatment is CI with all single excitations (CIS) [72, 93, 94] where all double, triple, quadruple, and higher order excitations are completely

neglected. Single excitations are important for their contribution for accurate evaluation of optical, electronic and nonlinear optical properties of the π-conjugated systems. CI-Singles is described by its developers as "An adequate zeroth-order treatment for many of the excited states of molecules" [95]. In fact, the results predicted by CIS calculations have shown close agreement with experimental results [45, 46, 62, 63, 66, 73, 80, 92, 94, 96, 97, 98, 99, 100, 101]. Therefore, to have deeper insight into the qualitative features of the conducting polymers CIS methodology appears very important [102] and hence we have chosen it for our calculations.

There have been a few excited state studies on thiophene. One such study by Bendazzoli *et al.* [96] used the CI method with a double zeta basis set to obtain the six lowest excited states (three singlet and three triplets). Palmer *et al.* [61] employed high level MRCI with several basis sets in their extensive investigation on the electronic states of thiophene. A previous comprehensive *ab initio* study of the excited states of thiophene used CASSCF wave functions followed by second order perturbation theory (CASPT2) [63]. Another semiempirical (AM1) study on thiophene oligomers followed by INDO-CI calculation was reported [64] depicting the interaction between negatively charged (electron) and positively charge (hole) polarons. Triplet and singlet excited states of fulvene were studied in the gas phase both experimentally and theoretically by Asmis *et al.*, [69] using electron-energy-loss spectroscopy and multiconfiguration second order perturbation calculations (CASSCF/CASPT2) - the reported results for the first two valence triplet and singlet transitions were within 0.19 eV of the experiment. A comparative study on geometric and electronic structures of polythiophene and polycyclopentadiene monomers up to heximers was carried out by Salzner *et al.* [103] using density

functional theory, where they have shown that band gaps increase with increasing π-donor strengths of the heteroatom. Recently, Subramanian and Lagowski [18] carried out an extensive study on thiophene- and cyclopentadiene-based polymers where they used the semi-empirical molecular orbital theory (MNDO, AM1) followed by *ab initio* Hartree-Fock method. They showed that the band-gaps in the cyano-substituted polymers, in comparison to their parent polymers were lowered and accompanied by a decrease in bond alternations in the aromatic forms and by an increase in bond alternations in the quinoid forms.

Bakhshi and Rattan [44, 104, 105] in their MNDO-AM1 solid-state calculations followed by HF crystal-orbital method reported two novel donor-acceptor polymers based on poly(cyclopentadiene), where the repeat unit was a bicyclopentadienylene bridged by an electron-accepting group. They showed that the small band gap values of these polymers in comparison with polythiophene arise chiefly due to the strong bonding interaction between the LUCO (Lowest Unoccupied Crystal Orbital) of the bithiophene skeleton and the LUMO of the electron accepting group. Toussaint and Brédas [106, 107] have investigated the same molecule with AM1 optimized geometry and Valence Effective Hamiltonian (VEH) method. They concluded that the introduction of the electron-withdrawing group between the two cyclopentadiene rings of the unit-cell has a weak influence on the aromatic (transcisoid) form and produces a very small band gap of 0.16 eV. Hong *et al.* [17] in their investigation on these π-conjugated systems, have used AM1 for geometry optimizations and modified extended Hückel method for calculating electronic properties of the polymers showing the variation of the band gaps with the electronic effect of the bridging groups.

1.3 Present Work

The goal of the present work is to investigate the excited state geometric and electronic properties of low band gap organic conducting oligomers (up to 8 monomer units) with thiophene and cyclopentadiene blocks as their backbones using the single configuration interaction technique. The theoretical study has been performed on the following systems: polythiophene (PT), polycyclopentadiene (PCY), polyfulvene (PFV), poly-(dicyanomethylene cyclopentadithiophene) (PCNTH), poly-(dicyanomethylene cyclopentadicyclopentadiene) (PCNCY), and poly- (dicyanomethylene cyclopentadifulvene) (PCNFV) oligomers respectively (refer to Fig. 1.5 for the monomer units). Most of these systems are extensively studied due to their electronic, mechanical and non-linear optical characteristics [18, 47, 65, 66, 70, 75, 81, 82, 83, 98, 100, 107, 108, 109, 110, 111, 112, 113, 114, 115].

As a part of this work we have also tried to shed light on the geometric and electronic modifications due to the presence of different electron donating and accepting end-groups as well as bridging-groups which form charge transfer complexes and hence improve conductivity. In this study an effort has been made to design the narrow band gap materials in their undoped state by decreasing the bond length alternation of a polyacetylene-like backbone by means of heteroatoms and/or side groups (i.e., variations in the occupancy of frontier molecular orbitals).

The two five membered fully conjugated cyclic systems, thiophene (C_4H_4S) and cyclopentadiene (C_5H_8), are prototype organic polymers which are studied rigorously within the framework of *ab initio* and different semiempirical methods on their electronic spectra and geometric properties [63, 77, 103]. Some qualitative and limited, though useful, information on the excited state geometries and energetics

of these molecules were reported [61, 65, 66, 69, 96, 116, 117, 118]. However, they do not contain enough information regarding the excited state geometries to be able to map the systems into their most stable conformation.

We have investigated a new polymer system which has not been investigated formerly either by theoretical or experimental means named PCNFV which has two fulvene rings bridged by a dicyano group as shown in Fig. 1.5. Numerous compounds have been synthesized with the inclusion of cyano and/or fulvene groups leading to enhanced conductivity with band gap values as low as 0.5 eV [46, 119]. Although not all of our proposed polymers have been synthesized, it is of course worth exploring their geometric and electronic properties prior to attempting their synthesis. Also for their successful design, it is necessary to have an overall understanding of the relationship between their structural chemistry and electronic properties like the excitation energies of different singlet and triplet excited states, dipole moments, oscillator strength, etc.

In the present study, we set our focus on investigating the geometric and electronic structures as well as the conducting properties of the above mentioned polymeric systems. The geometric and electronic investigations have been carried out on the basis of *ab initio* Hartree-Fock method followed by single configuration interaction (CIS) calculations [90] for the description of the excited states, in order to ensure an adequate treatment of the electron correlation effects. For every optimized geometry, the polymers are treated as infinite pseudo-one-dimensional systems, i.e., inter-chain interactions are neglected. In other words, oligomer models were used to simulate isolated single polymer chains. It is worth mentioning here that the molecular backbone planarity is one of the essential features of these π-

conjugated polymers which accounts for their unique electronic features such as the delocalized wavefunctions over long portions of the polymer chain [2].

A few molecular modelling packages and graphical viewer interface software packages have been used in order to construct the molecular structures under investigation. The first generation monomer units were generated using the MOPAC 93 software [120]. The initial input geometries i.e., the bond length and the bond angles for PT are taken from the gas phase electron diffraction data on α-bithiophene (hereafter denoted αT_2) [121]. For PCY the input geometries are obtained from the semiempirical AM1 optimized values [106]. For the remaining polymers *i.e.,* PFV, PCNTH, PCNCY, and PCNFV the input geometries are estimated from the data obtained for PT and PCY with the AM1 calculations [18, 106]. The second generation conformers of these compounds are build with the Cerius^2 molecular modelling package [122] using its polymer builder section.

Ground state geometries of the most stable forms of the oligomers have been optimized using the *ab initio* restricted Hartree-Fock procedure using *Gaussian 94* [118]. Throughout this study, the 3-21G* basis set has been used; except for the purpose of determining the basis set effect on the small α-bithiophene molecule, we have used several other minimal and split-valence basis sets with polarization and diffuse functions added to heavy atoms. The 6-31G* basis set has been used for all the monomers and dimers [73, 123]. We are interested in studying what simple modifications made to the basis sets can provide an almost adequate description of most properties. On the basis of the Hartree-Fock geometry, we have performed configuration interaction calculations involving singly excited configurations (CIS) to describe the lowest singlet and triplet states. The excited states

of the molecules are generated by considering single electron promotion from the occupied (valence) to one of the virtual (conduction) molecular orbitals using the optimized ground state molecular geometries, and this has been followed by optimization of the excited state geometries. The Berny algorithm has been employed for geometry optimization [124]. In most cases hydrogen atoms have been used as end groups in the oligomer calculations and compounds remained *planar*. An attempt has also been made to study the effects of appending push-pull nitro and amino groups at the two ends of the thiophene dimer molecule.

Ab initio molecular orbital methods for determining the wavefunctions and energies of molecules in their ground electronic states are well characterized. Extensive tabulations of the results of such calculations on most of these systems (especially thiophene, cyclopentadiene and fulvene), performed at a variety of basis sets and levels of sophisticated theories, have allowed predictive quantum chemistry reliable for understanding those molecular structures [17, 65, 66, 78, 79, 106]. In addition, algorithmic advances designed to take advantage of newly developed computer technology have increased both the number of atoms and the number of basis functions which can be practically treated in a standard calculation. However, a comparable situation does not exist for molecules in their electronically excited states. This is especially true for events where the ground-state methodology is not directly transferable (cases for which excited states of the same symmetry as the ground states are required). It is worth pointing out here that relatively few *ab initio* evaluations with inclusion of electron correlation effects [117, 125] have been reported for compounds of the size considered in this study. Most studies deal with smaller molecular systems [65, 66, 106, 114, 126]. Our main purpose here is to re-evaluate

the CIS method in the context of its ability to deal with large systems.

Care should be taken while considering the size of the unit cell which is a fundamental part of the cluster size. For the systems we have studied, the optimum cluster size is an octamer [18] where the monomeric units are PT, PCY, PFV respectively, and tetramer for PCNTH, PCNCY, PCNFV polymers with larger repeat units (refer to Fig. 1.5). It is typical in the molecular calculations that one monomer (e.g., one ring in PT) is considered to be the fundamental unit of the polymer. To keep consistent with the solid state computations, calculations are carried out using two monomers per unit cell. The important finding of these calculations is that with two monomers per unit cell a planar structure is obtained with the two rings pointing in the opposite directions (i.e., *anti* orientation) [127, 128]. Whereas with one monomer per unit cell one obtains a twisted out-of-plane structure [129] because of the steric interaction (repulsion) between the rings pointing in the same direction (i.e., *syn* orientation) preventing the formation of a planar structure and would eventually form a narrow helix in the infinite chain. Hence, it is clear that these five-membered ring polymers can exist in two mesomeric forms (see Fig. 1.4)

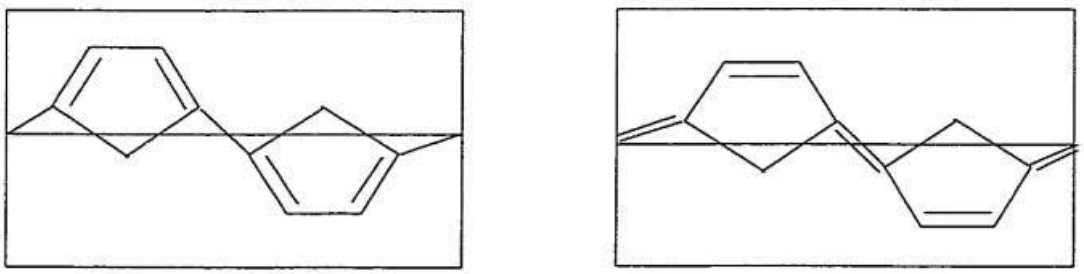

Aromatic (or s-cis or trans-cisoid) Quinoid (or s-trans or cis-transoid)

Figure 1.4: Two monomers per repeat unit in *anti* orientation.

1. aromatic: a geometric structure where a longer "single" bond appears between

the rings and between the β carbons; by analogy with the terminology used for cis-polyacetylene, this structure is named trans-cisoid;

2. quinoid: a structure where a shorter "double" bond appears between the rings and the β carbons; termed as cis-transoid [83].

In this thesis, the *ab initio* Hartree-Fock self consistent field (SCF) procedure and the post-SCF configuration interaction (CI) methods along with a synopsis of the CI-background are outlined in Chapter 2. In Chapter 3, we discuss the computational approach in detail. We attempt to provide a full analysis therein to state the approximations involved in CI-singles process. The ground and the excited state geometric structures along with the geometry relaxation phenomena of these five membered heterocycles are discussed in Chapter 4. Chapter 5 is devoted to the investigations of different electronic properties like excitation energies, singlet-triplet transitions, delocalization of molecular orbitals, charge distribution, dipole moments, oscillator strengths etc., within the microscopic realm of the polymeric systems. Chapter 5 also contains discussions about bond length alternation, and variation of excitation energy due to chain length and different end-groups. An effort has been made to determine the relationship between the electronic and geometric conformations of these systems. Wavefunctions of the highest occupied molecular orbital and the lowest unoccupied molecular orbital are also discussed in the same chapter. The bulk properties of these pseudo-one-dimensional polymers are then extrapolated to show the trends in band gaps from their excitation energies. Finally, we try to show the relative success of our CI-singles model-calculation as a function of basis set, indicating that a judicious choice of basis set is indeed important in order to evaluate the performance of these basis sets adequately.

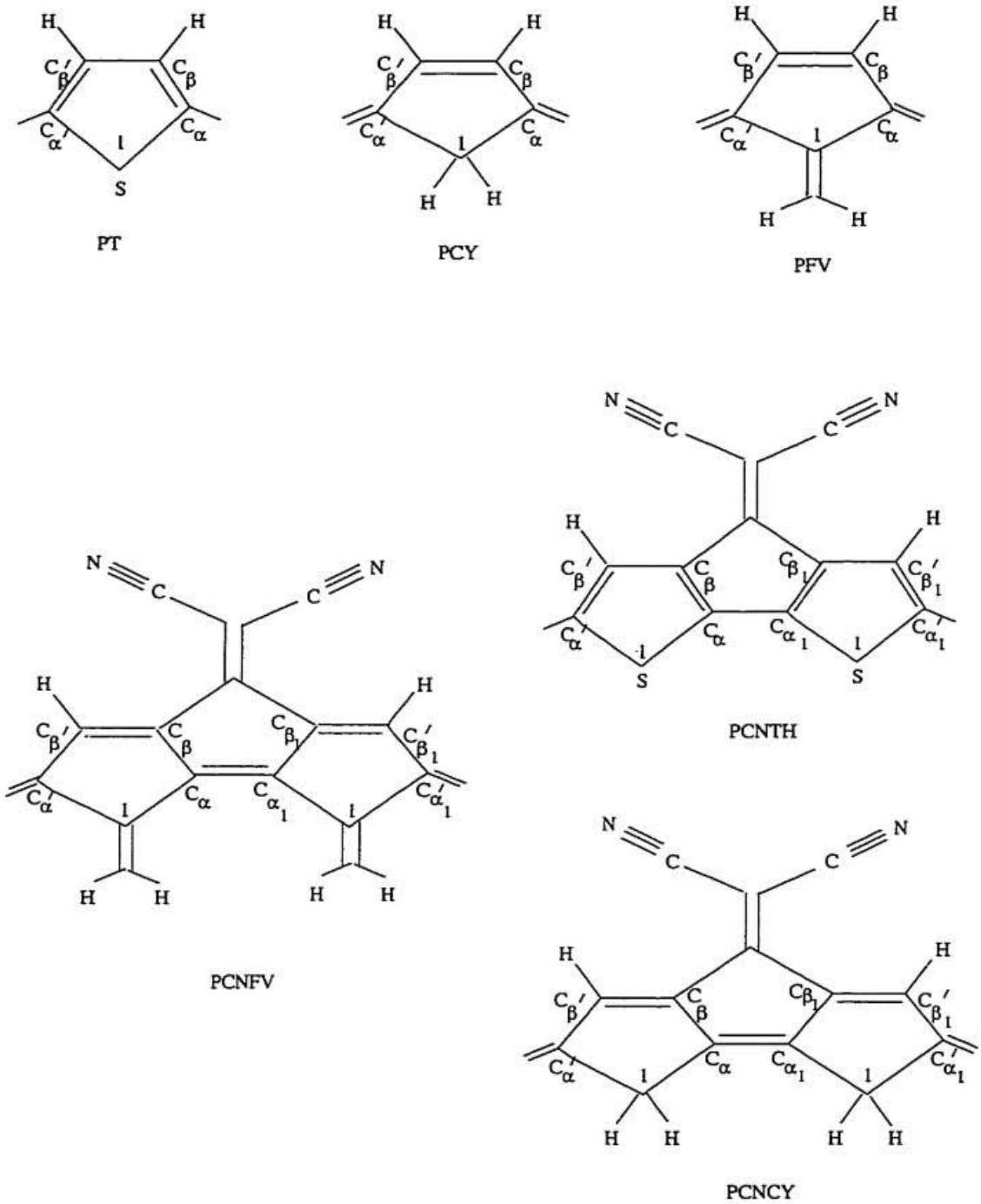

Figure 1.5: Monomer units of the π conjugated systems studied.

Chapter 2

Theoretical Approach

2.1 *Ab Initio* Hartree-Fock (HF) Theory

A primary objective of molecular quantum mechanics is to find a solution of the nonrelativistic, time-independent Schrödinger's equation

$$H\psi(\mathbf{r},\mathbf{R}) = E(\mathbf{R})\psi(\mathbf{r},\mathbf{R}) \tag{2.1}$$

where $\mathbf{R}$ denotes nuclear and $\mathbf{r}$ electronic coordinates. Due to their relative massiveness, the nuclei move slowly compared to the electrons. Hence, according to the Born-Oppenheimer approximation (or adiabatic approximation) the electrons in a molecule can be thought of as moving in the field of fixed nuclei [90]. The electronic Hamiltonian (in atomic units) for a molecular system containing N nuclei and $2n$ electrons is given by

$$\hat{H}_{elec} = -\sum_{i=1}^{2n}\frac{1}{2}\nabla_i^2 - \sum_{i=1}^{2n}\sum_{A=1}^{N}\frac{Z_A}{r_{iA}} + \sum_{i=1}^{2n}\sum_{j>i}^{2n}\frac{1}{r_{ij}} \tag{2.2}$$

where, $r_{iA} = |\mathbf{r}_{iA}| = |\mathbf{r}_i - \mathbf{R}_A|$ is the distance between the ith electron and the Ath nucleus, and $r_{ij} = |\mathbf{r}_i - \mathbf{r}_j|$ is the distance between the ith and jth electron. The Schrödinger equation involving the electronic Hamiltonian is given by

$$\hat{H}_{elec}\psi_{elec}(\mathbf{r_i}, \mathbf{R_A}) = E_{elec}(\mathbf{R_A})\psi_{elec}(\mathbf{r_i}, \mathbf{R_A}), \tag{2.3}$$

where $\psi_{elec}(\mathbf{r_i}, \mathbf{R_A})$ is used to describe the motion of the electrons. The total energy E_{tot} for a given nuclear geometry ($\mathbf{R_0}$) is given by the sum of the electronic energy $E_{elec}(\mathbf{R_0})$, and the constant nuclear repulsion energy $\sum_{A=1}^{N}\sum_{B>A}^{N}\frac{Z_A Z_B}{R_{AB}}$:

$$E_{tot} = E_{elec}(\mathbf{R_0}) + \sum_{A=1}^{N}\sum_{B>A}^{N}\frac{Z_A Z_B}{R_{AB}}. \tag{2.4}$$

2.1.1 Many-Electron Wavefunction

In a molecular many-body problem, the complex motion of *2n* electrons in the field of N nuclei can be approximated by a single-electron effective-field model. In this model, each electron moves in the (effective) electrostatic potential constructed from the average electron density estimated from the motions of the remaining *2n-1* electrons in the presence of N fixed nuclei. Electrons are fermions, hence the total many-electron wavefunction must obey the Pauli exclusion principle (i.e., $\psi(\mathbf{r})$ is antisymmetric). Taking the electronic spin into account we introduce **spin orbitals**, Φ_i, which are given by the product of an orbital wavefunction and one of

the two possible $\pm\frac{1}{2}$ spin functions

$$\Phi_i(r_i, m_{si}) = \psi_i(\mathbf{r_i})\zeta(m_{si}) \tag{2.5}$$

where $\zeta(m_{si}) = \alpha$ for $m_{si} = +\frac{1}{2}$ and $\zeta(m_{si}) = \beta$ for $m_{si} = -\frac{1}{2}$. The overall wavefunction is then written in the form of a Slater determinant [130],

$$\psi_i(\mathbf{r}, m_s) = \frac{1}{\sqrt{2n!}} \begin{vmatrix} \psi_1(1)\alpha(1) & \psi_1(2)\alpha(2) & \cdots & \psi_1(2n)\alpha(2n) \\ \psi_1(1)\beta(1) & \psi_1(2)\beta(2) & \cdots & \psi_1(2n)\beta(2n) \\ \cdots & \cdots & & \cdots \\ \psi_n(1)\alpha(1) & \psi_n(2)\alpha(2) & \cdots & \psi_n(2n)\alpha(2n) \\ \psi_n(1)\beta(1) & \psi_n(2)\beta(2) & \cdots & \psi_n(2n)\beta(2n) \end{vmatrix}. \tag{2.6}$$

The factorial term is necessary for normalization. In the HF approximation [90] each Φ is an eigenfunction of a single-electron equation of the form

$$\hat{H}^{eff}(i)\Phi(i) = E_i\Phi(i). \tag{2.7}$$

2.1.2 Basis Set Details

Typically, a complete set of basis functions can be used to represent molecular orbitals exactly, i.e., each molecular orbital ψ_i can be expanded as a linear combi-

nation of a pre-defined set of functions known as basis functions χ_μ

$$\psi_i = \sum_{\mu=1}^{N} c_{\mu i}\chi_\mu. \tag{2.8}$$

Normally, χ_μ are atomic like orbitals usually centered on the nuclei. The molecular orbital expansion coefficients $c_{\mu i}$ are determined from the variational principle [130]. The use of an infinite number of basis functions would result in a Hartree-Fock energy equal to that given by the variational expression which involves minimizing the Rayleigh ratio

$$\mathcal{E} = \frac{\int \psi^*(\mathbf{x};\mathbf{R})H\psi(\mathbf{x};\mathbf{R})d\mathbf{x}}{\int \psi^*(\mathbf{x};\mathbf{R})\psi(\mathbf{x};\mathbf{R})d\mathbf{x}}. \tag{2.9}$$

This limiting energy is called the **Hartree-Fock limit**. The HF limit is not the exact ground-state energy of the molecule because it still ignores effects of electron correlation. An infinite basis set is not computationally feasible. A finite basis set is always used, and the error due to the incompleteness of the basis set is called the **basis-set truncation error**. The difference between the Hartree-Fock limit and the computed lowest energy in a Hartree-Fock SCF calculation is a measure of the basis-set truncation error. Hence, a key computational consideration is to keep the number of basis functions high enough to minimize the basis-set truncation error and low enough to minimize the computational effort. In *Gaussian 94* [131] and other *ab initio* programs, Gaussian-type atomic functions are used (due to the faster evaluation of two-electron integral) as basis functions which have the general form

$$g(\alpha,\mathbf{r}) = cx^n y^m z^l e^{-\alpha r^2}, \tag{2.10}$$

where α is a positive exponent. The actual basis functions (termed *contracted gaussians*) are formed from a linear combination of the *primitive gaussians* giving

$$\chi_\mu = \sum_{p=1}^{N} d_{\mu p} g_p \tag{2.11}$$

where $d_{\mu p}$'s are contraction coefficients. Thus we have

$$\psi_i = \sum_\mu c_{\mu i} \chi_\mu = \sum_\mu c_{\mu i} (\sum_p d_{\mu p} g_p). \tag{2.12}$$

2.1.3 Electronic Energy

The expression for the electronic energy is obtained by evaluating the expectation value of the Rayleigh ratio, $\mathcal{E}$, (see Eq. (2.9)) with ψ given by Eq. (2.6) and $\hat{H} = \hat{H}_{elec}$ given by Eq. (2.2). Dividing $< \hat{H}_{elec} >$ into one- and two-electron contributions, performing the integrations over space coordinates and summing over all the spin orbitals according to rules explained elsewhere [90], the total electronic energy is given by

$$E = 2\sum_{i=1}^{n} \langle i|\hat{h}^N|i\rangle + \sum_i^n \sum_j^n (2J_{ij} - K_{ij}), \tag{2.13}$$

$$\text{where} \qquad \langle i|\hat{h}^N|i\rangle = \int \psi_i^*(1)\hat{h}^N\psi_i(1)d\mathbf{v}_1 = H_{ii}^N \tag{2.14}$$

are the one electron integrals obtained from the first and the second term of Eq. (2.2). $\hat{h}^N$ is referred to as the *one-electron Hamiltonian operator*. The two electron

contribution consists of two parts: the Coulomb and the exchange integrals. The Coulomb integral can be represented as

$$J_{ij} = \int \psi_i^*(1)[\int \psi_j^*(2)\frac{1}{\mathbf{r_{12}}}\psi_j(2)d\mathbf{v}_2]\psi_i(1)d\mathbf{v}_1 \tag{2.15}$$

and the exchange integrals can be represented as

$$K_{ij} = \int \psi_i^*(1)[\int \psi_i^*(2)\frac{1}{\mathbf{r_{12}}}\psi_j(2)d\mathbf{v}_2]\psi_j(1)d\mathbf{v}_1. \tag{2.16}$$

The terms within the square brackets in the above integrals are referred to as the Coulomb operator $\hat{J}_{ij}$, and the exchange operator $\hat{K}_{ij}$ respectively.

2.1.3.1 Variational Principle

Hartree-Fock theory is based on a variational principle. A brief summary of obtaining the integro-differential HF equations and subsequent formulation of HF matrix equation is given in Appendix A.

2.1.4 Population Analysis

Once we have obtained a converged value for the density matrix, Fock matrix, etc., (see Appendix A) there are a number of ways we might use the wavefunction Ψ to analyze the results of our calculation. Most of the properties of molecules that one might evaluate from a molecular wavefunction, such as the dipole moment, quadruple moment, field gradient at a nucleus, diamagnetic susceptibilities etc.,

are described by sums of one-electron operators of the general form

$$\mathcal{O}_1 = \sum_{i=1}^{n} h(i), \tag{2.17}$$

where $h(i)$ is not necessarily the core-Hamiltonian here, but any operator depending only on the coordinates of a single electron. The expectation values for such operators will have the form

$$\langle \mathcal{O}_1 \rangle = \langle \Psi | \mathcal{O}_1 | \Psi \rangle = \sum_{i}^{n} (\psi_i | h | \psi_i) = \sum_{\mu\nu} P_{\mu\nu} (\nu | h | \mu), \tag{2.18}$$

so that, in addition to the density matrix, we need only evaluate the set of one-electron integrals $(\mu|h|\nu)$ to calculate one-electron expectation values. For example, in order to calculate the dipole moment we need in addition to $\mathbf{P}$ only the dipole integrals

$$(\nu | x | \mu) = \int d\mathbf{r}_1 \psi_\nu^* \mathbf{r}_1 x_1 \psi_\mu^* \mathbf{r}_1. \tag{2.19}$$

The charge density

$$\rho(\mathbf{r}) = \sum_{\mu} \sum_{\nu} P_{\mu\nu} \psi_\mu(\mathbf{r}) \psi_\nu^*(\mathbf{r}) \tag{2.20}$$

represents the probability of finding an electron in various regions of space. Though there is no unique definition of the number of electrons to be associated with a given atom or nucleus in a molecule, it is still useful to perform such population analysis. Since

$$n = 2 \sum_{i}^{n} \int d\mathbf{r} |\psi_i(\mathbf{r})|^2 \tag{2.21}$$

divides the total number of electrons into two electrons per molecular orbital, by substituting the basis expansion of ψ_i into the above equation we have

$$n = \sum_{\mu} \sum_{\nu} P_{\mu\nu} S_{\nu\mu} = \sum_{\mu} (\mathbf{PS})_{\mu\mu} = tr\, \mathbf{PS} \tag{2.22}$$

where, $(\mathbf{PS})_{\mu\mu}$ represents the number of electrons associated with ψ_μ. This is called the **Mulliken population analysis**.

2.2 Electron Correlation Effects in Molecules

The optimum evaluation of structure and energies of molecules from first principles has long been a primary goal of both quantum physics and quantum chemistry. One of the major stumbling blocks to achieving this goal has been the lack of an accurate theory of electron correlation which is practical enough for a reasonable application to interesting problems in physics and chemistry. The use of mean-field models or orbital models is one of the first steps towards the theoretical determination of the electronic structure of molecules. An orbital model such as Hartree-Fock self-consistent field theory provides an excellent starting point which accounts for the bulk ($\sim$ 99%) of the total energy of the molecule [89]. The remaining component of the energy results from the neglect of instantaneous interactions (correlations) between electrons, and is crucial for the description of chemical bond formation and for the accurate and quantitative evaluation of molecular energies [132]. The term "electron correlation energy" is usually defined as the difference between the exact non-relativistic energy of the system ($\mathcal{E}$) and the Hartree-Fock energy (E)

[133] obtained in the limit that the basis set approaches completeness.

$$E_{corr} = \mathcal{E} - E. \tag{2.23}$$

Because the HF energy is an upper bound to the exact energy, the correlation energy is negative. Further discussion of correlation effects in molecules is given in Appendix B. Currently within the independent-electron theories, three approaches can be used to calculate the correlation energy as described above. One is perturbation theory, another is density functional theory and the last is configuration interaction theory. The configuration interaction is the approach that we take in this work. The background for this theory is summarized in Appendix C.

2.3 Configuration Interaction Theory

Configuration interaction is a straightforward application of the linear variational technique to the calculation of electronic wavefunctions [134]. The term configuration interaction was introduced in atomic electronic structure theory to deal with electronic states which could not be characterized adequately using the single configuration wavefunctions. It implied perturbation of an electronic configuration by neighbouring configurations. Correlation of the motion of the electrons with the spin is partly but not completely, accounted for by virtue of the determinantal form of the single determinant wavefunction. The basic idea is to diagonalize the n-electron Hamiltonian in a basis of n-electron functions (Staler determinants). In other words, CI represents the exact wavefunction as a linear combination of n-electron trial functions. In principle, CI can provide an arbitrarily accurate so-

lution to the exact many-electron wavefunction problem. But in practice, we can handle only a finite set of n-electron trial functions. Consequently, CI provides only an upper bound to the exact energy.

2.3.1 Configuration State Functions (CSF)

The HF method yields a finite set of spin orbitals when a finite basis set expansion is used. In general, a system comprising n-electrons described by a basis set of N functions ϕ_μ, results in $2N$ different spin orbital basis functions of the type ϕ_μ^β, which in turn may be linearly combined into $2N$ spin orbitals χ_i. Now, by ordering the spin orbitals energetically and taking the n lowest in energy (to be occupied by the n electrons), we can form the Hartree-Fock wavefunction ϕ_0. However, there remains $2N - n$ virtual orbitals. Clearly, many Slater determinants can be formed from the $2N$ spin orbitals; ϕ_0 is just one of them. By using the single determinantal wavefunction ϕ_0 as a convenient reference, it is possible to classify all other determinants according to how many electrons have been promoted from occupied orbitals to virtual orbitals. To simplify the appearance of the Slater determinants we omit the normalization factor and hence denote Φ_0 as

$$\Phi_0 = |\phi_1\phi_2 \cdots \phi_i\phi_j \cdots \phi_n| \tag{2.24}$$

where ϕ_i and ϕ_j are among the n occupied spin orbitals for the HF ground state. Here we have specified the determinant Eq. (2.6) in abbreviated form. A singly excited determinant corresponds to one for which a single electron from an occupied

spin orbital ϕ_i has been promoted to a virtual spin orbital ϕ_a

$$\Phi_i^a = |\phi_1\phi_2\cdots\phi_a\phi_j\cdots\phi_n|. \tag{2.25}$$

A doubly excited determinant is one in which two electrons have been promoted, one from ϕ_i to ϕ_a and the other from ϕ_j to ϕ_b.

$$\Phi_{ij}^{ab} = |\phi_1\phi_2\cdots\phi_a\phi_b\cdots\phi_n|. \tag{2.26}$$

In a similar fashion, we can form other multiply excited determinants. Each of the determinants, or a linear combination of a small number of them constructed so as to have the correct electronic symmetry (*e.g.*, to be an eigenfunction of S^2), is called a configuration state function (CSF). To be precise, a CSF is an eigenfunction of all the operators that commute with the Hamiltonian. These excited CSFs can be taken to approximate excited-state wavefunctions or, as we now see, they can be used in linear combination with ϕ_0 to improve the representation of the ground and/or excited-state wavefunction.

2.3.2 Full CI

The exact ground-state and excited-state wavefunctions can be expressed as a linear combination of all possible n-electron Slater determinants arising from a complete set of spin orbitals [133]. Hence, we can write the exact electronic wavefunction Φ for any state of the system in the form

$$\Phi = C_0\Phi_0 + \sum_{i,a} C_i^a \Phi_i^a + \sum_{i<j,a<b} C_{ij}^{ab} \Phi_{ij}^{ab} + \sum_{i<j<k,a<b<c} C_{ijk}^{abc} \Phi_{ijk}^{abc} \cdots \tag{2.27}$$

where the 0-indexed term is the Hartree-Fock level, the C's are the set of expansion coefficients and where the limits in the summation ensures that we sum over all unique pair of spin orbitals in doubly excited determinants, over all unique triplets of spin orbitals in triply excited determinants, and so on. In other words, a given excited determinant appears only once in the summation. The full CI method forms the wavefunction Φ as a linear combination of the Hartree-Fock determinant and all substituted determinants:

$$\Phi = C_0\Phi_0 + \sum_{s>0} C_s\Phi_s. \tag{2.28}$$

The summation $\sum_{s>0}$ runs over all possible substituted determinants with expansion coefficients C_s for the state s. On a physical level, Eq. (2.27) represents a mixing of all of the possible electronic states of the molecule, all of which have some probability of being attained according to the laws of quantum mechanics. The C's are determined by minimizing the energy of the resultant wavefunction using the linear variational method, leading to the following equation:

$$\sum_s (H_{st} - E_i S_{st}) C_{si} = 0 \qquad t = 0, 1, 2, \cdots \tag{2.29}$$

Here, H_{st} is a **configuration matrix** element,

$$H_{st} = \int \cdots \int \Phi_s^* H \Phi_t d\tau_1 d\tau_2 \cdots d\tau_n, \tag{2.30}$$

$$\text{and} \qquad S_{st} = \int \cdots \int \Phi_s^* \Phi_t d\tau_1 d\tau_2 \cdots d\tau_n \tag{2.31}$$

and E_i is an energy. The lowest root E of Eq. (2.29) is the energy of the electronic ground state. The matrix form of Eq. (2.29) is

$$HC = ESC \tag{2.32}$$

where the elements of the $L \times L$ square matrices **H** and **S** are H_{st} and S_{st}, respectively; **E** is the diagonal matrix of energies E_s; **C** is an $L \times L$ matrix of coefficients. Because the Slater determinants form an orthonormal set ($S_{st} = \delta_{st}$), Eq. (2.32) becomes

$$HC = EC. \tag{2.33}$$

The full CI method represents the most complete non-relativistic treatment possible within the limitations imposed by the chosen basis set. It exhibits the possible quantum states of the system in modelling the electron density in accordance with the definition and constraints of the basis set in use [89]. The difference between the HF energy with a given basis set and the full CI energy is the *correlation energy within the basis.* As the basis set becomes more complete, i.e., $N \to \infty$, the result of a full configuration interaction treatment will approach the exact solution of the nonrelativistic Schrödinger equation.

The full CI method is well-defined, size-consistent, and variational. However, it is very expensive and impractical except for very small systems because of the very large number of substituted determinants, the total number of which in Eq. (2.27) is $(2N!)/[n!(2N-n)!]$. For example, with 10 electrons and 20 basis set functions, the number of determinants to consider is

$$\begin{pmatrix} 2N \\ n \end{pmatrix} = 8.477\cdots\times 10^8. \tag{2.34}$$

In practice, therefore, the expression in Eq. (2.27) must always be truncated. Nonetheless, although the calculation is limited to a finite set of spin orbitals and only a fraction of all possible determinants, CI is a popular method for the calculation of accurate molecular wavefunctions and potential energy surfaces. Even with a small number of CSFs it can correct for one of the deficiencies that stem from the use of only double occupied orbitals in the restricted HF method, the incorrect behaviour for the dissociation of a molecule.

2.3.3 Limited CI

Conventional CI calculations are usually of the order of 10^4 SCFs, and because full CI results in a list far beyond this number, it is necessary to employ a truncation scheme so that the list of SCFs is kept to a manageable size. The most straightforward way of limiting the length of the CI expansion (Eq. (2.27)) is to truncate the series at a given level of substitution. If no substitutions are performed, $\Phi = \Phi_0$, corresponds to the HF solution. Inclusion of single substitution functions only,

termed **Configuration Interaction Singles** or CIS leads to,

$$\Phi_{CIS} = C_0\Phi_0 + \sum_{i}^{occ}\sum_{a}^{virt} C_i^a \Phi_i^a. \tag{2.35}$$

Single excitations mix indirectly with $|\Phi_0\rangle$; i.e., they interact with the doubles which in turn interact with $|\Phi_0\rangle$. Therefore singly excited determinants will have a small but nonzero effect on the calculation of the ground-state energy because they have nonzero matrix elements with doubly excited determinants, which themselves mix with Φ_0. Moreover, single excitations do affect the electronic charge distribution and therefore properties such as the dipole moment. Inclusion of double substitution functions, termed *Configuration Interaction Doubles* or CID leads to

$$\Phi_{CID} = C_0\Phi_0 + \sum_{i}^{occ}\sum_{<j}\sum_{a}^{virt}\sum_{<b} C_{ij}^{ab}\Phi_{ij}^{ab}. \tag{2.36}$$

Two major computational tasks are involved here. The first is a transformation of two-electron integrals $(\mu\nu|\lambda\sigma)$ over basis functions, into corresponding integrals with the Hartree-Fock spin orbitals χ_a replacing the basis functions ϕ_μ. The second is the determination of the lowest (or lowest few) energy solution of Eq. (2.27) and the associated wavefunction coefficients. Both the tasks are significant computationally, and considerable effort has been put towards the development of efficient algorithms.

At a slightly higher level of theory, both single and double substitutions can be included in the CI treatment. The model is termed **Configuration Interaction,**

Singles and Doubles, or CISD. The trial wavefunction is given by

$$\Phi_{CISD} = C_0\Phi_0 + \sum_{i}^{occ}\sum_{a}^{virt} C_i^a\Phi_i^a + \sum_{i}^{occ}\sum_{<j}\sum_{a}^{virt}\sum_{<b} C_{ij}^{ab}\Phi_{ij}^{ab} \tag{2.37}$$

where triple, quadruple, and higher order excitations are completely neglected. Double excitations contribute dominantly to the electron correlation energies. Single excitations contribute relatively little to the correlation energies, though they appear to be important for accurate evaluation of molecular properties such as geometries, vibrational frequencies, dipole moments, oscillator strengths, etc. [135] Strengths and weaknesses of the CI approach are discussed in Appendix C.

2.4 The CI-Singles Wave Functions and Energy

The Hartree-Fock single determinant wavefunction for the ground state of a system is

$$\psi_{HF} = (2n!)^{-1/2} det\{\chi_1\chi_2....\chi_i\chi_j...\chi_n\} \tag{2.38}$$

where $2n$ is the number of electrons and χ_p are spin orbitals represented in a convenient basis of N atomic basis functions, ϕ_μ:

$$\chi_p = \sum_{\mu}^{N} c_{\mu p}\phi_\mu. \tag{2.39}$$

This reference state need not be the ground state but could be any excited HF state as well. For convenience we will use the following subscript notation throughout: $\mu, \nu, \lambda, \sigma, \cdots$ denote atomic basis functions; $i, j, k, l, \cdots$ denote occupied molecular

orbitals in the ground state; $a, b, c, d, \cdots$ denote virtual molecular orbitals, unoccupied in the ground state; $p, q, r, s, \cdots$ denote generic molecular spin orbitals. The molecular orbital coefficients, $c_{\mu p}$, are determined by standard self-consistent field (SCF) procedures which solve the **Roothaan-Hall equations**:

$$\sum_{\mu}(F_{\mu\nu} - \epsilon_p S_{\mu\nu})c_{\nu p} = 0. \tag{2.40}$$

Here $F_{\mu\nu}$ represents the elements of the $N \times N$ **Fock matrix**

$$F_{\mu\nu} = H_{\mu\nu} + \sum_{\lambda\sigma}\sum_{i} c^*_{\mu i}c_{\nu i}(\mu\lambda\|\nu\sigma) \tag{2.41}$$

given in terms of the one-electron core Hamiltonian, $H_{\mu\nu}$, representing the energy of a single electron in a field of "bare" nuclei. Its elements are

$$\begin{aligned} H_{\mu\nu} &= \int \phi^*_{\mu}(1)\hat{H}(1)\phi_{\nu}(1)dx_1dy_1dz_1, \\ \hat{H}(1) &= -\frac{1}{2}\left(\frac{\partial^2}{\partial x_1^2} + \frac{\partial^2}{\partial y_1^2} + \frac{\partial^2}{\partial z_1^2} - \sum_{A=1}^{M}\frac{Z_A}{r_{1A}}\right). \end{aligned} \tag{2.42}$$

Here Z_A is the atomic number of atom A, and the summation is carried out over all atoms. The quantities $(\mu\lambda\|\nu\sigma)$ are the usual antisymmetrized two-electron repulsion integrals:

$$(\mu\lambda\|\nu\sigma) = \int\int \phi^*_{\mu}(1)\phi_{\nu}(1)\left(\frac{1}{r_{12}}\right)\phi^*_{\lambda}(2)\phi_{\sigma}(2)\; d\tau_1 d\tau_2 \tag{2.43}$$

$S_{\mu\nu}$ represents the $N \times N$ **overlap matrix** elements,

$$S_{\mu\nu} = \int \phi_\mu^* \phi_\nu \, d\tau, \tag{2.44}$$

and ϵ_p is the one-electron energy of the molecular orbital ψ_p. After having solved these equations, the total energy of the ground-state single determinant can be expressed as

$$E_{HF} = \sum_{\mu\nu} P_{\mu\nu}^{HF} H_{\mu\nu} + \frac{1}{2} \sum_{\mu\nu\lambda\sigma} P_{\mu\nu}^{HF} P_{\lambda\sigma}^{HF} (\mu\lambda \| \nu\sigma) + V_{nuc}, \tag{2.45}$$

where P^{HF} is the HF density given as a sum over the occupied orbitals,

$$P_{\mu\nu}^{HF} = \sum_{i=1}^{n} c_{\mu i}^* c_{\nu i}, \tag{2.46}$$

and V_{nuc} is the nuclear repulsion energy.

Equation (2.38) represents only one of the several possible determinants for a one electron wavefunction of the system. Now, considering the $2n(N-2n)$ possible singly excited determinants made by replacing one occupied spin orbital by a virtual spin orbital, the wavefunctions and associated energies can be written as

$$\psi_{ia} = (2n!)^{-1/2} det\{\chi_1 \chi_2 \cdots \chi_a \chi_j \cdots \chi_n\} \tag{2.47}$$

$$E_{ia} = E_{HF} + \epsilon_a - \epsilon_i - (ia \| ia) \tag{2.48}$$

where the general antisymmetrized two-electron integrals in the molecular orbital basis have the following form

$$(pq\|rs) = \sum_{\mu\nu\lambda\sigma} c^*_{\mu p} c_{\nu q} c^*_{\lambda r} c_{\sigma s} (\mu\nu\|\lambda\sigma). \tag{2.49}$$

These singly excited wavefunctions and energies can be considered as the first approximation to the molecular excited states of the system. The disadvantages [90] encountered in using Eq. (2.47) as a wavefunction are well known: (i) It is not an eigenfunction of the spin-squared operator and therefore does not yield pure spin states for the closed-shell systems; (ii) The spin orbitals involved in the transition have been determined variationally for the ground state. Forcing the virtual orbital to be occupied is more closely related to ionization rather than excitation; (iii) The wavefunction is not at all appropriate for excitation into degenerate spin orbitals. For example, the $\pi \rightarrow \pi^*$ excitation in benzene can be understood only as a mixture of four singly excited determinants.

These limitations are partially overcome if the excited-state wavefunction is expressed as a linear combination of all the possible singly excited determinants:

$$\Psi_{CIS} = \sum_{ia} a_{ia} \psi_{ia}. \tag{2.50}$$

The configuration interaction (CI) coefficients a_{ia} can be deduced as normalized eigenvectors of the Hamiltonian matrix:

$$\langle \psi_{ia} | H | \psi_{jb} \rangle = [E_{HF} + \epsilon_a - \epsilon_i]\delta_{ij}\delta_{ab} - (ja\|ib). \tag{2.51}$$

This procedure can be referred to as full configuration interaction in the space of single substitutions or "CI singles". The total energies, E_{CIS}, of the CIS for various excited states are the eigenvalues of Eq. (2.51). In this context, a few points should be mentioned:

(1) The excited state wavefunction Ψ_{CIS} is orthogonal to the ground-state wavefunction Ψ_{HF} by virtue of Brillouin's theorem, i.e.,

$$\langle \psi_{ia} | H | \psi_{HF} \rangle = 0. \tag{2.52}$$

(2) The CIS coefficients are determined variationally. This allows the overall wavefucntion to relax so that Ψ_{CIS} more properly represents an excited state rather than an ionized state. (3) Regarding the closed-shell systems, Ψ_{CIS} has the ability to describe pure sign singlets and triplets with no spin contaminations by allowing positive and negative combinations of α and β excitations from one doubly occupied orbital to one virtual orbital. (4) Since CIS lead to a well-defined wavefunction and differentiable energy, the analytical gradient techniques to determine properties and optimized excited-state geometries are straightforward to apply. (5) Finally, CIS is also found to be a size-consistent method (see Appendix B) [73]. The last point is well established, since size-consistency is exploited by the various CEPA methods [136, 137] which is widely used to approximate ground-state correlation energies. A brief derivation of the analytical first order derivative of the CI-Singles energy is given in Appendix D.

2.5 Electron Correlation in Excited States

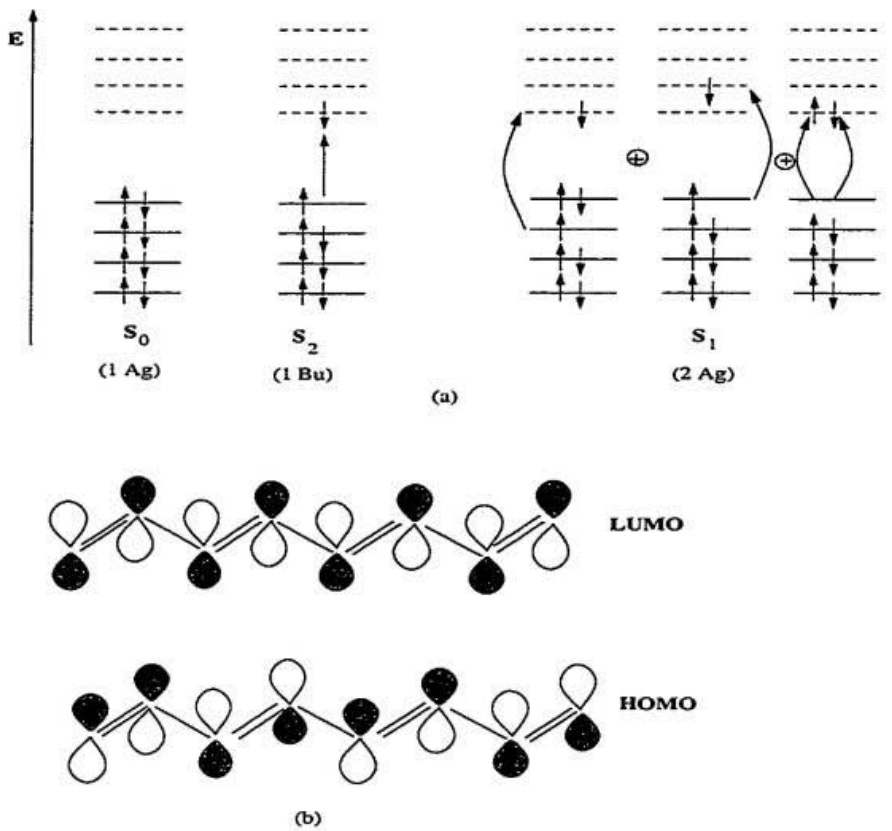

Figure 2.1: (a) The main electronic configurations contributing to the ground state S_0 and the lowest singlet excited states S_1 and S_2, (b) the bonding-antibonding pattern of the HOMO and LUMO levels.

Properties like luminescence, electron-hole separation, nonlinear optical response, etc., require a proper description of electronic excited states and hence many-body effects. In this context, the theoretical treatment of π-conjugated systems often becomes very elaborate in order to (i) incorporate electron correlation effects and (ii) account for the strong connection between, and mutual influence of the electronic and geometric structures. The importance of electron correlation is well depicted

in the analysis of the ordering of the lowest singlet excited states in polyenes and polyacetylene [138]. With a simple example this can be clarified in octatetraene (see Fig. 1.1 and Fig. 2.1). A one-electron treatment (*e.g.*, Hückel or Hartree-Fock) produces 8 π-molecular orbitals whose symmetries alternate between "gerade" (g) and "ungerade" (u)[1] and energies which increase with the number of nodes in the wavefunction [139]. The 8 π electrons distribute among the 8 π-MOs; each of their repartitions defines a so-called electronic configuration whose individual wavefunction can be cast in the form of one Slater determinant. The wavefunction can be cast in the form of one Slater determinant. The lowest energetic configuration is the one in which the π electrons occupy 2 by 2 the four lowest π MOs and defines the singlet ground state S_0 of A_g symmetry. At the one-electron level, the lowest one photon allowed (i.e., if transition dipole moment is finite)[2] excited state of B_u symmetry is described by the promotion of a single electron from HOMO to LUMO. Any one photon forbidden A_g excited state would lie higher in energy because it requires promotion of a single electron from HOMO to LUMO+1 or HOMO-1 to LUMO or promotion of two electrons from HOMO to LUMO and these processes nominally cost a larger energy as illustrated in Fig. 2.1a. The singly excited HOMO to LUMO+1 and HOMO-1 to LUMO configurations and the doubly excited HOMO to LUMO configuration strongly mix and result in the $2A_g$ state being located below the $1B_u$ state. Therefore, in polyenes (longer than butadiene), the lowest excited

[1]The symmetric combination of two localized AOs leads to a delocalized bonding MO of *gerade* symmetry (i.e., symmetric with respect to inversion about the point centered between the nuclei), and the antisymmetric combination leads to an antibonding MO of *ungerade* symmetry.

[2]A transition is allowed if the product of the vacated orbital and the newly occupied orbital belongs to (or contains) the same symmetry species as at least one component of the electronic dipole moment operator. See also ref. [139]

state, S_1, is one-photon forbidden, vs. the ground state S_0 [138]. The consequence is that polyenes and polyacetylene do not luminesce according to Kasha's rule [140] (which says that luminescence takes place from the lowest excited state). Hence in order to observe strong fluorescence, a large one-photon coupling between S_0 and S_1 is required.

An interesting and important feature which is specific to all conjugated polymers, is the interconnection between their electronic and geometric structures. We present here another example of octatetraene. In the first case we take only the σ backbone into consideration where all the carbon-carbon bond lengths are roughly the same and equal to 1.51 Å (typical single bond length between two sp^2 carbons). Now, as the π electrons are introduced, they are distributed *unevenly* over the bonds and in such a way that there appears alternating larger and smaller π bond densities. As a result we find a dimerization (i.e., alternation) of longer double-like (1.35 Å long) and shorter single-like (1.45 Å long) carbon-carbon π-bonds starting from one end of the molecule. This geometrical characteristic is reflected in the bonding-antibonding pattern of the HOMO wavefunction while the LUMO wavefunction displays the exactly opposite pattern (Fig. 2.1b).

There is another manifestation of the twinning between the geometric and the electronic structures: the dependence of the ordering of the lowest singlet excited states on the effective degree of bond-length alternation δ_r, along the backbone [141]. As δ_r increases, for example, when switching from a purely polyenic backbone (as in polyacetylene) to a mixed aromatic-polyenic backbone (as in poly (*p*-phenylenevinylene)), or to an aromatic backbone (as in poly(*p*-phenylene)), the $2A_g$ state is destabilized up to the point that the $1B_u$ state becomes the lowest singlet

S_1 state [141]. Hence, PPV and its derivatives can strongly luminesce and are the prime candidates for emissive layers in the polymer-based light-emitting devices [142, 143].

Physical properties like the band gap can be interpreted more precisely with the introduction of electron correlation [144, 145]. In an excited state, the electron distribution is not a closed shell. In semiconductor physics, the band gap is the energy required to move an electron from the top of the valence band to the bottom of the conduction band. In the e-h picture it is the minimum energy required to create an electron-hole pair. The correlation gap E_{CG} is defined as a contribution due to the correlation effect, i.e., it is the difference between the exact band gap and the HF band gap, $E_{CG} = E_{gap} - E_{gap}^{HF}$.

In order to get a better insight into the significance of correlation effects, we have compared the results obtained via the CIS approach to those from Hartree Fock and other calculations [65, 75, 77, 105, 106, 118], which are known to provide a reliable description of the one-electron structure of π-conjugated systems.

Chapter 3

Computational Approach

3.1 Methods and Computational Details

A few molecular modelling packages and graphical viewer interface software packages have been used in order to construct the molecules under investigation. Of them, xmol - an X-based molecule viewer and format converter [146] is used to view and convert 3D molecular models produced by other software packages for further use. The Z-matrices[1] of the first generation monomer units (see Fig. 1.5) are generated using the semiempirical MOPAC 93[2] software [120]. The Cerius[2] molecular modelling package [122] is used to construct the second generation conformers. All the *ab initio* calculations are carried out within the framework of *Gaussian 94*,[131] a commercial connected system of programs for performing semiempirical and *ab initio* molecular orbital calculations. Finally Gaussview [147] is used to construct the molecular orbitals from the Gaussian checkpoint files.

[1] A Z-matrix specifies the connections between atoms using bond lengths, bond angles, and dihedral (torsion) angles.

[2] It is a general-purpose semiempirical molecular orbital package for the study of solid state and molecular structures and reactions. Internal coordinates are used to specify the input molecular structures.

The electronic and geometric structures of molecules can be determined using empirical, semi-empirical or *ab initio* methods. Empirical methods (*e.g.*, Molecular Mechanics) are not used to treat these classes of compounds (but they could be used to obtain the geometry for initial guess) because of their inability to include the electrons explicitly in the calculations [89]. Semiempirical methods, like AM1, have been selectively employed and were shown to give some resemblance to the experimental results [18] for large systems. However, they are less reliable than the *ab initio* calculations. For example, it has been shown that AM1 overestimates the band gaps (by more than 4 eV) and the bond lengths due to the errors in the semiempirical-parametrization [118], which are basically designed to reproduce experimental results for molecules in their ground states. Hence for looking into the ground as well as the excited states, *ab initio* methods are the most suitable. *Ab initio* methods like HF neglect the important electron correlation effect, and density functional theory underestimates IPs and EAs by the same amount as the HF theory. It has been reported that the inclusion of hybrid functionals like Becke's three-parameter hybrid functional in combination with the Lee-Yang-Parr correlation functional (B3LYP) etc., ameliorate the band gap problems [75]; but still there are problems associated with them. In general, the CIS method can perform better than all of these methods [73]. The validity of the computational methods can best be checked by the comparison with experimentally determined values. The calculations are performed using the closed-shell restricted CIS (i.e., for singlet excited states) where one set of MOs for both spin up and spin down electrons (i.e., the MOs are either doubly occupied or unoccupied) is used.

To investigate the lattice deformation taking place in the lowest excited states of

these oligomers, the following approach has been considered. Initially, we optimize the ground state geometries by means of the RHF technique. The excited state geometries are then characterized by the promotion of one electron from the HOMO to the LUMO using the CIS procedure. Subtracting the ground state geometrical parameters calculated at the HF level from the excited state parameters at the CIS level allows us to estimate the geometry relaxation for the $\pi \rightarrow \pi^*$ transitions.

3.2 Basis Sets and Geometry

We are interested in finding suitable basis sets to reliably describe the geometric and electronic properties of the oligomers with the different hetaroatomic side/end groups. Therefore, before carrying out the calculations on a series of oligomers, we investigate basis set effects on one system in more detail. For this purpose αT_2 (stoichiometry $C_8H_6S_2$, two thiophene rings in aromatic conformation, see also Fig. 1.4) is chosen. For a molecule the size of αT_2, a systematic investigation of basis sets is feasible. We are also interested in the accuracy which can be achieved with different basis sets from such an investigation. Later the experience gathered from these studies will also be beneficial for calculations on much larger oligomers where smaller basis sets are required for economy reasons. The following issues are addressed here by our selection of basis sets:

1. The influence of polarization functions (p, d and f functions)[3] on the heavy atoms like C and S of αT_2.

[3]Split valence basis sets allow orbitals to change size, but not to change shape. Polarized basis sets remove this limitation by adding orbitals with higher angular momentum beyond what is required for the ground state to describe each atom.

2. The importance of additional diffuse p functions[4] on C, N and S.

While the correlation effects within a given basis set are partially treated by the CIS method, the convergence of the calculated results with respect to basis set expansion is rather slow [148, 149]. Basis sets involving higher angular momentum functions (spdf) are typically necessary to get accurate results when we deal with the problems like explicit bond breaking etc. The slow convergence of the electron correlation energy with the size of the basis set results from the singularity in the inter-electronic Coulomb repulsion energy at small separations, which can be depicted as an existence of a cusp in the electronic wavefunction that approaches $(1 + \frac{1}{2}r_{ij})$ at small inter-electronic distance r_{ij} [132]. The solution to this slow convergence can be found elsewhere [150, 151].

3.3 Evaluation of Methods

In this study we examine the results due to application of three quantum mechanical methods to the calculation of the excitation energies of the low-lying singlet and triplet states of the three parent oligomers and their derivatives. The methods are:

1. Applying split valence 3-21G* basis[5] with no CI (at the Hartree-Fock level)

2. Applying 3-21G* basis with CIS and

[4]Basis sets with diffuse functions are important for systems where electrons are relatively far from the nucleus: molecules with lone pairs, systems in their excited states, systems with low IP etc.

[5]Split valence basis sets have two or more sizes of basis functions for each valence orbitals. In 3-21G* the first number indicates 3 *Gaussian* type basis functions per atomic core orbital, the latter two numbers 2 and 1 indicate two and one *Gaussian* type basis functions per atomic valence orbital.

3. Applying 6-31G* basis with geometry optimized by Hartree-Fock level followed by CI-singles excitations.

The results, together with the experimental data where available, will be compiled to evaluate the basis set and methodological dependency in the next two chapters. We employed various basis sets ranging from the rather small split-valence STO-3G basis set and, in order to assess the consistency of results produced with it, the more sophisticated 3-21G*, 3-21G**, 3-21+G*, 6-31G*, 6-31G**, and 6-31+G* basis sets are also used for optimizing αT_2 [89]. The 3-21G* basis set adds polarization functions in the form of six *d*-type functions for each atom other than hydrogen to the split-valence 3-21G basis. Another star indicates an additional polarization function, *e.g.* 3-21G** indicates the addition to 3-21G* of a set of three *p*-type polarization function for each H atom. The 3-21+G* basis set is the 3-21G* basis with diffuse functions added to the heavy atoms. These additions are usually relatively inexpensive, but seldom make a difference in accuracy [95]. By performing electronic structure calculations on a small molecule using this hierarchy of basis sets, it is possible to gain some insight into the size and characteristics of the basis set needed to obtain a given level of calculational accuracy. By restricting our sample calculations to a limited set of molecules (ranging from monomers to octamers) and the above basis sets, we have attempted to illustrate in a systematic way how specific attributes of a basis set affect calculated quantities. Choosing a model chemistry with an appropriate basis set almost always involves a trade-off between accuracy and computational cost as we know that more accurate methods and larger basis sets make the job run longer. Specific examples of these effects will be presented in Chapters 4 and 5.

3.4 Influence of Methods and Basis Sets on Geometry Optimization

In order to see the effects of methods and basis sets on geometric and electronic structures we have analyzed the carbon-carbon bond lengths and transition energies of αT_2 using different methods along with different basis sets (see Table 3.1 and Fig. 3.1). The αT_2 geometrical structures optimized using restricted HF and CIS methods with different basis sets augmented with polarization functions and diffuse functions added to heavy atoms show very small fluctuations (see Figs. 3.2 and 3.3). The agreement between the calculated and experimental ground state geometries can be arranged in the order HF, CID, B3LYP, B3PW91, MP4(DQ), MP2, AM1, and MNDO from the best to the worst. Although B3LYP and B3PW91 optimized geometries are slightly better than the MP2 optimized geometry, the MP2 optimized geometry avoids large errors in predicting some coordinates observed by the B3LYP optimized geometry [75]. The effect of changing the basis set on bond angles is minor with the exception of CIS method. The bond lengths are better calculated by 3-21G*, followed by 3-21G**, 6-31+G*, 6-31G*, 6-31+G** and STO-3G basis sets.

Among the electron correlation methods MP2 has the bigger average error relative to MP4, accounted for the 3-21G* basis set. The scenario is even worse in cases of STO-3G basis set (see Table 3.1). The calculated bond lengths are overestimated in most of the methods except for the two semiempirical methods: AM1 and MNDO which basically underestimate the bond lengths. The *ab initio* HF method is found superior in comparison to the rest in describing the ground state geometrical parameters closely. In fact, perusal of Table 3.1 shows that a better agreement

Table 3.1: Comparison of optimized geometries (see Figs. 1.4 and 1.5 for labels) and transition energies (HOMO-LUMO gap) for α-bithiophene. The α'-β', β'-β, β-α and intra-cell bond distances are in Å.

Method/basis set	α'-β'	β'-β	β-α	Intra-cell [a]	δ_r [b]	E (eV)
RHF/STO-3G	1.335	1.448	1.346	1.478	-0.123	11.84
RHF/3-21G [c]	1.334	1.444	1.341	1.441	-0.105	10.14
RHF/3-21G	1.335	1.442	1.342	1.441	-0.103	10.14
RHF/3-21G*	1.347	1.433	1.354	1.456	-0.095	10.16
RHF/3-21G**	1.348	1.435	1.355	1.457	-0.095	10.15
RHF/6-31G*	1.344	1.433	1.352	1.464	-0.101	10.16
RHF/6-31+G*	1.346	1.434	1.354	1.465	-0.099	9.60
AM1	1.368	1.438	1.378	1.423	-0.058	8.02
MNDO	1.374	1.447	1.388	1.447	-0.066	7.95
CIS/STO-3G	1.375	1.393	1.426	1.389	0.010	5.06
CIS/3-21G*	1.380	1.387	1.423	1.374	0.021	4.11
CIS/6-31G*	1.377	1.388	1.420	1.381	0.014	4.00
CIS/6-31G**	1.378	1.390	1.421	1.383	0.017	3.98
CIS/6-31+G*	1.379	1.390	1.422	1.380	0.016	3.79
CIS/6-31+G**	1.379	1.390	1.421	1.380	0.015	3.78
RCISD/STO-3G	1.357	1.459	1.367	1.491	-0.113	2.96
RCID/3-21G*	1.357	1.437	1.364	1.459	-0.088	2.98
MP2/3-21G*	1.382	1.435	1.391	1.459	-0.061	2.98
MP4(DQ)/3-21G*	1.370	1.448	1.377	1.467	-0.084	2.99
B3LYP/3-21G*	1.370	1.428	1.380	1.448	-0.063	4.31
B3LYP/6-31G*	1.367	1.424	1.379	1.451	-0.065	4.23
B3PW91/3-21G*	1.371	1.425	1.381	1.446	-0.060	4.35
Experimental [d]	1.346	1.410	1.352	1.451	-0.082	(4.05)[e](4.13)[f](4.12)[g]

[a]The distance between two consecutive monomers

[b]$\delta_r = \frac{1}{2}\left[(C_{\alpha'-\beta'}) - (C_{\beta'-\beta}) + (C_{\beta-\alpha}) - (C_{\alpha-\alpha'})\right]$

[c]Reference [80]

[d]The C–C bond lengths were taken from reference [152]. The experimental C=S bond length was given as 1.73 Å[153]

[e]Reference [62]

[f]Reference [92]

[g]Reference [100]

with the ground state experimental results can be obtained for PT dimer using the HF approximation [62, 92, 100, 152, 153]. The δ_r value is seen to be highest with STO-3G basis set followed by 3-21G*, 6-31+G*, 6-31G*, and 3-21G basis set. It is shown here that the use of a minimal basis set exaggerates the degree of bond length alternation along the carbon-carbon backbone of the dimer. For instance, using STO-3G basis set, the bond length alternation in PT dimer is calculated to be 20% larger than the results obtained by using a double-ζ basis set, while the MNDO results give a δ_r value of -0.066 Å (see Table 3.1 and Figs. 3.1 through 3.3). The two basis sets 3-21G* and 3-21G** produce the same δ_r value of -0.095 Å.

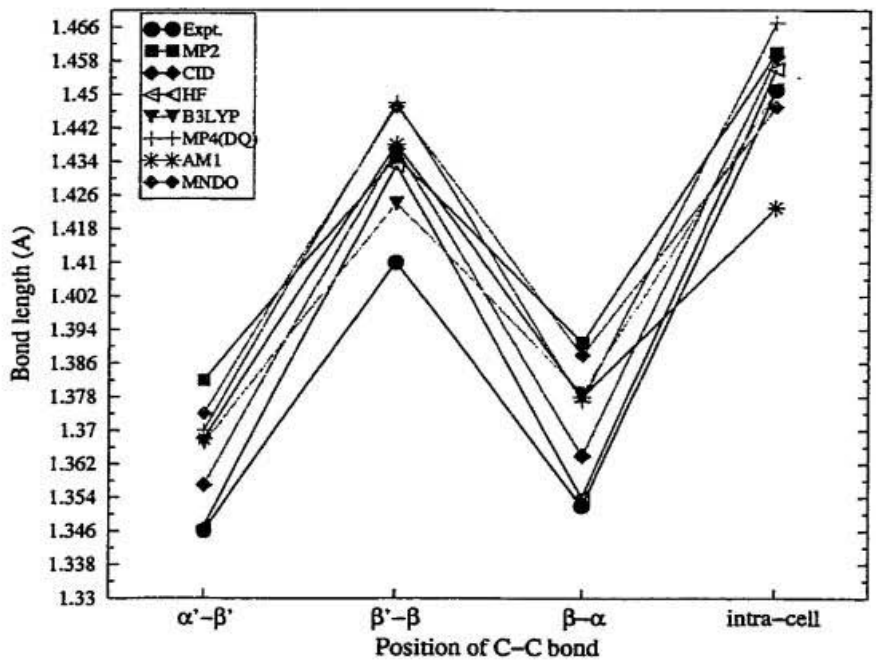

Figure 3.1: Carbon-Carbon bond lengths of αT_2 calculated using different methods (in all cases 3-21G* basis set is used).

Using CI-singles calculation with the identical basis sets we can see quite a different trend. The values for δ_r are as expected, all positive, with the highest being obtained with the 3-21G* followed by 6-31G**, 6-31+G* and 6-31G*. The B3LYP method with 6-31G* basis set gives δ_r value equal to -0.065 Å. For the MP_2 and the MP_4 geometrical results the corresponding values of δ_r are -0.061 and -0.084 Å respectively. Compared to HF theory [74], density functional theory with slightly modified B3LYP and B3PW91 hybrid functional yields longer C=C double bonds and shorter intra-cell bonds (see Table 3.1). As we associate electron correlation with perturbation theory (MP2, MP4 etc.), all the carbon-carbon bond lengths are elongated, though not equally, as the double bonds show larger elongation than the single bonds. The unpolarized 3-21G basis set leads to shorter intra-cell C−C bonds and C=C bonds but longer C-S bonds (1.81 Å in comparison to experimental 1.73 Å). But with polarization function added to heavy atoms the intra-cell C−C bond and C=C bond lengths are found to increase. The C−C bonds have decreased and the C−S bonds are in closer agreement with the experiment than with the 3-21G basis set. Hence 3-21G is found to be the most inefficient basis set with regards to others. Larger basis sets like 6-31G* plus extra diffuse function added to account for the excited state geometry calculations basically lead to longer C−C and C−S bonds but shorter C=C bonds.

The bond length alternation is underestimated with DFT, semiempirical and perturbation theories, and overestimated with HF theory compared to experiment. Although these methods demonstrate some resemblance to the experimental ground state geometries, they fail hopelessly to account for the transition energies corresponding to the experimentally obtained results (see Table 3.1 for details).

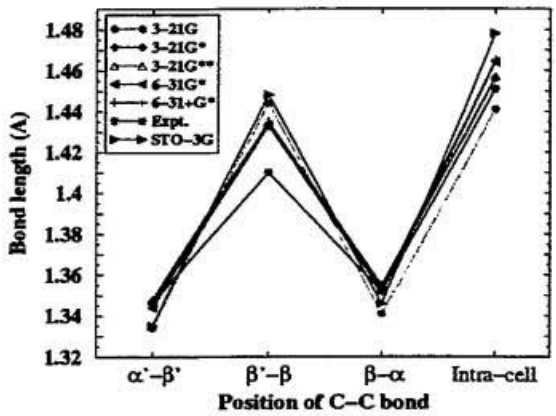

Figure 3.2: C—C bond lengths of αT_2 in HF method for different basis sets.

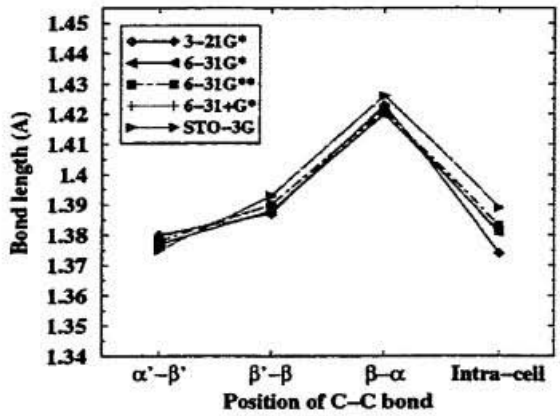

Figure 3.3: C—C bond lengths of αT_2 in CIS method for different basis sets.

Bond delocalization results in zero to minor bond length variations around a ring system, while bond localization results in large bond length variations, corresponding to localized single and double bonds [154]. HF theory seems to underestimate electron delocalization slightly, which results in shorter C=C and longer C—C bonds. All the CI-singles geometries show the localized nature of the bonds producing large variations in bond length at the central parts of the rings where drastic variations of single and double bond lengths can be observed (see also Figs. 4.2 to 4.7). Hence, in HF calculations, the π-electrons are more localized. This is most probably due to the lack of electron correlation.

Figures 3.2 and 3.3 show the basis set dependency in both the HF and CIS approximations for thiophene dimer respectively. As can be found from these plots that 3-21G* basis set is successful in accounting for the αT_2 structure, whereas in case of the larger basis sets 3-21G**, 3-21+G*, 6-31G*, 6-31G** and 6-31+G*, essentially produce closer results to one another. As mentioned above, the difference in the degree of bond length alternation in going from one end of the molecules to

the centre, as well as their evolutions with the increasing chain length, are very similar to those obtained for larger basis sets like 6-31G*, 6-31G** and 6-31+G*. The effect of electron correlation is generally to increase the bond length. The differences among the various correlation levels (MP4 and B3YLP) are usually quite small; the only exception with a large difference between experimental and MP2/3-21G*. Electron correlation via the MP2 perturbation increases the bond lengths for the same method used whereas adding *d*-polarization functions decrease the bond lengths which can be observed from Table 3.1 and Fig. 3.1.

Close examination of the absolute errors shows that improvement of the basis set does not necessarily lead to improvement in results. The greatest improvement occurs with the 3-21G* basis set (see Figs. 3.2 and 3.4). A few points are worth noting here regarding the optimization of excited state geometries using CIS. Because the CIS excited state wavefunction depends on the HF ground state reference, there may be difficulty encountered in cases where the structure is quite distorted from the ground state equilibrium geometry and a HF solution may be either difficult to find or inappropriate. It has been suggested that in these cases, simply using a more sophisticated SCF procedure (such as quadratic convergence, QCSCF) may be sufficient to determine the reference [155]. Also, since the CIS procedure leads directly to a variety of excited states, following the state of interest during a geometry optimization may be confusing. For instance, the second excited vertical state may become the first excited state at the optimized geometry of that state. In our implementations the density from the last geometry point is taken and that state is followed as the guess for the CI. Still, there is the possibility that significant mixing among states in distorted geometries will cause the optimization procedure

jump from state to state (either in the HF ground state or in the CIS part of the calculation). These occasions become obvious when large energy and wavefunction changes are observed, and a restart of the optimization may be required in some cases using QCSCF to get the correct ground state reference or marking a new state to follow in the CI.

On one occasion we had troubles with the excited state geometry of PFV octamer. As geometry optimization for the first excited state (S_1) of PFV proceeds, the intra-ring and inter-ring distances continued changing, particularly in respect of elongation and twisting of all the inter-ring bridging C=C bonds which are displaced on the two opposite sides of the ring plane giving it an arch-like (semi-circle) shape. The rings also become more and more non-planar and deformed. Further, a fluctuation in the minimum total energy is observed, and eventually the calculation failed due to the lack of convergence. This twisting of the inter-ring and the external ring C=C bonds in the S_1 excited state of PFV is reminiscent of the established fact that the two CH_2 fragments of ethylene become perpendicular to each other following the $\pi - \pi^*$ excitation [156]. Although no dissociation of any kind is observed, it is interesting to note that due to this twisting and other accompanying changes (oscillator strength, excitation energy etc.) that follow its $\pi - \pi^*$ excitation, quinoid PFV could be photo reactive. An essential requirement for an optimized molecular geometry to correspond to the global minimum of the potential energy surface is that the vibrational frequencies computed using the Hessian are real. We have not done any frequency studies in this work, but it would have been interesting to account for them as well [62]. Finally, the S_1 state of PFV is obtained by restricting to a tight convergence criteria by introducing two sulfur

atoms at the two ends of the chain thereby preventing the chain deformation and keeping its planar structure unaffected.

It is useful to compare computational time required among the various methods for the energy evaluation of αT_2. With the *Gaussian 94* package and different basis sets used, the HF/3-21G* approach took approximately 10 minutes processor time on an SGI OCTANE1 IRIX64 machine, the HF/3-21G** calculations took 13 minutes cpu time, the HF/6-31G* calculation required roughly 49 minutes cpu time, the HF/6-31+G* calculation required roughly 1 hour and 51 minutes cpu time, the CIS/3-21G* calculation required 38 minutes cpu time, with CIS/6-31G* calculation the job cpu time is 7 hours and 46 minutes, and with CIS/6-31G** it took approximately 4 hours. The MP2/3-21G* perturbation technique required about 1 hour 49 minutes cpu time. The B3LYP/6-31G* method took 1 hour 34 minute cpu time.

3.5 Influence of Methods and Basis Sets on Energetics

In order to compare the effects of different methods with different basis sets on energetics, we consider here the same αT_2 molecule for which we have already compared their influences on different geometrical parameters like bond length, bond angle and bond length alternation etc. First we wish to see the influence on the excitation energies. Among the methods used in our study, the CIS/3-21G* calculated excitation energies for the thiophene and PA oligomers have the lowest average errors as can be observed from the $\sim 1-6\%$ absolute deviation with respect to the experimental results (see Tables 3.1 and 5.14).

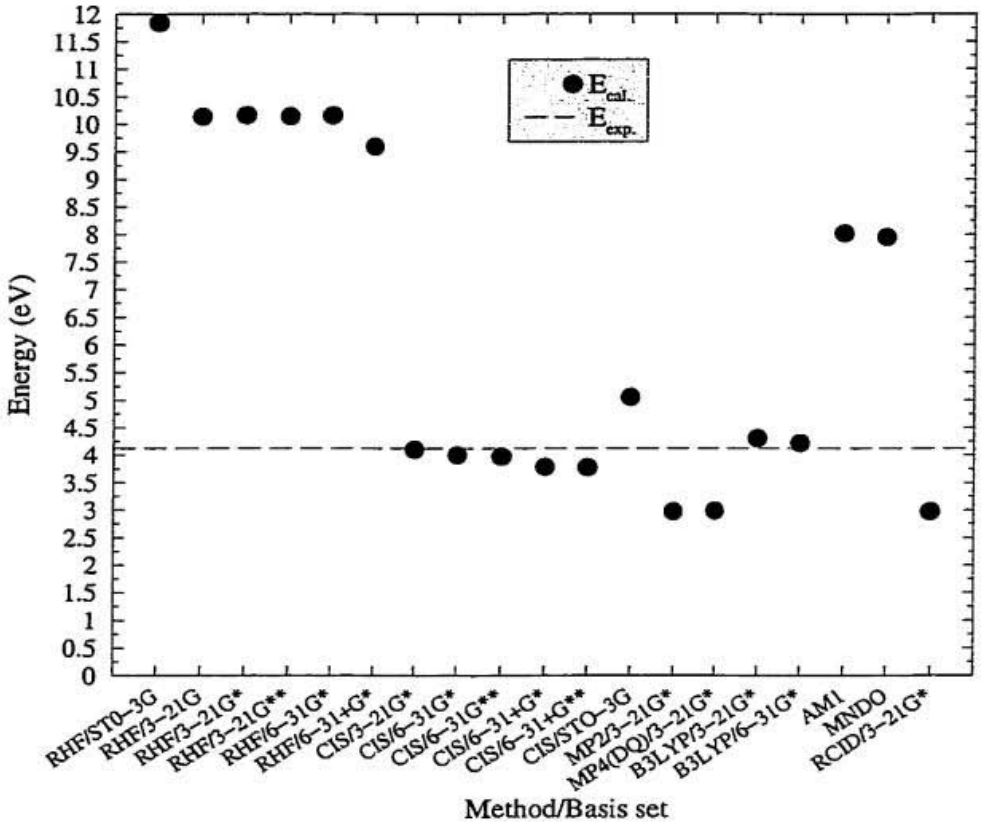

Figure 3.4: Plot comparing the CIS/3-21G* energy (in eV) for αT_2 with the experimental energy [100] and that obtained with several other methods/basis sets.

Among the four electron correlation methods considered here, those excitation energies calculated by the MP4/3-21G* have the highest deviation from the experimentally obtained result (see Table 3.1 and Fig. 3.4). Basically, perturbation theory underestimates the transition energies ($E_{cal.}$) up to 40% with respect to the experimental energies. The dipole moments calculated using MP2 and MP4 methods are also found underestimated in the limited case of thiophene when compared to the experimental result. The hybrid B3LYP method is also unable to approximate for the excitation energies and overestimated the values by an amount of ~0.3eV (even

for the larger basis set like 6-31G*, the deviation is around 4% compared to the experimental result). The worst scenario is observed with the HF approximations which overestimate the transition energies to an extent of 60% compared to the experiments. Even larger basis sets with diffuse and polarization functions do not give better results to the required limit. CI-singles calculations on the other hand are found quite efficient in producing the closest plausible result in comparison to the experiments. The dipole moments problem is also found ameliorated when we switch over to CIS method. It is found that the Quadratic Singles-Double substitutions (QCISD) is not computationally feasible as we ran out of disk space trying to optimize αT_2 with 3-21G* basis set.

It is beyond our scope to provide a comparative general review of all the possible basis sets for the current calculations. Though the basis sets we used are not necessarily optimum, they do have the characteristics that can be used to illustrate the qualitative nature of the systems which are covered in our study. Here, we have used a relaxed geometry "no-freeze" environment for our calculations of excitation energies along with several other transition properties of the lowest excited π^* states. SGI-IRIX64 Octane workstation has been employed for carrying out closed-shell SCF and CI-singles calculations for relatively shorter (dimer) molecules, whereas for the remaining cases DEC-AXP-OSF machine is used.

3.6 Absolute Deviations

Most of our results fall within a 1% - 5% deviation from the experimentally determined ground state conformational results for PT oligomers using HF method. the best comparison is obtained with the 3-21G* basis set followed by 3-21G**,

6-31+G*, 6-31G*, 6-31+G**, and STO-3G basis set. The STO-3G basis set shows ~20% larger errors than other double-ζ basis sets. Bond lengths are overestimated in most of the methods except in the HF method for the S_0 state when compared to the experimental results. Due to unavailability of experimental geometries in the lowest singlet excited states (S_1) comparisons can not be made.

From the results obtained for the lowest $\pi - \pi^*$ optically allowed transition energies we can see that the absolute deviations at the CIS level fall within a 1% - 5% deviation from the experimentally determined results for αT_2. The absolute deviations ($|E_{expt.} - E_{calc.}|$) from the experimental results for energies are compared for a particular method and basis set. The CIS/3-21G* is found to give the lowest deviation followed by the 6-31G*, 6-31G**, 6-31+G* and 6-31+G** basis sets with respect to the experimental results. Including electron correlation with perturbation approaches like MP2 and MP4(DQ) results in ~27% underestimation of the transition energy for αT_2. The CI-double substitution is also found to underestimate the transition energy by the same amount as with the Møller-Plesset perturbation method. The restricted single-doubles substitution (RCISD) also underestimates the band gap by almost the same amount.

Chapter 4

Geometric Structure Investigation

In this chapter the geometries of the oligomers in the ground and in the lowest excited states are discussed. The structural relationship between the cyano-substituted oligomers and their parent polymers is also examined in detail. The influence of the electron-withdrawing and electron-donating groups on the respective parent geometries is analyzed. We have also compared our calculated geometries with the experimental ones where available. The geometric structure parameters are labelled according to Fig. 1.5. The variation of the average bond length alternation, δ_r along the backbone is also discussed.

The initial geometries for PT are taken from the gas phase electron diffraction data on α-bithiophene [121]. For PCY the input geometries are obtained from the semiempirical AM1 optimized values [106]. For the remaining polymers (*i.e.*, PFV, PCNTH, PCNCY, and PCNFV) the input geometries are estimated from the data obtained for PT and PCY with the AM1 calculations [106, 18]. The AM1-optimized geometric structures of the neutral oligomers are in very good agreement with the higher level *ab initio* calculations [80, 111, 116, 118, 157] and experimental data [45, 62, 66, 67, 68, 70, 92, 98, 100, 158, 159, 160]. In summary, in this work we

have used the AM1 geometries [18] as our input geometries in the *ab initio* HF calculations of the optimized ground state geometries which are followed by the excited state calculations using the CI-singles method.

The most stable conformation for the five-membered polyheterocyclic rings corresponds to a situation where the adjacent rings are coplanar, connected through the α positions and ordered in such a way that the heteroatoms point in the opposite directions (*i.e., anti-orientations*) [74]. In a former study [118] that employed AM1 and MNDO methodologies, the authors examined the relative stability of the compounds by comparing heats of formation in two mesomeric forms – quinoid vs. aromatic. In all cases they found that the lower band gaps were obtained for the less stable mesomeric forms i.e., the s-*trans* (quinoid) form for PT and PCNTH and the s-*cis* (aromatic) structures for PFV, PCY, PCNFV and PCNCY. However, since we would like to consider the most stable forms, in the present study we have taken the aromatic forms for PT and PCNTH oligomers and quinoid structures for the rest of the oligomers. These selections are consistent with other findings: in their ground states PT and its cyano-derivative PCNTH have been found to have aromatic forms [13, 14], whereas the nonheterocyclic polymers PCY, PFV and their cyano-derivatives PCNCY and PCNFV respectively, show strong preference for quinoid structures [15, 16, 17, 18].

In view of the large unit cells of these polymers (63 basis functions for PT, 61 for PCY, 70 for PFV, 172 for PCNTH, 164 for PCNCY and 182 for PCNFV) all of the computations are performed using the 3-21G* for large oligomers and the 6-31G* split-valence basis sets for monomers and dimers [73, 123]. The 3-21G* basis set is selected for larger systems since we found that this is the smallest basis set which

can give a reliable description of the structural parameters for the five membered rings containing the heterocycles.

The C−C bond lengths, bond angles and the transition energies of the six molecular systems are determined for both the Hartree-Fock ground state and the CIS excited state. These optimized geometries of the oligomers starting from monomer are given in Tables 4.1 through 4.14. The average bond length alternations (δ_r) of the C−C backbone of the polymers are provided in the second last columns of the corresponding tables. It is defined as the average of the difference of neighbouring long (single) and short (double) C−C bonds. It plays a very important role in the analysis of the excitation energy [79]. A detailed relationship between bond length alternation and several other energetic parameters are explained in Section 5.3. The values of δ_r indicate whether the system is in the quinoid or the aromatic conformation.[1] For PT, PCY and PFV it is calculated as [78]

$$\delta_r = \frac{1}{2}\left[(C_{\alpha'-\beta'}) - (C_{\beta'-\beta}) + (C_{\beta-\alpha}) - (C_{\alpha-\alpha'})\right],$$

and for their cyano-substituted derivatives δ_r is given by

$$\begin{aligned}\delta_r = \frac{1}{4}\Big[&(C_{\alpha'-\beta'}) - (C_{\beta'-\beta}) + (C_{\beta-\alpha}) - (\text{Intra-cell}) + (C_{\alpha_1-\beta_1}) - (C_{\beta_1-\beta_1'}) \\ &+ (C_{\beta_1'-\alpha_1'}) - (\text{Inter-cell})\Big].\end{aligned}$$

where 'Inter-cell' is the distance between unit cells and 'Intra-cell' is the distance between monomers.

[1] δ_r shows the difference between neighbouring single and double carbon-carbon bonds. (+ for quinoid and − for aromatic)

4.1 Ground State (HF) Geometries

Polythiophene. Because of the numerous experimental and theoretical studies of its electronic states and the interesting conformational nature of this chromophore, PT seems to be a logical starting point for the evaluation of our CI-singles theoretical treatment. Further, thiophene is the classic case of close behavioural relationships in physical and chemical properties between six- and five-membered heterocycles where the portion (−CH=CH−) in the six-membered benzoid ring is replaced by (−S−) in the five membered ring. Thus significant aromaticity is thought to occur in thiophene [61]. Tables 4.1 and 4.2 list the HF ground state optimized geometries of the aromatic PT oligomers from monomer to decamer. The HF optimized structures presented in Table 4.1 show that the $C_{\alpha'}$-$C_{\beta'}$, $C_{\beta'}$-C_{β}, intra-cell, and inter-cell bond lengths along the carbon-carbon backbone compare well with their respective experimental values of 1.346, 1.410, 1.352, and 1.451 Å for αT_2 [152]. The theoretical angular structure obtained in the HF calculation matches very well with the microwave spectral results [61] (see Table 4.2). The disagreement between the computed and experimental bond lengths and bond angles are approximately 0.01 Å and 0.5° respectively. The δ_r values are found to range from -0.095 Å (for the dimer) to -0.084 Å (for the decamer) and show a very weak transformation towards the quinoid conformation within the central portion of the longer oligomers (from more negative to less negative δ_r values).

Polycyclopentadiene. Tables 4.3 and 4.4 summarize the ground state geometries of the PCY oligomers. Except for the hydrogen atoms attached to the sp_3 carbons, the chain is constrained to have a planar geometry. The inter-cell length is 1.326 Å and the intra-cell bond distances vary between 1.323 and 1.326 Å. Ta-

ble 4.3 shows that the $C_{\alpha'}$-$C_{\beta'}$, $C_{\beta'}$-C_{β}, and $C_{\beta'}$-C_{α} bond lengths differ only very slightly with regards to their initial AM1 input geometries (the maximum deviation is 0.052 Å). Since the inner repeat units for large oligomers remain unchanged, the structural data reported for the planar tetramer are representative of the whole series of oligoclopentadiene. The bond angles $1C_{\alpha}C_{\beta}$, $C_{\alpha}C_{\beta}C_{\beta'}$, $C_{\beta}C_{\beta'}C_{\alpha'}$, $C_{\beta'}C_{\alpha'}1$, and $C_{\alpha'}1C_{\alpha}$ are found to be nearly the same for the larger oligomers, but for the monomer the angles $1C_{\alpha'}C_{\beta'}$ and $C_{\beta'}C_{\alpha'}1$ are about 3° smaller, while $C_{\alpha'}1C_{\alpha}$ is about 2° larger than other bond angles. The δ_r values for quinoid PCY oligomers are found to be 0.173 Å and 0.137 Å for the dimer and the octamer respectively. In the case of the octamer, the difference between the δ_r values for the outer rings and the central rings is found to be 0.034 Å.

Polyfulvene. The optimized geometries for polyfulvene are presented in Tables 4.5 and 4.6. The inter-ring distances are found to vary between 1.336 and 1.346 Å. The $C_{\alpha'}$-$C_{\beta'}$ and C_{β}-C_{α} bonds range from 1.473 to 1.520 Å. For longer oligomers these bonds remain the same, but for monomer they are found to be longer ($\sim$ 1.520 Å). The $C_{\beta'}$-C_{β} bond length ranges from 1.318 to 1.334 Å, for the octamer this bond length is found to be elongated inside the central rings. The intra-cell distances range from 1.336 to 1.346 Å and the inter-cell distances range from 1.336 to 1.349 Å. The $C{=}CH_2$ bond lengths located outside the ring are evaluated between 1.314 Å and 1.323 Å. The bond angles are also found to vary more for shorter oligomers than for the longer octamer (in the case of $1C_{\alpha}C_{\beta}$ angle it is found to vary approximately by 2°). For quinoid PFV the δ_r values range between 0.163 Å (for the dimer) and 0.128 Å (for the octamer), which shows a weak transformation towards the aromatic conformation at the centre.

Poly (dicyanomethylene cyclopentadithiophene). The geometric structures of aromatic PCNTH oligomers are given in Tables 4.7 and 4.8. The inter-unit bond lengths are either 1.453 or 1.454 Å while the intra-unit bond lengths are found to vary between 1.454 and 1.463 Å. The C-S bond lengths are either 1.697 or 1.749 Å long and along the backbone the $C_{\alpha'}$-$C_{\beta'}$, $C_{\beta'}$-C_{β}, C_{β}-C_{α} bond lengths are analogous to their counterparts $C_{\beta'_1-\alpha'_1}$, $C_{\beta_1-\beta'_1}$, and $C_{\alpha_1-\beta_1}$. The bond angle $C_{\alpha_1}1C_{\alpha'_1}$ between the backbone and the S atom ranges between 90° and 91° which is the smallest angle. All other angles vary between 108° and 113°. The bond length alternations vary from -0.080 to -0.075 Å in going from smaller to larger oligomers and towards their central-rings.

Poly (dicyanomethylene cyclopentadicyclopentadiene). The geometric conformations for the quinoid PCNCY oligomers are provided in Tables 4.9 and 4.10. Differences are observed in the optimized bond lengths within each ring: the C−CH_2 bonds are 1.58 and 1.51 Å in length. The shortest bond ($C_{\beta'}$-C_{β}) on the dicyanomethylene-group side is 1.324 Å in length, whereas the $C_{\alpha'}$-$C_{\beta'}$ and $C_{\beta'_1-\alpha'_1}$ bond lengths are 1.471 to 1.529 Å long which are the longest bonds on the dicyanomethylene-group side. The intra-cell bond distances range between 1.324 and 1.326 Å, while the inter-cell bonds are a little longer (1.329 Å). The calculated bond angles vary between 102° and 112° with the $C_{\alpha'}1C_{\alpha}$ and the $C_{\alpha_1}1C_{\alpha'_1}$ angles being smaller than the rest. The δ_r values for quinoid PCNCY oligomers are calculated to range from 0.162 (external-parts) to 0.144 Å (central-part).

Poly (dicyanomethylene cyclopentadifulvene). The HF optimized geometries of the quinoid PCNFV are given in Tables 4.11 and 4.12. The intra-cell distances are calculated to be 1.337 to 1.344 Å while the inter-cell distances remain

the same for the dimer and tetramer as 1.348 Å. For other bond lengths we find the values for $C_{\alpha'}$-$C_{\beta'}$ and $C_{\beta_1'}$-$C_{\alpha_1'}$ range from 1.473 to 1.523 Å. For $C_{\beta'}$-C_{β} and C_{β_1}-$C_{\beta_1'}$ this range is between 1.325 and 1.331 Å and for C_{β}-C_{α} and C_{α_1}-C_{β_1} the range is from 1.470 to 1.490 Å. The outer C=CH_2 bonds are calculated between 1.319 and 1.325 Å. The bond angles for quinoid PCNFV oligomers vary from 104° to 112°. The average bond length alternations are obtained either 0.154 Å or 0.136 Å depending on the ring position.

In the ground state, the Hartree-Fock ground state optimized structures agree very closely with the experimental ground state results. In particular the balance among the $C_{\alpha'}$-$C_{\beta'}$, C_{β}-C_{α}, and intra-cell bond lengths [152, 161] is excellent. For the $C_{\alpha'}$-H bond the calculated value is 1.067 Å, compared to the experimental value of 1.077 Å [162]. The calculated value for $C_{\beta'}$-H bond length is 1.069 Å compared to its experimental value of 1.0805 Å [163]. The HF optimized structures show that for a given oligomer all the inner rings of the constituent oligomer present approximately the same geometry, which is somewhat different from that of the outer units due to chain-end effects (see Tables 4.1 through 4.14). This correlates well with their corresponding δ_r values. The difference in the δ_r values between the central and the outer parts is found to be comparatively smaller for PCNTH than for PCNCY and PCNFV.

Table 4.1: Comparison of optimized geometries and excitation energies for Polythiophene (PT) oligomers. Bond distances are in Å. See Fig. 1.5 for labels.

Oligomer/method	α'-β'	β'-β	β-α	Intra-cell	Inter-cell	δ_r	E_{cal}(eV)
Monomer (HF)[a]	1.348	1.438	1.348				12.80
Monomer (CIS)[b]	1.435	1.363	1.435				5.57
Dimer (HF)	1.347	1.433	1.354	1.456		-0.095	10.16
Dimer (CIS)	1.380	1.387	1.423	1.374		0.021	4.11
Tetramer (HF)	1.347	1.433	1.355	1.454		-0.093	8.50
	1.354	1.427	1.354		1.453	-0.086	
Tetramer (CIS)	1.354	1.418	1.376	1.416		-0.052	3.19
	1.396	1.378	1.410		1.384	0.022	
Seximer (HF)	1.347	1.433	1.355	1.454		-0.093	7.96
	1.354	1.427	1.354		1.452	-0.086	
	1.355	1.426	1.355	1.452		-0.084	
Seximer (CIS)	1.349	1.427	1.362	1.439		-0.078	2.92
	1.371	1.402	1.382		1.408	-0.029	
	1.395	1.380	1.402	1.391		0.013	
Octamer (HF)	1.347	1.433	1.355	1.454		-0.093	7.71
	1.354	1.427	1.354		1.452	-0.086	
	1.355	1.426	1.355	1.452		-0.084	
	1.355	1.426	1.355		1.452	-0.084	
Octamer (CIS)	1.348	1.431	1.358	1.448		-0.087	2.83
	1.366	1.416	1.361		1.431	-0.060	
	1.375	1.399	1.383	1.409		-0.025	
	1.398	1.383	1.393		1.397	0.006	
Decamer (HF)	1.347	1.433	1.355	1.454		-0.093	7.59
	1.354	1.427	1.354		1.452	-0.086	
	1.355	1.426	1.355	1.452		-0.084	
	1.355	1.426	1.355		1.452	-0.084	
	1.355	1.426	1.355	1.452		-0.084	
Decamer (CIS)	1.347	1.432	1.356	1.452		-0.091	2.82
	1.357	1.422	1.359		1.443	-0.075	
	1.363	1.413	1.368	1.429		-0.056	
	1.376	1.398	1.382		1.410	-0.025	
	1.390	1.385	1.394	1.400		-0.0005	

[a]The ground state geometries and energies are calculated at the HF level.
[b]The first excited state geometries and energies are calculated at the CIS level.

Table 4.2: Magnitudes (in degrees) of bond angles of optimized geometries for polythiophene (PT) oligomers.

Oligomer	$1C_\alpha C_\beta$	$C_\alpha C_\beta C_{\beta'}$	$C_\beta C_{\beta'} C_{\alpha'}$	$C_{\beta'} C_{\alpha'} 1$	$C_{\alpha'} 1 C_\alpha$	$C_\beta C_\alpha C_{\alpha'}$	$C_\alpha C_{\alpha'} C_{\beta'}$
PT HF monomer	111.93	112.39	112.39	111.93	91.35		
PT CIS monomer	113.14	112.75	112.75	113.15	88.21		
PT Expt. monomer[a]	111.47	112.45	112.45	111.47	91.54		
PT HF dimer	110.70	113.18	112.53	111.93	91.67	127.87	127.87
	111.93	112.53	113.18	110.70	91.67		
PT CIS dimer	109.99	112.53	113.83	112.83	90.82	128.24	128.24
	112.83	113.83	112.53	109.99	90.82		
PT HF tetramer	110.73	113.15	112.51	111.97	91.64	127.84	128.02
	110.67	113.33	113.34	110.69	91.98	128.03	128.03
	110.69	113.34	113.33	110.66	91.99	128.02	127.84
	111.97	112.51	113.15	110.74	91.64		
PT CIS tetramer	110.15	113.15	112.96	112.09	91.65	127.85	127.64
	109.95	113.58	114.22	110.57	91.67	127.76	127.76
	110.57	114.22	113.58	109.95	91.67	127.64	127.84
	112.09	112.96	113.15	110.15	91.65		
PT HF Sexamer	110.73	113.15	112.50	111.98	91.64	127.86	128.04
	110.66	113.33	113.34	110.69	91.99	128.04	128.04
	110.67	113.34	113.33	110.68	91.98	128.04	128.04
PT CIS Sexamer	110.46	113.19	112.67	111.99	91.69	127.89	127.86
	110.00	113.51	113.91	110.56	92.01	127.92	127.70
	109.98	113.79	114.11	110.31	91.82	127.73	127.73
PT HF octamer	110.73	113.14	112.50	111.99	91.64	127.86	128.04
	110.66	113.33	113.33	110.69	91.99	128.04	128.04
	110.68	113.33	113.33	110.68	91.98	128.04	128.03
	110.68	113.33	113.33	110.68	91.97	128.03	128.03
PT CIS octamer	110.63	113.16	112.56	111.99	91.65	127.87	127.96
	110.31	113.44	113.59	110.62	92.04	128.01	127.84
	110.02	113.61	113.90	110.45	92.02	127.88	127.71
	109.98	113.84	114.04	110.21	91.93	127.74	127.74

[a]see reference [61]

Table 4.3: Comparison of optimized geometries and excitation energies for polycyclopentadiene (PCY) oligomers. Bond distances are in Å.

Oligomer/method	α'-β'	β'-β	β-α	Intra-cell	Inter-cell	δ_r	E_{cal}(eV)
Monomer (HF)	1.519	1.316	1.519				14.77
Monomer (CIS)	1.482	1.541	1.482				6.35
Dimer (HF)	1.520	1.323	1.472	1.323		0.173	10.53
Dimer (CIS)	1.512	1.373	1.406	1.415		0.065	4.79
Tetramer (HF)	1.520	1.324	1.471	1.325		0.171	8.52
	1.468	1.333	1.469		1.326	0.139	
Tetramer (CIS)	1.518	1.335	1.447	1.355		0.138	3.36
	1.402	1.388	1.420		1.385	0.025	
Seximer (HF)	1.500	1.324	1.471	1.325		0.161	7.95
	1.468	1.333	1.467		1.326	0.138	
	1.467	1.334	1.467	1.326		0.137	
Seximer (CIS)	1.519	1.328	1.462	1.336		0.159	2.94
	1.446	1.357	1.429		1.361	0.079	
	1.416	1.382	1.407	1.375		0.033	
Octamer (HF)	1.520	1.324	1.471	1.325		0.171	7.72
	1.468	1.333	1.467		1.326	0.138	
	1.467	1.334	1.467	1.326		0.137	
	1.467	1.334	1.467		1.326	0.137	
Octamer (CIS)	1.519	1.325	1.467	1.329		0.166	2.81
	1.449	1.343	1.459		1.342	0.112	
	1.439	1.360	1.427	1.360		0.073	
	1.412	1.377	1.418		1.369	0.042	
s-*trans* PA Octamer	1.509	1.325	1.461	1.330		0.158	7.74
(HF)	1.457	1.333	1.456		1.332	0.124	
	1.456	1.333	1.456	1.332		0.124	
	1.456	1.333	1.455		1.332	0.123	
s-*trans* PA Octamer	1.509	1.327	1.457	1.335		0.152	2.91
(CIS)	1.448	1.342	1.439		1.347	0.099	
	1.429	1.359	1.417	1.365		0.061	
	1.408	1.376	1.403		1.375	0.030	

Table 4.4: Magnitudes (in degrees) of bond angles of optimized geometries for polycyclopentadiene (PCY) oligomers.

Oligomer	$1C_\alpha C_\beta$	$C_\alpha C_\beta C_{\beta'}$	$C_\beta C_{\beta'} C_{\alpha'}$	$C_{\beta'} C_{\alpha'} 1$	$C_{\alpha'} 1 C_\alpha$	$C_\beta C_\alpha C_{\alpha'}$	$C_\alpha C_{\alpha'} C_{\beta'}$
PCY HF monomer	103.77	113.10	113.10	103.77	106.26		
PCY CIS monomer	106.73	109.54	109.54	106.73	107.47		
PCY HF dimer	106.75	112.12	112.53	103.63	104.97	126.73	126.73
	103.62	112.54	112.12	106.75	104.97		
PCY CIS dimer	108.93	112.16	110.62	103.79	104.50	127.73	127.73
	103.79	110.62	112.16	108.93	104.50		
PCY HF tetramer	106.82	112.09	112.51	103.64	104.94	126.74	126.79
	106.55	111.60	111.63	106.48	103.74	126.82	126.82
	106.48	111.63	111.60	106.55	103.74	126.79	126.74
	103.64	112.51	112.09	106.82	104.94		
PCY CIS tetramer	107.54	112.23	111.93	103.55	104.75	127.04	127.69
	107.56	111.36	110.77	106.90	103.40	127.86	127.86
	106.90	110.77	111.36	107.56	103.40	127.69	127.04
	103.55	111.93	112.23	107.54	104.75		
PCY HF octamer	106.83	112.06	112.54	103.62	104.95	126.73	126.80
	106.56	111.58	111.65	106.48	103.73	126.82	126.83
	106.55	111.58	111.63	106.53	103.71	126.83	126.83
	106.55	111.60	111.61	106.54	103.71	126.83	126.83
	106.54	111.61	111.60	106.55	103.71	126.83	126.83
	106.53	111.63	111.58	106.55	103.71	126.83	126.82
	106.48	111.65	111.58	106.56	103.73	126.80	126.73
	103.62	112.54	112.06	106.83	104.95		
PCY CIS octamer	106.94	112.09	112.45	103.61	104.91	126.79	126.95
	106.84	111.65	111.43	106.44	103.64	127.06	127.29
	107.05	111.59	111.22	106.61	103.53	127.37	127.60
	107.14	111.34	111.14	106.93	103.44	127.62	127.62
	106.93	111.14	111.34	107.14	103.44	127.60	127.37
	106.61	111.22	111.60	107.05	103.53	127.29	127.06
	106.44	111.43	111.65	106.84	103.64	126.95	126.79
	103.61	112.45	112.09	106.94	104.91		

Table 4.5: Comparison of optimized geometries and excitation energies for polyfulvene (PFV) oligomers.

Oligomer/method	α'-β'	β'-β	β-α	Intra-cell	Inter-cell	δ_r	E_{cal}(eV)
Monomer (HF)	1.520	1.318	1.520				14.06
Monomer (CIS)	1.520	1.323	1.520				6.46
Dimer (HF)	1.507	1.322	1.483	1.342		0.163	9.38
Dimer (CIS)	1.502	1.343	1.446	1.443		0.081	4.00
Tetramer (HF)	1.504	1.322	1.485	1.346		0.161	7.92
	1.469	1.326	1.464		1.349	0.129	
Tetramer (CIS)	1.502	1.330	1.468	1.379		0.131	3.05
	1.417	1.372	1.409		1.414	0.020	
Seximer (HF)	1.503	1.322	1.485	1.346		0.160	7.53
	1.464	1.326	1.469		1.349	0.129	
	1.465	1.326	1.466	1.350		0.128	
Octamer (HF)	1.503	1.322	1.485	1.346		0.160	
(endgroup H_2)	1.464	1.326	1.469		1.349	0.129	7.37
	1.465	1.326	1.466	1.350		0.128	
	1.466	1.326	1.466		1.350	0.128	
Octamer (CIS)	1.503	1.323	1.483	1.350		0.157	
(endgroup H_2)	1.456	1.334	1.455		1.365	0.106	2.650
	1.440	1.348	1.432	1.385		0.070	
	1.420	1.364	1.415		1.397	0.037	
Octamer (CIS)	1.464	1.329	1.479	1.351		0.132	
(endgroup CH_2)	1.455	1.335	1.454		1.365	0.105	2.646
	1.440	1.348	1.432	1.385		0.070	
	1.420	1.364	1.416		1.396	0.038	
Octamer (CIS)	1.450	1.337	1.469	1.352		0.115	
(endgroup S)	1.452	1.336	1.452		1.366	0.101	2.649
	1.439	1.348	1.432	1.383		0.070	
	1.422	1.362	1.418		1.393	0.043	

Table 4.6: Magnitudes (in degrees) of bond angles of optimized geometries for polyfulvene (PFV) oligomers.

Oligomer	$1C_\alpha C_\beta$	$C_\alpha C_\beta C_{\beta'}$	$C_\beta C_{\beta'} C_{\alpha'}$	$C_{\beta'} C_{\alpha'} 1$	$C_{\alpha'} 1 C_\alpha$	$C_\beta C_\alpha C_{\alpha'}$	$C_\alpha C_{\alpha'} C_{\beta'}$
PFV HF monomer	102.99	112.72	112.71	102.99	108.59		
PFV CIS monomer	102.86	111.44	111.44	102.86	111.40		
PFV HF dimer	104.94	111.69	112.03	102.38	107.32	126.81	126.82
	102.38	112.04	111.68	104.94	107.32		
PFV CIS dimer	106.60	112.56	109.98	103.36	107.50	125.78	125.77
	103.36	109.98	112.56	106.60	107.50		
PFV HF tetramer	104.16	112.97	112.02	103.24	107.61	127.62	125.03
	103.85	112.59	112.53	104.25	106.78	126.48	126.48
	104.25	112.53	112.59	103.85	106.78	125.03	127.62
	103.24	112.02	112.97	104.16	107.61		
PFV CIS tetramer	104.93	112.94	111.32	103.15	107.67	127.62	125.81
	104.66	112.62	111.74	104.44	106.55	127.23	127.22
	104.44	111.74	112.62	104.66	106.55	125.81	127.62
	103.15	111.32	112.94	104.93	107.67		
PFV HF octamer	105.11	111.60	112.05	102.40	107.29	126.65	127.27
	104.73	111.22	111.34	104.59	106.43	127.18	127.09
	104.77	111.23	111.28	104.75	106.39	127.11	127.11
	104.76	111.25	111.26	104.75	106.40	127.11	127.11
PFV CIS octamer	104.27	112.95	111.95	103.21	107.62	127.60	125.17
	104.06	112.65	112.35	104.18	106.77	126.74	126.72
	104.20	112.81	112.37	103.77	106.85	126.86	127.14
	104.20	112.68	112.41	103.95	106.76	127.14	127.13

Table 4.7: Comparison of optimized geometries and excitation energies for poly (dicyanomethylene cyclopentadithiophene) (PCNTH) oligomers. Bond distances are in Å.

Oligomer/method	α'-β'	β'-β	β-α	Intra-cell	Inter-cell	α_1-β_1	β_1-β_1'	β_1'-α_1'	δ_r	$E_{cal}(eV)$
Monomer (HF)	1.352	1.428	1.366	1.463		1.366	1.428	1.352		8.36
Monomer (CIS)	1.354	1.416	1.451	1.369		1.451	1.416	1.354		1.93
Dimer (HF)	1.353	1.427	1.367	1.461	1.454	1.365	1.421	1.361	-0.080	7.34
	1.361	1.421	1.365	1.461		1.367	1.427	1.353		
Dimer (CIS)	1.354	1.425	1.369	1.455	1.431	1.374	1.409	1.372	-0.063	1.78
	1.372	1.409	1.374	1.370		1.445	1.418	1.353		
Tetramer (HF)	1.353	1.427	1.367	1.461	1.453	1.365	1.421	1.361	-0.079	6.75
	1.361	1.421	1.365	1.454	1.454	1.366	1.420	1.361	-0.074	
	1.361	1.420	1.366	1.458	1.453	1.366	1.420	1.361	-0.075	
	1.361	1.420	1.366	1.461		1.367	1.427	1.353		
Tetramer (CIS)	1.353	1.426	1.367	1.460	1.453	1.365	1.420	1.361	-0.078	1.63
	1.363	1.418	1.368	1.452	1.432	1.374	1.409	1.372	-0.059	
	1.373	1.398	1.443	1.369	1.433	1.443	1.398	1.372	0.008	
	1.371	1.410	1.373	1.455		1.369	1.425	1.354		
C-C backbone	1.322	1.473	1.328	1.468	1.454	1.330	1.465	1.331	-0.137	7.35
equivalent to	1.331	1.464	1.331	1.466	1.454	1.331	1.464	1.331	-0.131	
tetramer length	1.331	1.464	1.331	1.466	1.454	1.331	1.464	1.331	-0.131	
(HF)	1.331	1.465	1.330	1.468		1.328	1.473	1.322		
C-C backbone	1.323	1.470	1.331	1.460	1.433	1.337	1.450	1.343	-0.120	2.47
equivalent to	1.351	1.429	1.361	1.419	1.404	1.369	1.411	1.371	-0.053	
tetramer length	1.371	1.411	1.369	1.419	1.433	1.361	1.429	1.351	-0.060	
(CIS)	1.343	1.450	1.337	1.460		1.331	1.470	1.323		

Table 4.8: Magnitudes (in degrees) of bond angles of optimized geometries for poly(dicyanomethylene cyclopentadithiophene) (PCNTH) oligomers.

Oligomer/method	$1C_\alpha C_\beta$	$C_\alpha C_\beta C_{\beta'}$	$C_\beta C_{\beta'} C_{\alpha'}$	$C_{\beta'} C_{\alpha'} 1$	$C_{\alpha'} 1 C_\alpha$	$C_\beta C_\alpha C_{\alpha_1}$	$C_{\alpha_1} 1 C_{\alpha'_1}$	$1 C_{\alpha'_1} C_{\beta'_1}$	$C_{\alpha'_1} C_{\beta'_1} C_{\beta_1}$	$C_{\beta'_1} C_{\beta_1} C_{\alpha_1}$
Monomer (HF)	112.44	112.81	110.97	112.99	90.78	109.00	90.77	113.00	110.97	112.82
Monomer (CIS)	111.83	111.45	111.71	115.10	89.91	108.05	89.91	115.10	111.71	111.45
Dimer (HF)	112.45	112.80	110.95	113.05	90.75	108.93	91.00	111.73	111.77	112.96
	112.54	112.97	111.76	111.73	91.00	109.12	90.75	113.06	110.94	112.80
Dimer (CIS)	112.45	112.77	110.86	113.24	90.68	108.99	90.90	111.53	111.85	112.90
	111.88	112.07	112.70	113.08	90.27	108.14	90.01	114.89	111.78	111.51
Tetramer (HF)	112.46	112.79	110.94	113.07	90.74	108.92	90.99	111.73	111.76	112.96
	112.52	112.97	111.75	111.76	90.99	109.05	90.99	111.76	111.76	112.96
	112.53	112.96	111.76	111.76	90.99	109.06	90.99	111.76	111.75	112.97
	112.55	112.96	111.77	111.73	90.99	109.12	90.74	113.07	110.94	112.79
Tetramer (CIS)	112.46	112.79	110.93	113.09	90.73	108.92	90.98	111.73	111.77	112.73
	112.46	112.99	111.73	111.84	90.97	109.14	90.93	111.54	111.85	112.96
	111.82	112.13	112.74	112.96	90.36	108.33	90.37	112.95	112.76	112.11
	112.77	112.94	111.84	111.52	90.93	109.05	90.69	113.21	110.88	112.77

Table 4.9: Comparison of optimized geometries and excitation energies for poly (dicyanomethylene cyclopentadicyclopentadiene) (PCNCY) oligomers. Bond distances are in Å.

Oligomer/method	α'-β'	β'-β	β-α	Intra-cell	Inter-cell	α_1-β_1	β_1-β_1'	β_1'-α_1'	δ_r [a]	E_{cal}(eV)
Monomer (HF)	1.529	1.325	1.484	1.324		1.484	1.325	1.529		8.68
Monomer (CIS)	1.573	1.358	1.444	1.373		1.444	1.358	1.516		3.58
Dimer (HF)	1.529	1.324	1.483	1.325	1.329	1.479	1.335	1.471	0.162	
	1.471	1.335	1.480	1.325		1.483	1.324	1.529		7.06
Dimer (CIS)	1.527	1.327	1.474	1.341	1.380	1.454	1.384	1.407	0.108	2.59
	1.407	1.384	1.454	1.380		1.474	1.327	1.527		
Tetramer (HF)	1.528	1.324	1.483	1.325	1.329	1.479	1.335	1.472	0.162	
	1.471	1.335	1.480	1.326	1.329	1.479	1.335	1.472	0.144	6.54
	1.472	1.335	1.479	1.326	1.329	1.480	1.335	1.471	0.144	
	1.472	1.335	1.479	1.325		1.483	1.324	1.528		
Tetramer (CIS)	1.528	1.324	1.483	1.325	1.329	1.479	1.335	1.472	0.162	
	1.471	1.335	1.479	1.326	1.331	1.478	1.336	1.470	0.143	2.57
	1.468	1.338	1.469	1.342	1.381	1.454	1.385	1.406	0.088	
	1.406	1.385	1.453	1.342		1.473	1.328	1.526		
C-C backbone	1.509	1.326	1.462	1.333	1.331	1.459	1.333	1.456	0.141	7.89
equivalent to	1.456	1.334	1.457	1.334	1.332	1.457	1.334	1.456	0.123	
tetramer length	1.456	1.334	1.457	1.334	1.331	1.457	1.334	1.456	0.123	
(HF)	1.456	1.333	1.459	1.333		1.462	1.326	1.509		
C-C backbone	1.509	1.327	1.459	1.337	1.347	1.450	1.343	1.440	0.126	2.97
equivalent to	1.430	1.359	1.420	1.369	1.374	1.410	1.376	1.404	0.047	
tetramer length	1.404	1.376	1.410	1.369	1.347	1.420	1.359	1.430	0.053	
(CIS)	1.440	1.343	1.450	1.337		1.459	1.327	1.509		

[a] δ_r is average bond length alternation.

Table 4.10: Magnitudes (in degrees) of bond angles of optimized geometries for poly(dicyanomethylene cyclopentadicyclopentadiene)(PCNCY) oligomers.

Oligomer/method	$1C_\alpha C_\beta$	$C_\alpha C_\beta C_{\beta'}$	$C_\beta C_{\beta'} C_{\alpha'}$	$C_{\beta'} C_{\alpha'} 1$	$C_{\alpha'} 1 C_\alpha$	$C_\beta C_\alpha C_{\alpha_1}$	$C_{\alpha_1} 1 C_{\alpha'_1}$	$1 C_{\alpha'_1} C_{\beta'_1}$	$C_{\alpha'_1} C_{\beta'_1} C_{\beta_1}$	$C_{\beta'_1} C_{\beta_1} C_{\alpha_1}$
Monomer (HF)	108.16	112.48	110.54	105.25	103.55	109.77	103.55	105.25	110.54	112.48
Monomer (CIS)	108.99	111.81	110.81	105.12	103.28	108.74	101.72	109.78	109.83	110.24
Dimer (HF)	108.23	112.41	110.58	103.54	109.65	102.25	108.29	109.71	111.90	111.90
	107.85	111.90	109.71	108.29	102.24	109.71	103.54	105.24	110.58	112.41
Dimer (CIS)	108.99	111.81	110.81	105.12	103.73	108.74	101.72	109.78	109.83	110.24
	108.42	110.24	109.83	109.77	101.72	109.30	103.28	105.12	110.81	111.81
Tetramer (HF)	108.24	112.39	110.59	105.24	103.54	109.67	102.24	108.30	109.66	111.95
	107.91	111.80	109.79	108.27	102.23	109.59	102.23	108.28	109.73	111.86
	107.90	111.86	109.73	108.28	102.23	109.58	102.23	108.27	109.79	111.80
	107.86	111.95	109.66	108.30	102.24	109.73	103.54	105.24	110.59	112.39
Tetramer (CIS)	108.24	112.39	110.59	105.24	103.54	109.67	102.24	108.31	109.64	111.96
	107.93	111.78	109.81	108.27	102.22	109.59	102.20	108.35	109.68	111.88
	108.55	111.38	109.92	108.18	101.98	108.70	101.75	109.75	109.85	110.27
	108.43	110.24	109.82	109.80	101.71	109.32	103.27	105.12	110.80	111.81

Table 4.11: Comparison of optimized geometries and excitation energies for poly (dicyanomethylene cyclopentadifulvene) (PCNFV) oligomers. Bond distances are in Å.

Oligomer/method	α'-β'	β'-β	β-α	Intra-cell	Inter-cell	α_1-β_1	β_1-β_1'	β_1'-α_1'	δ_r	E_{cal}(eV)
Monomer (HF)	1.525	1.326	1.487	1.337		1.487	1.326	1.525		8.26
Monomer (CIS)	1.512	1.359	1.451	1.391		1.451	1.359	1.512		3.47
Dimer (HF)	1.523	1.325	1.490	1.340	1.348	1.471	1.332	1.475	0.154	6.57
	1.475	1.332	1.471	1.340		1.490	1.325	1.523		
Dimer (CIS)	1.522	1.328	1.481	1.359	1.405	1.445	1.376	1.412	0.098	2.35
	1.412	1.376	1.445	1.359		1.481	1.328	1.522		
Tetramer (HF)	1.523	1.325	1.490	1.340	1.348	1.470	1.331	1.476	0.154	6.05
	1.474	1.330	1.474	1.344	1.348	1.475	1.330	1.473	0.136	
	1.473	1.330	1.475	1.344	1.348	1.474	1.330	1.474	0.136	
	1.476	1.331	1.470	1.340		1.490	1.325	1.523		
Tetramer (CIS)	1.523	1.325	1.490	1.340	1.348	1.470	1.332	1.476	0.154	2.34
	1.473	1.330	1.475	1.345	1.348	1.474	1.330	1.473	0.134	
	1.473	1.332	1.467	1.362	1.406	1.449	1.374	1.410	0.088	
	1.411	1.377	1.443	1.360		1.480	1.328	1.521		
C-C backbone	1.509	1.326	1.462	1.333	1.331	1.459	1.333	1.456	0.141	7.89
equivalent to	1.456	1.334	1.457	1.334	1.332	1.457	1.334	1.456	0.123	
tetramer length	1.456	1.334	1.457	1.334	1.331	1.457	1.334	1.456	0.123	
(HF)	1.456	1.333	1.459	1.333		1.462	1.326	1.509		
C-C backbone	1.509	1.327	1.459	1.337	1.347	1.450	1.343	1.440	0.126	2.97
equivalent to	1.430	1.359	1.420	1.369	1.374	1.410	1.376	1.404	0.047	
tetramer length	1.404	1.376	1.410	1.369	1.347	1.420	1.359	1.430	0.053	
(CIS)	1.440	1.343	1.450	1.337		1.459	1.327	1.509		

Table 4.12: Magnitudes (in degrees) of bond angles of optimized geometries for poly(dicyanomethylene cyclopentadifulvene) (PCNFV) oligomers.

Oligomer/method	$1C_\alpha C_\beta$	$C_\alpha C_\beta C_{\beta'}$	$C_\beta C_{\beta'} C_{\alpha'}$	$C_{\beta'} C_{\alpha'} 1$	$C_{\alpha'} 1 C_\alpha$	$C_\beta C_\alpha C_{\alpha_1}$	$C_{\alpha_1} 1 C_{\alpha_1'}$	$1 C_{\alpha_1'} C_{\beta_1'}$	$C_{\alpha_1'} C_{\beta_1'} C_{\beta_1}$	$C_{\beta_1'} C_{\beta_1} C_{\alpha_1}$
Monomer (HF)	107.03	112.34	110.02	104.39	106.22	109.33	106.22	104.39	110.02	112.33
Monomer (CIS)	109.44	110.17	110.51	103.96	105.91	107.90	105.91	103.96	110.51	110.17
Dimer (HF)	106.68	112.54	110.02	104.44	106.33	108.97	105.10	105.87	110.44	111.72
	106.88	111.72	110.44	105.87	105.10	109.29	106.33	104.44	110.02	112.53
Dimer (CIS)	107.43	111.96	110.18	104.19	106.24	108.01	104.76	107.07	110.81	110.07
	107.29	110.07	110.81	107.07	104.76	108.96	106.24	104.19	110.18	111.96
Tetramer (HF)	106.67	112.53	110.03	104.43	106.33	108.98	105.10	105.80	110.44	111.78
	106.43	111.96	110.51	105.85	105.25	108.87	105.26	105.78	110.50	112.02
	106.44	112.02	110.50	105.78	105.26	108.88	105.25	105.85	110.51	111.96
	106.88	111.78	110.44	105.80	105.10	109.30	106.33	104.43	110.03	112.53
Tetramer (CIS)	106.67	112.53	110.04	104.43	106.34	108.98	105.10	105.81	110.43	111.79
	106.44	111.94	110.52	105.86	105.25	108.89	105.25	105.82	110.45	112.05
	107.14	111.52	110.62	105.60	105.11	107.94	104.91	107.09	110.84	110.37
	107.32	110.09	110.81	107.03	104.76	108.96	106.25	104.18	110.16	111.97

Table 4.13: Optimized geometries and excitation energies for *trans-cisoid* polyacetylene oligomers. Bond distances are in Å.

Oligomer/method	α'-β'	β'-β	β-α	Intra-cell	Inter-cell	δ_r	E_{cal}(eV)
Monomer (HF)	1.320	1.479	1.320				12.22
Monomer (CIS)	1.410	1.389	1.410				5.24
Dimer (HF)	1.322	1.472	1.328	1.458		-0.140	9.75
Dimer (CIS)	1.354	1.417	1.395	1.392		-0.030	4.12
Tetramer (HF)	1.322	1.471	1.329	1.456		-0.138	8.14
	1.331	1.463	1.331		1.454	-0.128	
Tetramer (CIS)	1.330	1.452	1.351	1.418		-0.094	3.03
	1.372	1.404	1.384		1.394	-0.021	
Seximer (HF)	1.322	1.472	1.329	1.456		-0.139	7.61
	1.331	1.463	1.331		1.454	-0.128	
	1.331	1.463	1.331	1.454		-0.128	
Seximer (CIS)	1.325	1.464	1.337	1.439		-0.121	2.67
	1.349	1.431	1.360		1.411	-0.067	
	1.372	1.405	1.378	1.397		-0.026	
Octamer(HF)	1.322	1.472	1.329	1.456		-0.139	7.38
	1.331	1.463	1.331		1.454	-0.128	
	1.331	1.463	1.331	1.454		-0.128	
	1.331	1.463	1.331		1.454	-0.128	
Octamer (CIS)	1.323	1.469	1.332	1.449		-0.132	2.56
	1.338	1.448	1.344		1.431	-0.099	
	1.352	1.427	1.361	1.411		-0.063	
	1.369	1.409	1.374		1.401	-0.034	

Table 4.14: Optimized geometries and excitation energies for *cis-transoid* polyacetylene oligomers. Bond distances are in Å.

Oligomer/method	α'-β'	β'-β	β-α	Intra-cell	Inter-cell	δ_r	E_{cal}(eV)
Monomer (HF)	1.510	1.319	1.510				14.88
Monomer (CIS)	1.472	1.531	1.472				6.35
Dimer (HF)	1.509	1.325	1.462	1.329		0.158	10.65
Dimer (CIS)	1.498	1.375	1.398	1.418		0.052	4.82
Tetramer (HF)	1.509	1.325	1.461	1.330		0.157	8.58
	1.457	1.333	1.456		1.331	0.125	
Tetramer (CIS)	1.506	1.337	1.436	1.361		0.122	3.48
	1.410	1.385	1.394		1.390	0.015	
Seximer (HF)	1.509	1.325	1.461	1.330		0.157	7.99
	1.457	1.333	1.456		1.332	0.112	
	1.456	1.333	1.456	1.332		0.124	
Seximer (CIS)	1.508	1.329	1.451	1.342		0.144	3.04
	1.435	1.356	1.419		1.366	0.066	
	1.406	1.380	1.398	1.381		0.062	
Octamer(HF)	1.509	1.325	1.461	1.330		0.157	7.74
	1.457	1.333	1.456		1.332	0.124	
	1.456	1.333	1.456	1.332		0.123	
	1.456	1.333	1.455		1.332	0.123	
Octamer(CIS)	1.508	1.327	1.457	1.335		0.152	2.91
	1.448	1.342	1.439		1.347	0.099	
	1.429	1.359	1.417	1.365		0.061	
	1.408	1.376	1.403		1.374	0.031	

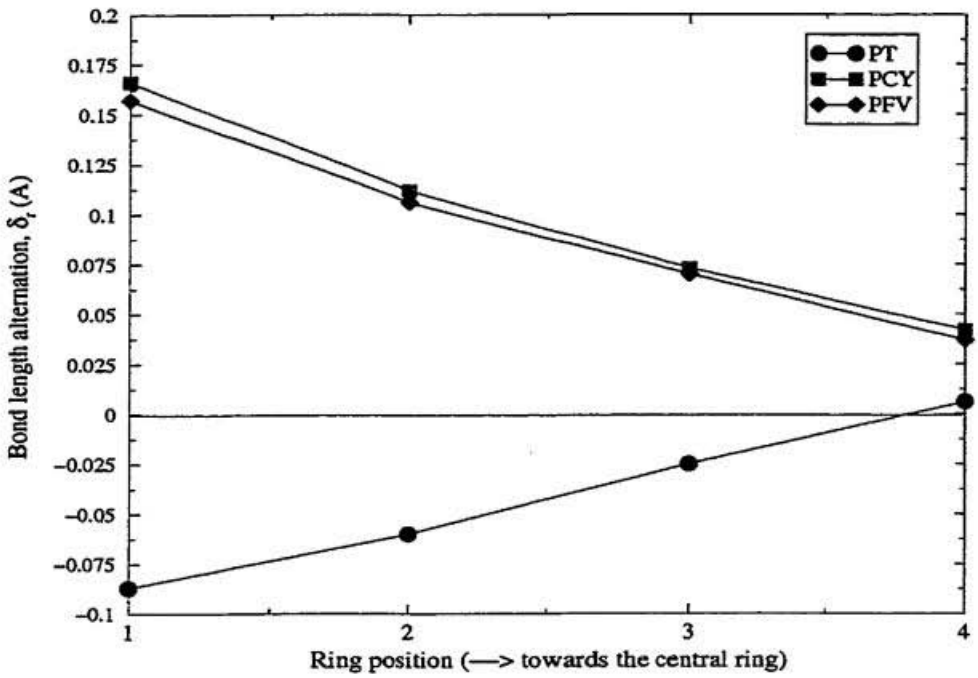

Figure 4.1: Bond length alternation of PT, PCY and PFV octamers in the first excited state in fully optimized geometries.

4.2 Excited State (CIS) Geometries

Polythiophene. The CIS results for the PT oligomers show fluctuations in the geometrical parameters. As the results presented in Table 4.1 show, the $C_{\alpha'}$-$C_{\beta'}$, $C_{\beta'}$-C_{β} and C_{β}-C_{α} bond lengths are either significantly increased or decreased, in going from the ground to the first ($\pi \rightarrow \pi^*$) excited state. This is reflected in the δ_r values shown in Fig. 4.1. For the central rings we observe an evolution towards a semiquinoid structure with the central inter-ring C—C bond reduced by 0.055 Å with respect to the ground state. The inter-ring distances vary from 1.384 to 1.431 Å, while the intra-ring distances vary between 1.374 and 1.448. For the dimers the C—C intra-ring bonds show a quite visible change from single to double

bond texture, while for larger oligomers this change is more discernible towards the central portion. For other bonds along the backbone of all the oligomers the evolution is quite similar i.e., single bond $\rightleftarrows$ double bond. The $1C_{\alpha}C_{\beta}$ and $C_{\beta'}C_{\alpha'}1$ bond angles are found to increase and the $C_{\alpha'}1C_{\alpha}$ bond angle is found to decrease appreciably in going from the ground to the first excited state. The bond length alternation (δ_r) values for PT oligomers range from -0.087 to 0.006 Å, evolving towards a benzene like structure at the central rings. With a sulfur end group the external $C_{\alpha'}$-$C_{\beta'}$ bond is seen to attain the smallest value (1.348 Å) due to the closeness of sulfur and hydrogen on the neighbouring carbons and also due to the fact that sulfur lone pair orbitals mix with the carbon frontier molecular orbitals (FMOs).

Polycyclopentadiene. The excited state geometries of quinoid PCY oligomers are given in Tables 4.3 and 4.4. As expected the carbon-carbon single and double bonds are altered considerably inside the oligomers: the C−C bonds are shortened while the C=C bonds are elongated with respect to their ground state values. The $C_{\alpha'}$-$C_{\beta'}$ bond distance ranges from 1.402 to 1.519 Å, the $C_{\beta'}$-C_{β} bond ranges from 1.325 to 1.377 Å, and the C_{β}-C_{α} bond ranges between 1.406 and 1.467 Å. The intra-ring and inter-ring bond distances increase by 0.03 Å at the central part. The $C_{\alpha'}$-$C_{\beta'}$ bond lengths are found to range from 1.412 to 1.519 Å, the $C_{\beta'}$-C_{β} bond distances vary from 1.325 to 1.541 Å – the largest being observed in case of the monomer, while the C_{β}-C_{α} bond lengths vary between 1.406 and 1.467 Å – the smallest length being found for the dimer. The bond angles are also observed to vary with respect to their ground state values by 1-2 degrees. The bond length alternation values range from 0.025 to 0.166 Å with the outer rings having close

resemblance to the ground state quinoid configurations while the inner parts show a transformation from quinoid (*cis-transoid*) to aromatic (*trans-cisoid*) conformation.

Polyfuleve. The geometries of PFV oligomers have also been found to develop an aromatic structure at the central part of the chain. The $C_{\alpha'}$-$C_{\beta'}$ bonds vary between 1.420 and 1.520 Å, the $C_{\beta'}$-C_{β} bonds vary between 1.323 and 1.372 Å, and the C_{β}-C_{α} bond lengths vary from 1.415 to 1.520 Å. As the ring number grows the bond lengths are seen to show a changeover from single to double bonded form and vice versa. The δ_r values, as observed for the octamers show a trend towards a semi-aromatic texture giving smaller numbers for δ_r values (0.157 − 0.037 Å) as we go from the exterior parts to the interior parts. We have also studied the PFV octamer with three different end groups: H_2, CH_2 and S which basically show the same trend in δ_r values. The highest variation in δ_r is obtained with the H_2 end group (0.120 Å) in going from the external rings towards the central rings. Regarding the bond angles, the $C_{\alpha}C_{\beta}C_{\beta'}$, $C_{\alpha'}1C_{\alpha}$ and $C_{\beta'}C_{\alpha'}1$ bond angles are found to increase within the central rings by an amount of $\sim 1^{\circ}$ while the $C_{\beta}C_{\beta'}C_{\alpha'}$, $1C_{\alpha}C_{\beta}$, and $C_{\alpha}C_{\alpha'}C_{\beta'}$ bond angles are found to decrease by almost the same amount in going from ground to the excited state. An identical trend is observed as well for the bond angles of oligomers with two other end groups *viz.* CH_2 and S.

Poly(dicyanomethylene cyclopentadithiophene). The excited state geometries of PCNTH oligomers are given in Tables 4.7 and 4.8. The bond lengths along the carbon-carbon backbone is found to show a trend similar to that of its parent thiophene polymers, though the variations are more profound in the cyano-derivative. The $C_{\alpha'}$-$C_{\beta'}$ bond is found to increase from 1.323 to 1.371 Å in traversing towards the central rings; the $C_{\beta'}$-C_{β} bonds are found to decrease from 1.470 to

1.411 Å; the C_β-C_α bond are found to increase from 1.331 to 1.369 Å; the intra-ring distances decrease from 1.460 to 1.419 Å, while the inter-ring distances changed from 1.433 to 1.404 Å. The bond-length alternation shows a transformation towards benzoid structure as seen from Table 4.7 where the the δ_r values for the outer-rings and that for the inner-rings are -0.078 and 0.008 Å respectively. The bond angles are also found varying - the smallest being $C_{\alpha'}1C_\alpha$ (90.4°) and the largest being $C_{\beta'}C_{\alpha'}1$ (115.1°). No particular trend is observed in the bond angles, except that the $C_{\alpha'}1C_\alpha$ angles decrease towards the centre of the polymer chain.

Poly(dicyanomethylene cyclopentadicyclopentadiene). The optimized excited state geometries are given in Tables 4.9 and 4.10. The $C_{\alpha'}$-$C_{\beta'}$ bonds are found to decrease gradually from 1.528 to 1.406 Å; the $C_{\beta'}$-C_β bonds are found to increase from 1.324 to 1.385 Å; the C_β-C_α bonds are found to decrease from 1.483 to 1.453 Å; the intra-ring bond lengths show an increasing trend towards the central rings: from 1.325 to 1.342 Å, also the same trend is observed in inter-ring bond-lengths: from 1.329 to 1.381 Å. The δ_r values show a weak evolution towards aromatic (s-*cis*) conformation as the values changes from 0.162 to 0.088 Å. The bond angles are also found to change randomly without any particular fashion (these changes are found to vary between 102° to 112°).

Poly(dicyanomethylene cyclopentadifulvene). The excited-state PCNFV optimized geometries are presented in Tables 4.11 and 4.12 respectively. The same trend is seen for differences in bond-lengths due to chain length. Along the C–C backbone the outer $C_{\alpha'}$-$C_{\beta'}$ bond attains the longest length of 1.523 Å, which shortens as we move towards the inner-rings to 1.411 Å; the $C_{\beta'}$-C_β double bond shows an increase from 1.325 to 1.377 Å; the C_β-C_α bonds are found to decrease

from 1.490 to 1.443 Å. The intra-ring and inter-ring distances are also found to increase from 1.340 to 1.360 (intra-ring) and from 1.348 to 1.406 Å (inter-ring). The δ_r values are found to decrease from 0.154 to 0.088 Å showing a very weak aromatic trend towards the central rings. The bond angles are seen to vary from 104° to 112° without showing any particular trend in them.

For all the oligomers, it is seen that in the calculated π-bond orders for the excited state geometries show a trend towards an aromatic benzoid-like structure (*i.e.,* the inter- and intra-ring carbon-carbon bond lengths are becoming almost equal). The CI-singles optimized geometries show considerable deformations at the central portions of the oligomers. The geometry modification in the outer rings are much weaker, adopting a geometry equivalent to that of the HF ground state.

4.3 Summary of Geometrical Findings

The ground state HF optimized geometries compare well with the experimental findings and hence also the average bond length alternation (δ_r) values. With the 3-21G* basis set, the carbon-carbon bonds in αT_8 are up to 0.023 Å longer than the experimental values, whereas the C-S bonds (~1.73 Å) are roughly the same, differing only at the third decimal place (~0.007 Å). The bond angles agree very closely with experiments to within 0.5° [61, 161, 164]. For PCY, PFV and their cyano-derivatives, the C−C single bond lengths are enlarged at the two ends of the molecular chain, whereas for PT and its cyano-derivative the opposite trend is observed. These topological differences in bond lengths at the two ends of the molecules suggest the end group effect due to the chain-end hydrogens.

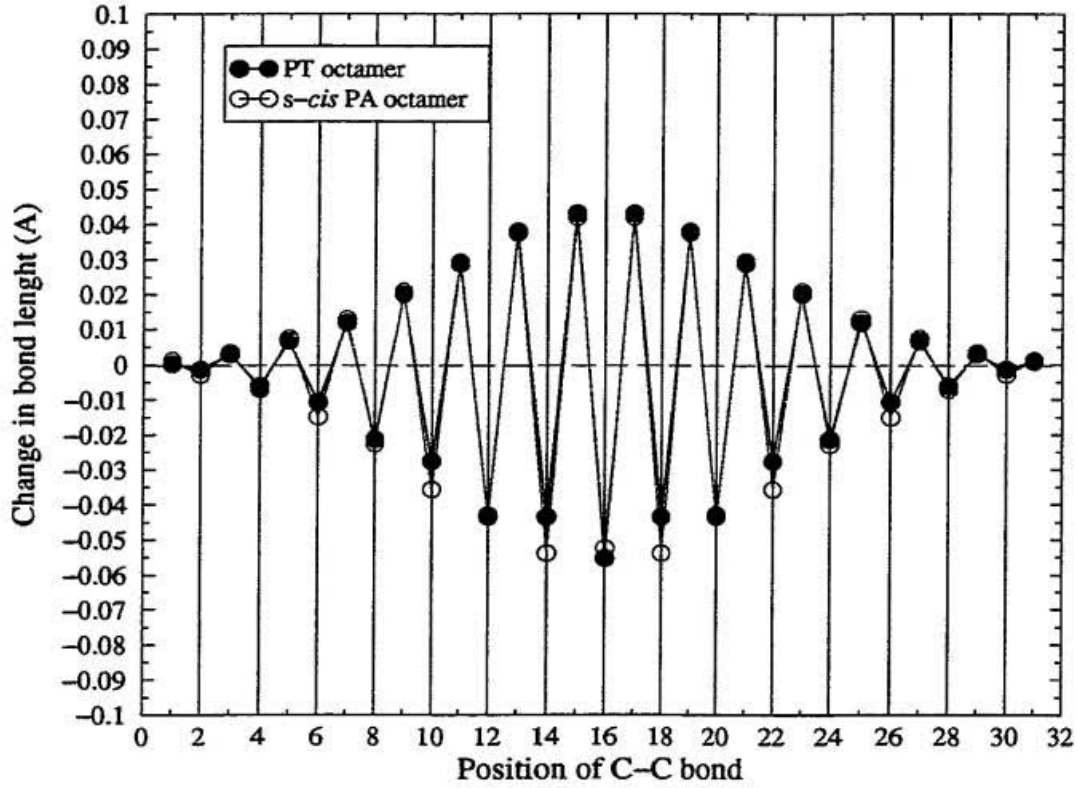

Figure 4.2: Changes in the HF calculated Carbon-Carbon bond lengths of PT octamer when going from the ground state to the first excited state in its fully optimized geometry. The deformations are calculated as the difference between the C–C bond lengths in the singlet excited and in the ground state.

Results obtained for bond length alternations using the CI-singles method show considerable variations depending on chain length and side groups. For PT and PCNTH moieties the δ_r values obtained using CIS calculations are found to change sign ($- \rightleftharpoons +$) in going from ground state to excited state. This basically reflects the transformation from aromatic (s-*trans*) to quinoid (s-*cis*) conformation. The neighbouring carbon-carbon bond length differences become even smaller as the molecular size grows longer, resulting in almost equal bond lengths especially across

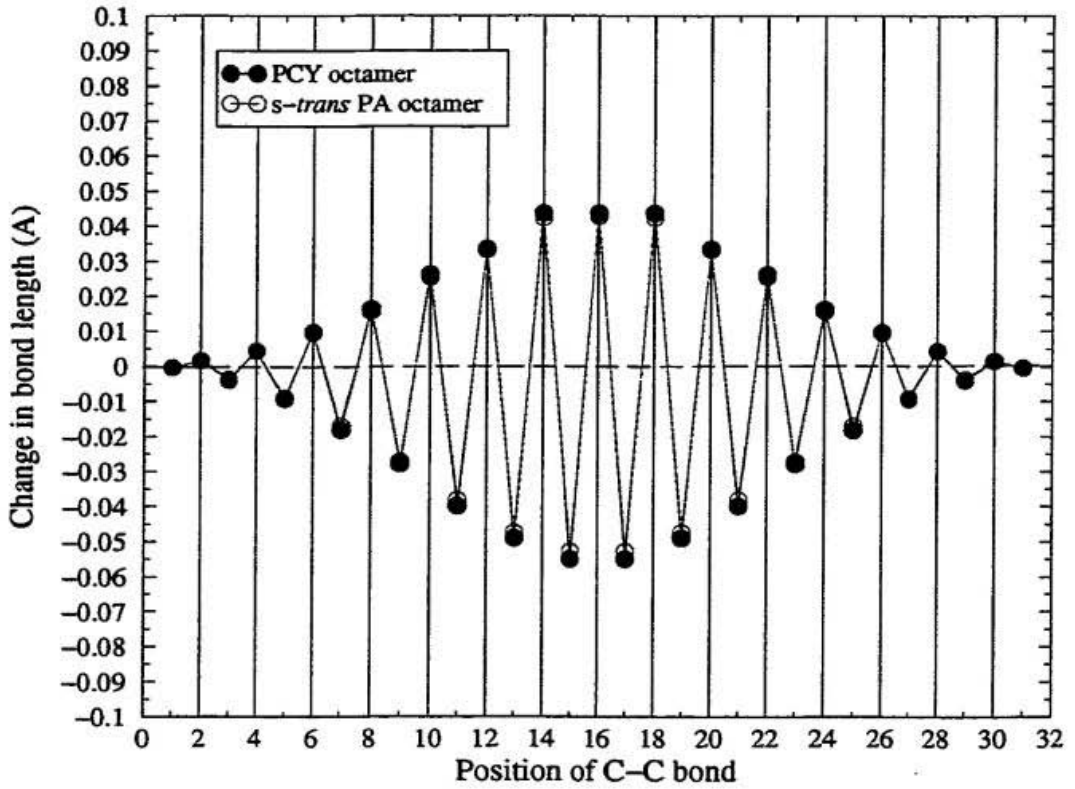

Figure 4.3: Changes in the HF calculated Carbon-Carbon bond lengths of PCY octamer when going from the ground state to the first excited state in its fully optimized geometry.

the central part of the systems. As the chain length increases, the effect of excitation on the geometry becomes prominent in the middle part of the molecules and much weaker near the ends. In CIS calculations, the bond lengths at the two ends do not really alternate much. This reflects the important role played by the creation of polaronic defects along the central portion of the molecules causing a changeover towards fully benzoid structure. The trend further shows that there is a similarity in the variation of bond lengths between the HF ground state and CI-singles excited

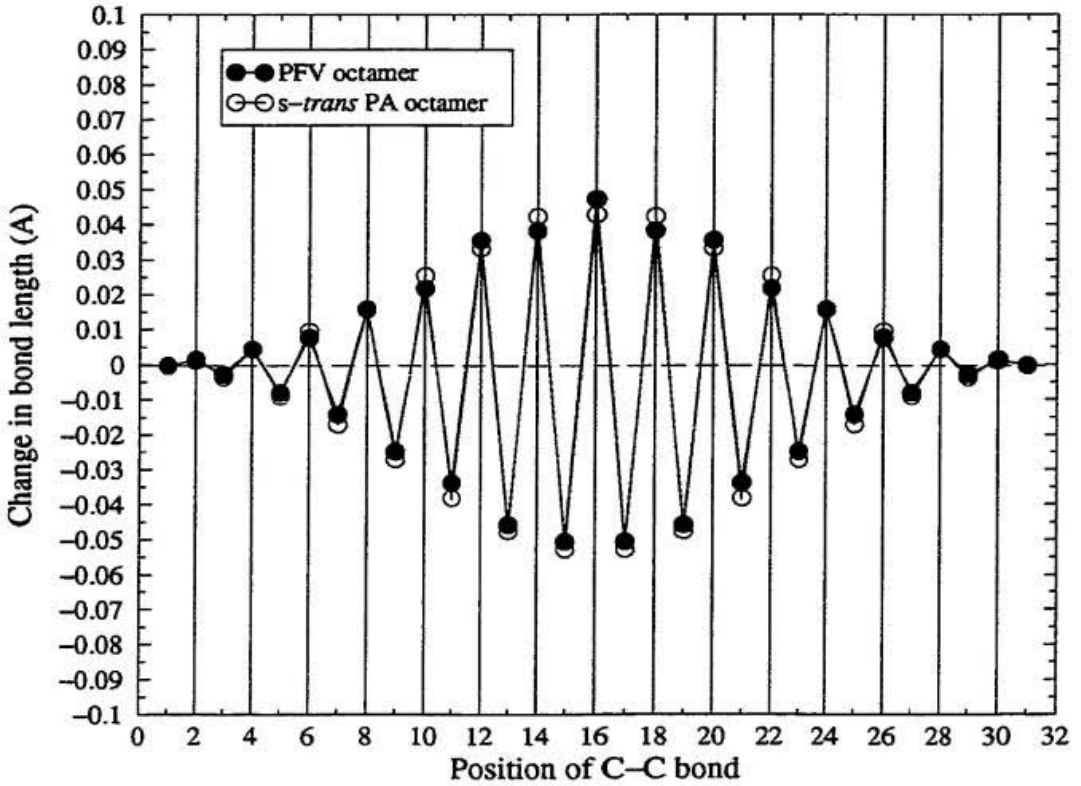

Figure 4.4: Changes in the HF calculated Carbon-Carbon bond lengths of PFV octamer when going from the ground state to the first excited state in its fully optimized geometry.

state results: the C—C single bonds get elongated towards the centre while the C=C double bonds are shortened. The central inter-ring bond in the PT octamer is 0.023 Å longer than that for its dimer. For the PCY octamer and dimer this difference is -0.046 Å. The same difference in inter-ring bond lengths is found between the fulvene octamer and dimer. The carbon-carbon double and single bonds are comparatively longer in octafulvene than in octacyclopentadiene. The intra-ring single bonds in octathiophene are shorter than those in octacyclopentadiene and octafulvene and

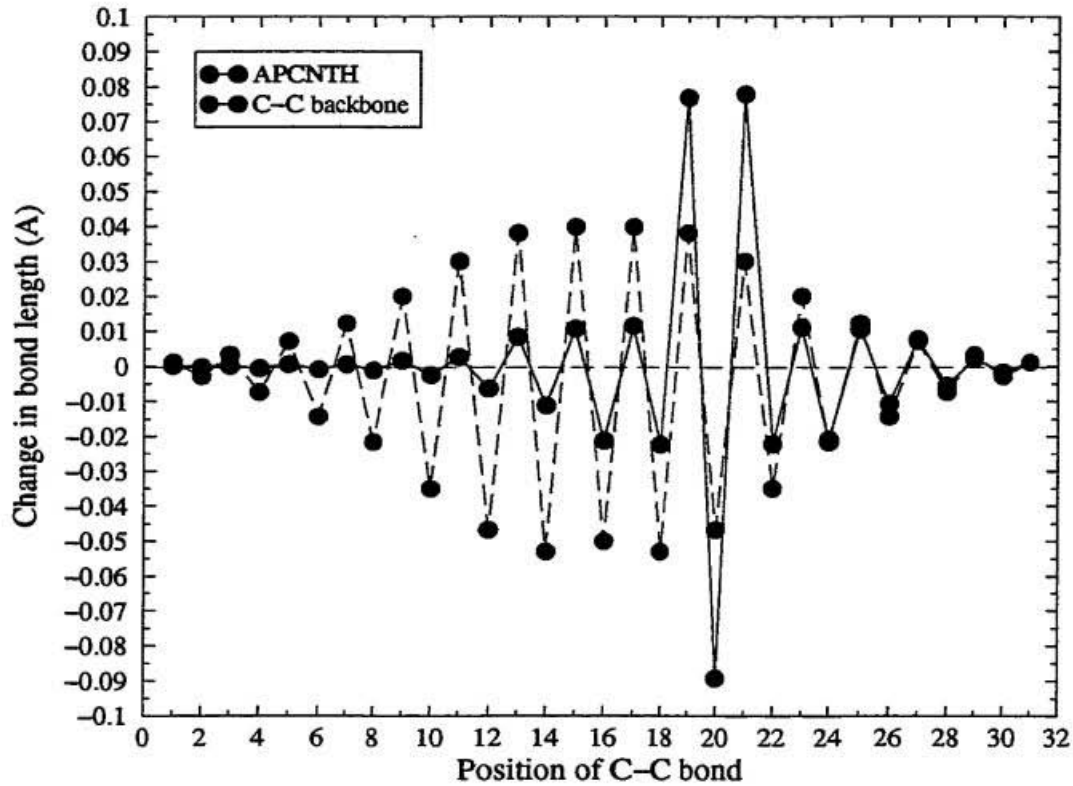

Figure 4.5: Changes in the HF calculated Carbon-Carbon bond lengths of PCNTH tetramer when going from the ground state to the first excited state in its fully optimized geometry. Changes occurring along the C–C backbone are also provided for $\pi - \pi^*$ transitions.

the C=C bonds are longer. The opposite trend have been observed for the input quinoid PT oligomers [165]. The angle parameters also show similarities when we compare them between the two methods. In addition, we compare these results with those obtained for the polyacetylene octamer geometries and we can see the same trends (see Table 4.13). The PA backbone shows an average bond length alternation from -0.139 to -0.128 Å in HF calculations, and from -0.132 to -0.034 Å in CIS calculations for a chain length similar to that of an octamer.

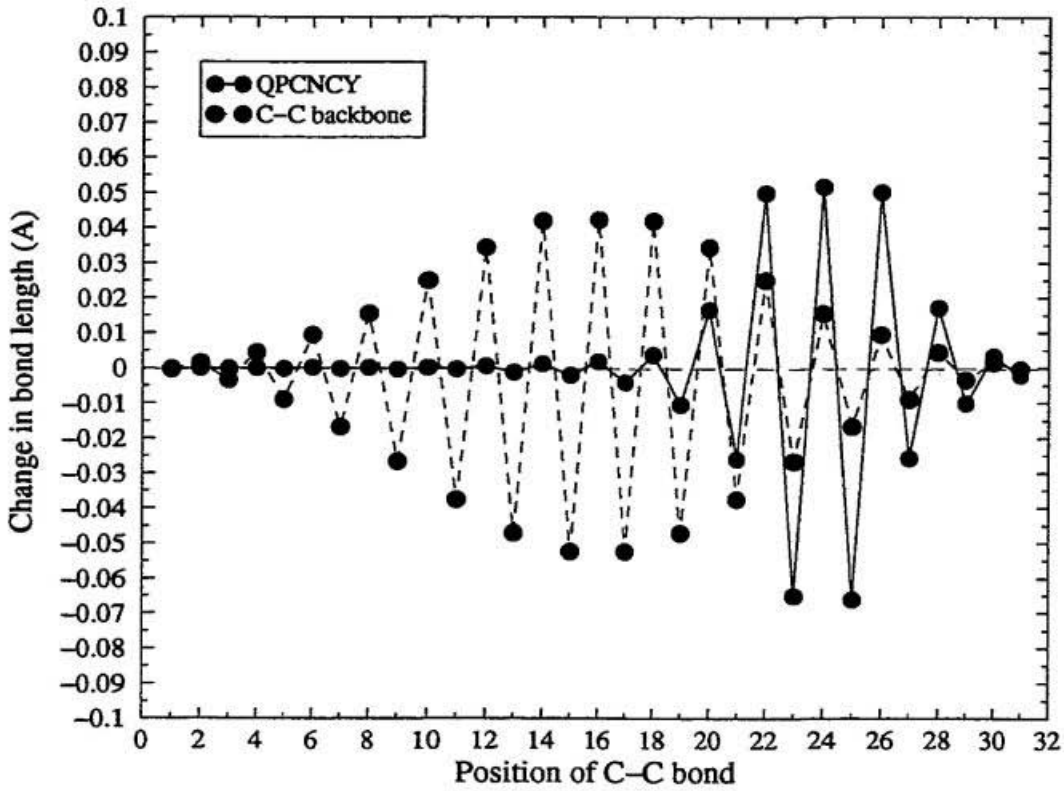

Figure 4.6: Changes in the HF calculated Carbon-Carbon bond lengths of PCNCY tetramer when going from the ground state to the first excited state in its fully optimized geometry. Changes occurring along the C–C backbone are also provided for $\pi - \pi^*$ transitions.

Regarding the total chain length of a PA octamer, the backbone for the cyano-substituted octamer gives a value of 34.48 Å while for aromatic PCNTH, quinoid PCNCY and quinoid PCNFV the chain lengths are 29.56, 28.34 and 28.56 Å respectively. It is found that the chain length is elongated for the PA molecule due to the fact that it experiences steric repulsion due to the end and/or side hydrogens. This is consistent with the trends calculated by Toussaint and Brédas [166]. Granville *et al.*, [167] have reported the optical absorption spectra for the transition from

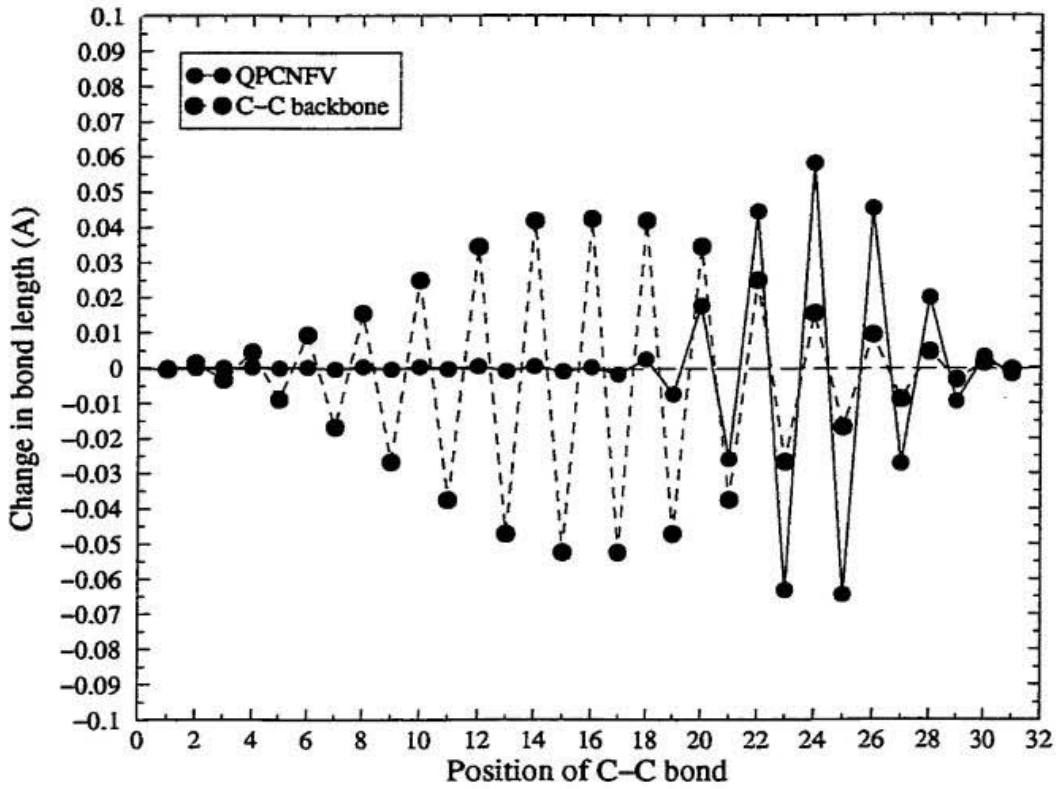

Figure 4.7: Changes in the HF calculated Carbon-Carbon bond lengths of PCNFV tetramer when going from the ground state to the first excited state in its fully optimized geometry. Changes occurring along the C–C backbone are also provided for $\pi - \pi^*$ transitions.

the ground to the first B_u excited state in linear polyenes with two to six double bonds. From a Franc-Condon analysis [167] of their spectra, they have been able to estimate the changes in single and double bond lengths upon excitation denoting an average δ_r value -0.08 Å for decapantaene. In our CIS-calculated geometries, the highest and the lowest δ_r values for *trans-cisoid* PA octamer are obtained as -0.132 and -0.034 Å, with an average bond length modification of -0.082 Å, matching well with the experimental results [50].

For PT octamer in the HF ground state C−C bonds ranged from 1.420 to 1.428 Å which are slightly overestimated in comparison to the experimental values (1.410 Å). While the CIS values for the C=C bonds are elongated for both the 3-21G* and 6-31G* basis sets, they are shortened with the 3-21G basis sets (see Table 4.1). The small δ_r value for the aromatic oligomers, relative to those obtained for the quinoid ones can be qualitatively explained as follows: For the decreases in δ_r in the aromatic PT oligomers the admixture of the LUMO into the ground state with anti-bonding character in the double bond region and bonding character in the single bond region causes a decrease in δ_{ring} [2] as we move towards the central rings. While for quinoid PCY oligomers, the HOMO attains a bonding character in the double bond region and anti-bonding character in the single bond region (see Fig. F.20) causing an increase in the δ_{ring} as we move from the outer rings to the inner ones, almost the same thing happens for quinoid PFV oligomers where the bonding nature is found across the double bond regions and anti-bonding nature across the single bond regions. The δ_r values for the smaller units (like dimers) are found rather dominating in our CI-singles calculations. As the chain length grows the values for δ_r changes proportionally as we go from the outer rings towards the central rings, this is reflected in Fig. 4.1. The dihedral values show that the rings are planar in the ground state as well as in the lowest excited states.

The HF/3-21G* optimized intra-cell C−C bonds for PT oligomers range between 1.452 and 1.456 Å (which are about 0.01 to 0.05 Å longer than the experimental results [152]). The C-S bond lengths are found to be ranging from 1.722 to 1.738

[2] δ_{ring} values are bond length alternation within the aromatic or quinoid ring, and are defined as $\delta_{ring} = r_{C_\alpha - C_\beta} - r_{C_\beta - C_{\beta'}}$. The trends in δ_{ring} parallel the δ_r values, and can be used for comparison purposes.

Å which are underestimated in comparison to the experimental value (1.739 Å). The bond length alternations, δ_r observed in the outer rings for PT octamer are found very close to that observed for the ground state geometries ($\sim$ -0.08 Å), which correspond to the experimentally obtained value for δ_r [80]. We note that for PT octamer the central inter-ring bond distance has reduced almost by 0.06 Å with respect to the HF ground state geometry (Fig. 4.2). In case of PCY the reduction in bond distance has been 0.04 Å, and it is 0.06 Å for the PFV octamer (Fig. 4.3 and 4.4 respectively), relative to their ground state geometries.

We also compare here the geometric structures optimized for PCNTH, PCNCY and PCNFV with those obtained for their parent polymers, and thus put an effort to see the influence of the electron withdrawing groups ($C_2(CN)_2$) on the geometries. It appears that:

(i) on the dicyano side, the outer $C_{\alpha'}$-$C_{\beta'}$ bonds in PCNTH tetramer (1.353 Å) have lengths that are similar to the ones optimized in s-*cis* polythiophene (1.354 Å); for PCNCY (1.528 Å) and PCNFV (1.523 Å) these bonds are found longer than their parents PCY (1.518 Å) and PFV (1.502 Å) in their excited states. The inner C_β-C_α bonds for PCNTH are found (1.367 Å) shorter than its precursor PT value (1.376 Å) but closer to that of its quinoid PT isomer [18], for PCNCY (1.325 Å) and PCNFV (1.340 Å) these values are found shorter than their corresponding lengths of predecessors PCY (1.447 Å) and PFV (1.468 Å). The variation in these bond lengths for the PCNTH oligomers are more dominating than those of PCNCY and PCNFV.

(ii) As a consequence the $C_{\beta'}$-C_β bonds for PCNTH are found to be elongated (1.426 Å) in comparison to the one optimized in PT (1.335 Å); for quinoid PCNCY

these bonds are found to decrease by ~0.010 Å compared to the one in PCY (1.335 Å), similarly for PCNFV the same bond (1.325 Å) is found to be decreased by an amount of 0.005 Å. These bond lengths for the aromatic PCNTH oligomers actually lie within the aromatic and quinoid values for their polythiophene precursor.

(iii) The intra-ring and the inter-ring bond lengths for PCNTH oligomers are also found to attain a value in between the single-double carbon-carbon bond lengths. On the other hand for PCNCY and PCNFV these changes are not as pronounced in their excited states.

To summarize, the excited state geometry of aromatic PCNTH is close to the one optimized in *cis-transoid* (quinoid) thiophene in ground state and there is also a weak contribution of the *cis-transoid* form in the ground-state geometry of aromatic PCNTH as was also observed by Toussaint and Brédas [106, 107]. On the other hand the excited-state geometries of PCNCY and PCNFV show a little change with respect to their *cis-transoid* PCY and PFV respectively. Hence from these optimized geometries one can easily infer that the introduction of the dicyanomethylene group between the thiophene rings has a strong influence on the geometric structure of *trans-cisoid* thiophene, resulting in an optimized geometry within the rings of PCNTH which is a combination of the ones appearing in the aromatic and quinoid forms of polythiophene. This situation is completely different from those taking place in PCNCY and PCNFV where the dicyanomethylene group inserted between the two cyclopentadiene and fulvene rings has only a weak influence on the geometric structure of *cis-transoid* PCY and PFV respectively.

Due to the closed shell nature of the molecules, we are able to extend our calculations to rather large oligomers containing up to 8 rings for PT, PCY, PFV

and for their cyano-derivatives. We can thus see from both the changes in carbon-carbon bond lengths and inter-ring twist angles, that the geometry modification extends over the six central rings of PT, PCY and PFV; whereas for their cyano-derivatives it is different, basically due to the presence of different heteroatoms on their side groups. The $C_{\alpha'}1C_{\alpha}$ angles reflect the hybridization of the heteroatoms. In PCY and PFV (angles in the order of 107°), the heteroatoms contribute to the σ backbone through a sp_{σ} hybrid, whereas in cases of polythiophene these bonds are described in terms of valence p_z orbitals due to the bond angle of about 90°.

The ground state geometries of PT oligomers show aromatic characteristics, whereas the PCY and PFV oligomers show quinoid characteristics. With regards to their excited state geometries, PT shows a tendency to evolve towards quinoid conformation and the latter two show a rather weak evolution towards aromatic conformation. In longer chains, the central rings of the oligomers adopt a changeover from one conformation to another in going from the ground (S_0) to the first excited state (S_1). From Figs. 4.2 through 4.4 it is quite clear that the central rings of the parent PT, PCY and PFV octamers are modified from aromatic to quinoid conformation and vice versa based on their ground state input geometries. For PT the central rings evolve in a close quinoid character with almost equal bond lengths (see Fig. 4.1), while the outer rings retain a geometry almost the same as that observed in the ground state (i.e., aromatic). For PCY and PFV we find a similar change in bond length which develop 0.04 and 0.05 Å deviations respectively for their central bonds following the respective $\pi - \pi^*$ singlet excitations.

4.3.1 Geometry Relaxation Phenomena

Geometry relaxation phenomena play a very important role in the turnovers from one kind of oligomer conformation to another (quinoid $\rightleftharpoons$ aromatic). For all the molecules, we find, as expected that a strong relaxation does indeed take place in their excited states, i.e., the geometry which is found to be optimal for their ground states do not constitute the optimal geometry in the lowest excited states. The equilibrium geometries optimized in both the HF and CIS techniques are given in Tables 4.1 through 4.14. For the ground state (S_0) optimized geometries, we observe relatively weak geometric deformation with respect to the AM1 input geometries (not shown in the tables). Inside the central rings, the small bond length modifications of $\sim$ 0.007 Å slightly weakens the aromatic character of PT octamer observed in the AM1 optimized geometries. In the linking bonds the modifications are found to be $\sim$ 0.002 Å at the outer rings and at the central portion this modifications are $\sim$ 0.008 Å (the bonds there are almost equal). The modifications are more pronounced for the S_1 states, the bond length alternation increases from -0.075 Å in S_0 to 0.008 Å in S_1, as result of the elongation of the double bonds and shortening of the single bonds due to conjugation effect. Going from the ends of the chain towards the centre of octathiophene (see Fig. 4.2), change in bond length increases, reaches 0.04 Å at the centre of the fourth ring and then evolves strongly and peaks at the connection between the fourth and the fifth ring of the octamer (where the single and double bond characters have exchanged with respect to the ground state and maximum absolute value of the bond length alternation is recovered). This state is thus characterized by a strong geometry relaxation.

In the lowest singlet excited states of PCY and PFV, the formation of a soliton-

antisoliton pair clearly emerges from the evolution of the geometry deformations along the chain axis. The aromatic PT and PCNTH oligomers acquire a semiquinoid character in their S_1 states, fully consistent with the formation of a polaron-like defect [56]. For the monomer and planar dimer of thiophene, similar geometric deformations have been predicted in the 3-21G*/CIS *ab initio* level and from semiempirical calculations including single and double excitations (QCFF/PI + CISD technique) [168]. The bond length variation between the C−C bonds joining the α-α carbons, amounts to ~ 0.04 Å (for aromatic PT octamer) and ~ 0.02 Å (for aromatic PCNTH tetramer). The single and the double bond character in the ring linkages are reversed. The quinoid PCY, PFV and their cyano-derivatives PCNCY, PCNFV acquire a very weak aromatic character though the changes are not as observable as in the cases of PT and PCNTH. In fact, the CIS results indicate that in the singlet state, the external rings of the oligomers are almost unaffected when going from S_0 to S_1.

We note, however that in the ground state the AM1 technique overestimated the bond length alternation with respect to the values calculated by other methods (see Table 3.1 as an example). Thus we can infer that the geometry modifications calculated at the AM1 level should be considered as maximal deformation for the ground state conformations, which could be due to the lack of electron correlation. But when we move on to CI-singles calculations the deformations are seen largest. For larger tetramers and octamers the geometric modifications are nearly independent of the charge of the species, and are strongly localized to the central rings and their surrounding bonds. The $C_{\alpha'}$-$C_{\beta'}$ bonds in the external rings for all the molecules display a value that is much closer to one calculated in their ground

states, these bond lengths are only modified by a thousandths of Angströms with respect to their values in the ground state.

The geometry relaxation phenomena involved in the singlet state formation are demonstrated in Figs. 4.2 to 4.7, where changes in bond lengths are shown along a path through the backbone of the molecule. For PT and PCNTH the thiophene units experience bond-order reversal, with the double bonds becoming longer and the single bonds shorter. Note that the carbon-sulfur bonds (and the carbon-carbon bonds off the backbone), that are only slightly modified in the excited states with respect to their values in the ground states are not considered here. These lattice distortions are similar to those associated to the formation of charged soliton-antisoliton pairs in polyacetylene [8, 144]. However, in oligothiophenes, the electron-hole pairs are bonded in the S_1 excited state by (i) the Coulombic attraction between opposite charges, (ii) the non-degenerate ground state of the thiophene oligomers, and (iii) the finite size of the systems, which prevents the separation between the opposite charge carriers occurring upon photo excitation in polyacetylene [8, 144].

The analysis of the CI-singles equilibrium geometries obtained for the lowest singlet states of the cyano-substituted oligomers indicates a general trend for structural modifications that are already observed in the cases of the unsubstituted oligomers. In the PCNTH tetramer, a pronounced enhancement of the quinoid character of the PT rings and reversal (reduction) of δ_r in the 20th bond linkage within the third repeating unit between the two dicyano rings of the triplet (singlet) polaron-exciton are observed (see Fig. 4.5). On the other hand, in cases of PCNCY and PCNFV the highest distortions are found taking place in the 24th inter ring bond linkage

(see Figs. 4.6 and 4.7). As a consequence, the lattice distortions associated with the lowest singlet-triplet excited states are more localized in the cyano-substituted oligomer moieties than the unsubstituted ones. The geometric deformations taking place in the excited states of cyano-substituted PCNTH, PCNCY and PCNFVs are however not symmetrical, in contrast to the situation prevailing for unsubstituted parent polymers, due to the presence of the electron accepting cyano-group Y terminated by hydrogen atoms (i.e., Y = CH_2=$C(CN)_2$). Actually, going from the singlet ground state (S_0) to the first excited state (S_1), as presented in Figs. 4.5, 4.6, and 4.7, we find that the cyano-substituted moieties show stronger bond length modifications with respect to their unsubstituted C–C backbone. For PCNTH tetramer these modifications occur at the carbon sites ranging from 10 to 20, for PCNCY and PCNFV tetramers the modifications are found pronounced at the carbon sites starting from 18 to 24. The geometric deformations that spread over the carbon skeleton are thus found to play a major role in the polaron-exciton generation. The energies are also lowered to a considerable amount due to the relaxed geometry as could be observed from Tables 4.1 through 4.14.

In polyacetylene (PA) another interesting phenomenon is the occurrance of bond alternation defects, which are often called solitons. The neutral soliton (carbon radical) has no charge but has spin ($s = 1/2, q = 0$). The solitons, represented as a localized radical electron in the neutral PA, separates two different bond-localized phases in the chain structure, which differ by the arrangement of their single/double bond sequence. The bond length difference is nearly zero near the soliton centre and increases only gradually with distance from this centre. Correspondingly, the probability density of the soliton wavefunction is not constrained to just one carbon

atom, but is smeared out over a certain range of carbon atoms, but not over the whole chain, for it is still pretty much localized. From our CI-singles study on the PA moiety the soliton is localized and non bonding with its energetic location in the middle of the Peierls gap between the π and π^* bands (i.e., the valence and conduction bands).

Chapter 5

Electronic Property Investigation

The wavefunctions describing the electronic states of the conducting systems extend throughout the conjugated chain. Unlike the atomic orbitals, which are localized around particular atoms, and decay exponentially away from the atoms, the MOs are referred to as delocalized in a sense that they are smeared over the molecules. Such delocalization gives rise to the formation of broad conduction and valence bands for very long conjugated chains in solids. Electronic charge delocalization is an important phenomenon. It is responsible for most of the electronic transport phenomena like conductivity and non-linear optical properties in solids. Some electronic and optical properties of π-conjugated systems are associated with the non-linear soliton, polaron and bipolaron excitations [169, 10]. Such excitations result from the coupling of the quasi-one-dimensional π electron systems to the polymer backbone structure via electron-phonon and electron-electron interactions. The electron-phonon coupling gives rise to structural relaxation which results in a self-localized electronic excitation around the local structural deformations giving rise to electronic states within the gap.

In this chapter we have the following sections: in Section 5.1 the general fea-

tures associated with the excitation energy are discussed; in Section 5.2 we study the lowest singlet and triplet excited states and relate them to other properties of the polymeric systems in greater details; in Section 5.3 we comment on the interrelation between excitation energy and bond length alternation; in Section 5.4 the correlation between the electronic and geometric structures is discussed; in Section 5.5 the resulting trends are extrapolated to the bulk polymers from their oligomeric moiety, and finally in Section 5.6 a brief summary is provided.

5.1 Excitation Energy

The excitation energy is simply one of the many features of a molecular excited state which is of interest to both physicists and chemists. Other information, such as the dipole moment and geometry relaxation is harder to obtain experimentally and so theory can play a key role in providing such details. The CI-singles calculations show that the lowest excited states correspond to a transition between the HOMO and the LUMO levels and get red shifted[1] as expected with increasing chain length. Detailed descriptions in terms of the configuration interaction expansion of these excitations in various oligomers are reported in Tables 5.1 through 5.6. It was observed earlier in qualitative comparisons of the spectra of closely related heterocyclic system [63] that the thiophene spectrum is closely related to the cyclopentadiene spectrum. The lowest $\pi \rightarrow \pi^*$ optically allowed transition has been reported to be located at about 5.3 eV both for cyclopentadiene and thiophene monomers [96]. This similarity was explained by the smaller and very similar

[1]Here the vertical transition energies represent the experimental absorption peaks [62] and since these excitation energies become smaller for longer oligomers the associated absorption wavelength increases (hence the term red shifted).

electronegativities of the bridging atoms: carbon and sulphur [63]. As expected, the electronic spectra calculated for molecules in their fully optimized geometries matched very well with experimental measurements. In Section 5.4 we compare the transition energies of the lowest singlet excited states of PT oligomers (from monomer to octamer) calculated via the CI-singles approach to experimental data obtained in gas phase. An excellent agreement between theory and experiment is observed. To achieve a reasonable correspondence between the experimental and calculated data, we have used gas phase values where available. It has to be noted here that due to the very low oscillator strength of the triplet transitions under investigation, the excitation energies for the $S_0 \rightarrow T_1$ transitions are not theoretically possible but they are experimentally important. This statement will be elaborated upon in Section 5.2.1.

5.2 Singlet and Triplet Excited States

Singlet and triplet excited states play a crucial role in the photo physics of conducting polymers [61, 66, 81, 98, 112, 114, 116, 170]. The electron-electron interaction has significant effects on various optical properties like photoluminescence, electroabsorption and third order optical susceptibilities [171]. On the basis of the HF ground state geometries, we calculate by means of the CIS technique the transition energies from the ground state (S_0) to the singlet excited state (S_1) forming the onset of the one-photon absorption (S_1, equivalent to the $1\ ^1B_u$ state of a polyene with C_{2h} symmetry [97]). The lowest one-photon energy transitions in the neutral oligomers of PT, PCY, PFV and their cyano-derivatives are basically related to a

one electron transition between the HOMO and the LUMO levels, denoted by H $\rightarrow$ L. Singlet and triplet excitation energies are calculated with the HF optimized ground-state geometries as initial guess. They are collected in Tables 5.1 through 5.6 providing the detailed descriptions of the lowest-energy transitions in terms of the configuration interaction expansions. It is clear from these tables that as the chain length increases the transition energy is red-shifted (see also Fig. 5.12), while the transition moments and hence the transition intensities increase due to the extension of the conjugation path. Our calculations indicate that the red shift is proportional to the number of repeat units. This trend has also been observed in several other conjugated organic polymers [66, 98, 103, 116, 118, 172]. This can be attributed to the greater delocalized nature of the HOMO and LUMO indicating that the HOMO and LUMO levels are merging.

The lowest transition energy associated with the various oligomers actually results from the mixing at the CI level of several one-electron transitions allowed by the selection rules within the C_{2h} symmetry of the oligomers. Analysis of the one-electron structure shows that the π-MOs alternatively belong to the a_g and b_u irreducible representations (A' and A'' respectively of the C_s point group symmetry) [95]. Note that, in the case of oligomers consisting of an even number of rings, the molecular symmetry is C_{2h}; transitions between π states belonging to the same a_u and b_g levels are totally forbidden [172, 116]. The large intensities (refer to Tables 5.1 through 5.6 for the corresponding oscillator strengths) reflect the extent of overlaps between the wavefunctions of the MOs involved in the one-electron HOMO $\rightarrow$ LUMO transitions. The MOs involved in the description of the lowest-lying symmetry-allowed excited states are formed from a linear combination

of atomic orbitals (LCAO) on atoms that give rise to bonding and antibonding patterns (see Appendix F). In PT and its cyano-derivative PCNTH, the sulfur atoms interact with the π electron clouds of the polyene backbone.

As in the case for the S_1 state, the lowest triplet state (T_1) is formed mainly by the spin-adapted electronic configuration resulting from the promotion of one electron from HOMO to LUMO. These triplet wave functions are composed of both singly excited configurations (the main configurations are characterized by the excitation of one electron from HOMO-1 to LUMO and the symmetric excitation from HOMO to LUMO+1, as well as other combinations where the HOMO-2, HOMO-1, HOMO, LUMO and LUMO+1, LUMO+2 levels are singly occupied). We find that the CIS expansion of the T_n state wavefunction is quite similar to the one of the S_n state (see Tables 5.1 through 5.6), which is coupled to the S_1 state and plays a principal role in the nonlinear optical properties of conjugated systems [80, 97].

5.2.1 Oscillator Strength

Oscillator strength is a useful measure of absorption intensity. For the transition n←0 it is expressed as

$$f_{n0} = \left(\frac{4\pi m_e \nu_{n0}}{3e^2\hbar}\right) |\mu_{n0}|^2 \tag{5.1}$$

which leads to an expression providing a link between spectroscopy and the prediction of polarizabilities

$$\overleftrightarrow{\alpha} = -\left(\frac{d^2 E_{n0}}{d\vec{\epsilon}^{\,2}}\right) = \frac{\hbar^2 e^2}{m_e} \sum_n{}' \frac{f_{n0}}{E_{n0}^2} \tag{5.2}$$

Table 5.1: Orbital symmetries, excitation (transition) energies, oscillator strengths (f), and main CI expansion coefficients of the lowest singlet and triplet excited states of PT oligomers (H and L refer to HOMO and LUMO).

Oligomer	State	Multiplicity	Symmetry	Energy (in eV)	(f)	Main CI expansion coefficients
monomer	T_1	Triplet	A′	1.0555	0.0000	0.68 [H→L]
	T_2	Triplet	A′	3.7352	0.0000	0.57 [H-1→L]-0.27 [H→L+1]0.25 [H→L+2]
	S_1	Singlet	A′	4.0950	0.0941	0.68 [H→L]
	T_3	Triplet	A′	4.8082	0.0000	0.49 [H→L+1]+0.39 [H-1→ L]-0.21 [H→L+2]
	S_2	Singlet	A′	5.6550	0.0620	0.57 [H-1→L+1]+0.39 [H→L+1]
	S_3	Singlet	A′	6.0977	0.0930	0.57 [H→L+1]-0.35 [H-1→L]+0.14 [H→L+2]
dimer	T_1	Triplet	A_U	1.5573	0.0000	0.65 [H →L]
	T_2	Triplet	A_G	3.3079	0.0000	0.48 [H →L+1]
	S_1	Singlet	A_U	4.1076	0.6240	0.68 [H →L]
	T_3	Triplet	A_U	4.4915	0.0000	0.53 [H-2 →L]
	T_4	Triplet	A_G	4.4991	0.0000	0.60 [H-1 →L]
	T_5	Triplet	A_U	5.7046	0.0000	0.57 [H →L+2]
tetramer	T_1	Triplet	A′	1.1980	0.0000	0.62 [H→L]+0.20 [H-1→L+1]
	T_2	Triplet	A′	2.2389	0.0000	0.45 [H→L+1]+0.42 [H-1→L]+0.15 [H-1→L+2]
	T_3	Triplet	A′	3.0902	0.0000	0.38 [H→L+2]+0.34 [H-1→L+1]-0.25 [H-5→L]
	S_1	Singlet	A′	3.1904	1.5382	0.66 [H→L]+0.17 [H-1→L+1]
	S_2	Singlet	A′	4.7263	0.0000	0.50 [H→L+1]+0.41 [H-1→L]
	S_3	Singlet	A′	5.7443	0.0000	0.50 [H-1→L]-0.39 [H→L+1]
Octamer	T_1	Triplet	A′	1.1802	0.0000	0.56 [H→L]+0.20 [H-1→L+1] -0.14 [H-2→L+2]+0.14 [H-2→L]
	T_2	Triplet	A′	1.7147	0.0000	0.40 [H→L+1]+0.37 [H-1→L]+0.16 [H-1→L+2]
	T_3	Triplet	A′	2.0968	0.0000	0.35 [H-1→L+1]+0.32 [H→L+2]-0.28 [H-2→L]
	S_1	Singlet	A′	2.8374	2.9661	0.62 [H→L]+0.23 [H-1→L+1]-0.13 [H-2→L+2]
	S_2	Singlet	A′	3.7435	0.0000	0.44 [H→L+1]+0.41 [H-2→L]+0.18 [H-1→L+2]
	S_3	Singlet	A′	4.3764	0.5040	0.37 [H→L+2]+0.36 [H-1→L+1]-0.32 [H-2→L]

Table 5.2: Orbital symmetries, excitation (transition) energies, oscillator strengths (f in arbitrary units), and main CI expansion coefficients of the lowest singlet and triplet excited states of PCY oligomers (H and L refer to HOMO and LUMO).

Oligomer	State	Multiplicity	Symmetry	Energy (in eV)	(f)	Main CI expansion coefficients coefficients
monomer	T_1	Triplet	A′	1.4917	0.0000	0.69 [H→L]-0.11 [H-3→L]
	S_1	Singlet	A′	6.3532	0.4413	0.67 [H→L]
	T_2	Triplet	A′	7.1101	0.0000	0.61 [H-4→L]-0.25 [H-2→L]-0.13 [H→L+6]
	S_2	Singlet	A′	7.8405	0.0000	0.63 [H-4→L]-0.27 [H-2→L]
	T_3	Triplet	A′	8.9650	0.0000	-0.48 [H→L+6]+0.32 [H→L+3]+0.22 [H→L+5]
	S_3	Singlet	A′	9.6243	0.0076	-0.52 [H-5→L]+0.34 [H→L+1]-0.29 [H→L+4]
dimer	T_1	Triplet	A′	1.1960	0.0000	0.66 [H→L]+0.17[H-1→L+1]
	T_2	Triplet	A′	3.3356	0.0000	0.46 [H-1→L]+0.45 [H→L+1]-0.19 [H-2→L+1]
	T_3	Triplet	A′	4.5686	0.0000	0.45 [H-2→L]-0.34 [H→L+2]-0.31 [H-1→L+1]
	S_1	Singlet	A′	4.7867	1.4857	0.69 [H→L]
	S_2	Singlet	A′	7.2624	0.0000	0.67 [H→L+1]+0.13 [H-1→L]
	S_3	Singlet	A′	7.8401	0.0000	0.66 [H-1→L]-0.15 [H→L+1]-0.13 [H-2→L+1]
tetramer	T_1	Triplet	A′	0.5176	0.0000	0.63 [H→L]+0.20 [H-1→L+1]-0.13 [H-2→L+2]
	T_2	Triplet	A′	1.8805	0.0000	0.45 [H→L+1]+0.42 [H-1→L]+0.16 [H-1→L+2]
	T_3	Triplet	A′	2.7586	0.0000	0.38 [H→L+2]-0.35 [H-2→L]+0.34 [H-1→L+1]
	S_1	Singlet	A′	3.2221	2.7132	0.68 [H→L]+0.16 [H-1→L+1]
	S_2	Singlet	A′	3.6012	0.0000	0.66 [H-3→L]+0.15 [H-1→L]+0.13 [H-1→L+2]
	S_3	Singlet	A′	4.3021	0.0000	0.31 [H-4→L]-0.16 [H-2→L+1]-0.13 [H→L+1]
octamer	T_1	Triplet	A′	0.7285	0.0000	0.62 [H→L]
	T_2	Triplet	A′	1.8217	0.0000	0.45 [H→L+1]
	T_3	Triplet	A′	2.7347	0.0000	0.38 [H→L+2]
	S_1	Singlet	A′	3.3599	2.7517	0.68 [H→L]
	S_2	Singlet	A′	5.1287	0.0000	0.66 [H→L+1]
	S_3	Singlet	A′	5.3439	0.0000	0.65 [H-1→L]

Table 5.3: Orbital symmetries, excitation (transition) energies, oscillator strengths (f in arbitrary units), and main CI expansion coefficients of the lowest singlet and triplet excited states of PFV oligomers (H and L refer to HOMO and LUMO).

Oligomer	State	Multiplicity	Transition	Symmetry	Energy (in eV)	(f) (in arb. unit)	Main CI expansion coefficients
monomer	T_1	Triplet	$\pi - \pi^*$	B_2	1.7765	0.0000	0.65 H $\rightarrow$ L
	T_2	Triplet	$\pi - \pi^*$	A_1	3.7665	0.0000	0.63 H-1 $\rightarrow$ L
	S_1	Singlet	$\pi - \pi^*$	B_2	6.4566	0.4642	0.68 H $\rightarrow$ L
	T_3	Triplet	$\pi - \pi^*$	A_1	7.8726	0.0000	0.61 H-3 $\rightarrow$ L
	S_2	Singlet	$\pi - \pi^*$	A_1	8.2778	0.4502	0.56 H $\rightarrow$ L+1
	T_3	Singlet	$\pi - \pi^*$	A_2	8.5125	0.0012	0.63 H-3 $\rightarrow$ L
dimer	S_1	Singlet	$\pi - \pi^*$	A'	4.0020	1.0053	0.69 H $\rightarrow$ L
	S_2	Singlet	$\pi - \pi^*$	A'	6.5541	0.0000	0.64 H $\rightarrow$ L+1
	S_3	Singlet	$\pi - \pi^*$	A'	6.5912	0.6718	0.65 H $\rightarrow$ L+2
tetramer	T_1	Triplet	$\pi - \pi^*$	A'	0.6468	0.0000	0.61 H $\rightarrow$ L
	T_2	Triplet	$\pi - \pi^*$	A'	1.3688	0.0000	0.48 H $\rightarrow$ L+1
	T_3	Triplet	$\pi - \pi^*$	A'	1.7826	0.0000	0.48 H $\rightarrow$ L+2
	S_1	Singlet	$\pi - \pi^*$	A'	3.0505	2.5910	0.68 H $\rightarrow$ L
	S_2	Singlet	$\pi - \pi^*$	A'	4.1469	0.0000	0.67 H $\rightarrow$ L+1
	S_3	Singlet	$\pi - \pi^*$	A'	4.4500	0.1564	0.66 H $\rightarrow$ L+2
Octamer	S_1	Singlet	$\pi - \pi^*$	A'	2.6503	4.8293	0.62 H $\rightarrow$ L
	S_2	Singlet	$\pi - \pi^*$	A'	3.5691	0.0000	0.52 H $\rightarrow$ L+1
	S_3	Singlet	$\pi - \pi^*$	A'	4.0269	0.7290	0.48 H $\rightarrow$ L+2

Table 5.4: Orbital symmetries, excitation (transition) energies, oscillator strengths (f in arbitrary units), and main CI expansion coefficients of the lowest singlet and triplet excited states of PCNTH oligomers (H and L refer to HOMO and LUMO).

Oligomer	State	Multiplicity	Transition	Symmetry	Energy (in eV)	(f) (in arb. unit)	Main CI expansion coefficients
	T_1	Triplet	$\pi - \pi^*$	A′	0.7190	0.0000	0.66 H → L
	T_2	Triplet	$\pi - \pi^*$	A′	1.7369	0.0000	0.62 H-1 → L
monomer	S_1	Singlet	$\pi - \pi^*$	A′	1.9330	0.0420	0.69 H → L
	T_3	Triplet	$\pi - \pi^*$	A′	3.6270	0.0000	0.44 H → L+3
	S_2	Singlet	$\pi - \pi^*$	A′	4.3957	1.0466	0.68 H-1 → L+1
	S_3	Singlet	$\pi - \pi^*$	A′	5.0431	0.1515	0.67 H-2 → L
	S_1	Singlet	$\pi - \pi^*$	A′	1.7811	0.1431	0.64 H → L
	S_2	Singlet	$\pi - \pi^*$	A′	2.8926	0.1921	0.56 H → L+1
dimer	S_3	Singlet	$\pi - \pi^*$	A′	4.4048	1.0543	0.64 H-2 → L
	S_1	Singlet	$\pi - \pi^*$	A′	1.6342	0.3386	0.63 H → L
	S_2	Singlet	$\pi - \pi^*$	A′	2.6732	0.5365	0.49 H → L+1
tetramer	S_3	Singlet	$\pi - \pi^*$	A′	2.9213	0.1609	0.44 H → L+2

Table 5.5: Orbital symmetries, excitation (transition) energies, oscillator strengths (f in arbitrary units), and main CI expansion coefficients of the lowest singlet and triplet excited states of PCNCY oligomers (H and L refer to HOMO and LUMO).

Oligomer	State	Multiplicity	Symmetry	Energy (in eV)	(f)	Main CI expansion coefficients
	T_1	Triplet	A′	1.3771	0.0000	0.61 [H→L]+0.24 [H-1→L]+0.19 [H-2→L+1]
	T_2	Triplet	A′	1.9687	0.0000	0.60 [H→L+1]+0.25 [H-2→L]-0.14 [H-1→L+1]
monomer	T_3	Triplet	A′	3.3334	0.0000	0.58 [H-1→L]-0.17 [H→L]-0.16 [H-2→L]
	S_1	Singlet	A′	3.5814	0.1551	0.70 [H→L]
	S_2	Singlet	A′	5.4701	0.7878	0.67 [H→L+1]-0.14 [H-1→L+1]-0.12 [H-2→L]
	S_3	Singlet	A′	5.6114	0.5089	0.68 [H-1→L]+0.10 [H-2→L+1]
	T_1	Triplet	A′	0.5150	0.0000	0.62 [H→L]-0.14 [H→L+2]-0.13 [H-1→L+1]
	T_2	Triplet	A′	1.7284	0.0000	0.42 [H→L+1]-0.41 [H-1→L]-0.17 [H-4→L]
dimer	T_3	Triplet	A′	2.3365	0.0000	0.39 [H-1→L+2]-0.38 [H→L+3]+0.18 [H-2→L]
	S_1	Singlet	A′	2.5913	1.6564	0.68 [H→L]-0.14 [H-1→L]
	S_2	Singlet	A′	3.8027	0.0000	0.54 [H→L+1]-0.41 [H-1→L]-0.13 [H-1→L+1]
	S_3	Singlet	A′	4.3999	0.0000	0.53 [H-1→L]+0.39 [H→L+1]+0.16 [H-2→L]
	T_1	Triplet	A′	1.2632	0.0000	0.45 [H→L]-0.30 [H-1→L+1]-0.22 [H-2→L+2]
	T_2	Triplet	A′	1.3594	0.0000	0.38 [H→L+1]-0.32 [H-1→L]-0.23 [H-1→L+2]
tetramer	T_3	Triplet	A′	1.5078	0.0000	0.35 [H→L+2]-0.28 [H-2→L]-0.27 [H-1→L+1]
	S_1	Singlet	A′	3.2746	2.0701	0.58 [H→L]-0.25 [H-1→L+1]-0.15 [H-2→L]
	S_2	Singlet	A′	3.3164	1.4088	0.46 [H-1→L+1]-40 [H-1→L]-0.19 [H-1→L+2]
	S_3	Singlet	A′	3.3338	1.5132	0.40 [H→L+2]-0.37 [H-1→L+1]-0.30 [H-2→L]

Table 5.6: Orbital symmetries, excitation (transition) energies, oscillator strengths (f in arbitrary units), and main CI expansion coefficients of the lowest singlet excited states of PCNFV oligomers (H and L refer to HOMO and LUMO).

Oligomer	State	Multiplicity	Transition	Symmetry	Energy (in eV)	(f) (in arb. unit)	Main CI expansion coefficients
	S_1	Singlet	$\pi - \pi^*$	A′	3.4738	0.0844	0.69 H → L
	S_2	Singlet	$\pi - \pi^*$	A′	4.3194	0.6501	0.67 H → L+1
monomer	S_3	Singlet	$\pi - \pi^*$	A′	5.3092	0.6763	0.66 H-1 → L
	S_1	Singlet	$\pi - \pi^*$	A′	2.3462	1.3749	0.68 H → L
	S_2	Singlet	$\pi - \pi^*$	A′	3.6457	0.0000	0.57 H-1 → L
dimer	S_3	Singlet	$\pi - \pi^*$	A′	4.0257	0.0000	0.54 H → L+1
	S_1	Singlet	$\pi - \pi^*$	A′	2.3367	1.7794	0.61 H → L
	S_2	Singlet	$\pi - \pi^*$	A′	2.9297	1.2090	0.33 H → L+1
tetramer	S_3	Singlet	$\pi - \pi^*$	A′	3.0282	1.5336	0.52 H-1 → L+1

where $\overleftrightarrow{\alpha}$ is the polarizability tensor, μ_{n0} is the transition dipole moment, E_{n0} is the associated transition energy, $\vec{\epsilon}$ is the applied electric field and ν_{n0} is the frequency of the oscillator. The prime denotes the fact that the summation excludes the ground state. The expression (Eq. 5.2) indicates that large contributions come from low energy, high intensity transitions; high energy or weak transitions make little contribution [91]. An implication is that if a molecule has intense, low-frequency transitions in its absorption spectrum, then it can be expected to be highly polarizable. Molecules that absorb only weakly or at high frequencies (*e.g.*, the colourless hydrocarbons) are expected to be weakly polarizable, while, intensely coloured molecules should be highly polarizable. From the above argument we should also expect large oscillator strengths to be associated with large absorption coefficients.

In practice, $f \approx 1$ for allowed electric dipole transitions and $f \ll 1$ for forbidden transitions. The oscillator strengths for the singlet and triplet transitions for the six molecular systems are listed in Tables 5.1 through 5.6. Oscillator strengths for the parent PT, PCY, PFV oligomers suggest that the S_1 states are more intense than all other singlet and triplet states. For their cyano-derivatives it is different, energetically higher transitions show larger intensities. As is observed in the case of PCNTH that the S_2 state is more intense than the S_1 state, for PCNCY monomer the same is true but for dimer and tetramer the S_1 state is found rather intense, for PCNFV oligomer moieties the S_1 state is weak in intensity for the monomer but for dimer and tetramer the S_1 states show higher intensities.

The triplet excited states of a few oligomers could not be studied, of them the aromatic PCNTH and quinoid PCNFV moieties did not converge for their triplet states. In an extended study [173] of the present work it has been observed that

the calculated polarizabilities for these molecules increase with increasing polymer length, which contrasts with the decrease in band gap with the chain length. This consistency between the polarizability and excitation energy indicates that the largest contribution to polarizability arises from transitions with the largest oscillator strength. As we consider higher excited states it is found that singlet states are producing oscillator strengths greater than zero (i.e., allowed transitions) while all the triplet states correspond to zero oscillator strengths (i.e., forbidden transitions). Hence the triplet states are not really significant with regards to the oscillator strengths in describing the optical absorption properties of the six molecular systems we studied.

5.2.2 Symmetry

Molecular symmetry in excited states is related to how the orbitals transform with respect to the ground state [95]. From group theory, we know that the overall symmetry of a molecule is a function of products of symmetry elements for the orbitals. Since the fully-occupied sets of symmetry-related orbitals are totally symmetric [2] only the singly-occupied orbitals are significant in determining the symmetry of the excited state. The theoretical/predicted symmetry of each excited state should be compared with the symmetry of the observed states. In some cases *Gaussian 94* could not identify the symmetry for a given excited state, these cases usually involve degenerate point groups [95].

All the molecules covered in this study lie in the x-y plane with the z-axis as axis of symmetry. Further symmetry considerations indicate that the inter-ring

[2] Indicates that an electron pair occupy the same spatial orbital, one of them has α spin and the other has β spin (total spin = 0 and multiplicity = 1).

bonds between the monomer units are not parallel to the chain axis direction [174]. For our systems, the primary centre of symmetry is typically situated at a half-way point on the intercell bond located between the monomers (a centre of symmetry, if there is one, is always at the centre of gravity of the system). Relative to this centre of symmetry, all the unit cells containing two monomers, could be characterized by C_{2h} point group symmetry which basically consists of eight symmetry operations *viz.* E, $C_2(x)$, $C_2(y)$, $C_2(z)$, i, $\sigma(yz)$, $\sigma(zx)$, $\sigma(xy)$ (see Fig. 5.1). In oligomer symmetry considerations we have not incorporated the non-primitive translational symmetry elements such as screw axis and glide plane. All-*trans* PT oligomers have

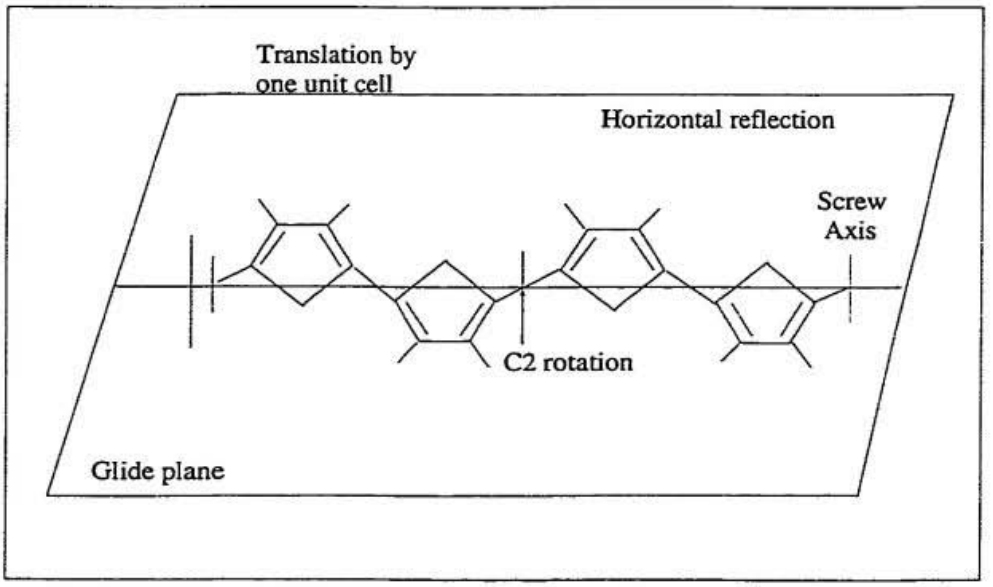

Figure 5.1: Space group operations for the polymer in the *anti* orientation

C_{2h} symmetry. In a simple molecular orbital treatment, all bonding one electron orbitals are doubly occupied, so the symmetry of the ground state S_0 is A_g. The promotion of one electron from the HOMO to the LUMO generates an excited state of symmetry B_u. Transitions between a_g and b_u is dipole allowed (see Fig. 5.4).

5.2.3 Molecular Orbital Analysis

In order to rationalize the electronic properties like excitation energy, oscillator strength etc., in relation with the observations of geometric structure analysis, we examine here the bonding-antibonding electronic patterns appearing on the HOMO and the LUMO levels of the conjugated skeleton and the cyano-derivatives of the parent oligomers. The molecular orbitals of these oligomers can be expressed as a linear combination of their respective monomer orbitals with the same symmetry as the constituent atoms. The MO coefficients of the lowest singlet excited states for the largest molecular systems are provided in Appendix E.

In order to rationalize the excitation energies calculated for the six heterocycles, we have examined the bonding-antibonding electronic patterns appearing on the HOMO and the LUMO levels of the FMO's and the molecules themselves. We have also compared these levels to those obtained for their unsubstituted parent polymers in both the aromatic and quinoid forms. The dominant MO plots for these six systems as well as their unsubstituted backbone are presented in Appendix F.

In a PT, PCY, or, PFV ring the highest occupied and lowest unoccupied levels are localized within the rings. Upon the formation of the oligomer chain, the strong interaction between the FMOs with high electron densities on the carbon atoms involved in forming the inter- and intra-ring bonds results in forming the *extended levels.*

We have illustrated in Figs. F.1 through F.54, the different molecular orbitals of our six systems of interest in comparison with their unsubstituted carbon-carbon backbone. Based on the wavefunctions, all these plots are obtained using Gaussview 1.0 - a Gaussian graphical user interface [147]. These figures show that the HOMO

and LUMO of aromatic PT, quinoid PCY and PFV all have a delocalized character while other levels present a more localized nature, as seen from the HOMO-2 and LUMO+2 orbitals of the respective molecules. While the localized orbitals for PT (Figs. F.11 and F.17) are confined within the five membered rings, the delocalized ones are dispersed along the C–C backbone (Figs. F.2 and F.5). In the cyano-derivative oligomers the distortion of the backbone introduced by the bridging group has a significant impact on the overall molecular orbitals and leads to a breaking of the charge conjugation symmetry.

The analysis of the bonding-antibonding texture on the FMOs of the aromatic conjugated skeleton as in Fig. F.1 shows that the HOMO possesses electronic characters identical to the ones observed on the HOMO of their parent aromatic polymers shown in Fig. F.2 and on the LUMO of the parent quinoid polymers. While the LUMO of the same (aromatic) skeleton exhibits the electronic characters that are also noticed on the LUMO of the parent polymers and on the HOMO of the respective quinoid parent polymers. These findings match very well with the ones observed by Toussaint and Brédas [106] in their study on PCNCY. Figs. F.3, F.6, F.21, F.24, F.27 and F.30 show the electronic characters appearing on the HOMO and LUMO of the cyano-substituted polymers. From Figs. F.1 and F.19 for the conjugated skeletons we can observe that the HOMO and LUMO wavefunctions of the cyano-derivative polymers describe situations which are opposite to that observed in the conjugated skeletons. In fact, the electronic character appearing on the HOMO of the aromatic PCNTH polymer corresponds to the LUMO of the aromatic PT and/or PA skeleton. It has also been observed separately for the dicyanomethylene group that it carries large MO coefficients on the HOMO of the

cyano-substituents. It is found that the electron-withdrawing cyano-group has no effect on the LUMO's of the cyano-substituents. Comparison between Figs. 5.2 and 5.3 show that the HOMO of the cyano-derivatives come from the strong bonding (i.e., stabilizing) interaction between the LUMO of the FMO's and the LUMO of the dicyanomethylene group. Thus, the HOMO of the cyano-derivatives are more stabilized relative to the LUMO of their skeletons.

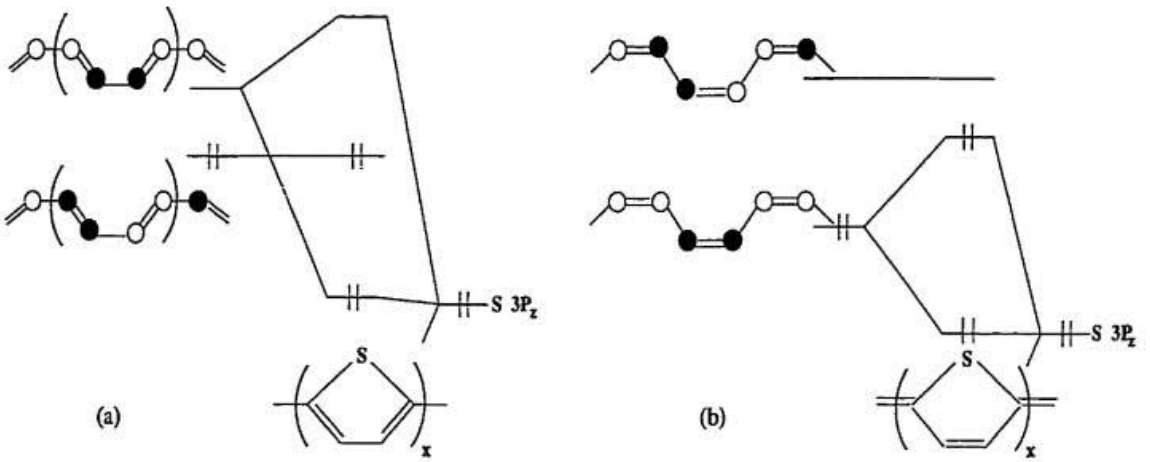

Figure 5.2: Interaction diagram for the HOMO, LUMO and sulfur orbitals for (a) aromatic, (b) quinoid thiophene. Figure taken from reference [79].

The LUMO of the heterocycle results from the interaction between the LUMO of the butadiene skeleton (Fig. 5.2) and the $p\pi$ orbital of the heteroatom since the heteroatom can only interact with orbitals of b_1 symmetry. For the aromatic thiophene monomer case (Fig. 5.2a), the LUMO of the PT backbone shifts upward by 0.33 eV (as obtained by the HF calculations) by interacting with the $3p_z$ orbital of sulfur atom, while the HOMO shows a downward shift of 0.24 eV, thereby enlarging the HOMO–LUMO gap. For quinoid PT (Fig. 5.2b), we see that the HOMO and the LUMO are interchanged, compared with those of the aromatic backbone of PT

(i.e., *trans-cisoid* PA). The HOMO for s-*trans* PT interacts with the sulfur lone pairs giving it a upward push by 0.45 eV and the LUMO is lowered by 0.58 eV which results in decrease in the band gap. For longer oligomers this is not the case where we see a different trend, as is observed for the aromatic thiophene oligomers the LUMO is not changed much while the HOMO is found lowered by $\sim$0.5 eV (for αT_6 as well).

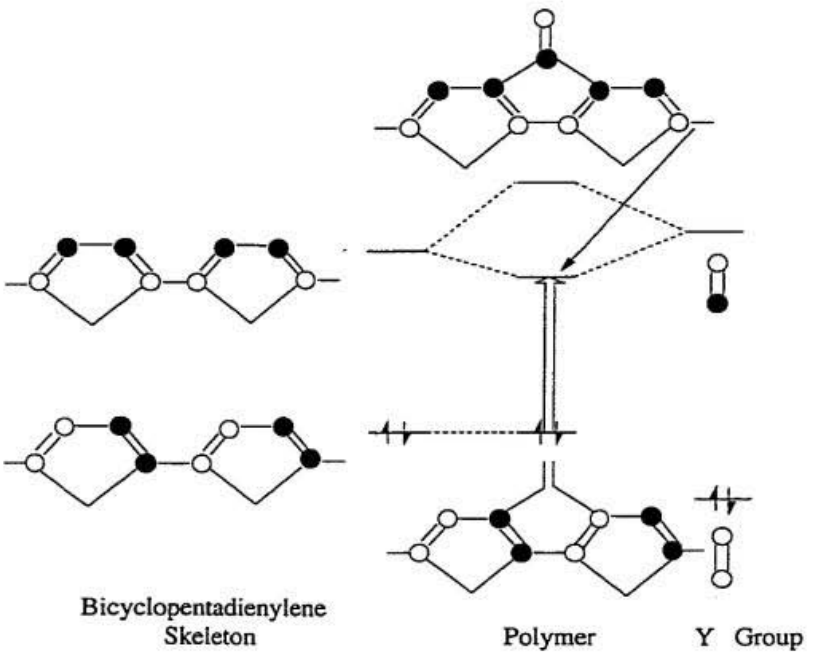

Figure 5.3: Interaction diagram showing the formation of polymers from the cyclopentadiene skeleton and the electron-accepting group Y terminated by H atoms [CH_2 =$C(CN)_2$]. The pseudo-orbitals of CH_2 are omitted. From reference [105].

The structure of the FMOs of the five-membered rings and their cyano derivatives can be qualitatively illustrated according to the interaction diagram shown in Fig. 5.3. The contribution of the electron accepting group Y= >C=$C(CN)_2$ to the HOMO of the C–C backbone is negligibly small, while it plays quite significantly in

contributing to the LUMO of these polymers. The interaction diagram, Fig. 5.3 of the bicyclopentadiene backbone with the electron-accepting group Y shows the formation of such polymers. In order to rationalize the excitation energy values in light of these results, it can be inferred that the energies of the cyano-substituted polymers are primarily determined by the strength of the bonding interaction between the LUMO of the bicyclopentadiene skeleton and the LUMO of the electron accepting group Y terminated by hydrogen atoms (*i.e.*, $Y{=}CH_2{=}C(CN)_2$). The smaller excitation energy of PCNTH as compared to the other two cyano-substituted polymers is, therefore, due to the low lying LUMO of $>C{=}C(CN)_2$ (with H atoms as end groups) and also due to orbital mixing of S electron lone-pairs with the frontier electron clouds (see also the LUMO of PCNTH tetramer in Fig. F.6). The presence of large LCAO coefficients on the electron withdrawing dicyano group (see Appendix E), the bonding/stabilizing interaction between the dicyano group and the thiophene rings as well as between the two thiophene rings of the unit cell (see Fig. 5.3) result in the lowering of band gaps for these cyano-derivatives oligomers. This could also be observed in the HOMO and the LUMO plots for the PCNTH tetramer (see Figs. F.3 and F.6).

Using the same approach as in PCNTH we can explain the small band gap value of PCNCY and PCNFV. It is observed that, on the HOMO of PCNCY (Fig. F.21) and PCNFV (Fig. F.24), the bonding-antibonding electronic patterns are identical to the ones appearing on the HOMO of the quinoid PCY (Fig. F.20) and PFV (Fig. F.23). On the LUMO, we can see that the dicyano group carries large LCAO coefficients as in PCNTH but the α carbon atoms carry very small LCAO coefficients (see Tables 11.5 and 11.6) which result in the absence of interactions between

the bicyclopentadiene and bifulvene units. This explains the flatness of the LUMO. Close examination of the LUMO of PCNCY and PCNFV show that no aromatic- or quinoid-like electronic characters/patterns appear on that band that correspond to any electronic characteristics of π bands of either aromatic or quinoid PCY and PFV. It could be due to the charge transfer from the cyclopentadiene/fulvene rings to the dicyanomethylene moiety in the first excited state causing the LUMO to be dominated by the electron withdrawing group with no electronic patterns (see Figs. F.24 and F.27).

The effect of the heteroatoms on the excitation energies is twofold. Due to symmetry, the mixing of the HOMO−LUMO is limited to orbitals symmetrical with respect to reflection through the vertical mirror plane containing the heteroatoms. Thus the LUMO in the aromatic PT case and HOMO in the quinoid PCY and PFV cases are mixing strongly. At the same time the C−C backbone also changes which is reflected in the calculated bond distance changes in Figs. 4.2 through 4.4. While this change has an effect on the excitation energy, the direct mixing plays a bigger role in the determination of excitation energy. The direct mixing enlarges the excitation energy for the aromatic PT oligomers, whereas it decreases the transition energies for the quinoid PCY and PFV cases. The strong mixing of the sulfur lone pairs with one of the FMOs of the carbon-carbon backbone network gives the aromatic form a higher stability as compared to the quinoid form [18, 79]. In contrast to fulvene and cyclopentadiene, the thiophene set has two well defined MOs of the p_z character – $2p_z$ and $3p_z$ respectively, with little or no mixing with the s-orbitals.

The six MOs *viz.* HOMO, LUMO, HOMO-1, HOMO-2, LUMO+1, and

LUMO+2 of PT all have the π character. We focus now on the nature of the transitions in fully optimized PT oligomers. The HOMO to LUMO transition is the most dominant transition in all its mesomers. For the largest oligomers αT_8 the dominant transition occurs at 2.83 eV as shown in Fig. 5.4. The weak transition at 4.38 eV is described by a linear combination of six Slater determinants involving H→ L+2, H-1→ L, H-2→ L, H-2→ L+2, H-1→ L+3 and H→ L+4 excitations shown in Table 5.1. It is also observed that the contributions from the higher-lying one-electron transitions increase as the chain length grows, due to reduction in the energetic difference between the various configurations (see Tables 5.1 through 5.6).

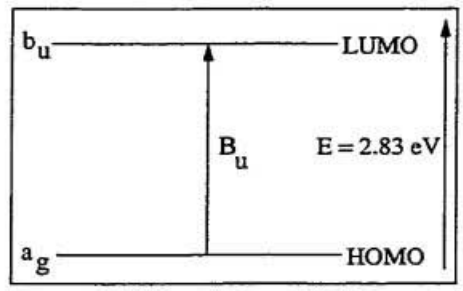

Figure 5.4: αT_8 one electron levels.

It is clear from the HOMO plot of the cyclopentadiene octamer presented in Fig. F.20 that there occurs a mixing between the '*s*' orbitals of hydrogen with the carbon p_z orbitals. The bonding antibonding nature of the orbitals at the centre differs from from that at the edges. The lowest energy transition for PCY octamer occurs at 2.81 eV which involves again a dominant H→ L transition. The second allowed excited state is located at 3.93 eV and is described by a superposition of the H→ L+1, H-1→ L, H-1→ L+2, H-2→ L+1, and H-2→ L+3 transitions. The oscillator strength of this second excitation is strongly reduced to zero with respect to the first excitation.

The three transitions calculated at 2.65, 3.57, and 4.03 eV for PFV octamer are originated from a large mixing of transitions from various delocalized occupied levels to localized levels. The lowest first excitation energy results due to the principal

transition from the delocalized HOMO to the localized LUMO (see Figs. F.23 and F.29) and a superposition of transitions between the H-1→ L+1 and H-2→ L+2 levels. The second singlet state shows a superposition of five distinct transitions: H→ L+1, H-1→ L, H-1→ L+2, H-2→ L+3, and H-2→ L+1. This weak intensity transition is characterized by a zero oscillator strength. While the third singlet state is optically dipole allowed with an oscillator strength of 0.73 in arb. unit with a combination of seven Slater determinants, of them the dominant one is for the H→ L+2 excitation.

To the extent that interactions between the π-electrons of the conjugated carbon chain and the sulfur atoms can be neglected, the electronic structures of the PT, PCY and PFV oligomers and that of the PA backbone are expected to be very similar [110].

5.2.4 Charge Distribution, Dipole Moment and Mulliken's Population Analysis

It is desirable to allocate the electrons in some fractional manner among the various parts of a molecule (atoms, bonds, etc.). It may be useful, for example, to define a total electronic charge on a particular atom in a molecule in order that quantitative meaning may be given to such concepts as electron withdrawing or donating ability. Suggestions about how to do this, starting from the density matrix as in Eq. (A.14), were made by Mulliken [156]. Mulliken population analysis, which partitions the total charge among the atoms in the molecule, is an arbitrary scheme for assigning charge. Atomic charges in a molecule - unlike the electron density - are not quantum mechanically observable, and can not be unambiguously predicted

from first principles. Based on the optimized geometries of the oligomers, we have calculated the charge distribution, as obtained from the Mulliken population analysis for both ground and excited states. From the results we can see that in the ground states, the charge appearance on the five-membered rings and their cyano derivatives indicates that relatively small charge transfer occurs in the polymeric ground states (see Table 5.7) in comparison to the excited states (see Table 5.8). Charge density accumulates predominantly on those carbon atoms which carry the negative charge in the valence bond formation. Charge is also transferred to the β carbons nearest to the central bonds. In case of the PT and PCNTH oligomers charge is also transferred from the sulfur atom (see Figs. 5.5 through 5.10).

Table 5.7: Calculated net charges on the basis of Mulliken's population analysis in HF/3-21G* ground state. Molecular volumes (in Å^3) are also provided.

Atom/Group	PT	PCY	PFV	PCNTH	PCNCY	PCNFv
C_1	-0.208154	-0.011801	0.005141	-0.212442	0.038838	0.048766
C_2	0.002444	0.004532	0.011154	0.111993	0.066573	0.086620
C_3	0.002444	0.004547	0.011154	-0.073591	-0.046498	-0.066030
C_4	-0.208154	-0.011815	0.005151	-0.287461	-0.024713	-0.031871
X[a]	0.411420	0.014537	-0.032601	0.539104	0.057980	0.045739
Y[b]				-0.155236	-0.184358	-0.166466
Molecular volume	72.0±1.6	77.2±1.4	91.7±3.1	189.1±5.4	195.9±3.7	220.6±5.5

[a]X = S(for PT and PCNTH), CH_2 (for PCY and PCNCY), $(CH)_2$ (for PFV and PCNFV) respectively.
[b]Y = >C=C(CN)$_2$.

In the MO picture of charge transfer the LUMO is the most important orbital. This LUMO which becomes the HOMO in the excited states are expected to receive

Table 5.8: Calculated net charges on the basis of Mulliken's population analysis at CIS/3-21G* for the S_1 excited state (Figs. 5.5 through 5.10). Molecular volumes (in Å^3) are also provided.

Atom/Group	PT	PCY	PFV	PCNTH	PCNCY	PCNFV
C_1	-0.201233	-0.017304	0.000769	-0.215236	0.037934	0.048248
C_2	0.006227	0.001341	0.013226	0.113199	0.105772	0.126864
C_3	0.006231	0.001341	0.013226	-0.089378	-0.079019	-0.101663
C_4	-0.201230	-0.017304	0.000769	-0.283633	-0.022331	-0.019009
X[a]	0.390005	0.031926	-0.027990	0.543428	0.054863	0.033797
Y[b]				-0.136761	-0.199444	-0.176473
Molecular volume	73.8±2.8	80.5±1.5	92.9±4.5	190.6±5.0	195.7±5.8	222.0±2.6

[a]X = S (for PT and PCNTH), CH_2 (for PCY and PCNCY), $(CH)_2$ (for PFV and PCNFV) respectively.
[b]Y = >C=C(CN)$_2$.

most of the charge. In order to justify this assumption, we compare in Figs. F.5 and F.2 for PT isosurface of the LUMO and the HOMO. One can see very clearly the migration of charge into the terminal positions of the aromatic arrangement and the formation of the central double bond. Besides that, charge depletion in the σ region due to the increased π charge takes place. Trends in structural properties also indicate that the lower transition energies in the cyano-substituted polymers are accompanied by greater charge delocalization in the aromatic (*trans-cisoid*) forms and by greater charge localization in the quinoid (*cis-transoid*) forms in comparison to their parent polymers.

The dipole moment is the first derivative of the energy with respect to an electric field. It is a measure of the asymmetry in the molecular charge distribution, and is

given as a vector in three dimensions. For Hartree-Fock calculations it is equivalent to the expectation value of X, Y, and Z. It was suggested by other investigators that the major portion of the dipole moment comes from the π electrons [175]. The π-electron theories predict an appreciable charge transfer from the exocyclic carbon into the ring [176]. For PFV and PCNFV, one can notice this as the fulvene molecules have a tendency to form a cyclic six π-electron system by intramolecular charge shifts even at their ground states. For PT and PNCTH this charge transfer is even stronger providing a bigger dipole moment than the ones observed in PCY and PFV. The Sulfur lone pairs play a significant role in this increment in dipole moment. The Mulliken charges obtained from the CI-singles calculations are shown in Figs. 5.5 through 5.10, where it is exhibited that a rather uniform charge distribution with the polarity of the CH bonds from CIS calculation being larger than that from the HF results. The corresponding dipole moments (μ) for the quinoid PCY, PFV and their cyano derivatives are rather small in HF calculations while the PT and PCNTH show larger values in comparison to the CIS values. These CIS values are in close agreement with the experimental results [89, 177]. This reveals that the contribution of the polar structures to the ground state is negligible. Previous investigations [178] show that the dipole moment is basis set dependent, but in our present calculations we have only used 3-21G* basis sets to estimate the magnitudes and directions of μ (see Table 5.9). The HF/3-21G* approach still requires higher order electron correlation and basis set corrections in order to account correctly for the ground state dipole moment calculations.

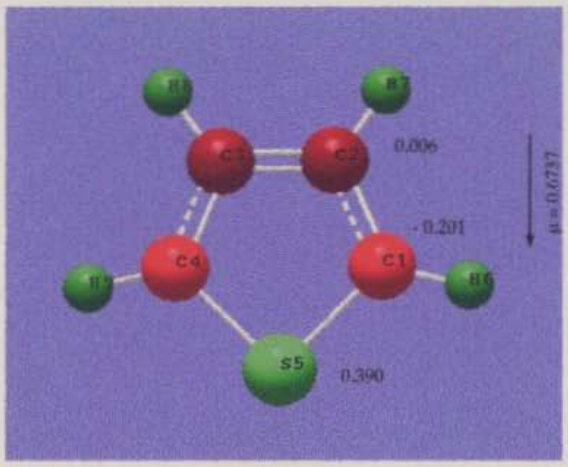

Figure 5.5: Mulliken charges and dipole moments in (D) for CIS/3-21G* excited state of thiophene (atomic colours: red→ negative, green→ positive).

5.2.5 Electron Correlation effects on Dipole Moment

Dipole moments are calculated with both HF/3-21G* and CIS/3-21G* calculations in order to observe the electron correlation effects. It has been reported by other investigators as well that the electron correlation corrects the π components of the dipole moment [101]. The six non-alternating oligomer systems that we have included in our present study show polar characteristics. For thiophene the ground state HF/3-21G* geometry shows a dipole moment of 0.764 D while the CIS/3-21G* geometry shows 0.674 D. For cyclopentadiene the calculated ground state dipole moment is found to be 0.136 D and for the first excited state it is 0.242 D. For fulvene the HF results show a dipole moment of 0.343 D and the CIS results show a dipole moment of 0.629 D. For the cyano-derivatives the calculated dipole moments are quite high: for aromatic PCNTH the HF and CIS values are found to be 4.864 D and 4.774 D respectively; for quinoid PCNCY these values are 6.837 D and 7.175 D respectively; and for quinoid PCNFV the corresponding values

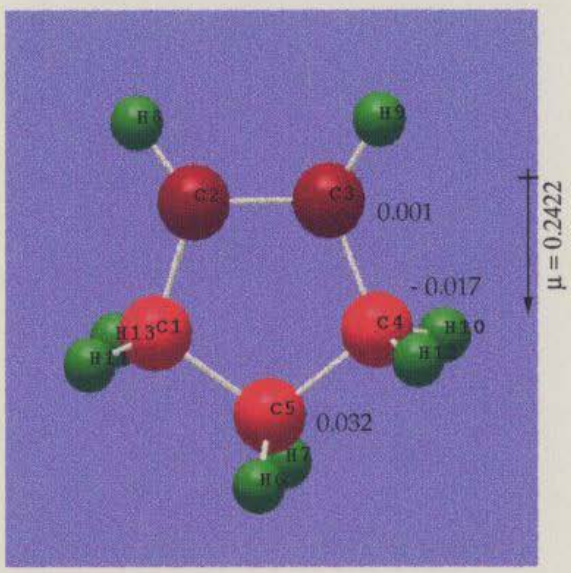

Figure 5.6: Mulliken charges and dipole moments in (D) for CIS/3-21G* excited state of cyclopentadiene.

are 6.345 D and 6.632 D respectively. The total dipole moments for optimized geometries and the charge distributions on several atoms are presented in Figs. 5.5 through 5.10. From Table 5.9 we can see that for quinoid PCY, PFV and their cyano-derivatives, the total dipole moments in excited state are larger than their ground state counterparts, on the other hand the aromatic PT and PCNTH show the opposite trend. For aromatic PA the total dipole moment in S_0 state is found to be larger than that for the S_1 state by an amount of 0.0075 D.

Due to the unavailability of experimental dipole moment data for the quinoid PCY and PFV molecules, we calculated the electron correlation effects on dipole moment for the aromatic unit cells of PCY and PFV by performing both HF and CIS optimizations on them. Table 5.9 shows the calculated data with the corresponding experimental values where available. Hartree-Fock calculations at 3-

Table 5.9: Summary of calculated ground (S_0) and excited (S_1) state dipole moments (μ) of different molecules.

Molecule	Repeating unit length (in Å)		Dipole moment (in debye)								$E_{cal.}$	
			Ground state (S_0)				Excited state (S_1)				S_0	S_1
	S_0	S_1	μ_x	μ_y	μ_z	Total[a]	μ_x	μ_y	μ_z	Total	(HF)	(CIS)
s-*cis* PA	5.19	5.01	0.0054	-0.0001	0.0124	0.0344	-0.0360	0.0000	0.0484	0.0269	12.22	5.24
s-*trans* PA	4.45	5.22	0.0308	0.0084	-0.0533	0.1579	0.0385	0.0000	-0.0667	0.3405	14.88	6.35
s-*cis* PT	4.53	4.55	-0.1103	-0.0005	0.2797	0.7642 [b]	-0.1781	-0.0003	0.4515	0.6737	12.80	5.57
s-*cis* PCY	4.40	4.37	0.0488	0.0038	0.1432	0.3846 [c]	-0.0373	-0.0029	0.1096	0.5103	12.37	4.77
s-*trans* PCY	4.14	4.17	0.0209	-0.0001	-0.0491	0.1357	0.0802	0.0000	-0.2010	0.2422	14.77	6.35
s-*cis* PFV[d]	4.38	4.30	0.0766	0.0001	-0.2188	0.5891 [e]	-0.2314	-0.0002	0.6609	1.5347	10.73	2.93
s-*trans* PFV	4.11	4.12	-0.0483	0.0001	0.1261	0.3432	-0.1062	0.0004	0.2537	0.6288	14.06	6.46
s-*cis* PCNTH	8.42	8.34	1.8714	0.0000	-0.3998	4.8640	1.4392	0.0000	-3.1177	4.7736	8.36	1.93
s-*trans* PCNCY	7.42	7.42	2.6900	0.0061	0.0000	6.8373	1.7730	0.0000	-4.1250	7.1754	8.68	3.58
s-*trans* PCNFV	7.60	7.40	1.0040	0.0009	-2.2855	6.3450	1.9392	0.0000	-4.5629	6.6316	8.26	3.47

[a]Magnitude of the total dipole moment
[b]The experimental value provided in Ref. [177] is 0.55 D.
[c]The experimental value provided in Ref. [179] is 0.419 ± 0.004 D
[d]The dipole moment for s-*cis* PFV calculted at the CID/3-21G* level is 0.1373 D.
[e]The experimental value provided in Ref. [180] is 0.424 ± 0.001 D.

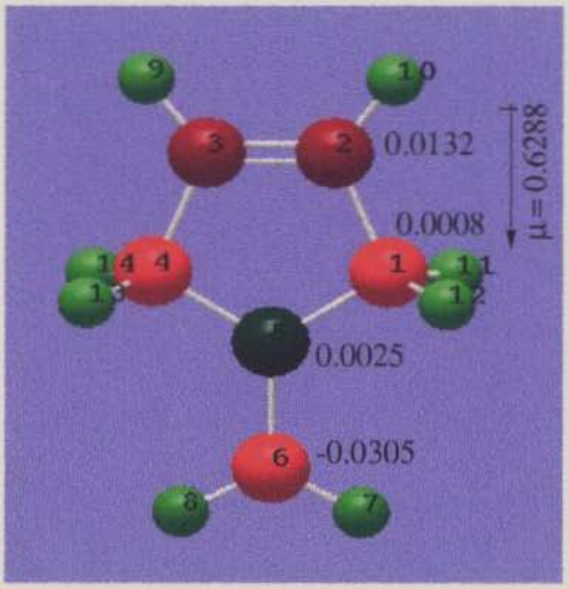

Figure 5.7: Mulliken charges and dipole moments in (D) for CIS/3-21G* excited state of fulvene.

21G* basis set provide dipole moments that are nearly 28% too high. The calculated results for dipole moments can be significantly improved by the inclusion of electron correlation effect at the CIS/3-21G* level reducing the calculated dipole moment by ~13% compared to the ground state.

Dipole moments of molecules in the gas phase are typically determined by microwave spectrometry to ±0.01 D or better [101]. A reasonable goal for the CIS theory is to calculate electronic properties like dipole moment as closely as possible to the experimental results. The dipole moment of aromatic fulvene is increased to 1.5347 D under the corresponding $\pi - \pi^*$ excitation, which is much larger than the corresponding HF as well as the experimentally observed ground state result. It is not quite understood as to why fulvene shows such an increase in dipole moment consequent to the $\pi - \pi^*$ excitation, although it is believed that the addition of

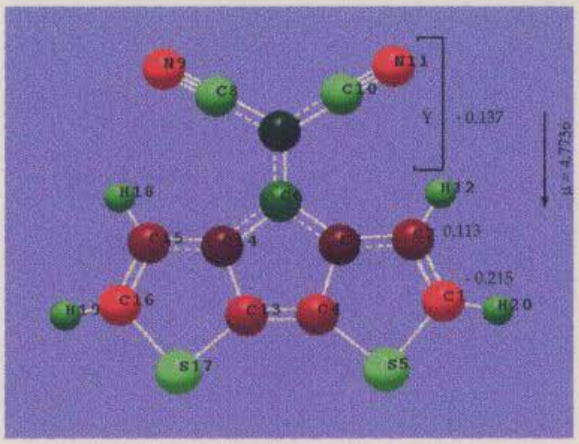

Figure 5.8: Mulliken charges and dipole moments in (D) for CIS/3-21G* excited state of PCNTH.

electron correlation to the wavefunction will improve the agreement between the calculated and experimental dipole moments [101]. Since we are unable to find the experimental results for excited state dipole moments, we can only compare our results with those observed for ground state dipole moments.

The dipole moments of all the monomers except the thiophene ones show the same trend, i.e., an increase in μ is observed following their $\pi - \pi^*$ excitation (see Table 5.9). For the cyano-derivatives electron correlation increases the total dipole moment for aromatic PCNTH monomer, but the reverse is observed for the quinoid PCNCY and PCNFV monomers which are in keeping with their parent quinoid monomers. In brief we can say that the effect of electron correlation on aromatic type polymers is to give dipole moments that are smaller than the corresponding HF results. For quinoid type polymers the opposite effect is observed. For the PA monomers the same electron correlation effect is identified. Still it is necessary to include electron correlation effects beyond single substitutions to adequately calculate the dipole moments of these heterocycles. This point is best illustrated

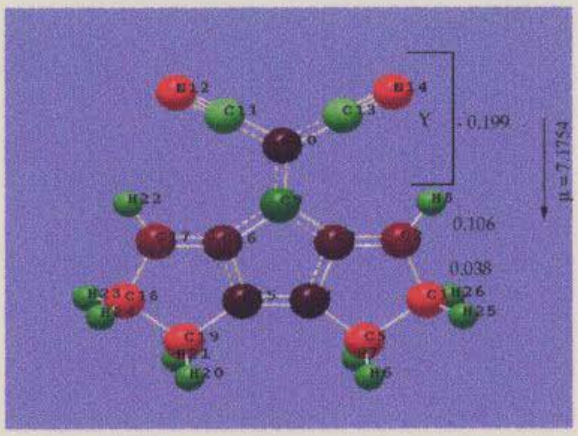

Figure 5.9: Mulliken charges and dipole moments in (D) for CIS/3-21G* excited state of PCNCY.

by a comparison with the results obtained with QCID/3-21G* for aromatic PFV, which has an essentially better agreement with the experimental one. The difference between the calculated and observed ground state dipole moments or the change in dipole moments following excitation may also be attributed to solvent effects in the experimental results [181]. The molecular unit lengths (see Table 5.9) as well as the molecular volumes (see Tables 5.7 and 5.8) of the monomer units in their ground and excited states are also calculated in order to see the relationship between their respective volume and electronic properties. The molecular volumes are determined using their Connolly [182, 183] surfaces (dot surfaces) by using Cerius[2] molecular simulation software [122]. A Connolly surface[3] is the Van der Waals surface of the molecule that is accessible to a solvent molecule. The surface is generated by rolling a probe sphere of a specified radius over the Van der Waal surface of the molecule. This feature could be used to "probe" a molecule, to map out the internal channel

[3]The Connolly [182, 183] function is used to calculate and display a Van der Waals surface or a Connolly surface for a molecular model.

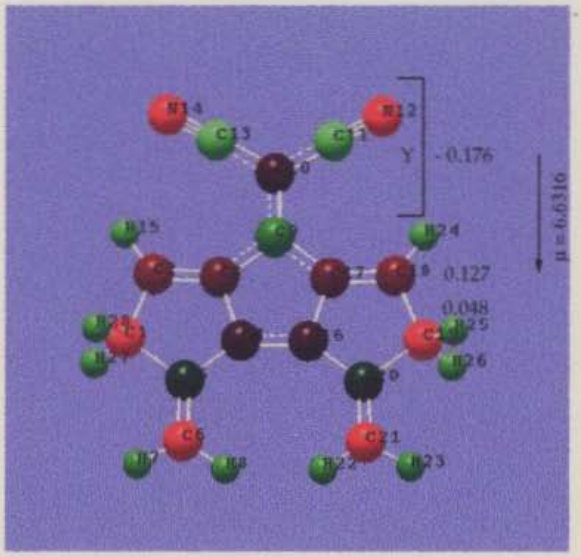

Figure 5.10: Mulliken charges and dipole moments in (D) for CIS/3-21G* excited state of PCNFV.

structure of a crystal, to consider the solvent accessible surface of a large molecule, or to understand the topography of a surface. In going from the ground to the excited states, the molecular volume of all the monomers are increased to some extent (~1 to 3 $Å^3$) except for the PCNCY monomer, which has not really shown a change in its molecular volume. None of the molecules show a large electronic charge diffusion and hence the compactness of the oligomers is sustained following the $\pi - \pi^*$ excitation.

5.3 Excitation Energy and Bond Length Alternation

In order to design a good intrinsic conducting polymer it is not enough only to find one with a small transition gap, but it is necessary also to consider the electron-phonon interaction to determine if a polymer is highly conducting [184]. The exci-

Table 5.10: Calculation of electron-photon coupling constant (ς) for different octamers with respect to excitation energy and bond length alternation calculated at CIS/3-21G* in their first excited states (Eq. 5.3).

Molecule	δ_r (Å)	E_{cal} (eV)	ς (eV/Å)
s-*cis* Polyacetylene	0.034	2.56	9.4
Polythiophene	0.006	2.83	58.9
Polycyclopentadiene	0.042	2.81	8.4
Polyfulvene	0.037	2.65	8.9
PCNTH	0.008	1.63	25.5
PCNCY	0.088	2.57	3.7
PCNFV	0.088	2.34	3.3

tation energy and bond dimerization are related to the electron-phonon coupling. The theoretical details could be found in the book by H. G. Kiess [185].

The Peierls instability [4] causes the chain of metallic equal bond lengths, which corresponds to a state of high symmetry, to distort. Hence the actual ground state has a broken symmetry, in the form of a *dimerized* or *bond altered* lattice. This broken symmetry state corresponds to the chemical picture of alternating short (double) and long (single) bonds. It is interesting to use the values of bond length alternation (bond dimerization) obtained from this study to calculate the magnitude of the electron-phonon coupling constant (ς), which basically relates the transition energy to the distortion via the following equation [50]:

$$E_{cal.} \equiv 2\triangle = 8\zeta\delta_r, \tag{5.3}$$

Here ζ is the electron-lattice coupling and $\triangle$, which has dimensions of energy, is a measure of the extent of the dimerization of the backbone (CH) lattice [185]. In physics terminology $\triangle$ is known as the dimerization or bond alternation order parameter and $2\triangle$ is our calculated pseudo-1D transition energy i.e., band gap, $E_{cal.}$. Table 5.10 shows the respective values of ζ for the octamers in the lowest excited state (S_1) calculated at the CIS/3-21G* level.

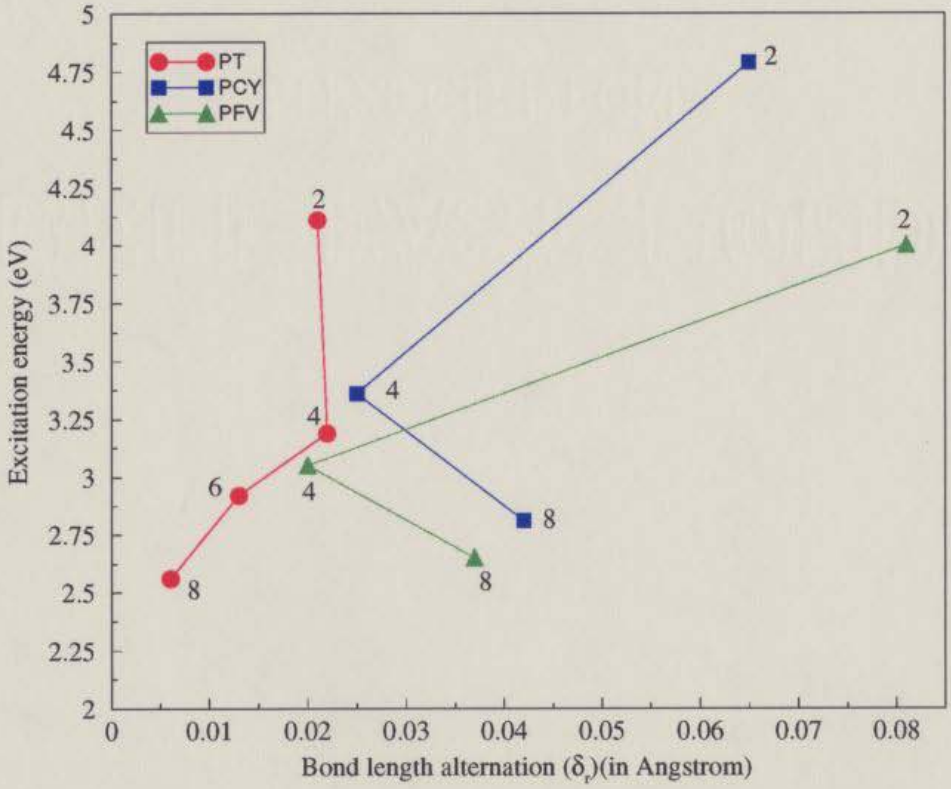

Figure 5.11: Bond length alternation (δ_r) plotted as a function of excitation energy for the parent heterocyclic oligomers PT, PCY and PFV.

Previous works on these molecules [18] show that these polymers undergo a polyacetylene-like bond length alternation [79]. Figure 5.11 has been plotted using the bond length alternation for the central ring of the oligomers vs. the respective excitation energy of that oligomer. The linear relationship could not be observed here probably due to the fact that strong electron-phonon coupling persists within the lattice. The polymers, optimized in this work, however, have different topologies. We have maintained the PA carbon backbone and the heteroatoms are attached additionally. To be precise, our calculations indeed show that a strong alternation persists. This is even evident from the interaction diagram (see Fig. 5.2). Our calculations on the polymers with X = S, CH_2 and $(CH)_2$ based on CI-singles geometry optimization, indicate a significant decrease of the δ_r values, relative to that of PA (see Tables 4.1, 4.3, 4.5, 4.7, 4.9, 4.11, 4.13 and 4.14). Cases for which the bond length alternation (δ_r) is relatively small, the ordering of the odd and even symmetry lowest excited states is $E(2A_g) < E(1B_u)$ [141]. For cases like PPV [141] when the "effective" bond length alternation is relatively large, the ordering of these states is reversed, giving rise to high photoluminescence efficiency and hence to improved LED devices. Experimentally it was verified also that the bond length alternation takes place over the whole molecule [92].

Therefore, we can see that in cases of PT and PCNTH oligomers, even though the sulfur appears to play a role in their π-electron structures, the bonding nature with neighbouring carbon atoms to form the heterocycle leads to significant change in the chain stiffness, electron-phonon coupling constant, geometry relaxation etc.

5.4 Variation of Excitation Energy due to Chain Length and End Groups

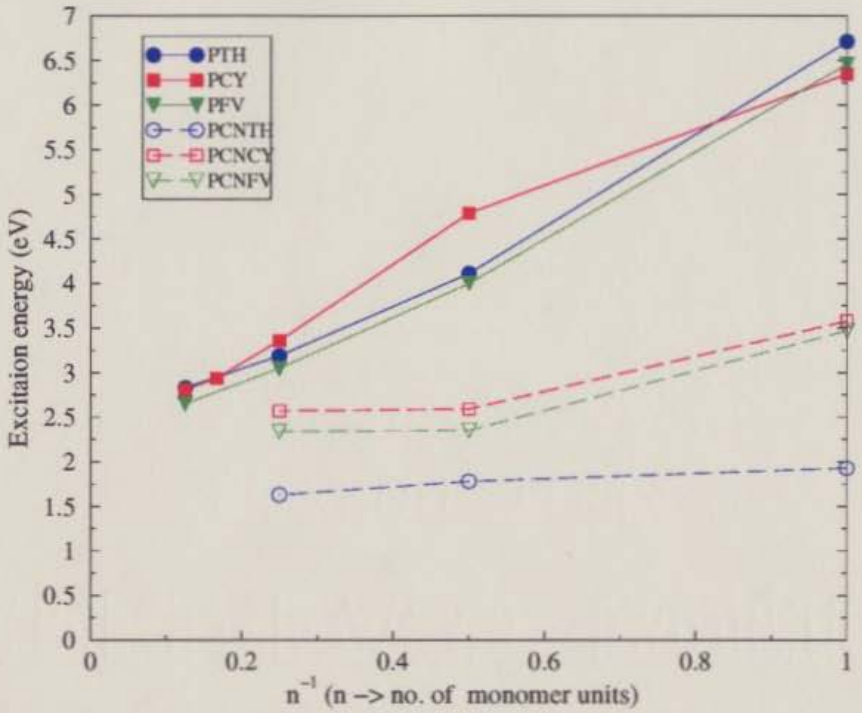

Figure 5.12: Excitation energy as a function of inverse chain length for the six heterocycles under study.

Figure 5.12 shows the evolution of the lowest singlet energies of the six polymers as a function of inverse number of their monomer units. It is discernible from Fig. 5.12 that as the chain length grows, the transition energy separation progressively decreases. The extent of π conjugated systems constitutes the essential structural parameters which controls the magnitude of the energy gap, conductivity and electro-activity of these conducting polymers. The effective mean conjugation length (MCL), which is defined as the number of undistorted sequences of the single and double bonds, is important in investigating finite polymers. Hence it is neces-

sary to follow the electronic structure trends with increasing chain length until a stabilization is reached, otherwise results cannot be reliably extrapolated to long chains. It has been reported in several works on the basis of the conductivities of short-chain oligomers or of Raman and IR spectra that the MCL values for PT range from 6 to 12 C_α-$C_{\alpha'}$ linked thiophene rings [81, 92]. The MCL value also indicates that the neutral polymers are not infinitely long but instead consist of a series of π-segments containing only 6-12 units, which could be generated by periodic bends and twists along the polymer chain. For such a conjugation length, the S_0–S_1 transition energy extrapolated quadratically from our theoretical results is 2.71 eV (i.e., for 12 repeat units of PT), to be compared with the 2.6 eV measured experimentally [186]. In an isolated thiophene chain study, Horowitz *et al.*, have shown that the band gap of long oligomers (n=12) and of the polymers is roughly independent of chain length and the transition from short and long oligomers occurs between 9 and 11 thiophene rings [92]. The theoretical chain length dependence of the S_0–S_n transition energies are in good agreement with the experimental ones (Fig. 5.13). Both theoretical and experimental [62, 92, 170, 186] data illustrate that the first absorption maximum is markedly shifted to lower energies as the chain length grows. A red shift proportional to the inverse number of repeat units also prevails in many other conjugated polymers [94, 141, 187].

Remarkably enough, the elongation of the thiophene ring from monomer to octamer, shifts the corresponding absorption peaks to red from 222 nm to 438 nm in the lowest singlet excited state, in ground state this shift is found from 96.9 nm to 160.8 nm. Hence the energy shift in going from monomer to octamer for excited state is more than three fold in comparison to the shift observed in

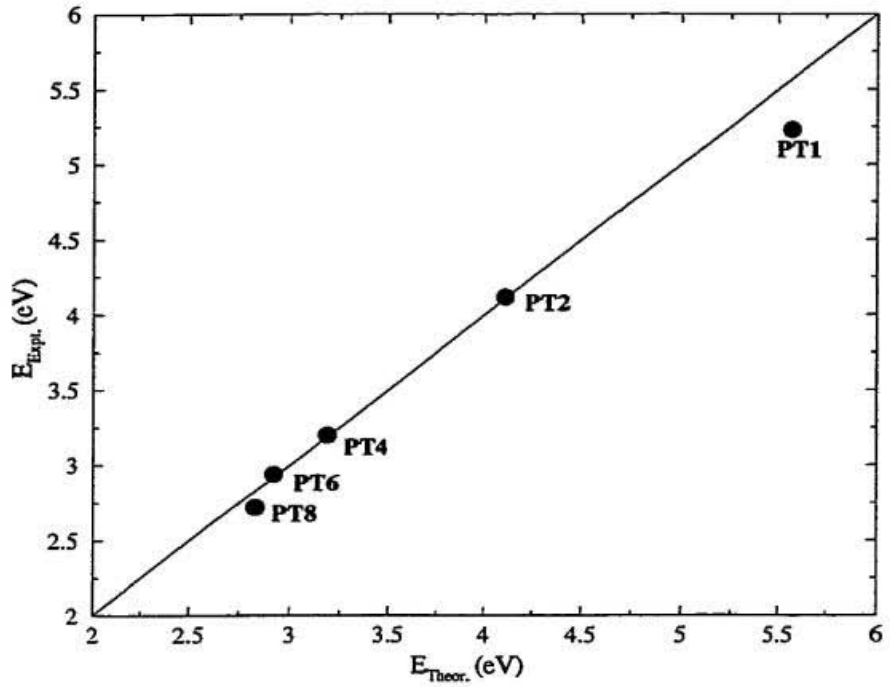

Figure 5.13: Plot comparing the CIS/3-21G* excitation energies (in eV) for the PT oligomers versus the experimental values obtained from several references [62, 81, 92, 170, 186].

ground state. Our results match well with the excited state property study of α-terthiophene (αT_3) by Reyftmann and others [170] using fluorescence and laser flash spectroscopy, where they have observed a red-shift of about 90 nm in going from αT_3 to αT_4. The shift suggests greater electron delocalization in the excited states of thiophene oligomers compared to their ground states, resulting from difference in geometry in their ground states and the lowest excited states. This can be generalized as well for other oligomers investigated in our study. The theoretical chain-length dependence of the $S_0 - S_1$ transition energies for thiophene oligomers with 2-8 monomer units are in good agreement with the experimental data [62, 186]

(see Table 5.14 and Fig. 5.13).

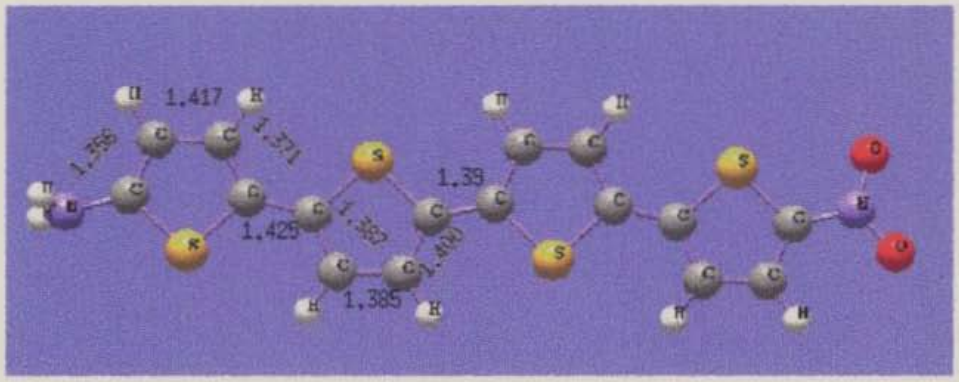

Figure 5.14: Structure of the amino (NH_2) and nitro (NO_2) group substituted aromatic PT tetramer. The numbers indicate bond lengths in Å.

Substitution or blocking of the oligothiophenes on both the α-carbons is very effective to enhance chemical stability, while the resulting compounds remain highly electroactive [188]. For the purpose of investigation, we have grafted the two electroactive groups – NH_2 and NO_2 – by substituting the two hydrogen end-groups of αT_4 along its conjugation path (see Fig. 5.14). The push-pull[4] type molecule has been constructed by appending an amino group to one end and a nitro group to the other end of the αT_4 chain. In such a case we see that the excitation energy is lowered to 2.97 eV in contrast to its unsubstituted analog with 3.19 eV. This red shift of the lowest electronic transition can be related to the fact that the derivatization gives rise to an asymmetric stabilization of the FMOs. This stabilization is asymmetric in a sense that the energy of the LUMO level is more affected than that of the HOMO level, a well documented feature [189, 190] of thiophene oligomers. Significant change in the colour of the light emitted by a light

[4]Electron donating (pushing) amino group and electron accepting (pulling) nitro group.

emitting device (LED) could occur due to the addition of such electroactive groups along the backbone of thiophene oligomers [191]. The addition of push-pull and electron-withdrawing $(C_2N)_2$ substituents has very different effects upon the energy levels. The appendage of either type of substitutes results in a decrease of the HOMO–LUMO energy gap, however this is accomplished in a different manner. When cyano-groups are added to the parent oligomers, the energy of the HOMO level is destabilized considerably but the energy of the LUMO level remains unchanged. The nitro and amino groups stabilize the LUMO and leave the HOMO unchanged. Our findings are analogous to the work carried out by Davis *et al.*, [94] on poly(*p*-phenylenevinylene) using Pariser-Parr-Pople-CIS method.

The effects on the ground state geometries of αT_4, of the NH_2/NO_2 groups grafted to the conjugated segment are very local. With respect to αT_4, only the geometry of the two thiophene end-rings to which the substituents are concatenated are significantly modified. These structural deformations lead to a small decrease in δ_{ring} within the external rings. However, in the singlet excited state, even stronger geometrical deformations are induced. It has been noticed that, if the main lattice distortions occur in the two end-thiophene rings, the geometry of the other rings is also modified (see Fig. 5.14). This difference can be explained by the fact that, in S_1, all the four thiophene rings are involved in the charge transfer process, while, in S_0, the charge supplied by the two electroactive groups is mainly injected to the two external rings. As observed in substituted polyenes [187] and on poly(*p*-phenylenevinylene) [94] derivatives, the electronic transition to the S_1 state, is red-shifted due to the appendage of these end-groups. The amplitude of this shift is proportional to the amount of charge transfer. Hence, it will be quite interesting

to see the effects of the cyano-bridging group connected to the sides along with the push-pull substituents acting as dangling end-groups on the geometry and the energy of these five-membered ring molecules.

5.4.1 Effects of Electron-Accepting and Donating Groups

It has been verified both theoretically [104, 105, 106, 107, 187, 192] and experimentally [45, 46] that the electron accepting and donating groups play a very important role in the formation of small band gap conjugated polymers. Havinga and his coworkers [42, 119] have proposed an efficient route to design and synthesize small band gap polymers by bringing together electron-donating and -withdrawing groups along the conjugated backbone. The reasons for this small band gap formation can be easily understood from the following fact: a conjugated polymer is developed by regular alternation of donor- and acceptor-like regions, possibly separated by neutral parts. If these donor and acceptor regions are extended, we have a polymer which is a one-dimensional analogue of an inorganic $n-i-p-i$ superlattice structure (see Ref. [193]). In such structures, it is well known that both the valence and the conduction bands are bent by space charge effects and a small band gap results when the spatial alternation of the edges of the bands is taken into account. The structure of the unit cells of PCNTH, PCNCY and PCNFV consist of two of their parent repeat units bridged by a strong electron-accepting dicyanomethylene group.

In a separate study the energy variation and bond length alternations at the CIS/3-21G* level for fulvene octamers are calculated for different end groups like H_2, CH_2, and S (see Table 5.11). It is seen that the lowest transition energy is

obtained for the CH_2 end group followed by the S and H_2 end groups.

Comparing the results obtained for PT, PCY, PFV with the PA skeletal (i.e., *trans-cisoid* polyacetylene in case of PT and *cis-transoid* polyacetylene in cases of PCY and PFV) energetics we find similarities if account is taken of the differences of structures and the presence of heteroatoms. These similarities suggest that PT can be viewed as being analogous to *trans-cisoid* PA with a structure formed by a sp^2 polyene chain with four carbon atoms in the unit cell and a sulfur heteroatom bound by covalent coupling to neighbouring carbon atoms to form the heterocycle. The influence of the sulfur atom on the electronic band structure mainly depends on the strength of the carbon-sulfur coupling. C-S coupling is weaker than the C-C coupling and the resonance integral for C-S is about three times smaller than that for the C-C ones [194]. Hence, the sulfur atom interacts weakly with the π-electrons of the C-C backbone. However, its presence modifies the band structure to a certain extent by breaking the electron-hole symmetry which exists for a carbon chain such as *trans*-$(CH)_x$.

The orbital patterns of the HOMO and the LUMO for the PCNCY and PCNFV octamers on the basis of CI-singles calculations are found to be similar and are shown in Figs. F.21, F.24, F.27, and F.30. It is an interesting finding that the contribution of the electron accepting group Y= >C=$C(CN)_2$ to the HOMO of the frontier backbone is negligibly small, while it plays quite significantly in contributing to the LUMO of these polymers. The reason why PCNTH has a larger electron affinity than the other two cyano-substituted polymers can be explained by looking into the fact that the HOMOs of the all three cyano-substituted polymers are more or less the same (and hence their respective ionization potentials) whereas

Table 5.11: Energy variation due to different side-groups in PFV oligomer. Comparison of excitation energies (in eV) and bond length alternations (in Å) at CIS/3-21G* in their most stable (planar) conformation are also provided.

Heterogroup	Oligomers	Point Group	δ_r (Å)	E (eV)	$\frac{(\alpha-\beta)}{(\beta-\beta')}$ [a]	δ_{ring} (Å)
H_2	monomer	C_{01}		6.458		0.197
H_2	dimer	C_S	0.081	4.002	1.077	0.103
H_2	tetramer	C_S	0.131	3.050	1.104	0.138
H_2	octamer	C_S	0.157	2.650	1.121	0.160
CH_2	octamer	C_S	0.132	2.646	1.113	0.150
S	octamer	C_S	0.115	2.649	1.099	0.132

[a]The ratio between C−C and C=C bonds. The values close to 1 indicate large bond lenth deformations.

the LUMO of each varies by different amount depending on their side groups. One can see from Tables 5.7 and 5.8 that the Y group of PCNTH has the smallest net negative charge (-0.136761) than that of PCNCY and PCNFV, showing that the Y group in PCNTH acts as a relatively stronger electron acceptor among the cyano-substituents. Whereas the X group (*i.e.,* S in this case) has the largest net positive charge among these three, which, in effect causes the lowering of the LUMO by electron donation as well as by strong orbital mixing. The electron donation ability of sulfur is hence higher than the rest two, thereby making PCNTH a potentially important conducting polymer.

According to Hong *et al.,* [15, 16, 78] PCY possesses a quinoid geometry exhibiting a band gap of 1.21 eV which was attributed to the decreased interference of the CH_2 group with the π-systems compared to the π-donating groups. Both PCNCY and PCNFV are found to have larger band gaps than the corresponding thiophene analogue, PCNTH. This means that the replacement of $>CH_2$ and $>(CH)_2$ groups in PCNCY and PCNFV by the strong electron-donating S atoms not only makes

the polymers better intrinsic conductors of electricity but also better candidates for forming conducting materials through doping (both p- and n-doping). Bakhshi *et al.*, [104, 105] in their *ab-initio* Hartree-Fock crystal orbital study has observed a different trend - where they have observed PCNCY to have smaller band gap than the thiophene analogue, PCNTH. This is contrary to our HF ground state as well as CI-singles excited state studies. Toussaint and Bredás [106] in their AM1/VEH studies on PCNCY polymer have reported a band gap of 0.16 eV and the conjugated skeleton associated to it as ~0.5 eV. We have followed here an identical rationalization for the transition energies obtained in our studies in relation with the bonding-antibonding electronic patterns appearing on the HOMO and the LUMO levels of the conjugated PA skeletons and their corresponding cyano-derivatives. We have also compared these levels to those appearing in *trans-cisoid* and *cis-transoid* type parent polymers. The transition energies calculated for the *trans-cisoid* and *cis-transoid* type parent monomers, and their cyano-derivatives along with the corresponding conjugated skeletons are compiled in Table 5.11. This skeletons posses the identical structure as their respective parents, except that the dicyanomethylene group and the S, CH_2, C_2H_2 on the X position are replaced by two hydrogen atoms.

The first calculated $\pi-\pi^*$ excitation energies of the cyano-substituted molecules and their parent molecules follows a different order, for parent oligomers the order is PFV<PCY<PT and for their derivatives it is PCNTH<PCNFV<PCNCY. The s-*trans* form of both PCY and PFV have smaller $E_{cal.}$ than the s-*cis* forms, these observations are in agreement with the results of CIS calculations on *trans-cisoid*- and *cis-transoid*-PA for which the *trans-cisoid* form exhibits a transition energy of

5.24 eV and that for *cis-transoid* form it is 6.35 eV. The trends observed in our results are comparable with those obtained by other investigators [17, 37, 75, 76, 77, 79, 106, 110, 118, 166, 195, 196].

5.5 Extrapolation of Trends in Bulk Polymers

For conjugated polymers the trends in band gaps can be extrapolated from excitation energy calculations in such a way as to show that from mesoscopic scale one can comment roughly on their bulk electronic properties. It is useful to consider the extrapolation of the data in Fig. 5.15 to the intercept, $m^{-1} = 0$, which corresponds to the limiting case of infinite chain length polymer. It has been shown previously by other investigators that extrapolation of this type yield good estimates for the transition energies of oligomer moieties [58, 74, 197].

For the purpose of showing the trends in excitation energy for bulk polymers we have employed the following two regression equations [74, 198]:

$$E = a_0 + a_1 m^{-1} \text{ (linear)} \tag{5.4}$$

$$E = a_0 + a_1 m^{-1} + a_2 m^{-2} \text{ (quadratic)} \tag{5.5}$$

where a_0 is the intercept corresponding to the transition energy in the polymer of infinite length, a_1 is the slope of the line and m^{-1} is the reciprocal length of the oligomer chain, where m denotes the number of carbon atoms located on the shortest pathway between the two ends of the chain. The results of the data using the regression Eqs. 5.4 and 5.5 are given in Table 5.12. The HF/3-21G* calculated

energies and corresponding intercepts a_0, of Eqs. 5.4 and 5.5 are about 2.5-3 eV higher than the CIS/3-21G* results. It has been observed [118] that MNDO results overestimates the band gap in polymers by 3-4 eV. Hence, CI-singles give results which are close to the respective experimental band gap in polymers. For example, the CIS calculated intercept of Eq. 5.4 (5.5), which corresponds to the transition energy in the polymer of infinite length is 2.36 (2.52) eV for polythiophene. These numbers compare quite favourably with the respective experimental estimates obtained by other researchers (2.0-2.8 eV [187, 197, 199, 200, 201, 202, 203, 204]).

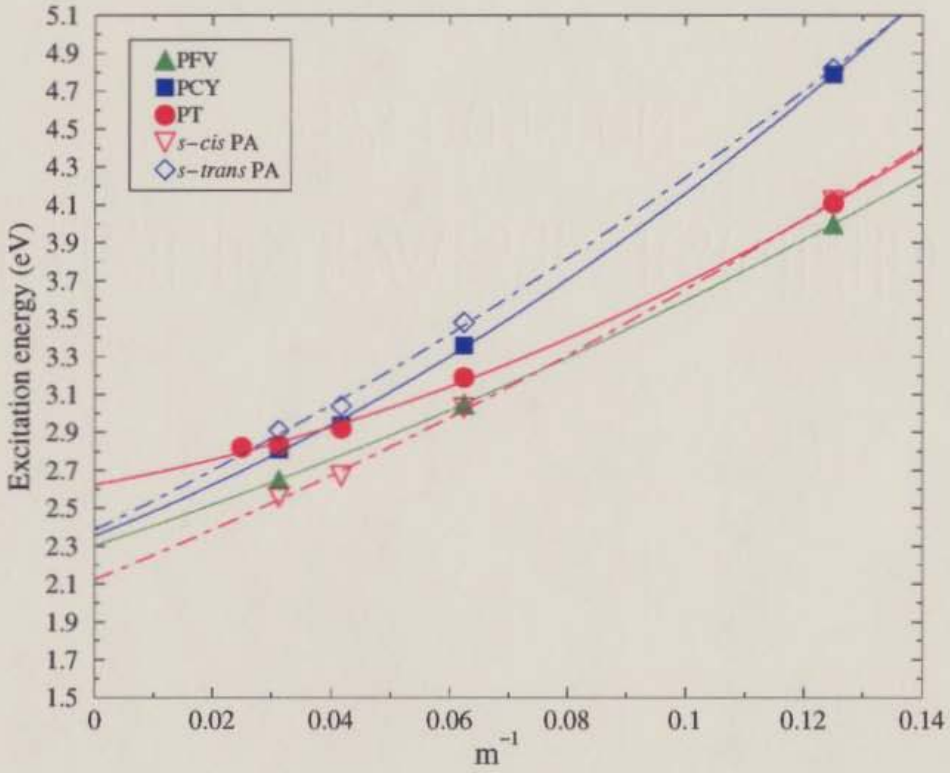

Figure 5.15: Quadratic relationship between the CIS calculated excitation energies (Eq. 5.5) and the inverse of the chain lengths (m^{-1}) for *s-cis*- and *s-trans*-PA, PT, PCY and PFV, where m denotes the number of carbon atoms located along the shortest pathway between the two ends of the chain.

In Fig. 5.15 we present for the PT, PCY, PFV oligomers and their unsubstituted s-*cis*- and s-*trans*-PA backbone, the evolutions of the inverse chain length: namely the transition from the ground state S_0 to the first singlet excited state S_1. We note that the excitation energies evolve almost linearly with inverse chain length. We also note that a linear relationship between the triplet transition energies and the inverse number of oligomer rings is developed as well (see Tables 5.1 through 5.6).

The excitation energies calculated for the cyano-substituted oligomers are compared in Table 5.14 to the values obtained for their parental moieties. The singlet excitation energies for the cyano-derivatives are consistently lower than those obtained for the unsubstituted oligomers which is consistent with others observations as well [104, 107]. Linear extrapolation of the calculated transition energies to the infinite chain length limit, leads to a transition energy gap in PCNTH that is around 0.81 eV lower than that in PT. The slope, a_1, and the non-linear energies $E_{n.l.}$ are presumably erroneous for the cyano-substituted polymers, since there are not enough points (three points for each oligomer moiety) on which a close approximation could not be achieved. In all three cases the transition energy of monomer (i.e., $m = 4$) does not fit well with that of the corresponding dimer and the tetramer values in the linear curve fitting (the larger values of correlation coefficients indicate the unacceptability of these extrapolated values of transition energies). The origin of this discrepancy is not clear to us, but is probably connected with the parameterization of the cyano-sidegroup in the CIS method. For this reason we have calculated the slopes for the cyano-derivatives with the x-axis taken as inverse of the number of carbon atoms located on the shortest pathway between the two

ends of the chain instead of the inverse of the number of monomer units.

The dependence of the calculated excitation energy E on m^{-1} levels off at the higher values of m and thus the non-linear extrapolation should lead to better results for these polymers. For this reason, we see that the linear curve fitting shows polyclopentadiene having the lowest transition energy when extrapolated, which is not acceptable (refer to Table. 5.12). Hence the quadratic non-linear curve fitting seems more reasonable for this purpose. The results obtained from quadratic fittings are also provided in Table 5.12 at the last column. Among the parent oligomer moieties, PFV is characterized by the smallest intercept, and therefore the corresponding polymer of PFV shows higher intrinsic electrical conductivity (since $\sigma \propto E^{-1}$) compared to PT and PCY.

5.6 Summary of Electronic Findings

One must be careful in comparing calculated CIS energies with experimental data. There may be states present with zero oscillator strengths which are seen in optical spectra, just as there may be states with non-zero oscillator strengths which are not seen. Diffuse functions sometimes have proven helpful in obtaining the complete manifold of excited states for a molecule basically for the purpose of determining the higher lying Rydberg states. Some states could have energies quite high in comparison to experimental results regardless of the basis sets used. It happens so because of the fact that this deficiency is related to the neglect of higher excitations (beyond single excitations) in the configuration interaction, which could be partially taken care of with the QCISD method. Still, the correct ordering of states

Table 5.12: Results of the regression treatments of CI-singles calculated excitation energies (in eV) for polymers according to Eqs. 5.4 and 5.5. The total CIS energies ($E_{Tot.}$) are also given (in a.u.).

Heterocycle	$E_{Tot.}$	$E_{expt.}$	$a_0 \pm \triangle a_0$ [a]	a_1 [b] $\pm \triangle a_1$	r[c]	$E_{n.l}$ [d]
s-cis PA	-154.03	1.9 [e]	1.99 ± 0.04	16.95 ± 0.52	0.999	2.12
s-trans PA	-155.20	N.A. [f]	2.21 ± 0.05	20.77 ± 0.68	0.999	2.53
PT	-548.36	2.0-2.8 [g]	2.36 ± 0.04	13.92 ± 0.56	0.998	2.52
PCY	-192.62	N.A.	2.07 ± 0.11	21.57 ± 0.93	0.998	2.35
PFV	-230.26	N.A.	2.17 ± 0.05	14.51 ± 0.59	0.999	2.30
PCNTH	-1353.65	0.8 [h]	1.55 ± 0.05	3.08 ± 0.59	0.982	1.43
PCNCY	-641.05	N.A.	2.08 ± 0.31	11.5 ± 3.76	0.950	2.86
PCNFV	-716.33	NA	1.78 ± 0.36	12.89 ± 4.35	0.947	2.69

[a]Linear intercepts calculated using Eq. 5.4

[b]Slopes are calculated with the x-axis taken as inverse of the number of carbon atoms located on the shortest pathway between the two ends of the chain.

[c]Correlation coefficient.

[d]Non-linear intercept results calculated using Eq. 5.5 corresponding to the transition energies in the polymers of infinite length.

[e]See reference [103]

[f]Not available.

[g]Band gap in the solid state or in solution [199, 203, 201, 202, 200, 204, 197].

[h]See refs. [46, 45].

and relatively good energetic results are obtained using the computationally less expensive CIS model. It is clear from Table 3.1 and Fig. 3.4 that only CIS results for transition energies match well with the experimental one - the CIS/3-21G* result being the closest among all. The data in Fig. 5.15 yields a value of $E_{tran.} = 2.52$ eV for polythiophene in agreement with the experimentally obtained value of 2.0-2.8 eV [197, 199, 200, 201, 202, 203, 204]. For aromatic cyclopentadiene monomer the CIS/3-21G* calculated value for excitation energy is 4.77 eV (see Table 5.9) whereas the experimental value for the same excited state was reported to be 5.26 eV by Frueholz *et al.*, [196]. The aromatic polyene monomer (C_2H_6) shows a transition gap of 5.24 eV compared to the 5.92 eV peak potential from UV absorption spectroscopy [75]. The CIS method thus underestimates the experimental excitation energies by only 0.5-0.7 eV (11% error). The transition energies for PA monomer through tetramer results also show very close agreement with the experimentally obtained vertical excitation energies from UV-absorption spectroscopy (see Table 5.14) [75]. The band gap determined as 2.12 eV which is slightly lower than the absorption onset λ_{max} of 1.9 eV [103]. The extrapolated band gap of PT is found lying at 2.52 eV which is also very reasonable in comparison to the experimental absorption maximum at 2.5 eV [199, 81]. It has been reported that the absolute error increases slightly with the increasing chain length [75].

The $\pi - \pi^*$ excitation energies of the parent polymers are ordered as

PFV<PCY<PT with *s-cis* PA<*s-trans* PA,

and for their cyano-substituted oligomers the order is

PCNTH<PCNFV<PCNCY.

Table 5.13: Comparison of excitation energies (in eV) for polymers and oligomers in their most stable (planar) configuration with other theoretical results.

Method/Basis set	Oligomer	PT	PCY	PFV	PCNTH	PCNCY	PCNFv
MNDO[a]	∞	6.48	6.75	6.37	5.73	6.34	5.90
AM1[a]	∞	6.43	6.52	6.32	5.70	6.07	5.78
RHF/3-21G*	dimer	10.16	10.53	9.25	7.34	7.06	6.57
LSDA/3-21G*	dimer	2.99	2.78	2.08	0.87	0.75	0.65
RCIS/3-21G* 1SCF	monomer				3.30	4.24	4.11
RCIS/3-21G* (Opt)	monomer	5.57	6.35	6.46	1.93	3.58	3.47
RCIS/3-21G* 1SCF	dimer	5.11	5.81	4.80	2.99	3.32	3.03
RCIS/3-21G* (Opt)	dimer	4.11	4.79	4.00	1.78	2.59	2.35
RCIS/6-31G* (Opt)	dimer	4.00	4.61	3.85	1.67	2.44	2.20
RCIS/3-21G* (Opt)	tetramer	3.19	3.36	3.05	1.63	2.57	2.34
RCIS/3-21G* (Opt)	octamer	2.83	2.81	2.65			

[a]Ref. [18]

Table 5.14: Comparison of experimental and calculated excitation energies (in eV) for different polymers and oligomers in their most stable (planar) configuration. Experimental values are given in parentheses.

Oligomer	PA	PT	PCY	PFV	PCNTH	PCNCY	PCNFV
monomer	5.24(5.92)[a]	5.57(5.23)[b](5.37)[c]	6.35	6.46	1.93	3.58	3.47
dimer	4.13(4.41)[d]	4.11(4.05)[e](4.13)[f](4.12)[g]	4.79	4.00	1.78	2.59	2.35
tetramer	3.03(3.02)[h]	3.19(3.22)[i](3.16)[j](3.20)[k](3.18)[k]	3.36	3.05	1.63	2.57	2.34
octamer	2.56	2.83(2.72)[l]	2.81	2.65			
∞	2.12(1.9)[m]	2.52(2.0-2.8)[n]	2.35	2.3	1.4(0.8)[o]		

[a]Ref. [75]
[b]Ref. [205]
[c]Ref. [100]
[d]Ref. [75]
[e]Ref. [62]
[f]Ref. [92]
[g]Ref. [100]
[h]Ref. [75]
[i]Ref. [170]
[j]Ref. [62]
[k]Ref. [92]
[l]Ref. [186]
[m]Ref. [103]
[n]Refs. [199, 203, 201, 202, 200, 204, 197]
[o]Refs. [46, 45, 104]

Chapter 6

Conclusions

We have shown that *ab initio* CI-singles calculations provide a deep understanding of the geometric and electronic properties of the thiophene and cyclopentadiene based conjugated organic materials. In this research we have described the one-electron structure of the unsubstituted and cyano-substituted neutral olgimers, distinguishing between the delocalized and localized characteristics of the molecular orbitals. An overall analysis of the CIS expansion of the excited states in comparison with the several experimental results points to the importance of the correlation effects. From the present study we can therefore derive the following important conclusions:

1. The molecular geometries for the five-membered ring oligomer moieties showed considerable modification in going from the ground (S_0) to the first excited state (S_1) evolving towards a full aromatic benzoid like structure with almost equal bond lengths along the molecular backbone.

2. Lattice distorsions in the lowest excited states are more localized and asymmetric in the cyano-derivatives in comparison to their parents.

3. HF theory underestimates electron delocalization, resulting in shorter C=C

and longer C–C bonds.

4. From the absolute deviations calculations, HF/3-21G* geometries show the lowest average errors in the S_0 state, while STO-3G basis set shows ~20% larger errors than most of the double-ζ basis sets.

5. Including electron correlation with perturbation approaches (MP2 etc.) results in elongated C–C bond lengths.

6. The S_1 geometries of PT evolve towards a quinoid structure while PCY and PFV evolve towards aromatic structures.

7. The geometry modification extends over the six central rings of PT, PCY, PFV.

8. The lowest electronic transitions of PT, PCY, PFV and their cyano-derivatives PCNTH, PCNCY and PCNFV are satisfactorily explained using CI-singles calculations.

9. In view of the molecular orbital analysis, for polymers containing aromatic and quinoid geometries, the heteroatomic substitutions and the geometry relaxation phenomenon contribute significanly in determining the excitation energy. Concatenation of electron withdrawing and donating groups lowers the excitation energy of the oligomers.

10. The transition energy is proportional to δ_r for constant electron-phonon coupling.

11. The excitation energies can be extrapolated to obtain the band gap for the bulk polymers. For PT the extrapolated band gap is 2.52 eV, for PCY it is 2.37 eV and for PFV it is 2.3 eV.

12. The S_1 state corresponds to a HOMO→LUMO transition and gets red shifted with increasing chain length.

13. The red shift for $\alpha T_1 \rightarrow \alpha T_8$ in the S_1 state is more than three fold in comparison to that in the S_0 state.

14. The different bridging and/or side-groups, when grafted along or beside the carbon backbone, lower the symmetry as well as the transition energies.

15. The transition energies in relation with the bonding-antibonding electronic patterns appearing on the HOMO and the LUMO levels of the conjugated PA skeletons and the corresponding cyano-derivatives of PT, PCY and PFV indicate that the replacement of $>CH_2$ and $>(CH)_2$ groups in PCNCY and PCNFV by the strong electron-donating S atoms not only make the polymers better intrinsic conductors of electricity but also better candidates for forming conducting materials through p- and n-type doping.

16. Electron correlation via CIS method gives better dipole moment agreement with the experimental results than other methods.

17. The singlet states have the largest oscillator strengths while the triplet states have oscillator strengths near zero.

18. Basis sets higher than 3-21G* underestimate the energies and do not show

much of difference in the geometry of molecules compared to the experimental results.

These theoretical results will be useful in explaining a variety of photo physical phenomena like picosecond photo induced absorption. By the very nature of our calculations, we have not included the dopant effects which indeed play a crucial role in the highly conducting polymer compounds. The interaction of the heteroatoms with the π-conjugated carbon backbone in the parent polymers show that in cases of PCY and PFV the respective heteroatoms $>CH_2$ and $>C{=}CH_2$ interact rather weakly compared to that found in PT where the $>C{=}S$ group interact strongly with the FMO of the C-C backbone thereby increasing the bandgap. Therefore, it is expected that the two polymers PCY and PFV could be doped with n-type dopants such as alkaline metals in order to produce even lower bandgap materials. Polythiophene can be both n- and p-dopable, although the stability of the n-doped form is relatively poor [103]. Neutral PT is an insulator. The highest conductivity observed for the p-doped form of PT is 2000 $S.cm^{-1}$ [206]. In the cases of cyano-derivatives a different trend is observed where the $>C_2{=}(C{\equiv}N)_2$ side group attracts electrons from the FMO and the bridging atoms (X = S, CH_2, C_2H_2). It will be, therefore, quite interesting to see the doping effects on these heterocycles.

Since the interaction of the bridging atoms of PCY and PFV oligomers with the π-electronic system of the conjugated backbone is very weak, the electronic effect of these bridging atoms on the excitation energy is also quite small. Because of this weak interaction, the bond length alternations of these oligomers change slightly in comparison with that observed in polyacetylene. On the other hand the sulfur lone pairs in PT oligomers interact rather strongly with the FMOs of the backbone

which is exposed in the nature of rather large alternation in the bond lengths compared to that observed in PA.

6.1 Future Work

On the basis of our theoretical results it is not straightforward to comment on the subtle phenomena occurring inside the microscopic domain of the π-conjugated polymers. In order to characterize for the suitable nonlinear optical (NLO) properties of these π-conjugated systems we need greater details. The ease with which these organic materials can be chemically modified along with their tunable properties make them ideal candidates for the optoelectronic and photonic applications. More attention is still required be paid to the evolution of the first- and third-order nonlinear optical response of these π-conjugated polymeric systems [114]. In order to understand the photophysics of excitation energy transfer we need to account for the following:

(i) to go beyond the frozen geometry models of polarizabilities and hyperpolarizabilities which can also prove to be essential in short moieties of PT, PCY, PFV and their cyano-derivatives where electron-lattice coupling effects are known to be important.

(ii) to calculate the nonlinear-optical properties in these molecules properly, the influence of soliton-pair relaxation effects are also required to be incorporated.

In this framework, it would be most useful to extend this work for the relaxation dynamics calculations, as carried out for PA [51], on these short and intermediate molecular moieties. Systematic studies could also be performed using the modalities

followed in this thesis in order to demonstrate the relative importance of geometry relaxation and several coupling effects in other conjugated compounds. More work is expected indeed to quantify the relative importance of the solitonic effect in determining the bond dimerization, in the excited states of these potential candidates of conjugated polymers. In order to rationalize a wide range of experimental measurements and to provide a guideline in the design of these novel attractive materials, more exploration into the phenomenon would likely be very interesting.

Bibliography

[1] W. H. Meyer. *Synth. Met.*, 10:255, 1985.

[2] W. R. Salaneck and J. L. Brédas. *Solid State Commun*, 92(1-2):31–36, 1994.

[3] J. L. Brédas, D. A. dos Santos, J. Cornil,D. Beljonne and Z. Shuai. Eelctronic structure of isolated and interacting π-conjugated oligomer and polymer chains: A quantum-chemical approach to optical and charge-transfer phenomena. In J. L. Brédas, editor, *Proceedings of the Fourth Francqui Colloquium, Conjugated Oligomers, Polymers, and Dendrimers: From Polyacetylene to DNA*, pages 133–162. DeBoeck Université, 1998.

[4] R.E. Peierls. *Quantum Theory of Solids.* Oxford University Press, London, 1955. p. 108.

[5] A. J. Heeger. *Polyacetylene New Concept and New Phenomena*, pages 729–755. Volume 2 of Skotheim [115], 1986.

[6] W. R. Salaneck, S. Stafström and J. L. Brédas. *Conjugated Polymer Surfaces and Interfaces.* Cambdrige University Press, 1996. p.53.

[7] M. J. Rice. *Phys. Lett.*, A 71:152, 1979.

[8] W. P. Su, J. R. Schrieffer and A. J. Heeger. *Phys. Rev. Lett.*, 42:1698, 1979.

[9] J. A. Pople and S. H. Walmsley. *Molec. Phys.*, 5:15, 1962.

[10] A. J. Heeger, S. Kivelson, J. R. Schrieffer and W. P. Su. *Rev. Mod. Phys.*, 60:781, 1988.

[11] D.Baeriswyl in. *Electronic Porperties of Conjugated Polymers III.* Springer-Verlag, Berlin, 1989. H. Kuzmany, M. Mehring and S. Roth (Eds), p. 54.

[12] R. Hoffmann, C. Janiak and C. Kollmar. *Macromolecules*, 24(13):3725–3746, 1991.

[13] K. Nayak and D. S. Marynick. *Macromolecules*, 23:2237, 1990.

[14] I. Hoogmartens, D. Vanderzande, H. Martens and J. Gelan. *Synth. Met.*, 41-43:513, 1991.

[15] S. Y. Hong and D. S. Marynick. *Macromolecules*, 28:4991–4995, 1995.

[16] S. Y. Hong, S. J. Kwon and S. C. Kim. *J. Chem. Phys.*, 103:1871, 1995.

[17] S. Y. Hong and J. M. Song. *Synth. Met.*, 85:1113–1114, 1997.

[18] H. Subramanian. Investigation of geometric and electronic properties of conducting polymers using semiempirical approach. Master's thesis, Memorial University of Newfoundland, 1997.

[19] M. Ozaki, Y. Ikeda and I. Nagoya. *Synth. Met.*, 18:485, 1987.

[20] A. L. S. de Rosa and C. P. De Melo. *Phys. Rev. B*, 38:5430, 1988.

[21] T. Yamabe, K. Tanaka, K. Ohzeki and S. Yata. *J. Phys.*, 44:C3–645, 1983.

[22] M. Kertesz, Y. S. Lee and J. P. Stewart. *Int. J. Quan. Chem.*, 35:305, 1989.

[23] S. Y. Hong, M. Kertesz, Y. S. Lee and O. K. Kim. *Chem. Mater*, 4:387, 1992.

[24] J. L. Brédas and R. H. Baughman. *J. Chem. Phys.*, 83:1316, 1985.

[25] M. Murakami and S. Yoshimura. *J. Chem. Soc., Chem. Commun.*, page 1649, 1984.

[26] J. L. Brédas. *Adv. Mater.*, 7:263, 1995.

[27] A. K. Bakhshi. *Ann. Rep. R. Soc. Sect. C*, 89:147, 1992.

[28] F. Wudl, M. Kobayashi and A. J. Heeger. *J. Org. Chem.*, 49:3381, 1984.

[29] F. Wudl, M. Kobayashi, N. Colaneri, M. Boysel and A. J. Heeger. *Mol. Cryst. Liq. Cryst.*, 118:195, 1985.

[30] M. Kobayashi, N. Colaneri, M. Boysel, F. Wudl and A. J. Heeger. *J. Chem. Phys.*, 82:5717, 1985.

[31] N. Colaneri, M. Kobayashi, A. J. Heeger and F. Wudl. *Synth. Met.*, 14:45, 1986.

[32] J. L. Brédas, A. J. Heeger and F. Wudl. *J. Chem. Phys.*, 85:4673, 1986.

[33] I. Hoogmartens, P. Adriaensens, D. Vandezande, J. Gelan, C. Quattrochi, R. Lazzaroni and J. L. Brédas. *Macromolecules*, 25:7347, 1992.

[34] A. Karpfen and M. Kertesz. *J. Phys. Chem.*, 95:7680, 1991.

[35] J. M. Toussaint, B. Theémans, J. M. André and J. L. Brédas. *Synth. Met.*, 28:205, 1989.

[36] J. M. Toussaint and J. L. Brédas. *J. Chem. Phys.*, 94:8122, 1991.

[37] J. M. Toussaint and J. L. Brédas. *Synth. Met.*, 43:3555, 1991.

[38] M Hanack and G. Dewald. *Synth. Met.*, 33:409, 1989.

[39] M Hanack, G. Hieber, G. Dewald and H. Ritter. *Synth. Met.*, 41:507, 1991.

[40] G. Hieber, M. Hanack, K. Quest and J. Strähle. *J. Chem. Ber.*, 124:1597, 1991.

[41] M Hanack, G. Hieber, G. Dewald, K. Mangold, H. Ritter and U. Röhrig. *Electronic Porperties of Polymers amd Related Compounds.* Springer Series in Solid State Sciences; Springer-Verlag, Berlin, 1992. H. Kuzmany, M. Mehring and S. Roth (Eds), p. 401.

[42] E. E. Havinga, W. ten Hoeve and H. Wynberg. *Synth. Met.*, 55-57:299–306, 1993.

[43] E. E. Havinga, W. ten Hoeve and H. Wynberg. *Synth. Met.*, 29:119, 1992.

[44] A. K. Bakhshi, Y. Yamaguchi, H. Ago and T. Yamabe. *Synth. Met.*, 79:115–120, 1996.

[45] T. L. Lambert and J. P. Ferraris. *J. Chem. Soc. Chem. Commun.*, Com. 1/00813G:752–754, 1991.

[46] J. P. Ferraris and T. L. Lambert. *J. Chem. Soc. Chem. Commun.*, 18:1268–1271, 1991.

[47] W. R. Salaneck, I. Lundström and B. Rånby. *Conjugated Polymers and Related Materials: The Interconnection of Chemical and Electronic Structure.* Oxford University Press, Oxford, 1993.

[48] C. B. Naarmann, 1963. DB Patent 1179715, 1197228, 1179716, BASF Corp., FRG.

[49] C. B. Naarmann. *Synth. Met.*, 22:1, 1987.

[50] C .R. Fincher, C. E. Chen, A. J. Heeger, A. G MacDiarmid and J. B. Hastings. *Phy. Rev. Lett.*, 48(2):100, 1982.

[51] W. P. Su, J. R. Schrieffer and A. J. Heeger. *Proc. Natl. Acad. Sci.*, 77:5626, 1980.

[52] W. P. Su, J. R. Schrieffer and A. J. Heeger. *Phys. Rev.*, B22:2099, 1980.

[53] C. K. Chiang, J. Fincher, Y. W. Park, A. J. Heeger, H. Shirakawa, E. J. Louis and A. G. MacDiarmid. *Phys. Rev. Lett.*, 39:1098, 1977.

[54] J. L. Brédas in. *Handbook of Conducting Polymers.* T. A. Skotheim (ed), Marcel Dekker Inc., New York, 1986. p. 859.

[55] C. Alemán and L. Julia. *J. Phys. Chem.*, 100:1524–1529, 1996.

[56] R. R. Chance, D. S. Boudreaux, J. L Brédas and R. Silbey in. *Handbook of Conducting Polymers*, volume 2. T. A. Skotheim (ed), Marcel Dekker Inc., New York. p. 825.

[57] J. L. Brédas and G. B Street. *Acc. Chem. Rev.*, 18:319, 1985.

[58] J. L Brédas, R. Silbey, D. S. Boudreaux and R. R. Chance. *J. Am. Chem. Soc.*, 105:6555–6559, 1983.

[59] J. L. Brédas, J. Cornil, F. Meyers and D. Beljonne in. *Handbook of Conducting Polymers.* T. A. Skotheim (ed), Marcel Dekker Inc., New York, 1998. p. 1.

[60] J. L. Brédas, C. Adant, P. Tackx, A. Persoons and B. M. Pierce. *Chem. Rev.*, 94:243, 1994.

[61] M. H. Palmer, I. C. Walker and M. F. Guest. *Chem. Phys.*, 241:275–296, 1999.

[62] R. Colditz, D. Grebner, M. Helbig and S. Rentsch. *Chem. Phys.*, 201:309–320, 1995.

[63] L. S. Andrés, M. Marchán, M. Fülscher and B. O. Roos. *Chem. Phys. Lett.*, 211(1):125–134, 1993. and references therein.

[64] J. Fagerström and S. Stafström. *Phys. Rev. B*, 54(19):13713–13720, 1996.

[65] F. Negri and M. Z. Zgierski. *J. Chem. Phys.*, 102(13):5165–5173, 1995.

[66] J. Dreyer and M. Klessinger. *J. Chem. Phys.*, 101(12):4337, 1994. and references therein.

[67] R. D. Brown, P. J. Domaille and J. E. Kent. *Aust. J. Chem.*, 23:1707–1720, 1970.

[68] P. J. Harman, J. E. Kent, M. F. O'Dwyer and M. H. Smith. *Aust. J. Chem.*, 32:2579–2587, 1979.

[69] K. R. Asmis, M. Allan, O. Schafer and M. Fülscher. *J. Phys. Chem. A*, 101(11):2089–2095, 1997.

[70] H. Nakano, T. Tsuneda, T. Hashimoto and K. Hirao. *J. Chem. Phys.*, 104:2312, 1996.

[71] J. W. Blatchford, T. L. Gustafson and A. J. Epstein. *J. Chem. Phys.*, 105(20):9214–9226, 1996.

[72] M. K. Shukla and P.C. Mishra. *Chem. Phys.*, 240:319–329, 1999.

[73] J. B. Foresman, M. Head-Gordon and J. A. Pople. *J. Phys. Chem.*, 96:135–149, 1992.

[74] H. O. Villar, P. Otto, M. Dupuis and J. J. Ladik. *Synth. Met.*, 59:97–110, 1993.

[75] U. Salzner, J. B. Lagowski, P.G. Pickup and R. A. Poirier. *J. Comp. Chem.*, 18(15):1943–1953, 1997. and references therein.

[76] S. Y. Hong and J. M. Song. *Synth. Met.*, 83:141–146, 1996.

[77] S. Y. Hong and J. M. Song. *J. Chem. Phys.*, 107(24):10607–10615, 1997.

[78] S. Y. Hong, S. J. Kwon and S. C. Kim. *J. Chem. Phys.*, 103(5):1871–1877, 1995.

[79] Y. S. Lee and M. Kertesz. *J. Chem. Phys.*, 88(4):2609–2617, 1988.

[80] D. Beljonne, Z. Shuai and J. L. Brédas. *J. Chem. Phys.*, 98(11):8819–8828, 1993.

[81] J. Roncali. *Chem. Rev.*, 92:711–738, 1992. and references therin.

[82] J. L. Brédas and R. Silbey. *Conjugated Polymers.* Kluwer Academic, Dordrecht, 1991.

[83] M. J. Winokur in. *Handbook of Conducting Polymers.* T. A. Skotheim (ed), Marcel Dekker Inc., New York, 1998. p. 709.

[84] G. Tourillon and F. Garnier. *J. Electroanal. Chem.*, 135:173, 1982.

[85] S. Bruckener and W Porzio. *Makromol. Chem.*, 189:961, 1988.

[86] A. Bolognesi, M. Catellani, S. Destri and W. Porzio. *Makromol. Chem. Rapid Commun.*, 12:9, 1991.

[87] J. Kurti and H. Kuzmany. *Phys. Rev. B*, 44:197, 1991.

[88] Terbeek, C. Zimmerman and D. S. Burnell. *Molecular Phys.*, 74:1027, 1991.

[89] W. J. Hehre, L. Radom, P.v.R. Schleyer and J. A. Pople. *Ab Initio Molecular Orbital Theory.* John Willey and Sons, USA, 1986.

[90] A. Szabo and N. S. Ostlund. *Modern Quantum Chemistry: Introduction to Advanced Electronic Structure Theory.* Macmillan, New York, 1982.

[91] P. W. Atkins and R. S. Friedman. *Molecular Quantum Mechanics.* Oxford University Press, Walton Street, Oxford, 0X2 6DP, third edition, 1997.

[92] G. Horowitz, A. Yassar and H.J. von Bardeleben. *Synth. Met.*, 62:245–252, 1994.

[93] I. Shavitt. *Methods of Electronic Structure Theory.* Plenum Press, New York, 1977. edited by H. F. Schaefer III,.

[94] W. B. Davis, M. R. Wasielewski and M. A. Ratner. *Int. J. of Quan. Chem.*, 72:463–471, 1999.

[95] J. B. Foresman, and A. Frisch. *Exploring Chemistry with Electronic Structure Methods: A Guide to Using Gaussian.* Gaussian Inc., Pittsburgh PA, 1993. and references therein.

[96] G.L. Bendazzoli, F. Bertinelli, P. Palmieri, A. Brillante and C. Taliani. *J. Chem. Phys.*, 69:5077–5081, 1978.

[97] D. Beljonne, Z. Shuai, R. H. Friend and J. L. Brédas. *J. Chem. Phys.*, 102(5):2042–2049, 1995.

[98] P. Swiderek, M. Michaud and L. Sanche. *J. Chem. Phys.*, 103(19):8424, 1995. and references therein.

[99] H. Tachikawa. *Chem. Phys. Lett.*, 265:455–459, 1997.

[100] A. F. Diaz, J. Crowley, J. Baryon, G. P. Gardini and J. B. Torrance. *J. Electroanal. Chem.*, 121:355–361, 1981.

[101] E. S. Replogle, G. W. Trucks and S. W. Staley. *J. Phys. Chem.*, 95:6908–6912, 1991.

[102] I. Shavitt. *Molecular Physics*, 94(1):3–17, 1998. and references therein.

[103] U. Salzner, J. B. Lagowski, P.G. Pickup and R. A. Poirier. *Synth. Met.*, 96:177–189, 1998.

[104] A. K. Bakhshi, Deepika and J. Ladik. *Solid State Commun.*, 101(5):347–350, 1997.

[105] A. K. Bakhshi and P. Rattan. *J. Chem. Soc., Faraday Trans.*, 94:2823–2826, 1998.

[106] J. M. Toussaint and J. L. Brédas. *Synth. Met.*, 69:637–640, 1995.

[107] J. M. Toussaint and J. L. Brédas. *Synth. Met.*, 61:103–106, 1993.

[108] A. Tol and G. Brocks. *J. Phys. Chem.*, 100:1838–1846, 1996.

[109] Intern. conf. on science and technology of synthetic metals. *Synth. Met.*, 55-57, 1992. Götenborg.

[110] P. Otto. *Int. J. of Quan. Chem.*, 52:353–364, 1994.

[111] J. M. Toussaint and J. L. Brédas. *Macromolecules*, 26:5240–5248, 1993.

[112] D. Birnbaum, D. Fichou and B. E. Kohler. *Chem. Phys.*, 96(1):165–169, 1991.

[113] R. A. J. Janssen, L. Smilowitz, N. S. Sariciftci and D. Moses. *J. Chem. Phys.*, 101:1787, 1994.

[114] C. Adant, J. L. Brédas and M. Dupuis. *J. Phys. Chem. A*, 101:3025–3031, 1997.

[115] T. A. Skotheim, editor. *Handbook of Conducting Polymers.* Marcel Dekker Inc., New York, 1986.

[116] J. Cornil, D. Beljonne and J. L. Brédas. *J. Chem. Phys.*, 103(2):842–849, 1995.

[117] M. Chandross, Y. Shimoi and S. Mazumdar. *Synth. Met.*, 85:1001–1006, 1997.

[118] H. Subramanian and J. B. Lagowski. *Int. J. of Quan. Chem.*, 66:229, 1998.

[119] E. E. Havinga, W. ten Hoeve and H. Wynberg. *Polym. Bull.*, 29:119, 1992.

[120] *Mopac 93.00 manual.* J. J. P. Stewart. Fujitsu Limited, Tokyo, Japan, 1993.

[121] A. Almenningen, O. Bastiansen and R. H. Baughman. *Acta. Chem. Scan.*, 12:1671, 1958.

[122] BIOSYM/Molecular Simulations Inc., 9685 Scranton Road, San diego, CA 92121, USA. *Cerius^2 User's Manual*, 1995.

[123] W. J. Hehre, R. F. Stewart and J. A. Pople. *J. Chem. Phys.*, 51:2657, 1969.

[124] H.B. Schlegel in D. R. Yakony(Ed). *Modern Electronic Structure Theory*, volume 2. World Scientific; Singapore, 1994.

[125] F. Sim, S. Chin, M. Dupuis and J. E. Rice. *J. Phys. Chem.*, 97:1158–, 1993.

[126] J. P. Das, A. T. Yeates and D. S. Dudis. *Chem. Phys. Lett.*, 212:671, 1993.

[127] S. Hotta, T. Hosaka and W. Shimotsuma. *J. Chem. Phys.*, 80:954, 1984.

[128] S. Hotta, T. Hosaka and W. Shimotsuma. *Synth. Met.*, 9:87, 1984.

[129] C. X. Cui and M. Kertesz. *Phys. Rev. B*, 40(14):9661, 1989.

[130] J. C. Slater. *Quantum Theory of Atomic Structure.* McGraw-Hill Book Company Inc., New York, 1960.

[131] M. J. Frisch, G. W. Trucks, H. B. Schlegel, P. M. W. Gill, B. G. Johnson, M. A. Robb, J. R. Cheeseman, T. Keith, G. A. Petersson, J. A. Montgomery, K.Raghavachari, M. A. Al-Laham, V. G. Zakrzewski, J. V. Ortiz, J. B. Foresman, C.Y. Peng, P. Y. Ayala, W. Chen, M. W. Wong, J. L. Andres, E. S. Replogle, R. Gomperts, R. L. Martin, D. J. Fox, J. S. Binkley, D. J. Defrees, J. Baker, J. P. Stewart, M. Head-Gordon, C. Gonzalez and J. A. Pople. *Gaussian 94.* Gaussian Inc., Pittsburgh PA, 1995.

[132] K. Raghavachari and J. B. Anderson. *J. Phys. Chem.*, 100(31):12960–12973, 1996.

[133] P. O. Löwdin. *Adv. Chem. Phys.*, 2:207, 1959.

[134] G. W. Kellner. *Z. Phys.*, 44(91):110, 1927.

[135] H. F. Schaefer, J. R. Thomas, Y. Yamaguchi, B. J. DeLeeuw and G.Vacek. *Modern Electronic Structure Theory.* World Scientific, Singapore, 1995. D.R. Yarkony, Ed.

[136] W. H. Meyer. *Int. J. Quantum Chem.*, 5:341, 1971.

[137] W. H. Meyer. *J. Chem. Phys.*, 58:1017, 1973.

[138] B. E. Kohler. *Chem. Rev.*, 93:41, 1993. and references therein.

[139] L. Salem. *Molecular Orbital Theory of Conjugated Systems.* Benjamin, New York, 1982.

[140] M. Pope and C. E. Swenberg. *Electronic Processes in Organic Crystals.* Oxford University Press, New York, 1982.

[141] Z. G. Soos, S. Ramasesha and D. S. Galvao. *Phys. Rev.*, 71:1609, 1993.

[142] J. H. Burroughes, D. D. C. Bradley, A. R. Brown, R. N. Marks, K. Mackay, R. H. Friend, P. L. Burn and A. B. Holmes. *Nature*, 347:539, 1990.

[143] G. Gustafsson, Y. Cao, G. M. Treacy F. Klavetter N. Colaneri and A. J. Heeger. *Nature*, 357:477, 1992.

[144] N. Suzuki, M. Okazaki, S. Etemad, A. J. Heege and A. G. MacDiarmid. *Phys. Rev. Lett.*, 45:1209, 1980. ibid 45: 1483, 1980.

[145] G. König and G. Stollhoff. *Phys. Rev. Lett.*, 65:1239, 1990.

[146] C. Wasikowski and S. Klemm. *MISC. REFERENCE MANUAL PAGES.* Research Equipment, Inc. d/b/a Minnesota Supercomputer Center, Inc., Minnesota, USA, 1993.

[147] A. B. Nielsen, and A. J. Holder. *Gaussview User's Reference.* Carnegie Office Park, Building 6, Pittsburgh, PA 15106, USA, 1997. Version 1.0.

[148] T. Helgaker and P. R. Taylor. *Modern Electronic Structure Theory.* World Scientific, Singapore, 1995. edited by D. R. Yarkony, p.725.

[149] J. Almlöf, B. J. Deleeuw, P. R. Taylor, C. W. Bauschlicher and P. Siegbahn. *Int. J. Quantum Chem. Symp.*, 23:345, 1989.

[150] W. Kutzelnigg and W. Klopper. *J. Chem. Phys.*, 94:1985, 1991.

[151] G. A. Patersson, T. G. Tensfeldt and J. A. Montgomery. *J. Chem. Phys.*, 94:6081, 1991.

[152] A. Willetts, J. E. Rice, D. M. Burland and D. P. Shelton. *J. Chem. Phys.*, 97:7590, 1992.

[153] G. Horowitz, B. Bachet, A. Yassar, P. Land, F. Demanze, J. L. Fave and F. Garnier. *Chem. Mater*, 7:1337–1341, 1995.

[154] C. I. Williams, M. A. Whitehead and B. J. Jean-Claude. *J. Mol. Struc. (Theochem)*, 389:13–25, 1997.

[155] J. B. Foresman and H. B. Schlegel. *Application of the CI-Singles method in predicting the energy properties and reactivity of molecules in their excited states.* Kluwer Academic, 1993. in "Recent experimental and computational advances in molecular spectroscopy, eds. R. Fausto, and J. M. Hollas".

[156] R. S. Mulliken. *J. Chem. Phys.*, 66:2448, 1977.

[157] J. L. Brédas, G. B Street, B. Thémans and J. M. André. *J. Chem. Phys.*, 83:1323, 1985.

[158] S. Hotta and K. Waragai. *J. Phys. Chem.*, 97:7427, 1993.

[159] S. Hotta and K. Waragai. *Adv. Mater.*, 5:896, 1993.

[160] F. van Bolhuis, H. Wynberg, W. W. Havinga, E. W. Meijer and E. G. J. Staring. *Synth. Met.*, 30:381, 1989.

[161] A. B. Trofimov, J. Schirner and H. Koppel. *J. Phys. Chem.*, 109:1025, 1998.

[162] J.H.D. Eland. *Int. J. Mass Spectrom. Ion Physics*, 2:471, 1969.

[163] R. Hakansson, B. Norden and E.W. Thulstrup. *Chem. Phys. Lett.*, 50:305, 1977.

[164] N. Kishimoto, H. Yamakado and K. Ohno. *J. Phys. Chem.*, 100:8204, 1996.

[165] D. Chakraborty and J. Lagowski. 2000. Unpublished data.

[166] J. M. Toussaint and J. L. Brédas. *J. Chem. Phys.*, 92(4):2624, 1990.

[167] M. F. Granville, B. E. Cohler and J. Bannon Snow. *J. Chem. Phys.*, 75:3765, 1981.

[168] F. Negri and M. Z. Zgierski. *J. Chem. Phys.*, 100:2571, 1994.

[169] Y. Lu. *Solitons and Polarons in Conducting Polymers.* World Scientific, Singapore, 1988.

[170] J. P. Reyftmann, J. Kagan, R. Santus and P. Morliere. *Photochem. Photobiol.*, 41(1):1–7, 1985.

[171] Z. V. Vardeny and X. Wei in. *Handbook of Conducting Polymers.* Marcel Dekker Inc. New York, 1998. Edited by T. A. Skotheim.

[172] J. Cornil, D. Beljonne and J. L. Brédas. *J. Chem. Phys.*, 103(2):834–841, 1995.

[173] J. B. Lagowski, S. Khare and D. Chakraborty. *Ab initio* polarizability studies of thiophene and cyclopentadiene based conducting polymers, 1999. Unpublished data.

[174] J. L. Brédas, G. B. Street, B. Themans and J. M. Andre. *J. Chem. Phys.*, 83(3):1316, 1985.

[175] L. Praud, P. Millie and G. Berthier. *Theor. Chem. Acta.*, 11:169, 1968.

[176] P. A. Straub, D. Meuche and E. Heilbronner. *Helv. Chim. Acta.*, 49:517, 1966.

[177] T. Ogata and K. Kozima. *J. Mol. Spectrosc.*, 42:38, 1972.

[178] A. A. El-Azhary and H. U. Suter. *J. Phys. Chem.*, 100:15056, 1996.

[179] L. H. Scharpen and V. W. Laurie. *J. Chem. Phys.*, 43:2765, 1965.

[180] P. D. Baron, R. D. Brown, F. R. Burden, P. J. Fomaille and J. E. Kent. *J. Mol. Spectrosc.*, 43:401, 1972.

[181] J. J. Aaron, M. D. Gaye, C. Parkanyi, N.S. Cho and L.V. Szentpaly. *J. Mol. Struct.*, 156:119, 1987.

[182] M. I. Connolly. *Science*, 221.

[183] M. I. Connolly. *J. Appl. Crystal.*, 16:548, 1983.

[184] J. J. Ladik. *Indian J. of Chem.*, 33A:449–452, 1994.

[185] *Conjugated Conducting Polymers.* Springer-Verlag, Heidelberg, Germany, 1992. Edited by H. G. Kiess.

[186] J. Guay, P. Kasai, A. Diaz, R. Wu, J. M Tour, and L. H. Dao. *Chem. Mater.*, 4:1097, 1992.

[187] D. Beljonne, J. Cornil, R. H. Friend, R. A. J. Janssen, and J. L. Brédas. *J. Am. Chem. Soc.*, 118:6453, 1996. and references therein.

[188] K. Waragai and S. Hotta. *Synth. Met.*, 41-43:519–522, 1991.

[189] J. Cornil, D.A. Dos Santos, D. Beljonne, and J. L. Brédas. *J. Phys. Chem.*, 99:5606, 1995.

[190] J. L. Brédas and A. J. Heeger. *J. Chem. Phys. Lett.*, 217:507, 1994.

[191] F. Demanze, J. Cornil, F. Garnier, G. Horowitz, P. Valat, A. Yassar, R. Lazzaroni, and J. L. Brédas. *J. Phys. Chem. B*, 101:4553–4558, 1997.

[192] H. A. Ho, H. Brisset, E. H. Elandaloussi, P. Frére, J. Roncali, and D. Beljonne. *Adv. Mater.*, 8(12):990–994, 1996.

[193] G. H Döhler. *CRC Critical Reviews in Solid State and Material Sciences*, 13(2):97, 1987.

[194] D. Bertho and C. Jouanin. *Phys. Rev. (B)*, 35(2):626–633, 1987.

[195] J. C. Grossman, W. A. Lester Jr., and S. G. Louie. *Mol. Phys.*, 96(4):629–632, 1999.

[196] R. P. Frueholz, W. M. Flicker, O. A. Mosher, and A. Kuppermann. *J. Chem. Phys.*, 70(04):2003, 1979.

[197] P. M. Lahti, J. Obrzut, and F. E. Karasz. *Macromolecules*, 20:2023, 1987.

[198] M. Karelson and M. Zerner. *Chem. Phys. Lett.*, 224:213–218, 1994.

[199] T. C. Chung, J. H. Kaufman, A. J. Heeger, and F. Wudl. *Phys. Rev. B*, 30(2):702–710, 1984.

[200] Z. Vardeny, E. Ehrenfreund, O. Brafman, M. J. Nowak, H. Schaffer, A. J. Heeger, and F. Wudl. *Phys. Rev. Lett.*, 56(6):671, 1987.

[201] S. Stafström and J. L. Brédas. *Phys. Rev. B*, 38:4180, 1988.

[202] Z. Vardeny, E. Ehrenfreund, J. Shinar, and F. Wudl. *Phys. Rev. (B)*, 35(5):2498, 1987.

[203] D. Fichou, G. Horowitz, B. Xu, and F. Garnier. *Synth. Met.*, 39:243–259, 1990.

[204] M. J. Nowak, S. D. D. V. Rughooputh, S. Hotta, and A. J. Heeger. *Macromolecules*, 20:965, 1987.

[205] *Sadler Handbook of Ultraviolet Spectra.* Sadler Research Laboratory, Pliladelphia, PA, USA, 1979.

[206] J. Roncali. *Chem. Rev.*, 97:173–205, 1997.

[207] C. C. J. Roothaan. *Reviews in Modern Physics*, 23:69, 1951.

[208] A. C. Harley. *Electron Correlation in Small Molecules.* Academic Press, New York, 1976.

[209] G. Fitzgerald and H. F. Shaefer III. *J. Chem. Phys.*, 83:1162, 1985.

[210] A. E. Hansen, and T. D. Bouman. *Adv. Chem. Phys.*, 44:545, 1980.

[211] C. W. McCurdy Jr., T. N. Rescigno, D. L Yeager, and V. Mckoy. Methods of electronic structure theory. 1977. edited by H. F. Schaefer III,.

[212] A. E. Hansen, and T. D. Bouman. *Adv. Chem. Phys.*, 1713:37, 1979.

[213] T. H. Dunning and V. Mckoy. *J. Chem. Phys.*, 47:1735, 1967.

[214] H. Koch, H. Jorgen, A. Jensen, P. Jorgense, and T. Helgaker. *J. Chem. Phys.*, 93:3345, 1990. and references therin.

[215] R. Colle, A. Fortunelli, and O. Salvetti. *Theo. Chem. Acta.*, 75:323, YEAR =.

[216] J. Del Bene, R. Ditchfield, and J. A. Pople. *J. Chem. Phys.*, 55:2236, 1971.

[217] R. Ditchfield, J. Del Bene, and J. A. Pople. *J. Amer. Chem. Soc.*, 94:703, 1972.

[218] In F. W. Bobrowicz, W. A. Goddard III. *Methods of Electronic Structure Theory.* Plenum, New York, USA, 1977. Ed. H. F. Schaefer III.

[219] E. R. Davidson and L. Z. Stenkamp. *Int. J. Quantum. Chem. Symp.*, 10:21, 1976.

[220] R. Pariser and R. G. Parr. *J. Chem. Phys.*, 21:466, 1953. ibid, 21:761,1953.

[221] J. A. Pople. *Trans. Faraday Soc.*, 49:1375, 1953.

[222] A. Volosov. *Int. J. Quantum Chem.*, 36:473, 1989.

[223] M. C. Zerner, G. H. Loew, R. F. Kirchner, and U. T. Mueller-Westerhoff. *J. Am. Chem. Soc.*, 102:589, 1980.

[224] T. Nagamiya. *Proc. phys.-math. SOc. Jap.*, 18:497, 1936.

[225] A. Papino and I. Shavitt. *Int. J. Quan. Chem.*, 2:741, 1968.

[226] C . D. Sherrill and H. F. Schaefer. *J. Phys. Chem.*, 100:6069, 1996.

[227] L. R. Kahn, P. J. Hay, and I. Shavitt. *J. Chem. Phys.*, 61:3530, 1974.

[228] C. W. Bauschlicher, S. R. Langhoff Jr., and P. R. Taylor. *J. Chem. Phys.*, 88:2540, 1988.

[229] B. O. Roos, P. R. Taylor, and P. E. M. Siegbahn. *Chem. Phys.*, 48:157, 1980.

[230] K. Ruedenberg, M W. Schmidt, M. M. Gilbert, and S. T. Elbert. *Chem. Phys.*, 71:41, 1982.

[231] J. Olsen, B. O. Roos, P. Jorgensen, and H. J. A. Jensen. *J. Chem. Phys.*, 89:2185, 1988.

[232] W. Duch and J. Karwowski. *Theor. Chim. Acta.*, 51:175, 1979.

[233] I. Shavitt. *Isreal J. Chem.*, 33:357, 1993.

[234] R. C. Raffenetti. *J. Chem. Phys.*, 58:4452, 1973.

[235] J. Almlöf and P. R. Taylor. *J. Chem. Phys.*, 86:4070, 1987. ibid **92**, 551, 1990.

[236] T. H. Dunning Jr. *J. Chem. Phys.*, 90:1007, 1989.

[237] J. L. Whitten. *J. Chem. Phys.*, 56:5458, 1972.

[238] S. Sæbo and P. Pulay. *Chem. Phys. Lett.*, 113:13, 1985.

[239] W. Meyer. *Methods of Electronic Structure Theory.* Plenum Press, New York, 1977. edited by H. F. Schaefer III, P.413.

[240] I. Shavitt. *J. Comput. Phys.*, 6:124, 1970.

[241] R .J. Bartlet and G. D. Purvis. *Int. J. Quantum. Chem.*, 14:561, 1978.

[242] G. S. Kedziora and I. Shavitt. *J. Chem. Phys.*, 106:8733, 1997.

[243] S. R. Langhoff and E. R. Davidson. *Int. J. Quantum. Chem.*, 8:61, 1974.

[244] J. A. Pople, M. Head-Gordon, and K. Raghavachari. *J. Chem. Phys.*, 87:5968, 1987.

[245] W. Duch and G. H. F. Diercksen. *J. Chem. Phys.*, 101:3018, 1994.

[246] B. R. Brooks, W. D. Laidig, P. Saxe, J. D. Goddard, Y. Yamaguchi, and H. F. Shaefer III. *J. Chem. Phys.*, 72:4652, 1980.

[247] R. Krishnan, H. B. Schlegel, and J. A. Pople. *J. Chem. Phys.*, 72:4654, 1980.

[248] J. A. Pople, R. Krishnan, H. B. Schlegel, and J.S. Binkley. *Int. J. Quantum Chem. Symp.*, 13:225, 1979. and references therein.

[249] J. Gerratt and I. M. Mills. *J. Phys. Chem.*, 49:1719, 1968. ibid 49:1730,1968.

[250] N. C. Handy and H. F. Schaefer III. *J. Chem. Phys.*, 81:5031, 1984.

[251] J. E. Rice and R. D. Amos. *Chem. Phys. Lett.*, 122:585, 1985.

[252] J. E. Rice, R. D. Amos, N. C. Handy, T. J. Lee, and H. F. Schaefer III. *J. Chem. Phys.*, 85:963, 1986.

Appendix A

HF Matrix Equation

We suppose ψ_{trial} to be an antisymmetric normalized trial function of the electronic coordinates used to approximate the exact eigenfunction ψ corresponding to the lowest energy eigenstate of a given system. Then according to the variational theorem for any ψ_{trial}

$$\mathcal{E} \geq E \tag{A.1}$$

where, E is the exact energy given by Eq. (2.13) for a true state wavefunction ψ. Therefore, it follows from this inequality that the best approximation of the expectation value of energy $\mathcal{E}$ to the eigenvalue E could be obtained by adjusting ψ_i (as in Eq. (2.8)) in order to minimize $\mathcal{E}$, i.e.,

$$\frac{\delta \mathcal{E}}{\delta \psi_i} = 0 \tag{A.2}$$

for all i. Applying unitary transformation and diagonalizing the matrix of Lagrange's multipliers leads to the eigenvalue equations called the spatial Hartree-

Fock integro-differential equations of the form

$$[\hat{h}^N(1) + \sum_{j=1}^{n}(2\hat{J}_j(1) - \hat{K}_j(1)]\psi_i(1) = \epsilon_i\psi_i(1), \qquad i = 1, 2, 3, \cdots n \tag{A.3}$$

which are equivalent to

$$\hat{H}^{HF}\psi_i = \epsilon_i\psi_i. \tag{A.4}$$

In order to interpret the Lagrange's multipliers, ϵ_i, we multiply Eq. (2.13) by $\psi_i^*(1)$ and integrate over the electronic coordinates, giving

$$\epsilon_i = \langle i|\hat{h}^N(1)|i\rangle + \sum_{j=1}^{n}\langle i|2\hat{J}_j(1) - \hat{K}_j(1)|i\rangle = \langle i|\hat{H}^{HF}|i\rangle \tag{A.5}$$

where $\hat{H}^{HF}$ is called the "Hartree-Fock Hamiltonian" or the effective "Fock operator" [90] which in turn is defined as

$$\hat{H}^{HF} = \hat{h}(i) + \sum_{j=1}^{n}(2\hat{J}_j(i) - \hat{K}_j(i)). \tag{A.6}$$

A.1 Roothaan Equations: Introduction of Basis Set Functions

In 1951, Roothaan [207] introduced the basis set functions, which together with the variational principle lead to a formulation of a matrix equation involving the molecular orbital expansion coefficients. The substitution of Eq. (2.8) into Eq. (2.19) (multiplying both sides by the basis function χ_ν^* and integrating over $d\mathbf{r}_1$)

yields

$$\sum_{\mu=1}^{N} c_{\mu i} \int \chi_\nu^*(1) H_{\mu\nu}^N \chi_\mu(1) d\mathbf{r}_1 = \epsilon_i \sum_{\mu=1}^{N} c_{\mu i} \int \chi_\nu^*(1) \chi_\mu(1) d\mathbf{r}_1. \tag{A.7}$$

The above quation is normally thought of as consisting of the **overlap matrix, S,** which indicates the overlap between orbitals, with elements

$$S_{\mu\nu} = \int \chi_\nu^*(1) \chi_\mu(1) d\mathbf{r}_1 \tag{A.8}$$

and the **Fock matrix, F**, with elements

$$F_{\mu\nu} = \int \chi_\nu^*(1) H_{\mu\nu}^N \chi_\mu(1) d\mathbf{r}_1. \tag{A.9}$$

The resultant equation can be wrtitten as

$$\sum_{\mu=1}^{N} F_{\mu\nu} c_{\mu i} = \epsilon_i \sum_{\mu=1}^{N} S_{\mu\nu} c_{\mu i}, \qquad i = 1, 2, \cdots n. \tag{A.10}$$

This set of N simultaneous equations (one for each value of ν) is known as the **Roothaan equations**. The entire set of equations can be written as the single matrix equation

$$\mathbf{Fc} = \mathbf{Sc}\epsilon \tag{A.11}$$

where $\mathbf{c}$ is an $N \times N$ matrix composed of elements $c_{\mu i}$ and ϵ is an $N \times N$ diagonal matrix of the orbital energies ϵ_i. The basis functions (χ_μ) are orthogonal and upon unitary transformation of the basis functions will produce molecular orbitals, i.e.,

$$\begin{aligned} \mathbf{S}^{-\frac{1}{2}}\mathbf{F}\mathbf{S}^{-\frac{1}{2}}\mathbf{S}^{\frac{1}{2}}\mathbf{c} &= \mathbf{S}^{\frac{1}{2}}\mathbf{c}\epsilon \\ \mathbf{F}'\mathbf{V}' &= \mathbf{V}'\epsilon. \end{aligned} \tag{A.12}$$

In Hartree-Fock method the total electronic energy is given by Eq. (2.13). With the use of Roothaan equations, the electronic energy can be written as:

$$E_{elec} = \frac{1}{2}\sum_{\mu\nu} P_{\mu\nu}(H^N_{\mu\nu} + F_{\mu\nu}). \tag{A.13}$$

where the $P_{\mu\nu}$ are defined as follows:

$$P_{\mu\nu} = 2\sum_{j}^{occ} c_{\mu j}c^*_{\nu j}. \tag{A.14}$$

The $P_{\mu\nu}$ are referred to as **density matrix** elements, and are interpreted as the total electron density in the overlap region of χ_μ and χ_ν. The coefficients are summed over the occupied orbitals only, and the factor of two comes from the fact that each orbital is occupied by two electrons.

A.1.1 Self-Consistent Field (SCF) Procedure

The Fock matrix as well as the density matrix and the orbitals depend on the molecular orbital expansion coefficients. Thus, Eq. (A.11) is not linear and must be solved iteratively. The procedure which does so is called the **Self-Consistent Field** method. At convergence, the energy is at a minimum, and the orbitals

generate a field which produces the same orbitals, hence the method's name. The solution produces a complete set of orbitals, both **occupied** ($\phi_{i,j...}$) and **virtual** ($\phi_{a,b...}$).

The following steps are followed in all SCF molecular orbital calculations:

1. Calculate the integrals for $\mathbf{F}$ and $\mathbf{S}$.
2. Diagonalize $\mathbf{S}$.
3. Form the Fock matrix $\mathbf{F}$.
4. Form $\mathbf{F}'$ as in Eq. (A.12).
5. Diagonalize $\mathbf{F}'$ for the MO eigenvalues ϵ.
6. Back transform $\mathbf{V}$ to obtain the MO coefficients.
7. Form the density matrix $\mathbf{P}$.
8. Check $\mathbf{P}$ for convergence. If $\mathbf{P}$ for the n^{th} cycle agrees with $\mathbf{P}$ for the previous cycle within a given tolerance, stop and go on to perform other parts of the calculation (e.g., population analysis). If not, extrapolate a new $\mathbf{P}$ matrix and repeat from step 3 until a self-consistent field (step 8) is satisfied.

Appendix B

Discussion on Correlation Effects in Molecules

Electron correlation effects, as defined above, are clearly not directly observable. Correlation is not a perturbation that could be turned on or off to have any physical consequences. Rather, this is a measure of the errors that are inherent in the HF theory or orbital models. This demands an explanation: while HF theory is well defined and unique for closed-shell molecules, several versions of HF theory are used for open-shell molecules. Correlation energy for an open-shell molecule is usually defined with respect to unrestricted Hartree-Fock (UHF) theory where the spatial orbitals are different for α and β spins. In general, a theory of electron correlation refers to any method for accurate treatment of interelectronic interactions starting from a suitable reference wavefunction. Another factor is also required to be considered in most theories of electron correlation. In actual computations, the orbitals are usually expanded in terms of a finite basis set, i.e., a set of finite atom-centered functions. This, in effect, introduces an additional error associated with basis set truncation effects. Typically, for any given method, the electron correlation energy is defined within the finite basis set used, and the convergence

with respect to increasing basis set size is then considered separately. For many of the popular quantum mechanical methods, the convergence with respect to the inclusion of higher angular momentum functions in the basis set is rather slow. The physical idea behind most theories of electron correlation can be understood from an analysis of the bonding in the simplest H_2 molecule. HF calculations with large basis sets show that correlation effects contribute about 25kcal/mol to the binding energy in H_2. In fact, correlation effects contribute about $\approx$1 eV (23 kcal/mol) for a pair of electrons in a well-localized orbital [208]. For many pairs of electrons in close proximity, correlation effects become very large. For example, they contribute more than 100 kcal/mol to the bond energy in N_2 [132]. The most important type of correlation effect which contributes to chemical bonding is usually termed "left-right" correlation [208]. For H_2 this refers to the tendency that when one electron is near the first hydrogen atom, the other electron tends to be near the second hydrogen. This is not what HF method yields where the spatial positions of the two electrons occupying the lowest bonding molecular orbital are uncorrelated. This problem gets worse as the two atoms move apart and dissociate. Qualitatively, this can be corrected by including a second configuration where both electrons occupy the anti bonding orbital. While this is unfavorable energetically, a mixture of the HF configuration with this second configuration provides even better description of the system. This is termed as "configuration interaction" and is the basis behind many of the electron correlation theories.

Another type of correlation effect is "in-out" correlation which corresponds to radial correlation in atomic systems. Such kind of effects can be included by having configurations with occupation of higher radial functions, e.g., $(1\sigma_g 2\sigma_g)$ configura-

tion in H_2 composed of 1s and 2s orbitals. A third type of correlation is "angular" correlation which is typically considered by the inclusion of the higher order angular momentum functions, e.g., $(\pi_u)^2$ configuration in H_2 composed of 2p orbitals. Large basis sets with higher radial and angular momentum functions are necessary to properly include the contribution of all the different correlation effects.

B.1 Requirements in Electron Correlation Theories

At this point it is useful to review the criteria which different theories of electron correlation should attempt to satisfy. In other words, a correlation theory constitutes a "theoretical model chemistry" [89] and should contain certain desirable characteristics. For example, it should provide a unique total energy for each electronic state at a given geometry and should also provide continuous potential energy surfaces as the geometry changes. The most important criterion for an accurate electron correlation theory is the property of size consistency or size extensivity [89]. This means that the method must give additive results when applied to an assembly of isolated molecules. Unless this is true, comparison of properties of molecules of different size will not lead to quantitatively meaningful results. While this appears to be a trivial requirement, popular methods like configuration interaction are not size-consistent and do not give additive energies for infinitely separated systems. The importance of size consistency was known for many years, but thought to be important only for large molecules. In the recent years, it has been realized that size consistency is necessary even for smaller molecules.

A very important aspect of any correlation scheme is its computational depen-

dence, it must not lead to such a rapid increase in the required computation with molecular size as to provide its use in systems of chemical interest.

A desirable property for a satisfactory model is that the resulting energy should be variational, i.e., it should be an *upper bound* to the energy that would derive from exact solution of Schrödinger equation. Again for many years, this was an important criterion, and approximate theories such as configuration interaction satisfies this requirement. However, successful theories of electron correlation like coupled cluster theory, do not provide variational total energies.

A final and useful criterion for an accurate correlation method is correctness for two-electron systems. The exact correlation treatment for electron pair within a given basis set is relatively easy to implement. Several of the popular electron correlation techniques do indeed correlate an electron pair exactly.

Turning specifically to excited states, there is an additional requirement. A given theoretical framework should lead to several accurate electronic states which have wavefunctions that are directly comparable. This qualification is necessary for calculating transition properties among the various possible states. It also ensures the capability of quantifying the difference between the structure of the ground and the excited states. Which, basically implies that, the excited-state wavefunction should be orthogonal to the ground-state wavefunction and to each other. If the state of interest is of identical symmetry and multiplicity as a lower state, then by introducing some means or being implicit in the model the variational collapse to the lower state should be prevented. This last point is important in studies of excited-states, since geometry relaxation often causes a reduction in symmetry [209].

B.2 Theories Based on Single-Configuration

The most widely used single-configuration techniques start from a Hartree-Fock self-consistent-field wavefunction [89], where the wavefunction ψ_i is a product of one-electron wavefunctions (referred to as molecular spin orbitals), antisymmetrized with respect to interchange of electronic coordinates. In HF calculation each electron moves in an average field due to all the other electrons, and the expansion coefficients of the molecular orbitals are determined in a self-consistent manner. Hence the wavefundtion in terms of a single configuration is inadequate to treat the correlation between the motions of different electrons. While the antisymmetry which is implicit in a determinantal wavefunction keeps electron of the same spin partially correlated, the correlation between the motions of electrons with opposite spins is neglected which is a shortcoming of HF theory.

Appendix C

Background of CI Method

Current electronic structure theories for excited-state can be naively classified into two categories: those which concentrate on the physics of the transitions and those which concentrate on the physics of the state [210]. The first type includes the schemes of random phase approximation (RPA). There are two ways to solve the actual equations for this formalism which are derived either by using the algebra of second quantization [211] or by imposing constraints on the ground- and excited-state wavefunctions based on hypervirial relations [212]. Transition based methodology has not quite found their way due to several difficulties, like producing complex excitation energies [213], in suitability for larger systems (due to the requirement for transformation of two electron-integrals), and for their nonvariational nature.

On the other hand, state-based methodology includes all treatments to calculate the wavefunction and energy of a given state without restricting to the physics connecting the states. The self-consistent-field (SCF) equations can be solved to obtain a spin-unrestricted HF wavefunction when the state of interest is the lowest energy state of a given multiplicity and symmetry: the traditional way to evaluate

a ground-state triplet. All is necessary is to provide an appropriate initial guess and to use a convergence procedure which finds the desired solution. For example, a crude approximation to the first excited singlet state of a particular symmetry may be found by forcing two electrons of opposite spins to occupy orbitals of different symmetry. These orbitals are chosen so that the product wavefunction yields the desired symmetry. Therefore, once the HF solution of this type is derived, the usual methodology for including electron correlation can be applied, either through configuration interaction (CI) or perturbation technique. Using UHF theory introduces spin contaminations, leading to inadequate evaluation of properties like optimized geometries and dipole moment. In addition to that, traditional solutions of HF equations do not allow for the second electronically excited state of a given symmetry to be found. Three different schemes are commonly used to solve this dilemma of variational collapse of the SCF procedure. The first involves adding constraints into the SCF equations which force the solution to be orthogonal to some lower solution [214]. This is not a well practised technique and the test cases are limited to small molecules [215]. The second solution is to use the orbitals of a HF state in an ordinary CI procedure, solving for the higher roots. Excited determinant are produced by replacing occupied orbitals with virtual orbitals and determining the overall wavefunction as a linear combination of such configurations. When a single occupied orbital is replaced by an unoccupied orbital, the single transition approximation (STA) is made. This is, generally, a poor level of theory since virtual orbitals are thought to be orbitals for ionized electrons, and excitation energies are overestimated. Now, if all the single excitations are taken in the manifold: i.e., the wavefunction is expressed as a linear combination of all determinants formed

by replacing a single occupied orbital with a virtual orbital then a level of theory is reached which was widely used under the names: single excitation configuration interaction (SECI), mono-excited configuration interaction, or the Tamm-Dancoff approximation (TDA), presently known as CI-singles. This is the simplest level of theory which can be used to include some of the effects of electron correlation via the mixing of excited determinants. It has been applied to calculate reasonable values for the π to π^* and n to π^* excitation energies of small organic molecules [216, 217]. Its utility for studying larger systems with higher basis sets has not been clearly evaluated except for a couple of recent cases [72, 62, 118]. Finally, the third solution to this problem is to expand the wavefunction to include configurations other than the HF determinant while continuing to optimize the molecular orbital coefficients in a variational sense. Multiconfigurational self-consistent field (MCSCF) calculations have been widely used to study correlated ground states as well as excited states by solving for the higher roots of the same basic equations. In MCSCF techniques [218, 219, 209] instead of using the ground-state HF wavefunction as a reference state for the CI, a multiconfigurational state of a particular symmetry ('parent' configuration) is used.

For many years another category of excited-state methodology has received considerable attention - they are basically state-based semiempirical treatments like PPP [220, 221] CNDO/OPTIC [222] and INDO-CI [223, 64, 80]. Because of low computational costs, these techniques can deal with extremely large number of electrons. These methods, however, were criticized for their inability to characterize excited-state surfaces [73], since parametrization is based on reproducing ground-state properties.

C.1 Developments and Adaptations

C.1.1 Infrastructural Development

The following steps are involved in a 'conventional' CI calculation [93]:

1. calculation of basis set integrals;
2. determination of orbitals, e.g., by an SCF calculation;
3. transformation of basis set integrals to orbital integrals;
4. calculation and storage of the Hamiltonian matrix elements;
5. solution of the matrix eigenvalue problem for the desired state.

A few things like the procedures for spin- and symmetry-adaptation of the configuration state functions (CSFs) have to be chosen, and methods for calculating Hamiltonian matrix elements between the CSFs have to be implemented [93]. The following choices need to be made for each calculation [93]:

- Selection of the basis set;
- Type of orbital to use (e.g., SCF, MCSCF, or natural orbitals);
- Choice of the configuration state functions to include in the CI expansion.

C.1.1.1 Structure of the CI expansion

Number of CSFs in the early CI calculations was very small [224, 102], and moreover, these CSFs were generally selected individually on the basis of physical considerations or by trial and error. In full CI the exponential growth of CSF number with the size of basis set demands the truncation in the CI expansion space to make

the calculation more practical. Most CI expansions can be grouped into either single reference (SRCI) or multireference (MRCI). In the first event, the expansion is based on one dominant CSF, which usually is the Hartree-Fock configuration constructed from the SCF orbitals. This includes the CSFs on the basis of their 'excitation levels', i.e., the number of electrons occupying orbitals which are empty in the Hartree-Fock configuration [225]. For further practical reasons, these calculations usually are limited to single and double excitations (CISD or, SR-CISD), though some reports on inclusion of higher excitations were presented [226]. In the multireference case, the expansion is based on a set of 'reference configurations' [227, 102], and again the expansion is limited to single and double excitations. In both single and multireference expansions, excitations from the inner-shell orbitals usually are omitted ('frozen-core CI'), since their contribution is supposedly small to the description of chemical processes, and since a meaningful treatment of inner-shell correlation technique requires a greatly expanded basis set [228, 149].

Earlier MRCI works included very few reference CSFs [102] but in later works a better idea based on an 'active space' i.e., a set of orbitals having variable occupancy in the reference configurations was used. This space is typically composed of the valence shell orbitals or a subset of them.

A highly desirable, but often not practical, form of the reference space is the 'complete active space' (CAS) [229], which consists of a full CI expansion within the active orbitals. However, inclusion of all the valence orbitals in the active space results in generating a quite large number of CSFs in the MRCI expansion [230]. Effective alternatives include the 'restricted active space' (RAS) and generalized valence bond form of active space, wherein restrictions in occupancy are place on

various subsets of the active orbitals [231].

C.1.1.2 Spin Adaptation

The spin of a single electron is described by the two spin functions $\alpha(\omega) \equiv \alpha$ and $\beta(\omega) \equiv \beta$, i.e., spin up ($\uparrow$) and spin down ($\downarrow$). For K orthonormal spatial orbitals $(\psi_i | i = 1, 2, \cdots, K)$ we can form a set of $2K$ spin orbitals $(\chi_i | i = 1, 2, \cdots 2K)$ by multiplying each spatial orbital by either the α or β function

$$\chi_{2i-1}(x) = \psi_i(r)\alpha(\omega) \tag{C.1}$$

$$\chi_{2i}(x) = \psi_i(r)\beta(\omega) \qquad i = 1, 2, \cdots K. \tag{C.2}$$

Such spin orbitals are *restricted* spin orbitals and the determinants formed from them are restricted determinants. A given spatial orbital ψ_i in such a determinant can be occupied either by a single electron (spin up or down) or by two electrons (one with spin up and the other with spin down). A determinant in which each spatial orbital is doubly occupied is called a *closed-shell* determinant and an *open shell* refers to a spatial orbital that is occupied by a single electron. All the electrons are paired in a closed-shell determinant, and a closed-shell determinant is a pure singlet, i.e., it is an eigenfunction of S^2 with eigenvalue zero. The simplest example of a closed-shell determinant is the Hartree-Fock ground state wavefunction of minimal basis H_2. Unitary group approach or symmetric group approach [232] are the tow common approaches used for the construction of complete set of S^2 eigenfunctions and for the calculation of Hamiltonian matrix elements between them. Spin

and symmetry adaptation are important not just for the increased efficiency of the calculation, but also to ensure that the resulting wavefunction describes an electronic state of the desired multiplicity and symmetry type and is not contaminated by contributions of the wrong type [225].

C.1.1.3 Spatial Symmetry Adaptation

In atomic calculations spatial symmetry is of particular importance. The use of full spin and spatial symmetry in atomic CI calculations can reduce the length of the CI expansion significantly in comparison to expansion in Slater determinants. It is important in focusing the calculations on the electronic states and in fully characterizing these states [102]. Symmetry adaptation is trivial in the case of molecules described by Abelian point-group symmetry. In these cases it is necessary only to use symmetry-adapted orbitals in the construction of the CSFs, and to limit the CI expansion to terms of the desired overall symmetry. Non-Abelian point group symmetry is often eschewed due to complications.

C.1.1.4 Basis Sets

In correlation corrections the requirements of basis set are much more demanding than those for SCF treatments [233]. In basis set formalism for the high level calculation, a very important advancement was the introduction of the 'generally contracted' Gaussian basis sets [234]. The generally contracted type gaussians can significantly produce more efficient basis sets than the usual 'segmented' contracted ones, because generally contracted basis functions can be chosen to reproduce atomic Hartree-Fock orbitals or atomic natural orbitals, or other desired

choices. In correlated calculations most of the computational effort is done in steps following the basis set integrals evaluation and SCF or MCSCF calculation. Besides, in the post-SCF stages this effort increases more steeply with basis set size (typically with the sixth power of the number of basis functions) than does the integral evaluation and SCF effort (proportional at most to the fourth power). Hence, it is desired to derive the maximum benefit out of the number of contracted basis functions; for example, by employing larger primitive Gaussian sets as well as general contraction, even at the cost of increased integral computation time.

Tow types of generally contracted Gaussian basis sets have been introduced in the recent years: viz., atomic natural orbital (ANO) [235] and 'correlation-consistent' polarized valence basis sets specifically designed for correlated calculations [236]. Basis sets designed for valence-shell electron correlation treatment cannot, in general, provide useful descriptions for core-core and core-valence correction effects [102]. With the addition of the extrapolation capabilities it is now possible, in many cases, to distinguish errors due to basis set incompleteness from errors due to electron correlation treatment.

C.1.1.5 Choices of Orbitals

In CI expansion, the configuration state functions are constructed from the canonical SCF (Hartree-Fock) orbitals of the molecules, both occupied and virtual. These CSFs are used most commonly in single reference CI expansions to study electronic states. In open shell cases, restricted SCF orbitals are generally used (or sometimes orbitals of a closely related closed-shell state). The use of different orbitals for α and β spins is rarely used in CI calculations [102].

Most attempts in improving SCF orbitals for use in CI calculations are focused upon the virtual orbitals. The virtual canonical SCF orbitals are obtained as eigenfunctions of a Fock operator representing an N electron potential, rather than an (N-1) electron potential acting on the electrons in occupied orbitals. As a consequence, the lower-energy virtual orbitals tend to be relatively diffuse and not very effective for correlating the electrons in occupied orbitals [237]. For larger molecules, expansion in terms of localized orbitals can lead to compact wavefunctions, though usually they entail giving up the use of spatial symmetry [238].

C.1.1.6 Integral Transformation

A very important step in CI calculation (basically in most correlated calculations) is the transformation of the one and two-electron basis set integrals to corresponding integrals over the orbitals. Although in some correlated treatments this step can be avoided [239], generally, it is simplest to formulate the Hamiltonian matrix element calculation in terms of fully transformed orbital integrals.

C.1.1.7 Matrix Eigenvalue Problem

Most Hamiltonian matrices that occur in CI calculations are sparse and diagonally dominant. Hence, iterative methods using simple element-by-element updates based on perturbation theory [240] usually are quite effective, at least for the lowest root. In conventional CI approach, the Hamiltonian matrix element are computed once, in the desired order, and stored thereafter.

C.2 Strengths and Weaknesses

The conceptual simplicity of configuration interaction method is very appealing, and its variational character is an important advantage, but its principal strength lies in its flexibility and generality. Its application to any electronic state is quite straightforward, and it can be spin- and symmetry-adapted relatively easily.

One of the weaknesses of truncated CI is its size-consistency problem. A satisfactory model in chemistry plays an important role in the selection of methods used in the study of electron correlation. *Size-consistency* is one of the prime requirements for a satisfactory model. In chemistry one is interested in the relative energies of molecules of different size. Suppose one wishes to calculate ΔE for the reaction

$$A + B \rightarrow C. \tag{C.3}$$

For the result to be meaningful, it is necessary to use approximation schemes that are equally good, in a certain sense, for molecules with different number of electrons. To define in just what sense, let us consider a supermolecule (e.g., dimer) composed of two identical but noninteracting molecules (monomers). Two monomers separated by a large distance will serve as an example of such a dimer. Physically, it is clear that the energy of the dimer should be just twice the energy of the monomer, since by assumption the monomers do not interact. An approximation scheme for calculating the energy of such a system that has this property is said to be size consistent. The Hartree-Fock approximation is an example of such a theory: the HF energy of a supermolecule composed of two noninteracting *closed shell* subsystems is just the sum of the HF energies of the subsystems.

The main weakness of truncated configuration interaction is its lack of proper scaling with the size of the system. The proper scaling of a computational approximation model, referred to as 'extensivity' or 'size extensivity' [241], is the main facet of the 'separability condition' [102]. The lack of extensivity also affects the accuracy of computed ionization potentials and electron affinities, unless appropriate corrections are applied. Another facet of the separability condition is 'size consistency' and truncated CI fails this test, as a result, when it is applied naïvely, fails to provide satisfactory dissociation energies and some other energy differences. Satisfactory dissociation energies also can be obtained by treating the dissociated limit as a 'supermolecule', using the same type of CI expansion as for the bound system employed in multireference treatments [242].

Although the use of higher order CSFs in CI calculation is easy in principle, the exponential increase in the size of a CI expansion with the level of excitation usually makes such calculations impractical [102]. The increased complexity in handling the coupling coefficient complicates the extension of the direct CI programs with higher excitation CSFs. Hence most attempts to include higher order excitations [226] or to implement full CI calculations use a determinantal formulation [102].

It is always difficult to extend the CI expansion to higher excitations because of its very slow convergence. Unlike the situations encountered in many body methods, the connected and disconnected cluster contributions to each excited CSF are inextricably combined in the CI formalism. The use of a multireference CISD expansion can account for some of the most important contributions arising from higher excitations in single-reference model but is not sufficient to offset the intrinsic limitation of the truncated CI approach. Overall, due to the approximate nature of

corrections and due to the efficient formulation of exactly size-consistent schemes, traditional methods such as CISD have lost their preference in ground state quantum chemical applications. For electronically excited states, however, the ease of definition of the CI method for any state of interest makes it an attractive method, and such calculations are performed fairly widely.

C.3 Modifications and Corrections

Full CI, as to be expected from a formally exact theory, is also size consistent. Unfortunately, truncated CI is devoid of this property. It should be noted that the magnitude of the size-consistency error increases as the size of the molecule increases, i.e., the truncated CI energy does not scale linearly with the size of the system and it is not additive for infinitely separated systems. However, using the Langhoff and Davidson method can reduce the error significantly [243]. Wherein they have proposed a correction for the effects of quadruple excitations, $\Delta E_{DC} = \Delta E_{CISD}(1 - C_0^2)$, where ΔE_{CISD} is the CISD correlation energy and C_0 is the coefficient of the Hartree-Fock configuration in the normalized CISD wavefunction. Alternative corrections for the lack of size consistency have also been reported [244, 245]. More accurate techniques are now available for evaluating the structure and properties of small molecules. However, successful methods like CCSD(T) are not yet currently applicable to large molecules because of the stringent basis set requirements and high-order scaling with system size [132].

The various approaches that have been employed to compensate for the deficiency of extensivity and size-consistency of truncated CI falls into two classes: the

first class applies 'post hoc' (often called 'quadruples correction') corrections, while the second method modifies the algorithm itself [102]. Numerous other analysis as well as proposed correction formulae and modifications for dealing with the extensivity problem have been published which are beyond the scope of this work. For a good reference, the paper of I. Shavitt is worth mentioning [102].

Appendix D

Analytical First Derivative of the CI-Singles Energy

For several years, the gradient of the generic CI energies have been evaluated using different schemes [246, 247]. Simple modifications of this existing programs can be utilized to generate the gradient of the CIS energy. In this section we will emphasize on the algebraic manipulation of the terms required for the purpose of determining the analytical first derivative of CIS energy. The simplicity of this special case provides us a technique which makes the computation of excited-state properties practicable for larger molecules.

The total energy for a CI-singles excited state is an eigenvalue of the Hamiltonian matrix given in Eq. (3.14). It can be rearranged as

$$E_{CIS} = E_{HF} + \sum_{ia} a_{ia}^2(\epsilon_a - \epsilon_i) - \sum_{ijab} a_{ia}a_{jb}(ja||ib). \tag{D.1}$$

The first derivative of E_{CIS} with respect to any external system parameter (e.g., a

geometric variable or an applied electric field) can be written as

$$E^x_{CIS} = E^x_{HF} + \sum_{ia} a^2_{ia}(\epsilon^x_a - \epsilon^x_i) - \sum_{ijab} a_{ia}a_{jb}[(j^x a\|ib) + (ja^x\|ib) + (ja\|i^x b) + (ja\|ib^x)] \tag{D.2}$$

where the superscript x refers to differentiation of the given term with respect to that parameter. The diagonalization of Eq. (3.14) ensures that there are no terms involving CI coefficient derivatives. The first term of Eq. (D.1) is handled by ordinary Hartree-Fock derivative theory [248], while the other terms require the knowledge of first-order changes in the Fock and overlap matrices

$$\epsilon^x_p = F^x_{pp} - S^x_{pp}\epsilon_p \tag{D.3}$$

molecular orbital (MO) coefficient derivatives

$$c^x_{\mu p} = \sum_q c_{\mu q} U^x_{qp} \tag{D.4}$$

and the two-electron integral derivatives. The molecular orbital coefficient derivatives evolves from the byproducts of solving the coupled-perturbed Hartree-Fock (CPHF) equations [249] for the unknown U matrix

$$\sum_{ia}[1 - A_{ijab}]U^x_{ia} = \frac{Q^x_{jb}}{\epsilon_j - \epsilon_b} \tag{D.5}$$

where Q_{jb} is a perturbation-dependent quantity given in Eq. (51) of reference [248]

and A_{ijab} is a matrix involving transformed two-electron integrals:

$$A_{ijab} = \frac{(ab\|ij) + (aj\|ib)}{\epsilon_i - \epsilon_a}. \tag{D.6}$$

Q_{jb} in Eq. (D.5) implies that the linear equation must be solved separately for each variable in the perturbation (one for each geometric degree of freedom in a geometry optimization). This method for evaluation of the gradient is inefficient [73]. Hence further enhancements have been introduced [250, 251] in the form of solving only one perturbation-independent CPHF equation and to derive an equation which does not require the transformation of the atomic orbital derivative integrals. Throughout the study, our program does not take advantage of the frozen core approximation described previously [252]. Thus calculations evaluating a gradient must involve CI contributions from all possible single substitutions. Therefore, the CIS gradient can be recasted in the following form:

$$E_x = \sum_{\mu\nu\lambda\sigma} \Gamma^{CIS}_{\mu\nu\lambda\sigma} (\mu\nu|\lambda\sigma)^x + \sum_{\mu\nu} P^{CIS}_{\mu\nu} H^x_{\mu\nu} + \sum_{\mu\nu} W^{CIS}_{\mu\nu} S^x_{\mu\nu} + V^x_{nuc.}. \tag{D.7}$$

The first term in the above equation involves the contraction of the two-particle CIS density matrix with two-electron integral derivatives. The second term involves the contraction of the CIS density matrix with the one-electron Hamiltonian derivatives. The third term depicts the contraction of an "energy-weighted" density matrix with the overlap integral derivatives. The final term is the nuclear repulsion energy derivative with respect to parameter x.

The two-particle CIS density matrix, Γ^{CIS} can be written in terms of the HF

ground-state density matrix and the ground-to-excited-state transition density matrix, T^{CIS}:

$$\Gamma^{CIS}_{\mu\nu\lambda\sigma} = \frac{1}{2}[P^{HF}_{\mu\nu}P^{HF}_{\lambda\sigma} + 2T^{CIS}_{\mu\nu}T^{CIS}_{\lambda\sigma} - P^{HF}_{\mu\sigma}P^{HF}_{\lambda\nu} - 2T^{CIS}_{\mu\sigma}T^{CIS}_{\lambda\nu}]. \tag{D.8}$$

$P^{HF}_{\mu\nu}$ is given in Eq. (3.9) and T^{CIS} can be expressed as:

$$T^{CIS}_{\mu\nu} = \sum_{ia} a_{ia}c_{\mu i}c_{\nu a}. \tag{D.9}$$

The CIS density matrix for excited-state, P^{CIS}, is also represented as a sum of HF as well as excited-state terms:

$$P^{CIS}_{\mu\nu} = P^{HF}_{\mu\nu} + P^{\Delta}_{\mu\nu} \tag{D.10}$$

where, $P^{\Delta}_{\mu\nu}$ are the elements of the CI-singles Δ density matrix, which is also called a "difference density matrix", since it represents the changes in the electronic orientations upon excitation. The Δ density matrix plays an important role in calculating accurate excited-state properties using the CIS framework, hence its evaluation and identification is important as well. It is, in fact, the use of the true CI-singles density matrix required by Eq. (D.7) and not the simple one-particle density matrix which allows the realistic computation of charge distribution, orbital population, and electronic moments of the excited state. In the MO basis, the Δ density matrix is symmetric matrix with both occupied-occupied (OO) and virtual-virtual (VV)

combinations:

$$P^{\Delta}_{ij} = -\sum_{ab} a_{ia}a_{jb} \tag{D.11}$$

$$P^{\Delta}_{ab} = +\sum_{ij} a_{ia}a_{jb} \tag{D.12}$$

with the occupied-virtual (OV) elements all zero. The true CIS density matrix required in Eq. (D.7) will have the same OO an VV contributions, but the OV terms are not all zero. The appearance of these off-diagonal block elements in the excited-state density matrix can be interpreted as orbital relaxation following the initial charge rearrangement due to excitation. These OV terms can be found by solving a single set of CPHF equations:

$$L_{ai} = \sum_{bj}[(ij\|ab) - (ib\|ja)]P^{\Delta}_{bj} + (\epsilon_a - \epsilon_j)P^{\Delta}_{ai} \tag{D.13}$$

where L is the Lagrangian of CI-singles given by

$$L_{ai} = C1_{ai} - C2_{ai} + \sum_{kl} P^{\Delta}_{kl}(al\|ik) + \sum_{bc} P^{\Delta}_{bc}(ab\|ic) \tag{D.14}$$

$$C1_{ci} = -2\sum_{jab} a_{ia}a_{jb}(cb\|ja) \tag{D.15}$$

$$C2_{bk} = -2\sum_{ija} a_{ia}a_{jb}(ik\|ja). \tag{D.16}$$

As the solution of Eq. (D.13) is implemented, *GAUSSIAN 94* does not require the transformed two-electron integrals to be stored on the disk [73]. Because of

the simple nature of the matrix elements, diagonalization can be carried out in a direct fashion, i.e., without the storage of the 2 electron integrals. Hence the appropriate matrix multiplication can be performed, using the two-electron integrals or by regeneration of them in each iteration. This opens the possibility of studying the excited states of molecules much larger than can be treated by methods such as MR-CI, since they involve the evaluation of more complicated matrix elements than above. The total CI-singles Δ density matrix presented in Eq. (D.10) can be generated by transforming the entire MO basis Δ density matrix defined by Eqs. (D.11), (D.12), and (D.13) respectively:

$$P^{\Delta}_{\mu\nu} = \sum_{pq} P^{\Delta}_{pq} c_{\mu p} c_{\nu q}. \tag{D.17}$$

The final term in Eq. (D.7) requires the energy weighted density matrix, which is also a sum of HF and excited state terms:

$$W^{CIS}_{\mu\nu} = W^{HF}_{\mu\nu} + W^{\Delta}_{\mu\nu} \tag{D.18}$$

$$\text{where} \qquad W^{HF}_{\mu\nu} = \sum_{i} \epsilon_i c_{\mu i} c_{\nu i} \tag{D.19}$$

while the second term have OO, VV and OV contributions in the MO basis:

$$W^{\Delta}_{ij} = -P^{\Delta}_{ij}\epsilon_i - S1_{ij} - \sum_{pq} P^{\Delta}_{pq}(ip\|jq) \tag{D.20}$$

$$W^{\Delta}_{ab} = P^{\Delta}_{ab}\epsilon_i - S2_{ab} \tag{D.21}$$

$$W^{\Delta}_{ai} = -C2_{ai} - P^{\Delta}_{ai}\epsilon_i \tag{D.22}$$

where the S matrices are defined by:

$$S1_{ij} = \sum_{ab} a_{ia} b_{jb} \tag{D.23}$$

$$S2_{ab} = \sum_{ij} a_{ia} b_{jb} \tag{D.24}$$

with the product vector

$$b_{jb} = \sum_{pq} W^{\Delta}_{pq} c_{\mu p} c_{\nu q} \tag{D.25}$$

which can be transformed to the AO basis for the use in Eq. (D.18) by:

$$W_{\mu\nu} = \sum_{pq} W^{\Delta}_{pq} c_{\mu p} c_{\nu q}. \tag{D.26}$$

Appendix E

Molecular Orbital Coefficients

Table E.1: Molecular orbital coefficients for the lowest excited states of PT octamer.

Atom	Atomic orbital contribution	Molecular orbital coefficients			
		HOMO	LUMO	HOMO-1	HOMO-2
C_2	$2p_z$	0.04282	0.03565	0.08767	-0.11737
C_2	$3p_z$	0.05973	0.06249	0.11912	-0.15570
S_3	$2p_z$	0.01098	0.01518	0.01746	-0.01668
S_3	$3p_z$	-0.02439	-0.03343	-0.03873	0.03698
S_3	$4p_z$	-0.02405	-0.04996	-0.03627	0.03296
C_4	$2p_z$	-0.03032	0.02135	-0.07478	0.11181
C_4	$3p_z$	-0.04617	0.03686	-0.10972	0.15779
C_5	$2p_z$	-0.04621	-0.04353	-0.08535	0.10064
C_5	$3p_z$	-0.06394	-0.07951	-0.11235	0.12677
C_6	$2p_z$	0.01973	-0.00085	0.04537	-0.06688
C_6	$3p_z$	0.02711	-0.00191	0.05979	-0.08504
C_9	$2p_z$	0.08127	0.07318	0.12573	-0.11084
C_9	$3p_z$	0.11380	0.12252	0.17519	-0.15593
C_{10}	$2p_z$	0.04626	-0.01797	0.08957	-0.10217
C_{10}	$3p_z$	0.06387	-0.03144	0.11785	-0.12893
C_{11}	$2p_z$	-0.07855	-0.07365	-0.10140	0.06266
C_{11}	$3p_z$	-0.10917	-0.13430	-0.13397	0.07904
C_{12}	$2p_z$	-0.06269	0.05200	-0.12075	0.12337
C_{12}	$3p_z$	-0.09370	0.08875	-0.17153	0.16479
S_{13}	$2p_z$	0.01224	0.02944	0.00456	0.01498
S_{13}	$3p_z$	-0.02700	-0.06407	-0.01003	-0.03291

continued overleaf

Atom	Atomic orbital contribution	Molecular orbital coefficients			
		HOMO	LUMO	HOMO-1	HOMO-2
S_{13}	$4p_z$	-0.02817	-0.10232	-0.01024	-0.03098
C_{16}	$2p_z$	0.11905	0.11202	0.10485	0.00272
C_{16}	$3p_z$	0.16982	0.18888	0.15191	-0.00589
S_{17}	$2p_z$	0.01216	0.04637	-0.01274	0.03368
S_{17}	$3p_z$	-0.02676	-0.10051	0.02804	-0.07387
S_{17}	$4p_z$	-0.02891	-0.16372	0.02767	-0.07146
C_{18}	$2p_z$	-0.09879	0.09080	-0.12083	0.02802
C_{18}	$3p_z$	-0.14826	0.15187	-0.16806	0.02772
C_{19}	$2p_z$	-0.10629	-0.09840	-0.06796	-0.03334
C_{19}	$3p_z$	-0.14878	-0.17761	-0.09070	-0.04236
C_{20}	$2p_z$	0.07436	-0.04369	0.09894	-0.04972
C_{20}	$3p_z$	0.10381	-0.07634	0.13142	-0.06325
C_{23}	$2p_z$	0.14107	0.13576	0.02741	0.10712
C_{23}	$3p_z$	0.20588	0.22866	0.04790	0.14310
C_{24}	$2p_z$	0.10016	-0.07604	0.06698	0.04097
C_{24}	$3p_z$	0.14102	-0.13310	0.08920	0.05279
C_{25}	$2p_z$	-0.11462	-0.10045	0.00160	-0.08516
C_{25}	$3p_z$	-0.16145	-0.17833	0.00154	-0.10908
C_{26}	$2p_z$	-0.13117	0.12609	-0.06568	-0.08882
C_{26}	$3p_z$	-0.19540	0.21050	-0.08480	-0.12989
S_{27}	$2p_z$	0.00562	0.05881	-0.02865	0.01869
S_{27}	$3p_z$	-0.01234	-0.12711	0.06291	-0.04093
S_{27}	$4p_z$	-0.01371	-0.20957	0.06414	-0.04045
C_{30}	$2p_z$	0.13117	0.12609	-0.06568	0.08882
C_{30}	$3p_z$	0.19540	0.21050	-0.08480	0.12989
S_{31}	$2p_z$	-0.00562	-0.02865	-0.01869	-0.01869
S_{31}	$3p_z$	0.01234	-0.12711	0.06291	0.04093
S_{31}	$4p_z$	0.01371	-0.20957	0.06414	0.04045
C_{32}	$2p_z$	-0.14107	0.13576	0.02741	0.10712
C_{32}	$3p_z$	-0.20588	0.22866	0.04790	-0.14310
C_{33}	$2p_z$	-0.10016	-0.07604	0.06698	-0.04097
C_{33}	$3p_z$	-0.14102	-0.13310	0.08920	-0.05279
C_{34}	$2p_z$	0.11462	-0.10045	0.00160	0.08516
C_{34}	$3p_z$	0.16145	-0.17833	0.00154	0.10908
C_{37}	$2p_z$	0.09879	0.09080	-0.12083	-0.02802
C_{37}	$3p_z$	0.14826	0.15187	-0.16806	-0.02772

continued overleaf

Atom	Atomic orbital contribution	Molecular orbital coefficients			
		HOMO	LUMO	HOMO-1	HOMO-2
C_{38}	$2p_z$	0.10629	-0.09840	-0.06796	0.03334
C_{38}	$3p_z$	0.14878	-0.17761	-0.09070	0.04236
C_{39}	$2p_z$	-0.07436	-0.04369	0.09894	0.04972
C_{39}	$3p_z$	-0.10381	-0.10381	0.13142	0.06325
C_{40}	$2p_z$	-0.11905	0.11202	0.10485	-0.00272
C_{40}	$3p_z$	-0.16982	0.18888	0.15191	0.00589
S_{41}	$2p_z$	-0.01216	0.04637	-0.01274	-0.03368
S_{41}	$3p_z$	0.02676	-0.10051	0.02804	0.07387
S_{41}	$4p_z$	0.02891	-0.16372	0.02767	0.07146
C_{44}	$2p_z$	0.06269	0.05200	-0.12075	-0.12337
C_{44}	$3p_z$	0.09370	0.08875	-0.17153	-0.16479
S_{45}	$2p_z$	-0.01224	0.02944	0.00456	-0.01498
S_{45}	$3p_z$	0.02700	-0.06407	-0.01003	0.03291
S_{45}	$4p_z$	0.02817	-0.10232	-0.01024	0.03098
C_{46}	$2p_z$	-0.08127	0.07318	0.12573	0.11084
C_{46}	$3p_z$	-0.11380	0.12252	0.17519	0.15593
C_{47}	$2p_z$	-0.04626	-0.01797	0.08957	0.10217
C_{47}	$3p_z$	-0.06387	-0.03144	0.11785	0.12893
C_{48}	$2p_z$	0.07854	-0.07365	-0.10140	-0.06266
C_{48}	$3p_z$	0.10917	-0.13429	-0.13397	-0.07904
C_{51}	$2p_z$	0.03032	0.02135	-0.07478	-0.11181
C_{51}	$3p_z$	0.04617	0.03686	-0.10972	-0.15779
C_{52}	$2p_z$	0.04621	-0.04353	-0.08535	-0.10064
C_{52}	$3p_z$	0.06394	-0.07951	-0.11235	-0.12677
C_{53}	$2p_z$	-0.01973	-0.00085	0.04537	0.06688
C_{53}	$3p_z$	-0.02711	-0.00191	0.05979	0.08504
C_{54}	$2p_z$	-0.04282	0.03565	0.08767	0.11737
C_{54}	$3p_z$	-0.05973	0.06249	0.11912	0.15570
S_{55}	$2p_z$	-0.01098	0.01518	0.01746	0.01668
S_{55}	$3p_z$	0.02439	-0.03343	-0.03873	-0.03698
S_{55}	$4p_z$	0.02405	-0.04996	-0.03627	-0.03296

Table E.2: Molecular orbital coefficients for the lowest excited states of PCY octamer.

Atom	Atomic orbital contribution	Molecular orbital coefficients			
		HOMO	LUMO	HOMO-1	HOMO-2
C_1	$2p_z$	0.00743	-0.00309	0.01729	0.02588
C_1	$3p_z$	0.01058	-0.00628	0.02327	0.03310
C_2	$2p_z$	-0.03777	0.03394	-0.03777	-0.07675
C_2	$3p_z$	-0.05488	0.06163	-0.10793	-0.13914
C_3	$2p_z$	-0.01541	-0.00775	-0.04015	-0.06434
C_3	$3p_z$	-0.02413	-0.01602	-0.05959	-0.09108
C_4	$2p_z$	0.06083	-0.05111	0.11103	0.12751
C_4	$3p_z$	0.08436	-0.07967	0.15170	0.17202
C_5	$2p_z$	-0.00887	0.00112	-0.01947	-0.02653
C_5	$3p_z$	-0.01249	-0.01056	-0.03079	-0.04487
H_6	$1s$	0.01092	-0.00792	0.02136	0.02654
H_6	$2s$	0.01889	-0.03253	0.03087	0.03214
H_7	$1s$	-0.01092	0.00792	-0.02136	-0.02654
H_7	$2s$	-0.01889	0.03253	-0.03088	-0.03215
C_{10}	$2p_z$	0.03259	0.01780	0.08024	0.11816
C_{10}	$3p_z$	0.05154	0.02400	0.11698	0.16169
C_{11}	$2p_z$	-0.07211	0.07361	-0.10557	-0.08548
C_{11}	$3p_z$	-0.10605	0.13438	-0.15143	-0.12104
C_{12}	$2p_z$	-0.04107	-0.03520	-0.09026	-0.11229
C_{12}	$3p_z$	-0.06392	-0.06638	-0.13181	-0.15503
C_{13}	$2p_z$	0.10102	-0.09322	0.11594	0.04732
C_{13}	$3p_z$	0.14320	-0.14531	0.16473	0.07256
C_{14}	$2p_z$	-0.01811	0.00145	-0.03119	-0.03012
C_{14}	$3p_z$	-0.02956	-0.01374	-0.05557	-0.05648
H_{15}	$1s$	-0.02202	0.01102	-0.03381	-0.02978
H_{15}	$2s$	-0.03357	0.04436	-0.04154	-0.02920
H_{16}	$1s$	0.02202	-0.01102	0.03381	0.02978
H_{16}	$2s$	0.03357	-0.04436	0.04154	0.02920
C_{19}	$2p_z$	0.06578	0.04905	0.12089	0.11085
C_{19}	$3p_z$	0.10163	0.07021	0.17055	0.14379
C_{20}	$2p_z$	-0.10570	0.11716	-0.07888	0.02142
C_{20}	$3p_z$	-0.15811	0.21435	-0.11767	0.02398
C_{21}	$2p_z$	-0.07201	-0.07494	-0.10723	-0.05789
C_{21}	$3p_z$	-0.13793	-0.13793	-0.15469	-0.07535

continued overleaf

Atom	Atomic orbital contribution	Molecular orbital coefficients			
		HOMO	LUMO	HOMO-1	HOMO-2
C_{22}	$2p_z$	0.13136	-0.12740	0.05446	-0.07955
C_{22}	$3p_z$	0.19121	-0.19795	0.08574	-0.09993
C_{23}	$2p_z$	-0.02740	0.00195	-0.02839	-0.00542
C_{23}	$3p_z$	-0.04785	-0.01187	-0.05320	-0.01010
H_{24}	$1s$	0.03283	-0.01169	0.03042	0.00540
H_{24}	$2s$	0.04705	-0.04449	0.03484	0.00540
H_{25}	$1s$	-0.03283	0.01168	-0.03041	-0.00540
H_{25}	$2s$	-0.04704	0.04450	-0.03483	-0.00539
C_{28}	$2p_z$	0.10256	0.09080	0.11040	-0.00008
C_{28}	$3p_z$	0.15640	0.13423	0.15025	-0.01009
C_{29}	$2p_z$	-0.11948	0.13842	-0.00201	0.09702
C_{29}	$3p_z$	-0.18244	0.25223	-0.00961	0.13400
C_{30}	$2p_z$	-0.10327	-0.11847	-0.07497	0.05015
C_{30}	$3p_z$	-0.16045	-0.21539	-0.10418	0.07559
C_{31}	$2p_z$	0.13101	-0.12614	-0.04186	-0.10354
C_{31}	$3p_z$	0.19587	-0.19215	-0.04863	-0.14376
C_{32}	$2p_z$	-0.03313	0.00102	-0.01126	0.02009
C_{32}	$3p_z$	-0.06097	-0.00462	-0.02199	0.04188
H_{33}	$1s$	-0.03913	0.00533	-0.01191	0.01920
H_{33}	$2s$	-0.05284	0.01954	-0.01270	0.01445
H_{34}	$1s$	0.03914	-0.00533	0.01192	-0.01920
H_{34}	$2s$	0.05287	-0.01956	0.01271	-0.01447
H_{37}	$1s$	-0.00862	0.00577	-0.01873	-0.02644
H_{37}	$2s$	-0.01325	0.01008	-0.02796	-0.03839
H_{38}	$1s$	0.00862	-0.00577	0.01872	0.02644
H_{38}	$2s$	0.01325	-0.01007	0.02796	0.03839
C_{39}	$2p_z$	0.13101	0.12614	0.04186	-0.10354
C_{39}	$3p_z$	0.19587	0.19215	0.04863	-0.14376
C_{40}	$2p_z$	-0.10327	0.11847	0.07497	0.05015
C_{40}	$3p_z$	-0.16045	0.21539	0.10418	0.07559
C_{41}	$2p_z$	-0.11948	-0.13842	0.00201	0.09702
C_{41}	$3p_z$	-0.18244	-0.25223	0.00961	0.13400
C_{42}	$2p_z$	0.10256	-0.09080	-0.11040	-0.00008
C_{42}	$3p_z$	0.15640	-0.13423	-0.15025	-0.01009
C_{43}	$2p_z$	-0.03313	-0.00102	0.01126	0.02009
C_{43}	$3p_z$	-0.06097	0.00462	0.02199	0.04188

continued overleaf

Atom	Atomic orbital contribution	Molecular orbital coefficients			
		HOMO	LUMO	HOMO-1	HOMO-2
H_{44}	$1s$	0.03913	0.00533	-0.01192	-0.01920
H_{44}	$2s$	0.05285	0.01955	-0.01270	-0.01446
H_{45}	$1s$	-0.03914	-0.00533	0.01192	0.01920
H_{45}	$2s$	-0.05286	-0.01956	0.01271	0.01446
C_{48}	$2p_z$	0.13136	0.12740	-0.05446	-0.07955
C_{48}	$3p_z$	0.19121	0.19795	-0.08574	-0.09993
C_{49}	$2p_z$	-0.07201	0.07494	0.10723	-0.05789
C_{49}	$3p_z$	-0.11231	0.13793	0.15469	-0.07535
C_{50}	$2p_z$	-0.10570	-0.11716	0.07888	0.02142
C_{50}	$3p_z$	-0.15811	-0.21435	0.11767	0.02398
C_{51}	$2p_z$	0.06578	-0.04905	-0.12089	0.11085
C_{51}	$3p_z$	0.10163	-0.07021	-0.17055	0.14379
C_{52}	$2p_z$	-0.02740	-0.00195	0.02839	-0.00542
C_{52}	$3p_z$	-0.04785	0.01187	0.05320	-0.01010
H_{53}	$1s$	-0.03283	-0.01169	0.03042	-0.00540
H_{53}	$2s$	-0.04704	-0.04450	0.03484	-0.00540
H_{54}	$1s$	0.03283	0.01169	-0.03042	0.00540
H_{54}	$2s$	0.04704	0.04449	-0.03483	0.00540
C_{57}	$2p_z$	0.10102	0.09322	-0.11594	0.04732
C_{57}	$3p_z$	0.14319	0.14531	-0.16473	0.07256
C_{58}	$2p_z$	-0.04107	0.03520	0.09026	-0.11229
C_{58}	$3p_z$	-0.06392	0.06638	0.13181	-0.15503
C_{59}	$2p_z$	-0.07211	-0.07361	0.10557	-0.08548
C_{59}	$3p_z$	-0.10605	-0.13438	0.15143	-0.12104
C_{60}	$2p_z$	0.03259	-0.01780	-0.08024	0.11816
C_{60}	$3p_z$	0.05154	-0.02400	-0.11698	0.16169
C_{61}	$2p_z$	-0.01811	-0.00145	0.03119	-0.03012
C_{61}	$3p_z$	-0.02956	0.01374	0.05557	-0.05648
H_{62}	$1s$	0.02202	0.01102	-0.03381	0.02978
H_{62}	$2s$	0.03357	0.04436	-0.04155	0.02921
H_{63}	$1s$	-0.02202	-0.01102	0.03381	-0.02978
H_{63}	$2s$	-0.03356	-0.04435	0.04154	-0.02919
C_{66}	$2p_z$	0.06083	0.05111	-0.11103	0.12751
C_{66}	$3p_z$	0.08436	0.07967	-0.15170	0.17202
C_{67}	$2p_z$	-0.01541	0.00775	0.04015	-0.06434
C_{67}	$3p_z$	-0.02413	0.01602	0.05959	-0.09108

continued overleaf

Atom	Atomic orbital contribution	Molecular orbital coefficients			
		HOMO	LUMO	HOMO-1	HOMO-2
C_{68}	$2p_z$	-0.03777	-0.03394	0.07675	-0.10191
C_{68}	$3p_z$	-0.05488	-0.06163	0.10793	-0.13914
C_{69}	$2p_z$	0.00743	0.00309	-0.01729	0.02588
C_{69}	$3p_z$	0.01058	0.00628	-0.02327	0.03310
C_{70}	$2p_z$	-0.00887	-0.00112	0.01947	-0.02653
C_{70}	$3p_z$	-0.01249	0.01056	0.03079	-0.04487
H_{71}	$1s$	-0.01887	-0.03252	0.03084	-0.03209
H_{71}	$2s$	-0.01887	-0.03252	0.03084	-0.03209
H_{72}	$1s$	0.01093	0.00793	-0.02138	0.02656
H_{72}	$2s$	0.01891	0.03253	-0.03092	0.03220
H_{75}	$1s$	-0.00861	-0.00576	0.01871	-0.02643
H_{75}	$2s$	-0.01323	-0.01005	0.02793	-0.03835
H_{76}	$1s$	0.00862	0.00577	-0.01874	0.02646
H_{76}	$2s$	0.01327	0.01010	-0.02799	0.03843

Table E.3: Molecular orbital coefficients for the lowest excited states of PFV octamer.

Atom	Atomic orbital contribution	Molecular orbital coefficients			
		HOMO	LUMO	HOMO-1	HOMO-2
C_1	$2p_z$	0.00694	-0.00125	0.01743	0.02687
C_1	$3p_z$	0.01079	-0.00752	0.02432	0.03467
C_2	$2p_z$	-0.03323	0.02145	-0.06858	-0.08804
C_2	$3p_z$	-0.04725	0.03823	-0.09508	-0.11939
C_3	$2p_z$	-0.01417	-0.00344	-0.03619	-0.05533
C_3	$3p_z$	-0.02318	-0.00793	-0.05596	-0.08122
C_4	$2p_z$	0.05620	-0.03319	0.10667	0.12210
C_4	$3p_z$	0.07762	-0.05035	0.14549	0.16450
C_5	$2p_z$	-0.00701	-0.00947	-0.02252	-0.03920
C_5	$3p_z$	-0.01301	-0.01530	-0.03754	-0.06103
C_6	$2p_z$	-0.03040	0.01798	-0.06443	-0.08512
C_6	$3p_z$	-0.04407	0.03674	-0.08852	-0.11151
C_{11}	$2p_z$	0.02876	0.01767	0.07588	0.11452
C_{11}	$3p_z$	0.04393	0.02324	0.10762	0.15402
C_{12}	$2p_z$	-0.06402	0.05974	-0.09177	-0.06768

continued overleaf

Atom	Atomic orbital contribution	Molecular orbital coefficients			
		HOMO	LUMO	HOMO-1	HOMO-2
C_{12}	$3p_z$	-0.09225	0.10518	-0.13103	-0.09810
C_{13}	$2p_z$	-0.03692	-0.02506	-0.08022	-0.09760
C_{13}	$3p_z$	-0.05844	-0.04725	-0.11803	-0.13409
C_{14}	$2p_z$	0.09310	-0.07937	0.10721	0.03857
C_{14}	$3p_z$	0.13008	-0.12105	0.15003	0.05810
C_{15}	$2p_z$	-0.01447	-0.01676	-0.03485	-0.04194
C_{15}	$3p_z$	-0.02614	-0.02852	-0.05742	-0.06491
C_{16}	$2p_z$	-0.05845	0.03208	-0.09488	-0.08751
C_{16}	$3p_z$	-0.08339	0.06614	-0.12773	-0.11189
C_{21}	$2p_z$	0.05973	0.05096	0.11469	0.10694
C_{21}	$3p_z$	0.08980	0.07152	0.15921	0.13867
C_{22}	$2p_z$	-0.09445	0.11132	-0.06608	0.02540
C_{22}	$3p_z$	-0.13940	0.19820	-0.10015	0.02683
C_{23}	$2p_z$	-0.06440	-0.06447	-0.09445	-0.05171
C_{23}	$3p_z$	-0.10057	-0.11829	-0.13500	-0.06452
C_{24}	$2p_z$	0.12192	-0.13020	0.04796	-0.08099
C_{24}	$3p_z$	0.17437	-0.19915	0.07370	-0.10299
C_{25}	$2p_z$	-0.02235	-0.02048	-0.03115	-0.00609
C_{25}	$3p_z$	-0.04086	-0.03464	-0.05180	-0.00936
C_{26}	$2p_z$	-0.08805	0.04291	-0.08407	-0.01296
C_{26}	$3p_z$	-0.12443	0.08604	-0.11229	-0.01668
C_{31}	$2p_z$	0.09436	0.10148	0.10458	-0.00028
C_{31}	$3p_z$	0.14047	0.14829	0.14116	-0.00795
C_{32}	$2p_z$	-0.10759	0.14016	0.00119	0.08567
C_{32}	$3p_z$	-0.16276	0.25042	-0.00661	0.11714
C_{33}	$2p_z$	-0.09286	-0.11577	-0.06720	0.04118
C_{33}	$3p_z$	-0.14346	-0.20803	-0.09112	0.06413
C_{34}	$2p_z$	0.12170	-0.14081	-0.04138	-0.10009
C_{34}	$3p_z$	0.17824	-0.21184	-0.04947	-0.13734
C_{35}	$2p_z$	-0.02701	-0.00983	-0.01204	0.02872
C_{35}	$3p_z$	-0.04974	-0.01655	-0.02013	0.04525
C_{36}	$2p_z$	-0.10462	0.02165	-0.03224	0.05876
C_{36}	$3p_z$	-0.14653	0.04279	-0.04269	0.07341
C_{41}	$2p_z$	0.12170	0.14081	0.04138	-0.10009
C_{41}	$3p_z$	0.17823	0.21184	0.04947	-0.13734
C_{42}	$2p_z$	-0.09285	0.11577	0.06720	0.04118

continued overleaf

Atom	Atomic orbital contribution	Molecular orbital coefficients			
		HOMO	LUMO	HOMO-1	HOMO-2
C_{42}	$3p_z$	-0.14346	0.20803	0.09112	0.06413
C_{43}	$2p_z$	-0.10759	-0.14016	-0.00119	0.08568
C_{43}	$3p_z$	-0.16277	-0.25042	0.00661	0.11714
C_{44}	$2p_z$	0.09436	-0.10148	-0.10458	-0.00028
C_{44}	$3p_z$	0.14047	-0.14829	-0.14116	-0.00795
C_{45}	$2p_z$	-0.02701	0.00984	0.01205	0.02871
C_{45}	$3p_z$	-0.04974	0.01656	0.02014	0.04524
C_{46}	$2p_z$	-0.10462	-0.02165	0.03225	0.05876
C_{46}	$3p_z$	-0.14653	-0.04280	0.04269	0.07341
C_{51}	$2p_z$	0.12191	0.13019	-0.04796	-0.08099
C_{51}	$3p_z$	0.17437	0.19914	-0.07370	-0.10299
C_{52}	$2p_z$	-0.06440	0.06447	0.09445	-0.05171
C_{52}	$3p_z$	-0.10057	0.11829	0.13499	-0.06453
C_{53}	$2p_z$	-0.09445	-0.11132	0.06608	0.02540
C_{53}	$3p_z$	-0.13940	-0.19821	0.10014	0.02683
C_{54}	$2p_z$	0.05973	-0.05096	-0.11469	0.10694
C_{54}	$3p_z$	0.08980	-0.07152	-0.15921	0.13867
C_{55}	$2p_z$	-0.02235	0.02049	0.03114	-0.00609
C_{55}	$3p_z$	-0.04086	0.03465	0.05180	-0.00937
C_{56}	$2p_z$	-0.08805	-0.04290	0.08407	-0.01297
C_{56}	$3p_z$	-0.12443	-0.08604	0.11229	-0.01668
C_{61}	$2p_z$	0.09309	0.07937	-0.10721	0.03857
C_{61}	$3p_z$	0.13008	0.12105	-0.15002	0.05810
C_{62}	$2p_z$	-0.03692	0.02505	0.08022	-0.09760
C_{62}	$3p_z$	-0.05844	0.04726	0.11802	-0.13409
C_{63}	$2p_z$	-0.06402	-0.05975	0.09177	-0.06769
C_{63}	$3p_z$	-0.09225	-0.10519	0.13103	-0.09810
C_{64}	$2p_z$	0.02876	-0.01767	-0.07588	0.11452
C_{64}	$3p_z$	0.04393	-0.02324	-0.10761	0.15402
C_{65}	$2p_z$	-0.01447	0.01676	0.03485	-0.04194
C_{65}	$3p_z$	-0.02614	0.02853	0.05742	-0.06492
C_{66}	$2p_z$	-0.05845	-0.03208	0.09488	-0.08751
C_{66}	$3p_z$	-0.08338	-0.06614	0.12773	-0.11190
C_{71}	$2p_z$	0.05620	0.03319	-0.10667	0.12210
C_{71}	$3p_z$	0.07762	0.05035	-0.14549	0.16450
C_{72}	$2p_z$	-0.01417	0.00344	0.03619	-0.05534

continued overleaf

Atom	Atomic orbital contribution	Molecular orbital coefficients			
		HOMO	LUMO	HOMO-1	HOMO-2
C_{72}	$3p_z$	-0.02317	0.00793	0.05596	-0.08122
C_{73}	$2p_z$	-0.03323	-0.02145	0.06857	-0.08804
C_{73}	$3p_z$	-0.04725	-0.03823	0.09508	-0.11939
C_{74}	$2p_z$	0.00694	0.00125	-0.01743	0.02687
C_{74}	$3p_z$	0.01079	0.00752	-0.02432	0.03467
C_{75}	$2p_z$	-0.00701	0.00947	0.02252	-0.03920
C_{75}	$3p_z$	-0.01301	0.01530	0.03753	-0.06103
C_{76}	$2p_z$	-0.03040	-0.01798	0.06443	-0.08512
C_{76}	$3p_z$	-0.04407	-0.03673	0.08852	-0.11151
H_{81}	$1s$	0.00798	-0.00193	0.01884	0.02750
H_{81}	$2s$	0.01071	0.00037	0.02550	0.03702
H_{82}	$1s$	0.00798	0.00193	-0.01884	0.02750
H_{82}	$2s$	0.01071	-0.00037	-0.02550	0.03702
H_{83}	$1s$	-0.00798	0.00193	-0.01884	-0.02750
H_{83}	$2s$	-0.01071	-0.00037	-0.02550	-0.03702
H_{84}	$1s$	-0.00798	-0.00193	0.01884	-0.02750
H_{84}	$2s$	-0.01071	0.00037	0.02550	-0.03702

Table E.4: Molecular orbital coefficients for the lowest excited states of PCNTH tetramer.

Atom	Atomic orbital contribution	Molecular orbital coefficients				
		HOMO	LUMO	HOMO-1	HOMO-2	HOMO-3
C_1	$2p_z$	-0.10431	0.02689	0.08615	-0.09156	-0.09707
C_1	$3p_z$	-0.15844	0.03937	0.11753	-0.13133	-0.12314
S_2	$2p_z$	0.01774	0.02649	0.01453	0.02118	-0.00929
S_2	$3p_z$	-0.03957	-0.05903	-0.03157	-0.04639	0.02036
S_2	$4p_z$	-0.04066	-0.07796	-0.03369	-0.04769	0.01650
C_3	$2p_z$	0.11795	0.05942	-0.05570	0.10170	0.08089
C_3	$3p_z$	0.16689	0.09249	-0.08076	0.13603	0.11123
C_4	$2p_z$	0.08682	-0.00602	-0.09317	0.05107	0.09981
C_4	$3p_z$	0.11651	-0.00735	-0.12240	0.06393	0.12282
C_5	$2p_z$	-0.10540	-0.04849	0.01454	-0.08517	-0.01599
C_5	$3p_z$	-0.14296	-0.08819	0.01826	-0.10693	-0.01968

continued overleaf

Atom	Atomic orbital contribution	Molecular orbital coefficients				
		HOMO	LUMO	HOMO-1	HOMO-2	HOMO-3
C_7	$2p_z$	0.00089	-0.01646	0.00031	-0.00431	0.00250
C_7	$3p_z$	0.00422	-0.02589	0.00528	0.00146	0.00220
C_8	$2p_z$	-0.00057	0.02470	-0.00634	-0.01630	0.00522
C_8	$3p_z$	-0.00370	0.03993	-0.01374	-0.02911	0.00792
C_9	$2p_z$	0.00026	0.00415	0.00106	0.00377	0.00059
C_9	$3p_z$	-0.00141	0.00274	0.00436	0.00537	-0.00298
N_{10}	$2p_z$	0.00190	-0.01173	0.00326	0.01115	-0.00060
N_{10}	$3p_z$	0.00321	-0.01705	0.00235	0.01285	0.00033
C_{11}	$2p_z$	0.00076	0.00497	0.00162	0.00296	-0.00284
C_{11}	$3p_z$	-0.00104	-0.01721	0.00754	0.00998	-0.00730
N_{12}	$2p_z$	0.00034	-0.01142	0.00575	0.00951	-0.00566
N_{12}	$3p_z$	-0.00104	-0.01721	0.00754	0.00998	-0.00730
C_{13}	$2p_z$	-0.07002	0.02116	0.13348	0.01685	-0.09558
C_{13}	$3p_z$	-0.10018	0.03609	0.18365	0.01787	-0.12925
C_{14}	$2p_z$	-0.09038	-0.03476	0.09630	-0.03875	-0.10445
C_{14}	$3p_z$	-0.12231	-0.05537	0.12482	-0.05022	-0.12849
C_{15}	$2p_z$	0.04767	-0.00113	-0.11169	-0.04551	0.02890
C_{15}	$3p_z$	0.06340	-0.00330	-0.14465	-0.05696	0.03479
C_{16}	$2p_z$	0.08877	0.02999	-0.12787	0.00609	0.10661
C_{16}	$3p_z$	0.12886	0.04916	-0.18535	0.00132	0.13683
S_{17}	$2p_z$	0.00324	0.01354	-0.03965	-0.05126	-0.00196
S_{17}	$3p_z$	-0.00658	-0.02943	-0.03965	-0.05126	-0.00196
S_{17}	$4p_z$	-0.01038	-0.04527	-0.03965	-0.05126	-0.00196
C_{19}	$2p_z$	-0.04767	0.00581	0.14634	0.10931	0.04520
C_{19}	$3p_z$	-0.07239	0.00880	0.20994	0.14705	0.05145
S_{20}	$2p_z$	0.01046	0.00664	-0.01339	0.00367	0.03443
S_{20}	$3p_z$	-0.02327	-0.01473	0.02984	-0.00791	-0.07487
S_{20}	$4p_z$	-0.02333	-0.01992	0.02885	-0.00682	-0.07285
C_{21}	$2p_z$	0.05618	0.01592	-0.14235	-0.09306	-0.01934
C_{21}	$3p_z$	0.07834	0.02510	-0.19628	-0.12838	-0.03268
C_{22}	$2p_z$	0.03779	-0.00037	-0.11972	-0.10468	-0.06728
C_{22}	$3p_z$	0.05037	-0.00065	-0.15537	-0.13260	-0.08162
C_{23}	$2p_z$	-0.05417	-0.01509	0.10913	0.04184	-0.01336
C_{23}	$3p_z$	-0.07281	-0.02607	0.14041	0.05185	-0.01529
C_{25}	$2p_z$	0.00064	-0.00332	0.00058	0.00040	-0.03163
C_{25}	$3p_z$	0.00285	-0.00491	-0.00198	0.00143	-0.03178

continued overleaf

Atom	Atomic orbital contribution	Molecular orbital coefficients				
		HOMO	LUMO	HOMO-1	HOMO-2	HOMO-3
C_{26}	$2p_z$	-0.00181	0.00537	0.00623	0.00043	-0.05990
C_{26}	$3p_z$	-0.00465	0.00839	0.01165	-0.00011	-0.08743
C_{27}	$2p_z$	0.00032	0.00083	0.02741	-0.00146	-0.00089
C_{27}	$3p_z$	-0.00015	0.00054	0.00023	0.00170	0.02299
N_{28}	$2p_z$	0.00178	-0.00249	-0.00545	-0.00188	0.03267
N_{28}	$3p_z$	0.00247	-0.00361	-0.00757	-0.00333	0.03558
C_{29}	$2p_z$	0.00050	0.00111	-0.00070	0.00101	0.01419
C_{29}	$3p_z$	0.00154	0.00066	-0.00433	-0.00155	0.02085
N_{30}	$2p_z$	0.00114	-0.00236	-0.00240	0.00185	0.03740
N_{30}	$3p_z$	0.00072	-0.00359	-0.00125	0.00316	0.04278
C_{31}	$2p_z$	-0.02380	0.00354	0.09215	0.10320	0.13842
C_{31}	$3p_z$	-0.03472	0.00598	0.13142	0.14284	0.18130
C_{32}	$2p_z$	-0.03751	-0.00889	0.11395	0.10278	0.12100
C_{32}	$3p_z$	-0.05034	-0.01400	0.14757	0.12880	0.14963
C_{33}	$2p_z$	0.01156	0.00073	-0.04637	-0.05385	-0.04636
C_{33}	$3p_z$	0.01500	0.00077	-0.05921	-0.06727	-0.05681
C_{34}	$2p_z$	0.03310	0.00686	-0.11058	-0.11238	-0.12734
C_{34}	$3p_z$	0.04723	0.01167	-0.15228	-0.14975	-0.16441
S_{35}	$2p_z$	0.00452	0.00300	-0.00953	-0.00323	0.02896
S_{35}	$3p_z$	-0.00988	-0.00654	0.02096	0.00737	-0.06208
S_{35}	$4p_z$	-0.01068	-0.00975	0.01958	0.00347	-0.07049
C_{39}	$2p_z$	-0.06502	0.02405	-0.07783	0.13523	-0.12165
C_{39}	$3p_z$	-0.09285	0.04095	-0.10724	0.18029	-0.15709
S_{40}	$2p_z$	-0.00906	0.01026	-0.00685	0.00401	0.02674
S_{40}	$3p_z$	0.01981	-0.02234	0.01508	-0.00917	-0.05731
S_{40}	$4p_z$	0.02147	-0.03352	0.01419	-0.00458	-0.06505
C_{41}	$2p_z$	0.04627	0.01154	0.06456	-0.12410	0.13179
C_{41}	$3p_z$	0.06806	0.01992	0.09249	-0.17212	0.17261
C_{42}	$2p_z$	0.07316	-0.03095	0.07957	-0.12262	0.11385
C_{42}	$3p_z$	0.09826	-0.04853	0.10316	-0.15384	0.14083
C_{43}	$2p_z$	-0.02280	0.00241	-0.03272	0.06491	-0.04514
C_{43}	$3p_z$	-0.02965	0.00240	-0.04185	0.08118	-0.05535
C_{45}	$2p_z$	-0.0010	-0.01057	0.00039	-0.00017	-0.02919
C_{45}	$3p_z$	-0.00511	-0.01628	-0.00123	-0.00154	-0.02900
C_{46}	$2p_z$	0.00249	0.01726	0.00336	0.00092	-0.05553
C_{46}	$3p_z$	0.00730	0.02712	0.00650	0.00242	-0.08132

continued overleaf

Atom	Atomic orbital contribution	Molecular orbital coefficients				
		HOMO	LUMO	HOMO-1	HOMO-2	HOMO-3
C_{47}	$2p_z$	-0.0009	0.00365	-0.00037	-0.00146	0.01326
C_{47}	$3p_z$	-0.00283	0.00219	-0.00279	0.00141	0.01936
N_{48}	$2p_z$	-0.00164	-0.00758	-0.00110	-0.00307	0.03484
N_{48}	$3p_z$	-0.00071	-0.01160	-0.00020	-0.00475	0.03986
C_{49}	$2p_z$	-0.00058	0.00269	-0.00094	0.00085	0.01026
C_{49}	$3p_z$	0.00050	0.00154	0.00041	-0.00247	0.02141
N_{50}	$2p_z$	-0.00295	-0.00793	-0.00329	0.00145	0.03031
N_{50}	$3p_z$	-0.00419	-0.01142	-0.00468	0.00306	0.03296
C_{51}	$2p_z$	-0.10809	0.05446	-0.09774	0.10817	-0.01643
C_{51}	$3p_z$	-0.15222	0.08422	-0.13602	0.15062	-0.02851
C_{52}	$2p_z$	-0.07202	0.00061	-0.08217	0.12326	-0.06460
C_{52}	$3p_z$	-0.09626	0.00323	-0.10680	0.15621	-0.07869
C_{53}	$2p_z$	0.10026	-0.05010	0.07152	-0.04454	-0.01649
C_{53}	$3p_z$	0.13544	-0.09035	0.09253	-0.05562	-0.01857
C_{54}	$2p_z$	0.09158	0.02052	0.10165	-0.13072	0.04274
C_{54}	$3p_z$	0.14012	0.02892	0.14616	-0.17556	0.04813
S_{55}	$2p_z$	-0.01911	0.02372	-0.00786	-0.00686	0.03272
S_{55}	$3p_z$	0.04244	-0.05296	0.01751	0.01490	-0.07105
S_{55}	$4p_z$	0.04396	-0.06854	0.01773	0.01319	-0.06986
C_{57}	$2p_z$	-0.15292	0.10034	-0.07416	-0.01990	0.10022
C_{57}	$3p_z$	-0.22508	0.16029	-0.11031	-0.01758	0.12972
S_{58}	$2p_z$	-0.00018	0.07116	0.01845	-0.03336	-0.00917
S_{58}	$3p_z$	-0.00055	-0.15539	-0.04064	0.07282	0.01967
S_{58}	$4p_z$	0.00505	-0.22767	-0.04169	0.07372	0.02429
C_{59}	$2p_z$	0.12513	0.16246	0.08828	-0.01888	-0.09622
C_{59}	$3p_z$	0.18791	0.24992	0.12233	-0.01460	-0.13222
C_{60}	$2p_z$	0.14135	-0.11897	0.04638	0.05645	-0.10155
C_{60}	$3p_z$	0.19696	-0.18505	0.06316	0.07289	-0.12989
C_{61}	$2p_z$	-0.08427	0.02245	-0.07165	0.05149	0.01304
C_{61}	$3p_z$	-0.11312	0.03828	-0.09304	0.06399	0.01615
C_{63}	$2p_z$	-0.00017	-0.17061	0.00144	0.00257	0.01558
C_{63}	$3p_z$	-0.00043	-0.27184	0.00625	-0.00226	0.01730
C_{64}	$2p_z$	-0.00004	0.19838	-0.00033	0.01138	0.02952
C_{64}	$3p_z$	0.00019	0.34167	-0.00503	0.02212	0.04355
C_{65}	$2p_z$	-0.00002	0.03630	0.00133	-0.00212	-0.00800
C_{65}	$3p_z$	-0.00428	0.02942	0.00008	-0.00611	-0.00989

continued overleaf

Atom	Atomic orbital contribution	Molecular orbital coefficients				
		HOMO	LUMO	HOMO-1	HOMO-2	HOMO-3
N_{66}	$2p_z$	0.00210	-0.10700	0.00265	-0.00678	-0.02059
N_{66}	$3p_z$	0.00474	-0.15612	0.00330	-0.00660	-0.02411
C_{67}	$2p_z$	-0.00005	0.03626	0.00069	-0.00364	-0.00404
C_{67}	$3p_z$	0.00422	0.02940	0.00255	-0.00394	-0.01173
N_{68}	$2p_z$	-0.00221	-0.10701	0.00073	-0.00958	-0.01497
N_{68}	$3p_z$	-0.00483	-0.15609	-0.00030	-0.01118	-0.01600
C_{69}	$2p_z$	-0.12948	0.16631	0.00367	-0.11163	0.03485
C_{69}	$3p_z$	-0.19339	0.25625	-0.00304	-0.15028	0.05683
C_{70}	$2p_z$	-0.14127	-0.11560	-0.05311	-0.06001	0.07939
C_{70}	$3p_z$	-0.19718	-0.17993	-0.07113	-0.07955	0.09947
C_{71}	$2p_z$	0.09000	0.01822	-0.02894	0.07897	0.01055
C_{71}	$3p_z$	0.12072	0.03123	-0.03774	0.09870	0.01149
C_{72}	$2p_z$	0.15525	0.09854	0.03416	0.10074	-0.06314
C_{72}	$3p_z$	0.22980	0.15753	0.04200	0.14404	-0.07588
S_{73}	$2p_z$	-0.00186	0.07173	0.02307	-0.02297	-0.02752
S_{73}	$3p_z$	0.00503	-0.15671	-0.05038	0.05026	0.05987
S_{73}	$4p_z$	-0.00079	-0.22942	-0.05367	0.05127	0.05827

Table E.5: Molecular orbital coefficients for the lowest excited states of PCNCY tetramer.

Atom	Atomic orbital contribution	Molecular orbital coefficients			
		HOMO	LUMO	HOMO-1	LUMO+1
C_1	$2p_z$	0.01053	0.00198	0.01905	-0.00449
C_1	$3p_z$	0.01486	-0.00138	0.02600	0.00208
C_2	$2p_z$	-0.04417	-0.01972	-0.07649	0.04582
C_2	$3p_z$	-0.06099	-0.03454	-0.10388	0.08106
C_3	$2p_z$	-0.02418	0.00450	-0.04597	-0.01189
C_3	$3p_z$	-0.03508	0.00741	-0.06578	-0.02038
C_4	$2p_z$	0.07194	-0.03598	0.10991	0.05507
C_4	$3p_z$	0.09725	-0.05087	0.14839	0.07831
C_5	$2p_z$	-0.01415	0.00367	-0.02272	-0.00520
C_5	$3p_z$	-0.02313	-0.00673	-0.03922	0.01353
H_6	1_s	0.01494	-0.00744	0.02322	0.01153

continued overleaf

Atom	Atomic orbital contribution	Molecular orbital coefficients			
		HOMO	LUMO	HOMO-1	LUMO+1
H_6	2_s	0.01870	-0.02057	0.02713	0.03388
H_7	1_s	-0.01495	0.00744	-0.02323	-0.01153
H_7	2_s	-0.01872	0.02058	-0.02715	-0.03389
H_9	1_s	0.01088	0.00430	0.01922	-0.00981
H_9	2_s	0.01522	0.01183	0.02673	-0.02608
H_{10}	1_s	-0.01089	-0.00430	-0.01922	0.00980
H_{10}	2_s	-0.01523	-0.01181	-0.02675	0.02606
C_{11}	$2p_z$	-0.00028	0.05734	0.00499	-0.10953
C_{11}	$3p_z$	0.00204	0.10036	0.01151	-0.19412
C_{12}	$2p_z$	0.05971	-0.05881	0.08938	0.10380
C_{12}	$3p_z$	0.08616	-0.10999	0.12674	0.19799
C_{13}	$2p_z$	0.00013	-0.01209	-0.00143	0.02350
C_{13}	$3p_z$	-0.00893	-0.01017	-0.01456	0.02272
N_{14}	$2p_z$	-0.02623	0.03237	-0.03993	-0.05942
N_{14}	$3p_z$	-0.03298	0.04737	-0.04981	-0.08826
C_{15}	$2p_z$	-0.00186	-0.01252	-0.00391	0.02418
C_{15}	$3p_z$	-0.00859	-0.01373	-0.01459	0.02763
N_{16}	$2p_z$	-0.02832	0.03383	-0.04242	-0.06139
N_{16}	$3p_z$	-0.03577	0.05076	-0.05295	-0.09291
C_{17}	$2p_z$	0.05188	-0.00495	0.08915	0.01015
C_{17}	$3p_z$	0.07720	-0.01039	0.12853	0.01725
C_{18}	$2p_z$	-0.07747	0.05676	-0.10398	-0.08468
C_{18}	$3p_z$	-0.10872	0.09540	-0.14523	-0.14313
C_{19}	$2p_z$	-0.05740	-0.04556	-0.09550	0.08663
C_{19}	$3p_z$	-0.08185	-0.08348	-0.13249	0.15689
C_{20}	$2p_z$	0.09366	-0.06274	0.10489	0.08150
C_{20}	$3p_z$	0.12901	-0.10180	0.14556	0.13171
C_{21}	$2p_z$	-0.02204	0.00313	-0.03161	-0.00402
C_{21}	$3p_z$	-0.03874	-0.00694	-0.05858	0.01738
H_{22}	1_s	0.02432	-0.01046	0.03330	0.01496
H_{22}	2_s	0.03105	-0.03550	0.03755	0.05448
H_{23}	1_s	-0.02433	0.01046	-0.03330	-0.01496
H_{23}	2_s	-0.03105	0.03550	-0.03756	-0.05448
C_{25}	$2p_z$	0.08172	0.04252	0.11834	-0.07718
C_{25}	$3p_z$	0.11699	0.06791	0.16284	-0.12515
C_{26}	$2p_z$	-0.08422	0.07778	-0.07026	-0.09180

continued overleaf

Atom	Atomic orbital contribution	Molecular orbital coefficients			
		HOMO	LUMO	HOMO-1	LUMO+1
C_{26}	$3p_z$	-0.11829	0.13870	-0.09785	-0.16608
C_{27}	$2p_z$	-0.08221	-0.05346	-0.10206	0.08367
C_{27}	$3p_z$	-0.11757	-0.08902	-0.14271	0.14219
C_{28}	$2p_z$	0.10924	0.05451	0.05210	-0.00061
C_{28}	$3p_z$	0.15319	0.07888	0.07926	-0.00285
C_{29}	$2p_z$	-0.03057	-0.00761	-0.02671	0.00283
C_{29}	$3p_z$	-0.05295	0.02002	-0.04961	-0.01669
H_{30}	1_s	-0.03332	-0.01858	-0.02848	0.01252
H_{30}	2_s	-0.04091	-0.05859	-0.03352	0.04806
H_{31}	1_s	0.03332	0.01858	0.02848	-0.01253
H_{31}	2_s	0.04091	0.05859	0.03352	-0.04806
C_{33}	$2p_z$	-0.00285	-0.14194	0.00217	0.10593
C_{33}	$3p_z$	0.00023	-0.25018	0.00638	0.18891
C_{34}	$2p_z$	0.10647	0.14006	0.06648	-0.09662
C_{34}	$3p_z$	0.15451	0.26449	0.09485	-0.18612
C_{35}	$2p_z$	-0.00087	0.03019	-0.00313	-0.02363
C_{35}	$3p_z$	-0.01518	0.02931	-0.02823	-0.00989
N_{36}	$2p_z$	-0.04854	-0.07970	-0.03239	0.05845
N_{36}	$3p_z$	-0.06131	-0.11815	-0.04083	0.08906
C_{37}	$2p_z$	-0.00125	0.03068	-0.00023	-0.02245
C_{37}	$3p_z$	-0.01483	0.03179	-0.01101	-0.02187
N_{38}	$2p_z$	-0.04906	-0.08058	-0.02904	0.05602
N_{38}	$3p_z$	-0.06211	-0.12034	-0.03609	0.08323
C_{39}	$2p_z$	0.10367	0.03630	0.09018	-0.05551
C_{39}	$3p_z$	0.14776	0.05494	0.11938	-0.07770
C_{40}	$2p_z$	-0.09720	-0.08322	-0.00815	-0.00088
C_{40}	$3p_z$	-0.13805	-0.13949	-0.01371	-0.00265
C_{41}	$2p_z$	-0.08766	0.09242	-0.05128	-0.04183
C_{41}	$3p_z$	-0.12404	0.16648	-0.06946	-0.07275
C_{42}	$2p_z$	0.10691	0.07945	-0.02441	0.02390
C_{42}	$3p_z$	0.15025	0.12822	-0.02775	0.04082
C_{43}	$2p_z$	-0.03285	-0.00711	-0.01298	0.00501
C_{43}	$3p_z$	-0.05682	0.01965	-0.02309	-0.01580
H_{44}	1_s	-0.03613	-0.02017	-0.01316	0.00916
H_{44}	2_s	-0.04544	-0.06671	-0.01262	0.02636
H_{45}	1_s	0.03613	0.02017	0.01316	-0.00916

continued overleaf

Atom	Atomic orbital contribution	Molecular orbital coefficients			
		HOMO	LUMO	HOMO-1	LUMO+1
H_{45}	2_s	0.04544	0.06671	0.01262	-0.02636
C_{47}	$2p_z$	0.10691	-0.07945	0.02441	0.02390
C_{47}	$3p_z$	0.15025	-0.12822	0.02775	0.04082
C_{48}	$2p_z$	-0.08766	-0.09242	0.05128	-0.04183
C_{48}	$3p_z$	-0.12404	-0.16648	0.06946	-0.07275
C_{49}	$2p_z$	-0.09720	0.08322	0.00815	-0.00088
C_{49}	$3p_z$	-0.13805	0.13949	0.01371	-0.00265
C_{50}	$2p_z$	0.10367	-0.03630	-0.09018	-0.05551
C_{50}	$3p_z$	0.14776	-0.05494	-0.11938	-0.07770
C_{51}	$2p_z$	-0.03285	0.00711	0.01298	0.00501
C_{51}	$3p_z$	-0.05682	-0.01965	0.02309	-0.01580
H_{52}	1_s	0.03613	-0.02017	-0.01316	-0.00916
H_{52}	2_s	0.04544	-0.06671	-0.01262	-0.02636
H_{53}	1_s	-0.03613	0.02017	0.01316	0.00916
H_{53}	2_s	-0.04544	0.06671	0.01262	0.02636
C_{55}	$2p_z$	-0.00285	0.14194	-0.00217	0.10593
C_{55}	$3p_z$	0.00023	0.25018	-0.00638	0.18891
C_{56}	$2p_z$	0.10647	-0.14006	-0.06648	-0.09662
C_{56}	$3p_z$	0.15451	-0.26449	-0.09485	-0.18612
C_{57}	$2p_z$	-0.00125	-0.03068	0.00023	-0.02245
C_{57}	$3p_z$	-0.01483	-0.03179	0.01101	-0.02187
N_{58}	$2p_z$	-0.04906	0.08058	0.02904	0.05602
N_{58}	$3p_z$	-0.06211	0.12034	0.03609	0.08323
C_{59}	$2p_z$	-0.00087	-0.03019	0.00313	-0.02363
C_{59}	$3p_z$	-0.01518	-0.02931	0.00989	-0.02823
N_{60}	$2p_z$	-0.04854	0.07970	0.03239	0.05845
N_{60}	$3p_z$	-0.06131	0.11815	0.04083	0.08906
C_{61}	$2p_z$	0.10924	-0.05451	-0.05210	-0.00061
C_{61}	$3p_z$	0.15319	-0.07888	-0.07926	-0.00285
C_{62}	$2p_z$	-0.08221	0.05346	0.10206	0.08367
C_{62}	$3p_z$	-0.11757	0.08902	0.14271	0.14219
C_{63}	$2p_z$	-0.08422	-0.07778	0.07026	-0.09180
C_{63}	$3p_z$	-0.11829	-0.13870	0.09785	-0.16608
C_{64}	$2p_z$	0.08172	-0.04252	-0.11834	-0.07718
C_{64}	$3p_z$	0.11699	-0.06791	-0.16284	-0.12515
C_{65}	$2p_z$	-0.03057	0.00761	0.02671	0.00283

continued overleaf

Atom	Atomic orbital contribution	Molecular orbital coefficients			
		HOMO	LUMO	HOMO-1	LUMO+1
C_{65}	$3p_z$	-0.05295	0.04961	-0.02002	-0.01669
H_{66}	1_s	0.03332	-0.01858	-0.02848	-0.01253
H_{66}	2_s	0.04091	-0.05859	-0.03352	-0.04806
H_{67}	1_s	-0.03332	0.01858	0.02848	0.01252
H_{67}	2_s	-0.04091	0.05859	0.03352	0.04806
C_{69}	$2p_z$	0.09366	0.06274	-0.10489	0.08150
C_{69}	$3p_z$	0.12901	0.10180	-0.14556	0.13171
C_{70}	$2p_z$	-0.05740	0.04556	0.09550	0.08663
C_{70}	$3p_z$	-0.08185	0.08348	0.13249	0.15689
C_{71}	$2p_z$	-0.07747	-0.05676	0.10398	-0.08468
C_{71}	$3p_z$	-0.10872	-0.09540	0.14523	-0.14313
C_{72}	$2p_z$	0.05188	0.00495	-0.08915	0.01015
C_{72}	$3p_z$	0.07720	0.01039	-0.12853	0.01725
C_{73}	$2p_z$	-0.02204	-0.00313	0.03161	-0.00402
C_{73}	$3p_z$	-0.03874	0.00694	0.05858	0.01738
H_{74}	1_s	-0.02433	-0.01046	0.03330	-0.01496
H_{74}	2_s	-0.03105	-0.03550	0.03756	-0.05448
H_{75}	1_s	0.02432	0.01046	-0.03330	0.01496
H_{75}	2_s	0.03105	0.03550	-0.03755	0.05448
C_{77}	$2p_z$	-0.00028	-0.05734	-0.00499	-0.10953
C_{77}	$3p_z$	0.00204	-0.10036	-0.01151	-0.19412
C_{78}	$2p_z$	0.05971	0.05881	-0.08938	0.10380
C_{78}	$3p_z$	0.08616	0.10999	-0.12674	0.19799
C_{79}	$2p_z$	-0.00186	0.01252	0.00391	0.02418
C_{79}	$3p_z$	-0.00859	0.01373	0.01459	0.02763
N_{80}	$2p_z$	-0.02832	-0.03383	0.04242	-0.06139
N_{80}	$3p_z$	-0.03577	-0.05076	0.05295	-0.09291
C_{81}	$2p_z$	0.00013	0.01209	0.00143	0.02350
C_{81}	$3p_z$	-0.00893	0.01017	0.01456	0.02272
N_{82}	$2p_z$	-0.02623	-0.03237	0.03993	-0.05942
N_{82}	$3p_z$	-0.03298	-0.04737	0.04981	-0.08826
C_{83}	$2p_z$	0.07194	0.03598	-0.10991	0.05507
C_{83}	$3p_z$	0.09725	0.05087	-0.14839	0.07831
C_{84}	$2p_z$	-0.02418	-0.00450	0.04597	-0.01189
C_{84}	$3p_z$	-0.03508	-0.00741	0.06578	-0.02038
C_{85}	$2p_z$	-0.04417	0.01972	0.07649	0.04582

continued overleaf

Atom	Atomic orbital contribution	Molecular orbital coefficients			
		HOMO	LUMO	HOMO-1	LUMO+1
C_{85}	$3p_z$	-0.06099	0.03454	0.10388	0.08106
C_{86}	$2p_z$	0.01053	-0.00198	-0.01905	-0.00449
C_{86}	$3p_z$	0.01486	0.00138	-0.02600	0.00208
C_{87}	$2p_z$	-0.01415	-0.00367	0.02272	-0.00520
C_{87}	$3p_z$	-0.02313	0.00673	0.03922	0.01353
H_{88}	1_s	-0.01495	-0.00744	0.02323	-0.01153
H_{88}	2_s	-0.01872	-0.02058	0.02715	-0.03389
H_{89}	1_s	0.01494	0.00744	-0.02322	0.01153
H_{89}	2_s	0.01870	0.02057	-0.02713	0.03388
H_{90}	1_s	0.01088	-0.00430	-0.01922	-0.00981
H_{90}	2_s	0.01522	-0.01183	-0.02673	-0.02608
H_{91}	1_s	-0.01089	0.00430	0.01922	0.00980
H_{91}	2_s	-0.01523	0.01181	0.02675	0.02606

Table E.6: Molecular orbital coefficients for the lowest excited states of PCNFV tetramer.

Atom	Atomic orbital contribution	Molecular orbital coefficients			
		HOMO	LUMO	HOMO-1	LUMO+1
C_1	$2p_z$	0.00256	-0.00045	0.01987	-0.02819
C_1	$3p_z$	0.00414	0.00059	0.02948	-0.03820
C_2	$2p_z$	-0.01063	0.00247	-0.07378	0.08973
C_2	$3p_z$	-0.01510	0.00422	-0.10246	0.12071
C_3	$2p_z$	-0.00516	-0.00044	-0.04132	0.06021
C_3	$3p_z$	-0.00718	-0.00047	-0.05780	0.08304
C_4	$2p_z$	0.02072	0.00735	0.12168	-0.11697
C_4	$3p_z$	0.02798	0.00996	0.16432	-0.15799
C_5	$2p_z$	-0.00428	0.00085	-0.03245	0.04463
C_5	$3p_z$	-0.00730	0.00223	-0.05468	0.07282
C_6	$2p_z$	-0.01285	-0.00431	-0.08044	0.08814
C_6	$3p_z$	-0.01772	-0.00786	-0.10715	0.11188
C_9	$2p_z$	-0.00169	-0.00920	-0.00239	-0.00547
C_9	$3p_z$	-0.00232	-0.01589	0.00008	-0.01391
C_{10}	$2p_z$	0.01591	0.01122	0.08430	-0.06893

continued overleaf

Atom	Atomic orbital contribution	Molecular orbital coefficients			
		HOMO	LUMO	HOMO-1	LUMO+1
C_{10}	$3p_z$	0.02366	0.02033	0.12146	-0.09468
C_{11}	$2p_z$	0.00061	0.00186	0.00129	0.00154
C_{11}	$3p_z$	-0.00187	0.00102	-0.01122	0.01055
N_{12}	$2p_z$	-0.00681	-0.00580	-0.03649	0.03088
N_{12}	$3p_z$	-0.00878	-0.00820	-0.04654	0.03890
C_{13}	$2p_z$	-0.00016	0.00185	-0.01196	0.00275
C_{13}	$3p_z$	-0.00190	0.00185	-0.01196	0.01185
N_{14}	$2p_z$	-0.00752	-0.00615	-0.03949	0.03162
N_{14}	$3p_z$	-0.00964	-0.00902	-0.04993	0.03925
C_{16}	$2p_z$	0.01282	0.00000	0.09257	-0.11834
C_{16}	$3p_z$	0.01905	0.00098	0.13158	-0.15892
C_{17}	$2p_z$	-0.02235	-0.01321	-0.10470	0.05879
C_{17}	$3p_z$	-0.03072	-0.02150	-0.14381	0.08152
C_{18}	$2p_z$	-0.01286	0.00714	-0.08877	0.09684
C_{18}	$3p_z$	-0.02003	0.01355	-0.12864	0.13064
C_{19}	$2p_z$	0.03208	0.01681	0.12322	-0.02108
C_{19}	$3p_z$	0.04399	0.02700	0.16965	-0.03432
C_{20}	$2p_z$	-0.00680	0.00160	-0.04491	0.04399
C_{20}	$3p_z$	-0.01188	0.00190	-0.07551	0.07073
C_{21}	$2p_z$	-0.02218	-0.00836	-0.11427	0.08551
C_{21}	$3p_z$	-0.03087	-0.01443	-0.15207	0.10715
C_{25}	$2p_z$	0.02118	-0.00833	0.12504	-0.09377
C_{25}	$3p_z$	0.03144	-0.01348	0.17402	-0.11956
C_{26}	$2p_z$	-0.03185	-0.01625	-0.08772	-0.03324
C_{26}	$3p_z$	-0.04617	-0.02853	-0.12661	-0.04128
C_{27}	$2p_z$	-0.02278	0.01003	-0.10711	0.03794
C_{27}	$3p_z$	-0.03173	0.01526	-0.14804	0.04915
C_{28}	$2p_z$	0.05604	-0.02517	0.09995	0.09025
C_{28}	$3p_z$	0.07639	-0.03460	0.14166	0.11363
C_{29}	$2p_z$	-0.01361	-0.00361	-0.04626	-0.00481
C_{29}	$3p_z$	-0.02297	-0.00945	-0.07836	-0.00713
C_{30}	$2p_z$	-0.04105	0.02007	-0.11857	-0.00574
C_{30}	$3p_z$	-0.05657	0.03634	-0.15798	-0.00619
C_{33}	$2p_z$	-0.00626	0.04153	-0.00529	0.00203
C_{33}	$3p_z$	-0.00880	0.07212	-0.00387	0.00605
C_{34}	$2p_z$	0.04686	-0.04787	0.09247	0.03479

continued overleaf

Atom	Atomic orbital contribution	Molecular orbital coefficients			
		HOMO	LUMO	HOMO-1	LUMO+1
C_{34}	$3p_z$	0.07009	-0.08768	0.13407	0.04788
C_{35}	$2p_z$	0.00151	-0.00836	-0.00065	0.00152
C_{35}	$3p_z$	-0.00539	-0.00562	-0.01156	-0.00577
N_{36}	$2p_z$	-0.02057	0.02544	-0.04271	-0.01315
N_{36}	$3p_z$	-0.02651	0.03637	-0.05464	-0.01637
C_{37}	$2p_z$	0.00041	-0.00881	0.00107	-0.00312
C_{37}	$3p_z$	-0.00493	-0.00833	-0.01221	-0.00485
N_{38}	$2p_z$	-0.02179	0.02644	-0.04081	-0.01826
N_{38}	$3p_z$	-0.02819	0.03884	-0.05199	-0.02318
C_{40}	$2p_z$	0.04021	-0.00496	0.12724	0.02646
C_{40}	$3p_z$	0.05874	-0.00979	0.17272	0.04374
C_{41}	$2p_z$	-0.05725	0.04545	-0.05065	-0.09748
C_{41}	$3p_z$	-0.07893	0.07384	-0.07093	-0.13175
C_{42}	$2p_z$	-0.03419	-0.02959	-0.08275	-0.06018
C_{42}	$3p_z$	-0.05298	-0.05502	-0.11616	-0.08484
C_{43}	$2p_z$	0.08109	-0.05576	0.03256	0.11883
C_{43}	$3p_z$	0.11194	-0.08997	0.05010	0.15901
C_{44}	$2p_z$	-0.01829	-0.00631	-0.03578	-0.03889
C_{44}	$3p_z$	-0.03203	-0.00904	-0.05961	-0.06349
C_{45}	$2p_z$	-0.05993	0.03111	-0.08881	-0.07938
C_{45}	$3p_z$	-0.08350	0.05458	-0.11772	-0.10042
H_{49}	$1s$	0.00278	-0.00084	0.02075	-0.02793
H_{49}	$2s$	0.00344	-0.00251	0.02648	-0.03598
H_{50}	$1s$	-0.00278	0.00084	-0.02075	0.02793
H_{50}	$2s$	-0.00344	0.00251	-0.02648	0.03598
C_{51}	$2p_z$	0.05411	0.03384	0.08079	0.11440
C_{51}	$3p_z$	0.07982	0.05487	0.10723	0.15407
C_{52}	$2p_z$	-0.08001	0.05367	0.00042	-0.06892
C_{52}	$3p_z$	-0.11619	0.09454	-0.00337	-0.09674
C_{53}	$2p_z$	-0.05778	-0.03817	-0.04621	-0.09985
C_{53}	$3p_z$	-0.08102	-0.05923	-0.06219	-0.13477
C_{54}	$2p_z$	0.13355	0.07488	-0.03264	0.03758
C_{54}	$3p_z$	0.18560	0.10624	-0.03912	0.05926
C_{55}	$2p_z$	-0.03381	0.01191	-0.00599	-0.04141
C_{55}	$3p_z$	-0.05806	0.02880	-0.01116	-0.06799
C_{56}	$2p_z$	-0.10201	-0.06602	-0.01973	-0.08461

continued overleaf

Atom	Atomic orbital contribution	Molecular orbital coefficients			
		HOMO	LUMO	HOMO-1	LUMO+1
C_{56}	$3p_z$	-0.13997	-0.11837	-0.02741	-0.10704
C_{59}	$2p_z$	-0.01742	-0.13691	0.00111	0.00204
C_{59}	$3p_z$	-0.02054	-0.23456	0.00022	0.00652
C_{60}	$2p_z$	0.11267	0.15013	-0.00825	0.03715
C_{60}	$3p_z$	0.16821	0.27508	-0.01205	0.05082
C_{61}	$2p_z$	0.00348	0.02681	-0.00148	-0.00266
C_{61}	$3p_z$	-0.01226	0.01967	0.00152	-0.00499
N_{62}	$2p_z$	-0.05124	-0.08210	0.00229	-0.01923
N_{62}	$3p_z$	-0.06635	-0.11803	0.00276	-0.02460
C_{63}	$2p_z$	0.00126	0.02815	0.00169	0.00158
C_{63}	$3p_z$	-0.01194	0.02508	0.00054	-0.00595
N_{64}	$2p_z$	-0.05329	-0.08370	0.00577	-0.01443
N_{64}	$3p_z$	-0.06906	-0.12246	0.00751	-0.01813
C_{66}	$2p_z$	0.10135	0.01880	0.01670	0.10246
C_{66}	$3p_z$	0.14743	0.03117	0.01674	0.13095
C_{67}	$2p_z$	-0.11947	-0.12048	0.05452	0.03403
C_{67}	$3p_z$	-0.17159	-0.18878	0.07612	0.04314
C_{68}	$2p_z$	-0.08335	0.11208	0.00880	-0.05022
C_{68}	$3p_z$	-0.12733	0.18934	0.01617	-0.06429
C_{69}	$2p_z$	0.12364	0.11757	-0.06900	-0.08130
C_{69}	$3p_z$	0.18162	0.17990	-0.09532	-0.10312
C_{70}	$2p_z$	-0.03788	0.01565	0.00911	-0.01148
C_{70}	$3p_z$	-0.06865	0.02845	0.01733	-0.01763
C_{71}	$2p_z$	-0.11778	-0.07398	0.02549	-0.01911
C_{71}	$3p_z$	-0.16035	-0.13332	0.03347	-0.02328
C_{75}	$2p_z$	0.12477	-0.13147	-0.03938	0.00622
C_{75}	$3p_z$	0.18064	-0.20237	-0.05896	-0.00022
C_{76}	$2p_z$	-0.07921	-0.09916	0.05072	0.08198
C_{76}	$3p_z$	-0.12259	-0.16767	0.07372	0.11139
C_{77}	$2p_z$	-0.11641	0.12924	0.04888	0.03652
C_{77}	$3p_z$	-0.16606	0.20400	0.06993	0.05392
C_{78}	$2p_z$	0.08093	0.00026	-0.05239	-0.09530
C_{78}	$3p_z$	0.12001	-0.00646	-0.07455	-0.12855
C_{79}	$2p_z$	-0.03457	-0.01405	0.02071	0.02979
C_{79}	$3p_z$	-0.06273	-0.02152	0.03594	0.04913
C_{80}	$2p_z$	-0.10762	0.06848	0.05129	0.05713

continued overleaf

Atom	Atomic orbital contribution	Molecular orbital coefficients			
		HOMO	LUMO	HOMO-1	LUMO+1
C_{80}	$3p_z$	-0.14629	0.12133	0.06681	0.07031
C_{83}	$2p_z$	-0.01203	0.10830	0.00219	-0.00318
C_{83}	$3p_z$	-0.01279	0.18461	-0.00022	-0.01044
C_{84}	$2p_z$	0.09404	-0.12433	-0.04511	-0.05179
C_{84}	$3p_z$	0.13941	-0.22596	-0.06492	-0.07109
C_{85}	$2p_z$	-0.00073	-0.02212	0.00099	0.00187
C_{85}	$3p_z$	-0.01124	-0.02027	0.00640	0.00886
N_{86}	$2p_z$	-0.04523	0.06921	0.02150	0.02411
N_{86}	$3p_z$	-0.05804	0.10126	0.02724	0.03003
C_{87}	$2p_z$	0.00348	-0.02120	-0.00074	0.00089
C_{87}	$3p_z$	-0.01043	-0.01326	0.00570	0.00752
N_{88}	$2p_z$	-0.04169	0.06647	0.02013	0.02370
N_{88}	$3p_z$	-0.05402	0.09462	0.02584	0.03011
C_{90}	$2p_z$	0.12238	-0.08201	-0.06481	-0.08892
C_{90}	$3p_z$	0.16850	-0.11442	-0.08919	-0.12232
C_{91}	$2p_z$	-0.03279	0.00615	0.02330	0.04789
C_{91}	$3p_z$	-0.04669	0.00779	0.03295	0.06629
C_{92}	$2p_z$	-0.06581	-0.02782	0.04098	0.07087
C_{92}	$3p_z$	-0.09330	-0.04779	0.05692	0.09556
C_{93}	$2p_z$	0.01610	0.00487	-0.01112	-0.02228
C_{93}	$3p_z$	0.02596	-0.00759	-0.01651	-0.03028
C_{94}	$2p_z$	-0.02674	-0.00954	0.01803	0.03498
C_{94}	$3p_z$	-0.04664	-0.02367	0.03092	0.05786
C_{95}	$2p_z$	-0.07918	0.05040	0.04458	0.06937
C_{95}	$3p_z$	-0.10847	0.09052	0.05914	0.08794
H_{99}	$1s$	0.01740	0.00942	-0.01160	-0.02208
H_{99}	$2s$	0.02164	0.02883	-0.01483	-0.02849
H_{100}	$1s$	-0.01740	-0.00942	0.01160	0.02208
H_{100}	$2s$	-0.02164	-0.02883	0.01483	0.02849

Appendix F

Schematic Diagrams of Molecular Orbitals

In this appendix we represent important molecular orbitals like the HOMO, LUMO, HOMO-1, HOMO-2, LUMO+1 and LUMO+2 for the six molecular systems of interest along with their unsubstituted carbon backbones i.e., the respective polyacetylene oligomers. These MOs are important in a sense that the electrons are excited from these HOMOs to the LUMOs. The calculated wavefunction is projected onto a local atomic orbital basis. The colours and size of the symbols represent the local phase and amplitude of the wavefunction (green: negative, red: positive). These LCAO (Linear Combination of Atomic Orbitals) molecular orbitals of the octamers for PA, PT, PCY, PFV and tetramers for PCNTH, PCNCY and PCNFV show that the Highest Occupied Molecular Orbitals and the Lowest Unoccupied Molecular Orbitals have a delocalized character while other levels present a localized nature, as exemplified by the HOMO-2 and LUMO+2 orbitals.

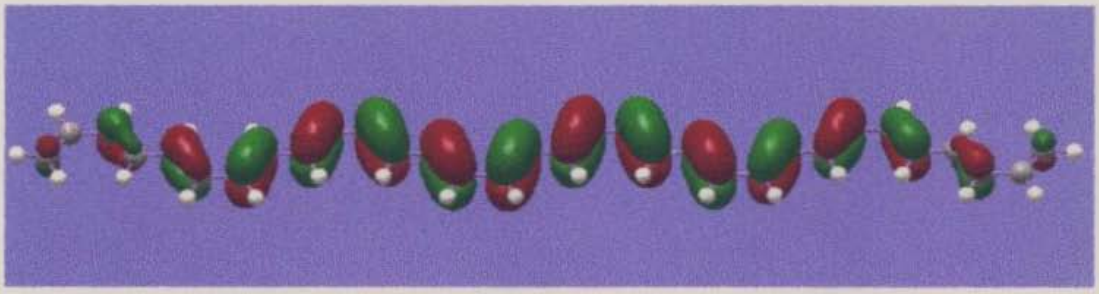

Figure F.1: Schematic representation of the HOMO for *trans-cisoid* PA octamer. Since the HOMO is a π state, only the p_z components are nonzero. The colours and size of the symbols represent the local phase and amplitude of the wavefunction (green:negative, red:positive).

Figure F.2: Schematic representation of the HOMO for aromatic PT octamer.

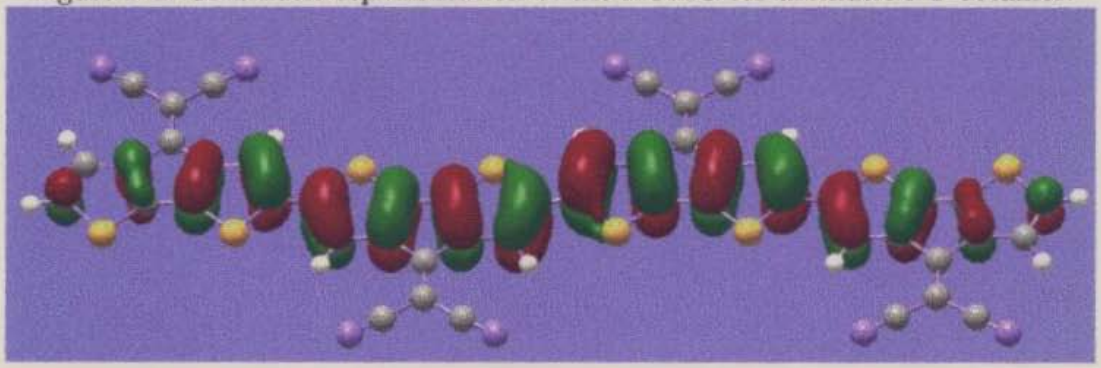

Figure F.3: Schematic representation of the HOMO for aromatic PCNTH tetramer.

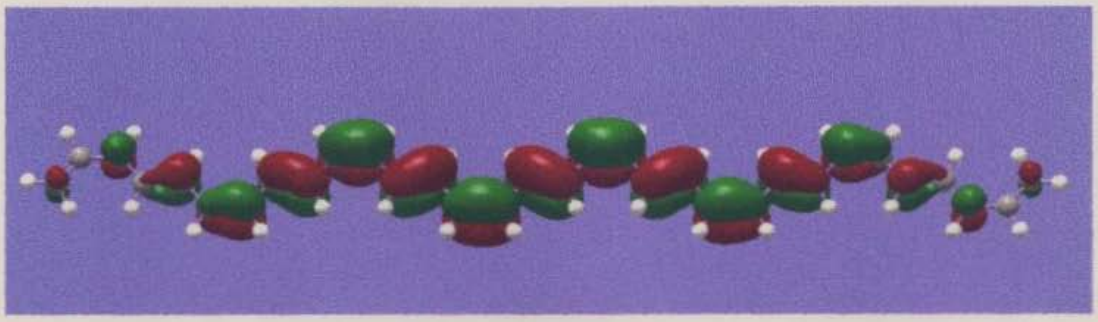

Figure F.4: Schematic representation of the LUMO for *trans-cisoid* PA octamer.

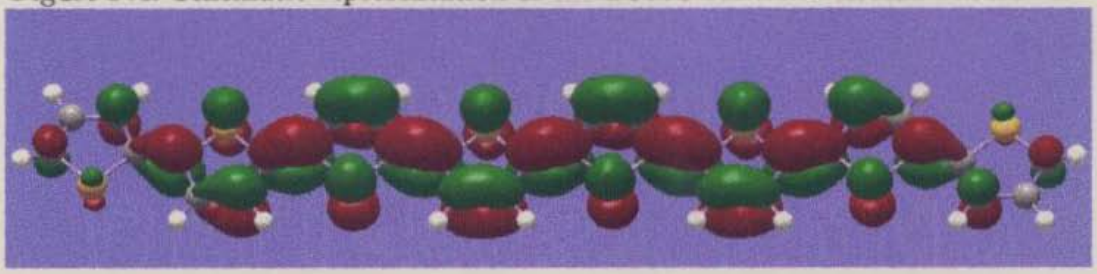

Figure F.5: Schematic representation of the LUMO for Aromatic PT octamer.

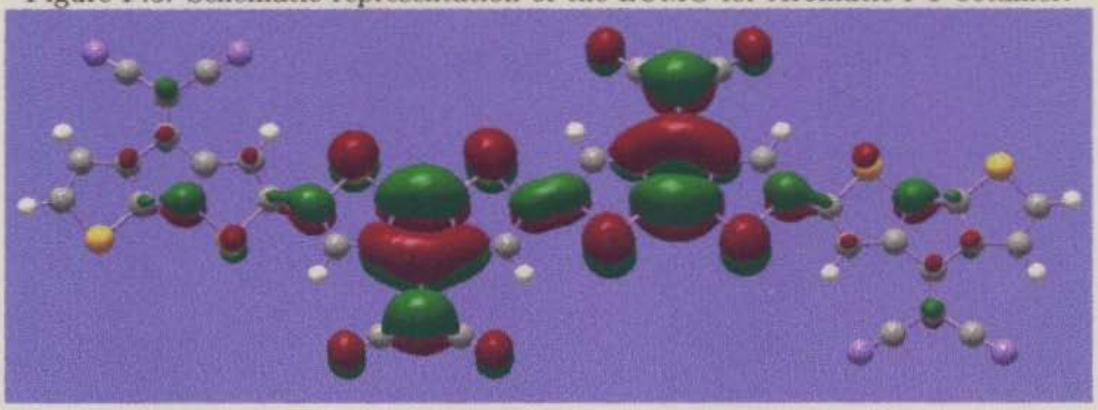

Figure F.6: Schematic representation of the LUMO for PCNTH tetramer.

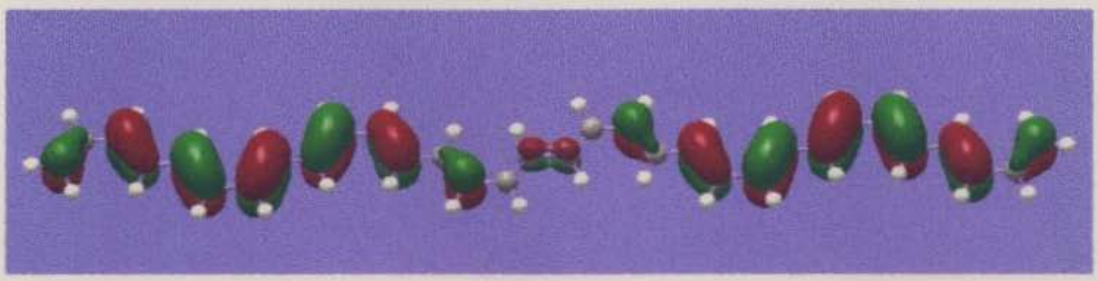

Figure F.7: Schematic representation of the HOMO-1 for *trans-cisoid* PA octamer.

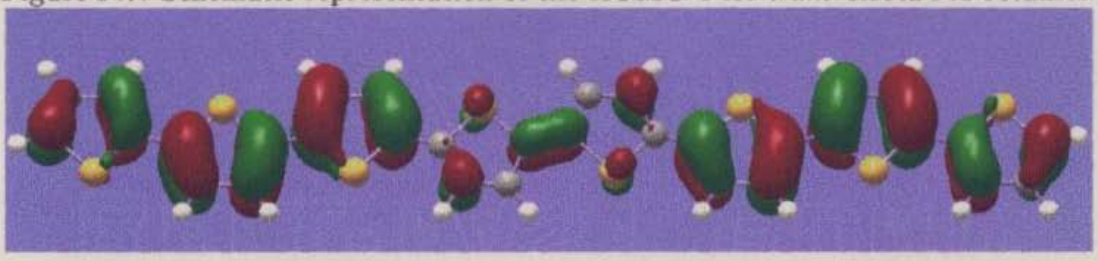

Figure F.8: Schematic representation of the HOMO-1 for aromatic PT octamer.

Figure F.9: Schematic representation of the HOMO-1 for PCNTH tetramer.

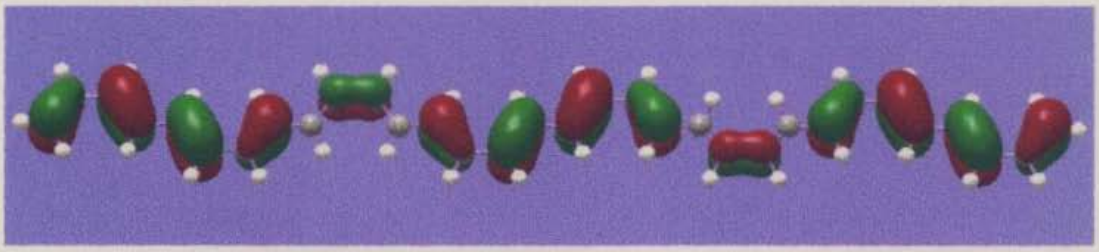

Figure F.10: Schematic representation of the HOMO-2 for *trans-cisoid* PA octamer.

Figure F.11: Schematic representation of the HOMO-2 for aromatic PT octamer.

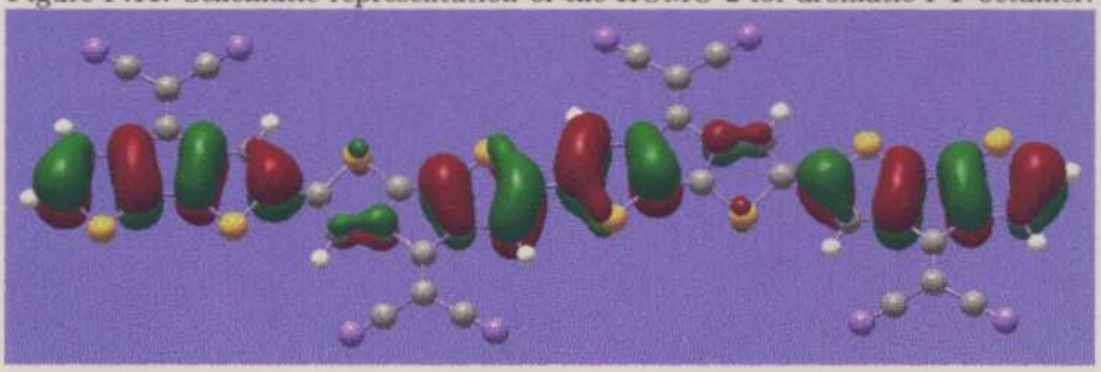

Figure F.12: Schematic representation of the HOMO-2 for PCNTH tetramer.

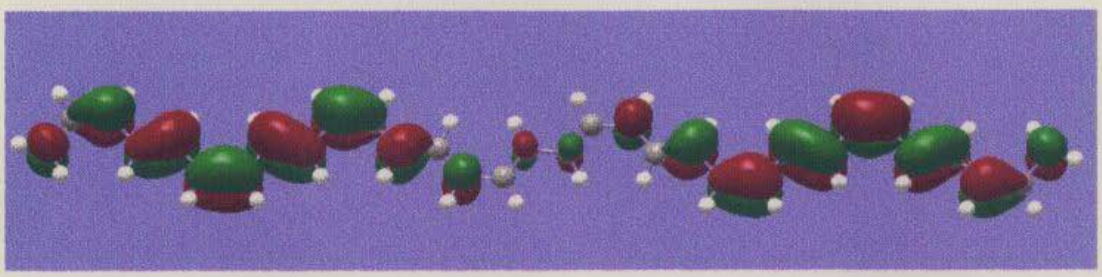

Figure F.13: Schematic representation of the LUMO+1 for *trans-cisoid* PA octamer.

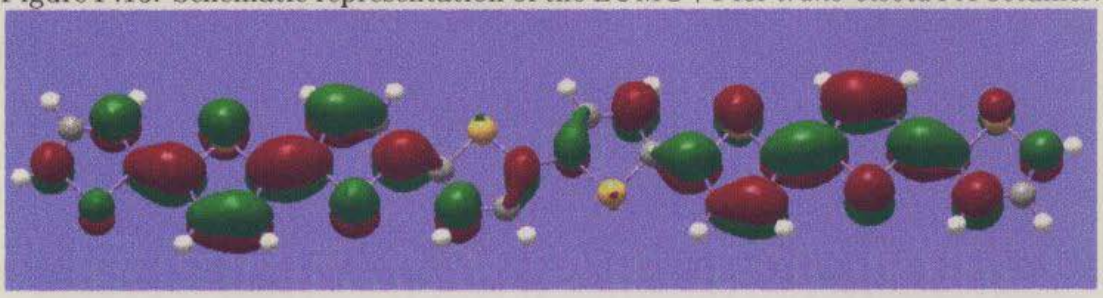

Figure F.14: Schematic representation of the LUMO+1 for aromatic PT octamer.

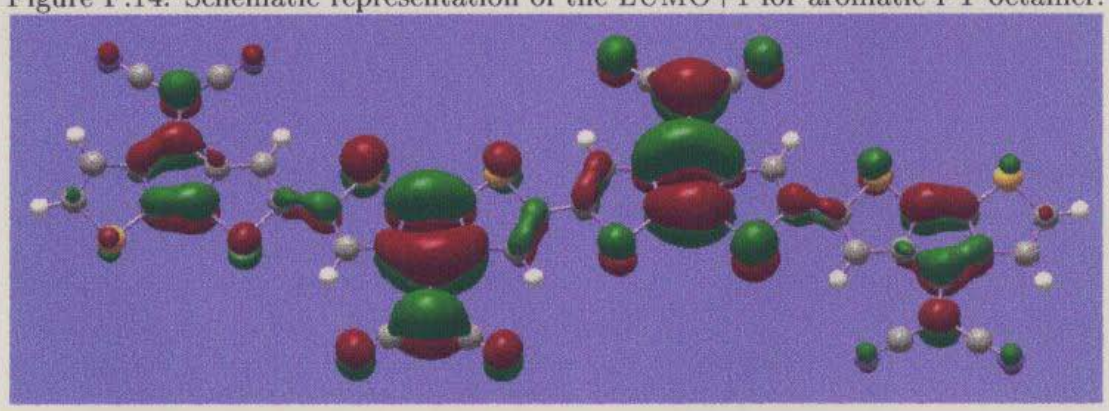

Figure F.15: Schematic representation of the LUMO+1 for PCNTH tetramer.

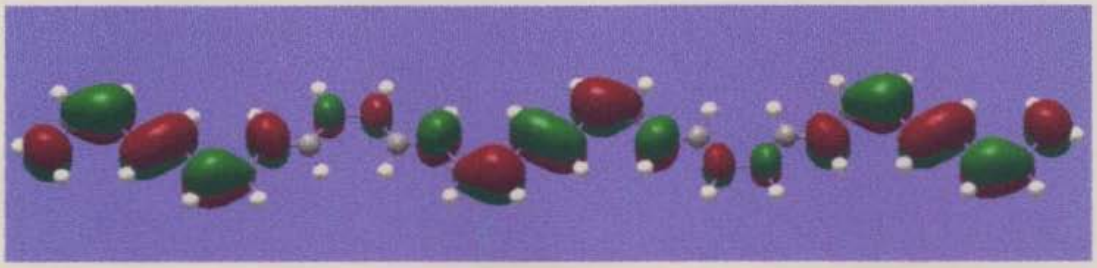

Figure F.16: Schematic representation of the LUMO+2 for *trans-cisoid* PA octamer.

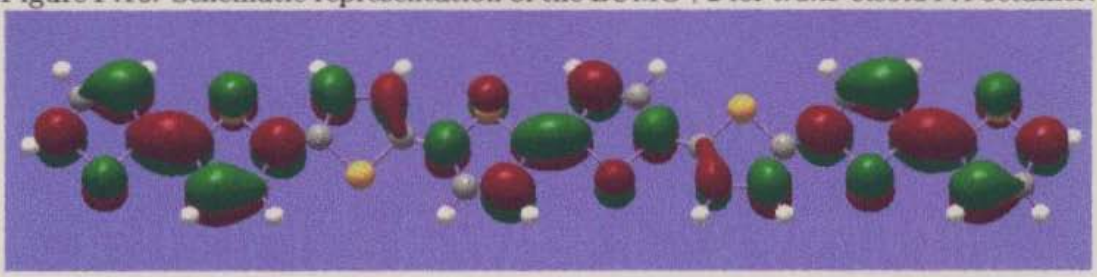

Figure F.17: Schematic representation of the LUMO+2 for aromatic PT octamer.

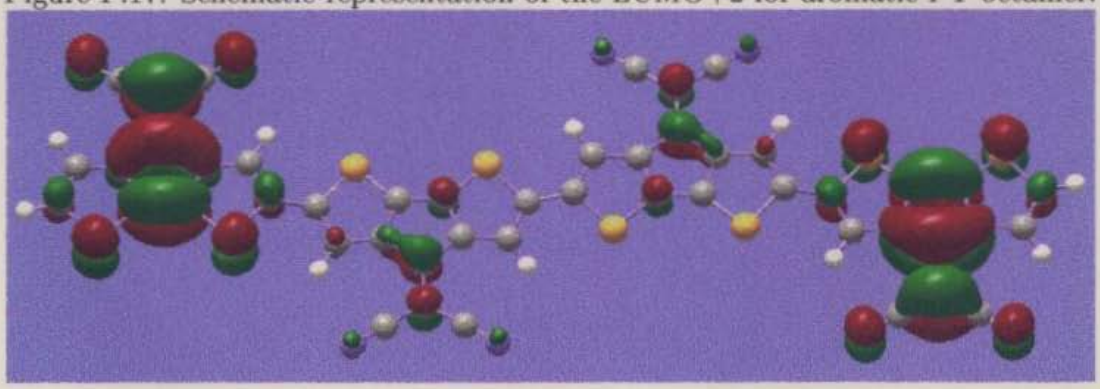

Figure F.18: Schematic representation of the LUMO+2 for PCNTH tetramer.

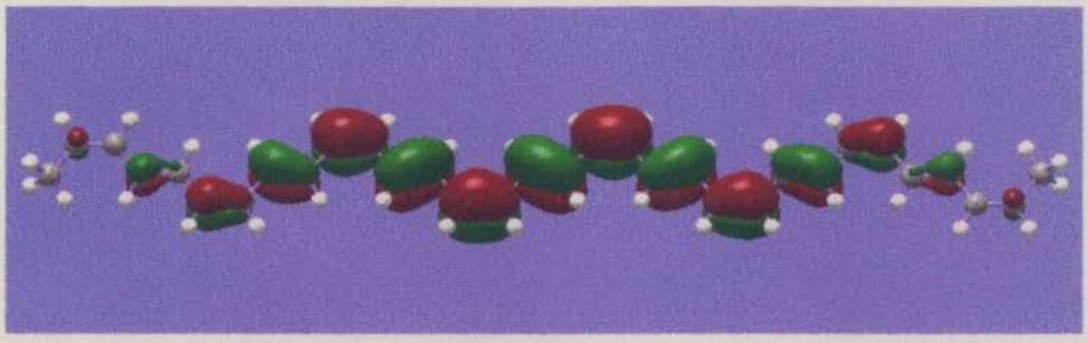

Figure F.19: Schematic representation of the HOMO for *cis-transoid* PA octamer.

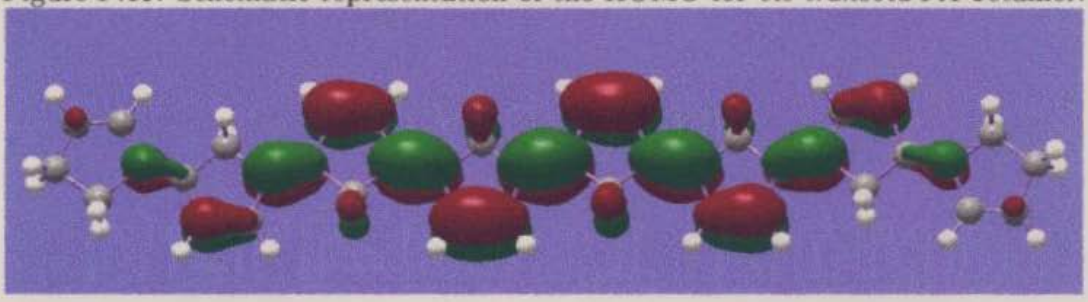

Figure F.20: Schematic representation of the HOMO for quinoid PCY octamer.

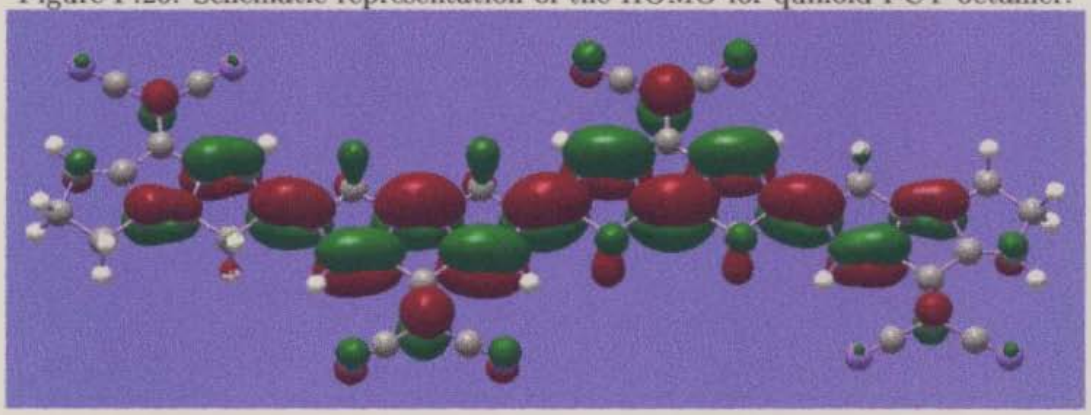

Figure F.21: Schematic representation of the HOMO for quinoid PCNCY tetramer.

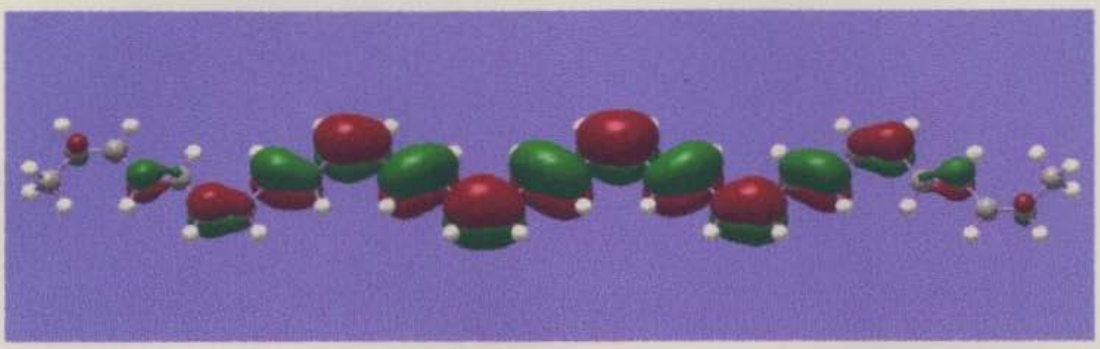

Figure F.22: Schematic representation of the HOMO for *cis-transoid* PA octamer.

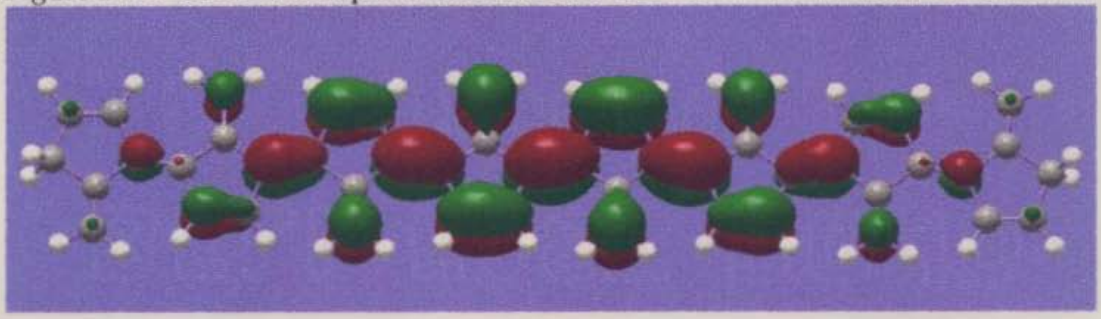

Figure F.23: Schematic representation of the HOMO for quinoid PFV octamer.

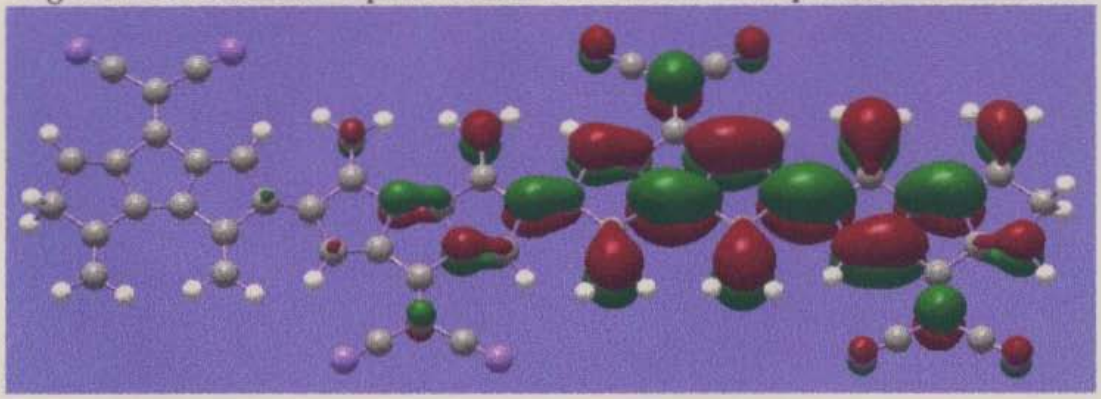

Figure F.24: Schematic representation of the HOMO for PCNFV tetramer.

Figure F.25: Schematic representation of the LUMO for *cis-transoid* PA octamer.

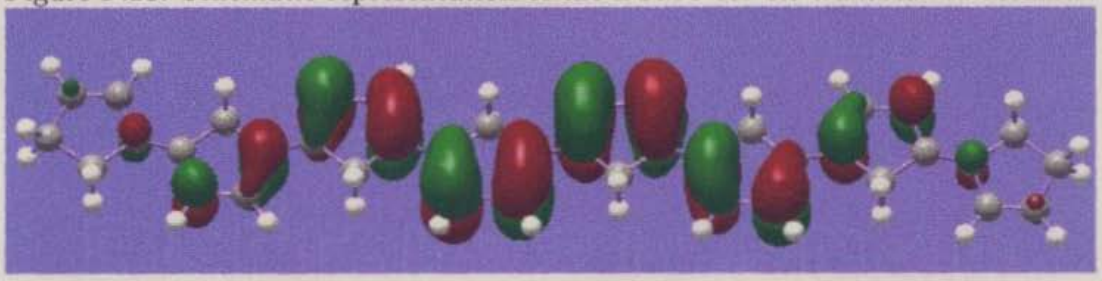

Figure F.26: Schematic representation of the LUMO for quinoid PCY octamer.

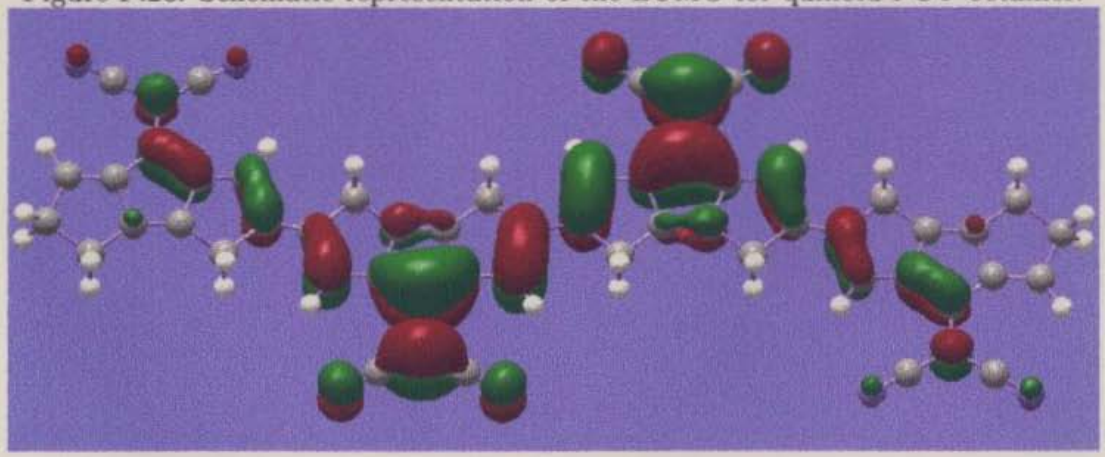

Figure F.27: Schematic representation of the LUMO for PCNCY tetramer.

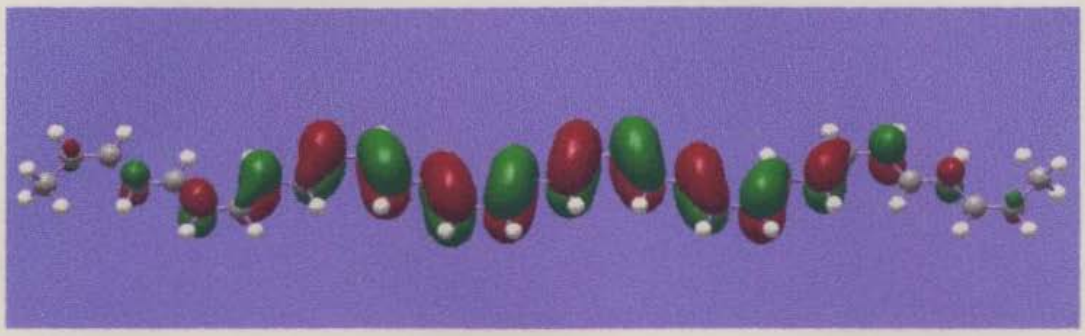

Figure F.28: Schematic representation of the LUMO for *cis-transoid* PA octamer.

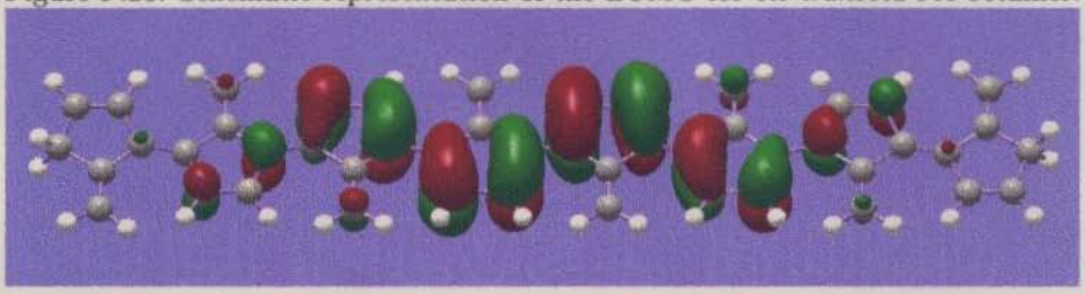

Figure F.29: Schematic representation of the LUMO for quinoid PFV octamer.

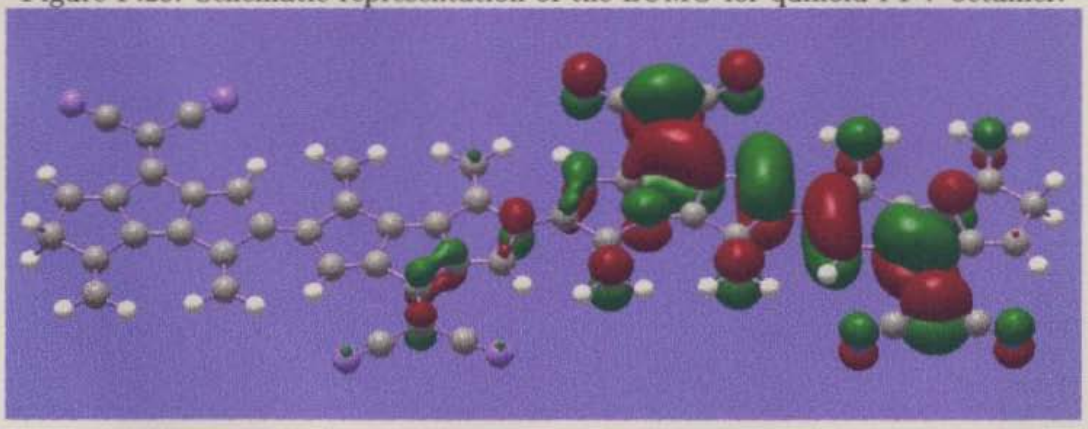

Figure F.30: Schematic representation of the LUMO for PCNFV tetramer.

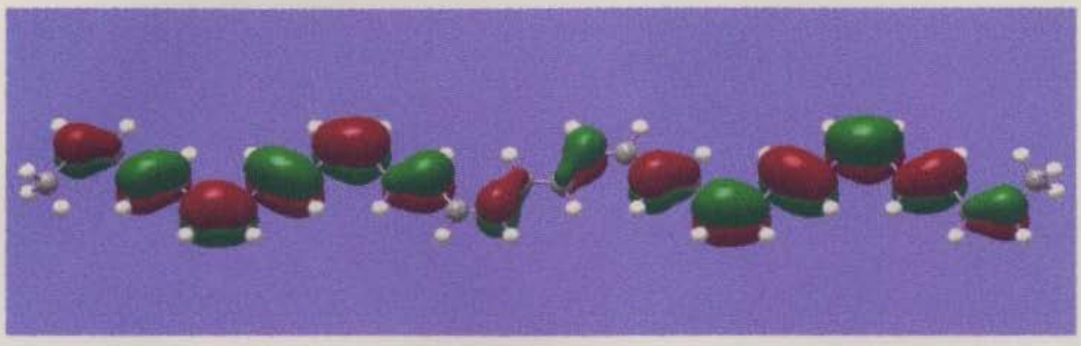

Figure F.31: Schematic representation of the HOMO-1 for *cis-transoid* PA octamer.

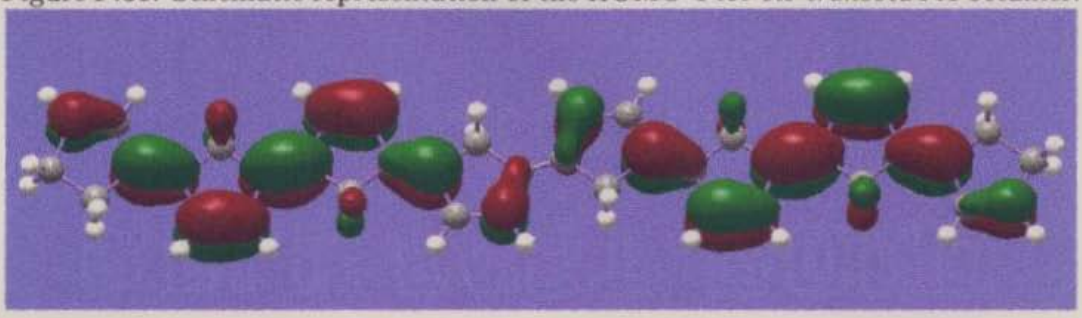

Figure F.32: Schematic representation of the HOMO-1 for quinoid PCY octamer.

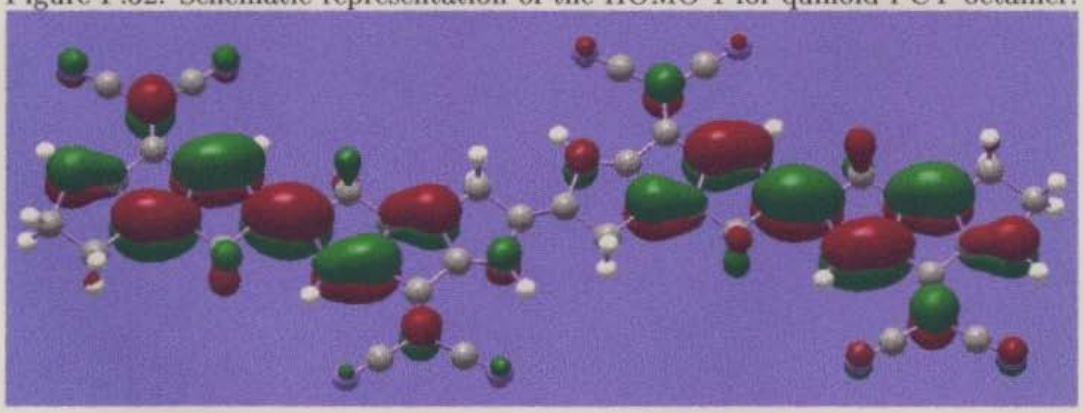

Figure F.33: Schematic representation of the HOMO-1 for PCNCY tetramer.

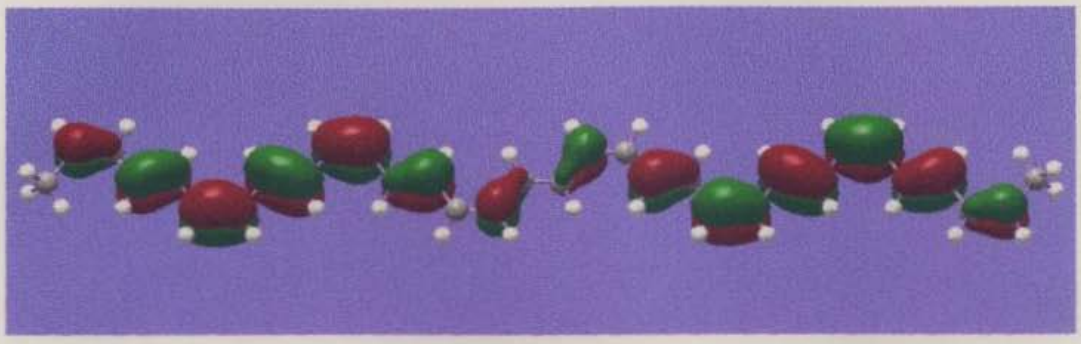

Figure F.34: Schematic representation of the HOMO-1 for *cis-transoid* PA octamer.

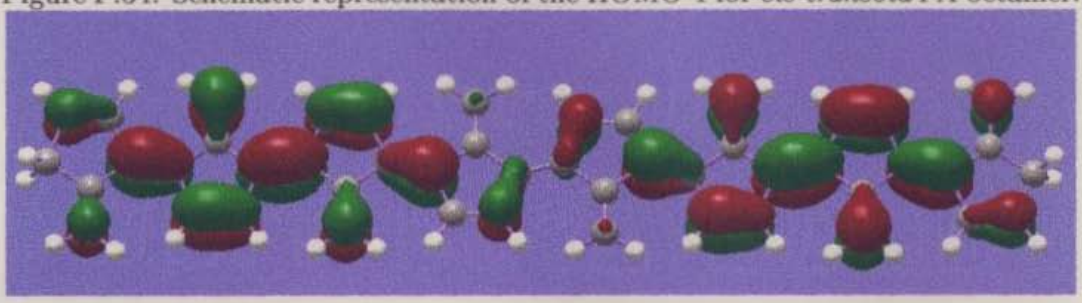

Figure F.35: Schematic representation of the HOMO-1 for quinoid PFV octamer.

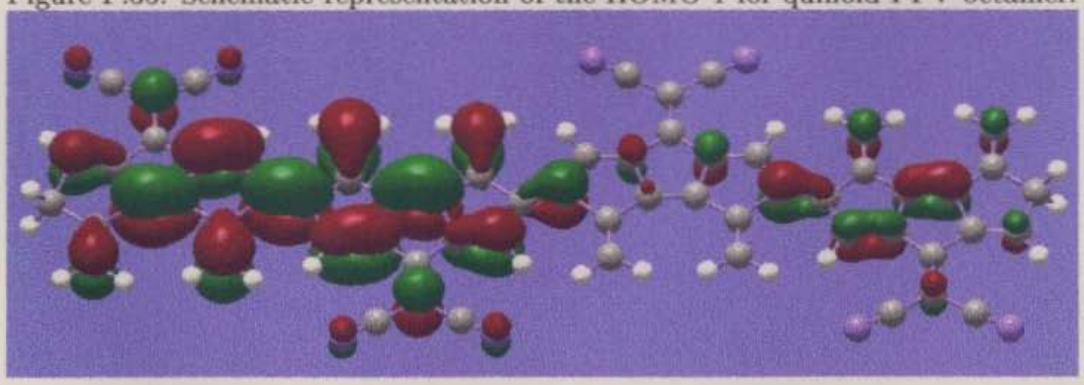

Figure F.36: Schematic representation of the HOMO-1 for PCNFV tetramer.

Figure F.37: Schematic representation of the HOMO-2 for *cis-transoid* PA octamer.

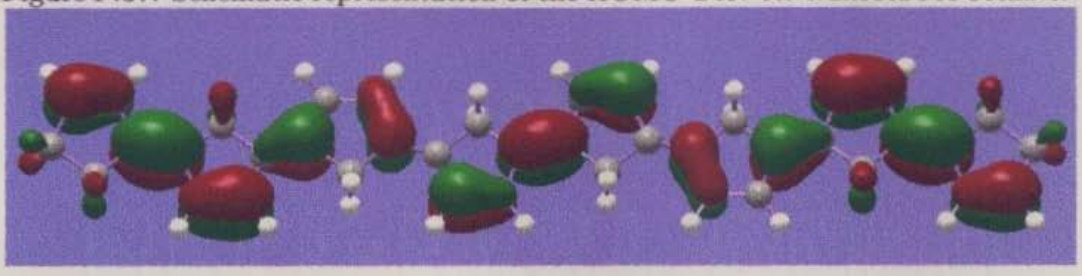

Figure F.38: Schematic representation of the HOMO-2 for quinoid PCY octamer.

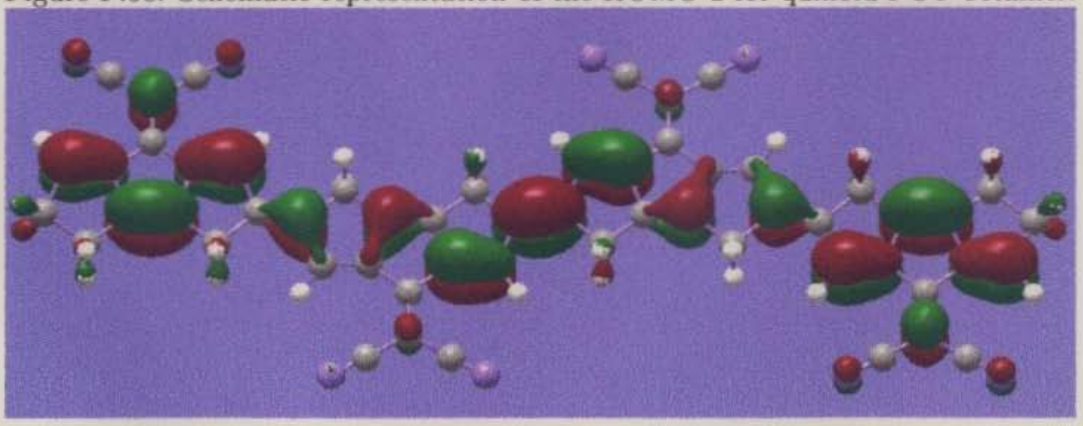

Figure F.39: Schematic representation of the HOMO-2 for PCNCY tetramer.

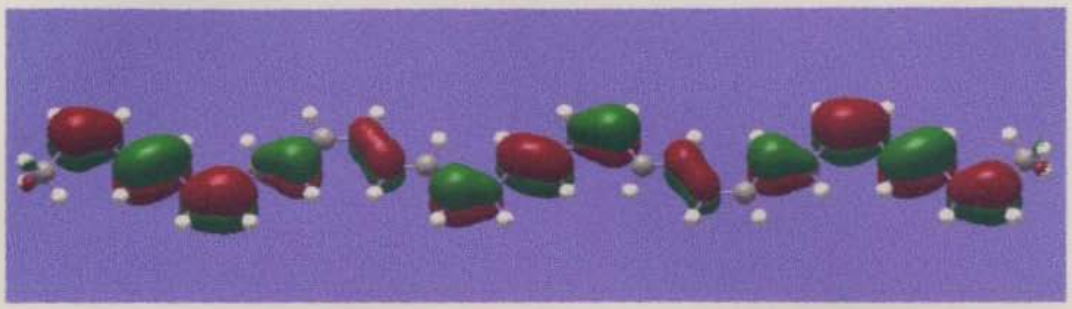

Figure F.40: Schematic representation of the HOMO-2 for *cis-transoid* PA octamer.

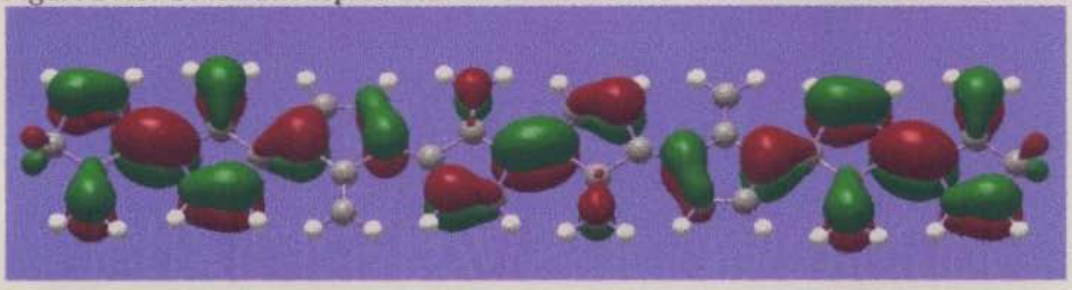

Figure F.41: Schematic representation of the HOMO-2 for quinoid PFV octamer.

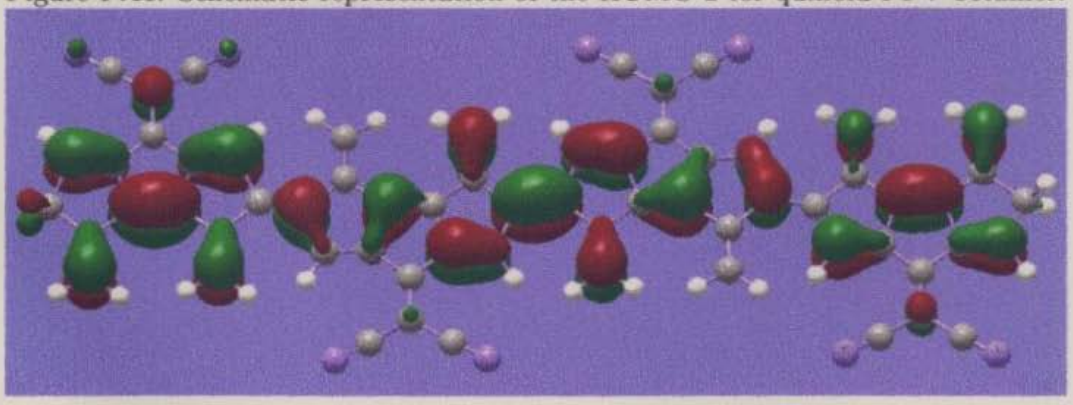

Figure F.42: Schematic representation of the HOMO-2 for PCNFV tetramer.

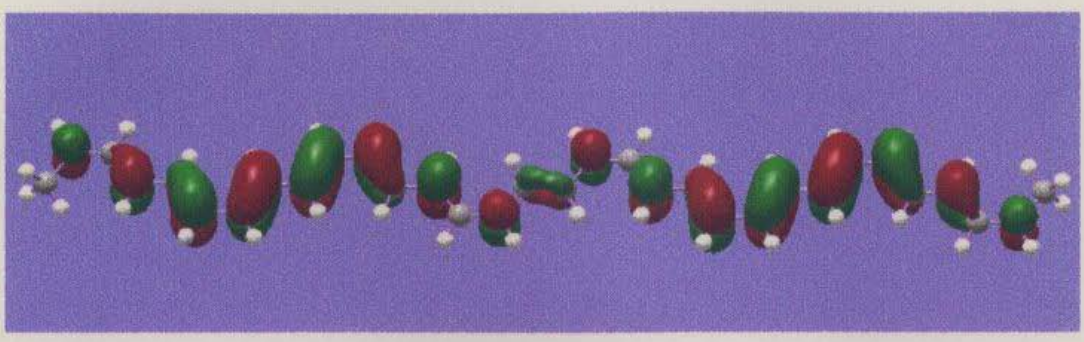

Figure F.43: Schematic representation of the LUMO+1 for *cis-transoid* PA octamer.

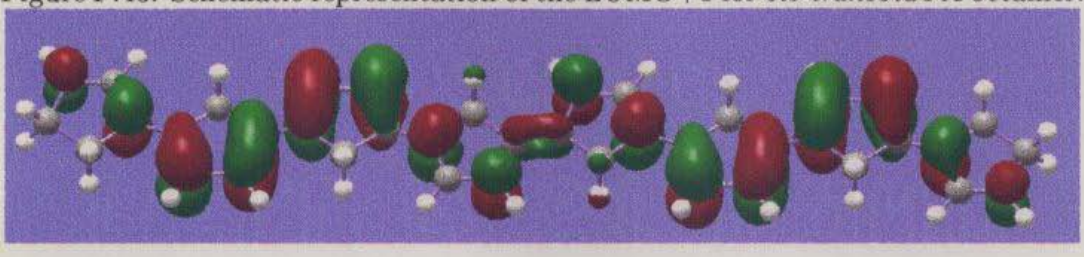

Figure F.44: Schematic representation of the LUMO+1 for quinoid PCY octamer.

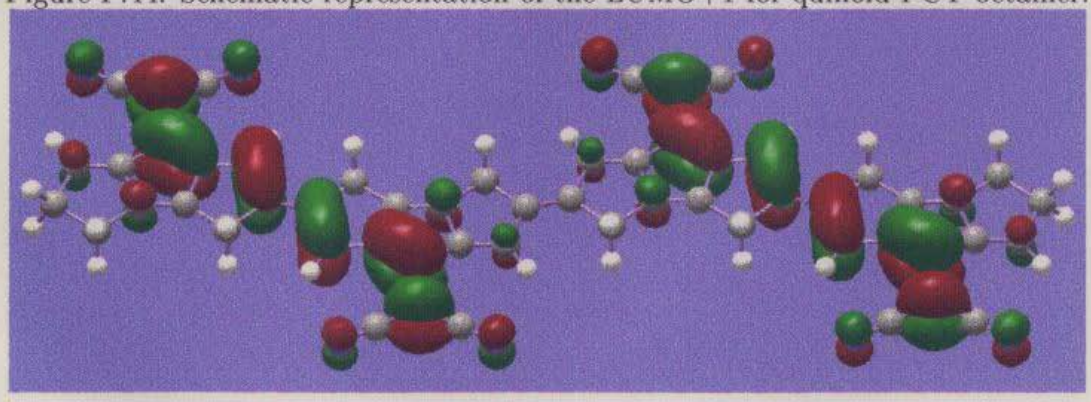

Figure F.45: Schematic representation of the LUMO+1 for PCNCY tetramer.

Figure F.46: Schematic representation of the LUMO+1 for *cis-transoid* PA octamer.

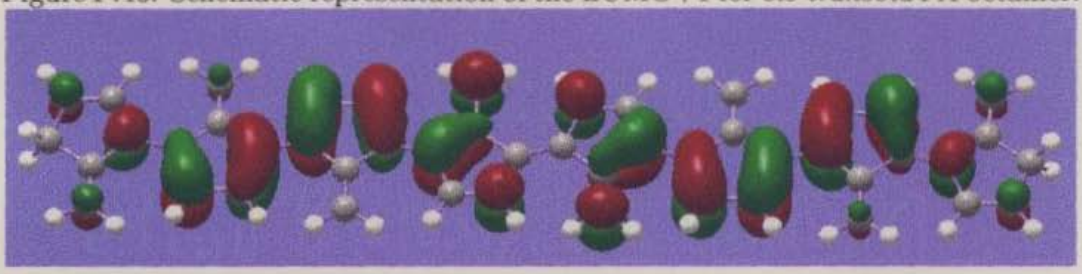

Figure F.47: Schematic representation of the LUMO+1 for quinoid PFV octamer.

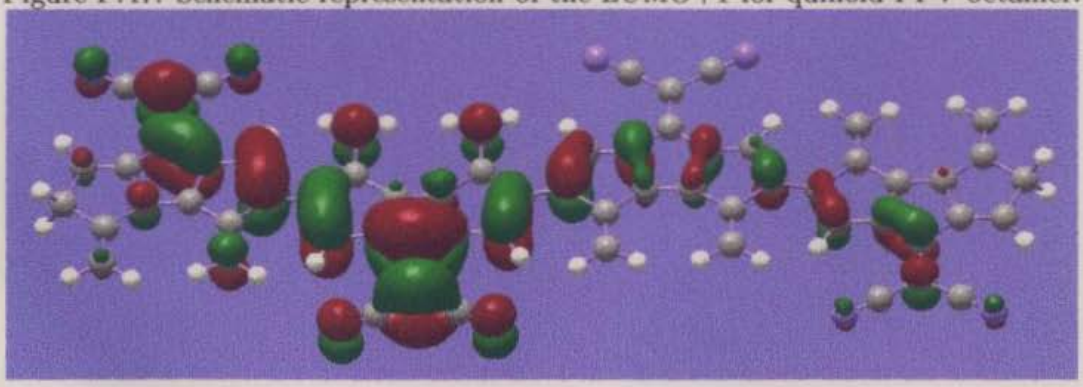

Figure F.48: Schematic representation of the LUMO+1 for PCNFV tetramer.

Figure F.49: Schematic representation of the LUMO+2 for *cis-transoid* PA octamer.

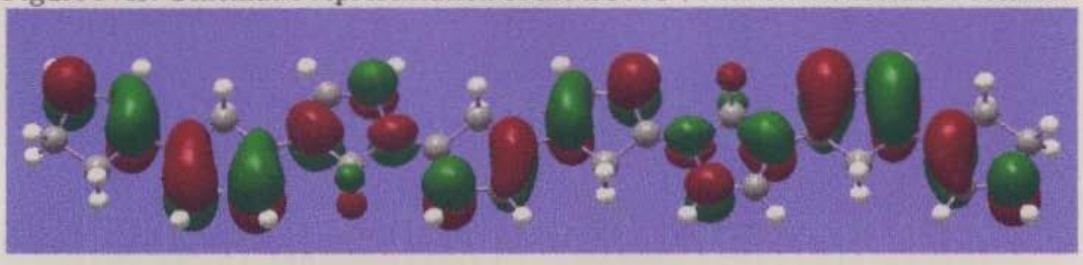

Figure F.50: Schematic representation of the LUMO+2 for quinoid PCY octamer.

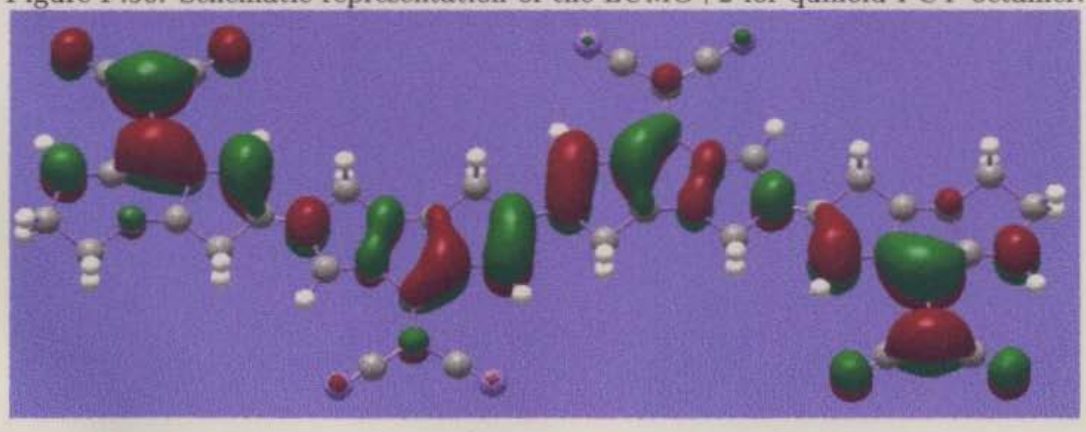

Figure F.51: Schematic representation of the LUMO+2 for PCNCY tetramer.

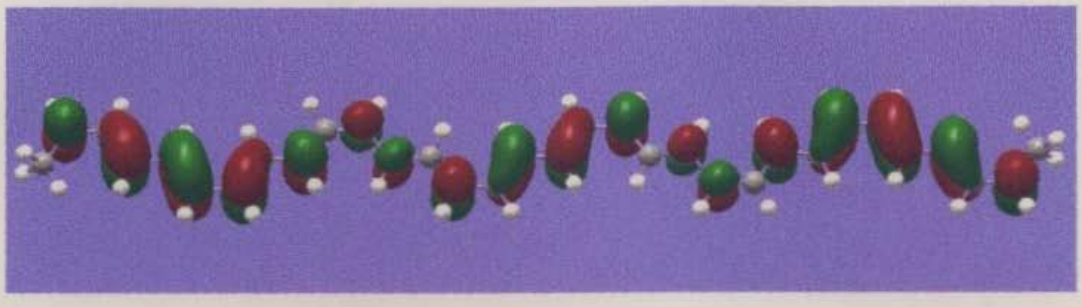

Figure F.52: Schematic representation of the LUMO+2 for *cis-transoid* PA octamer.

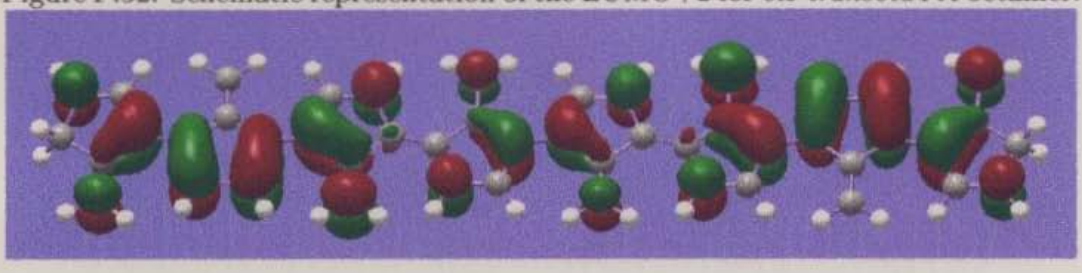

Figure F.53: Schematic representation of the LUMO+2 for quinoid PFV octamer.

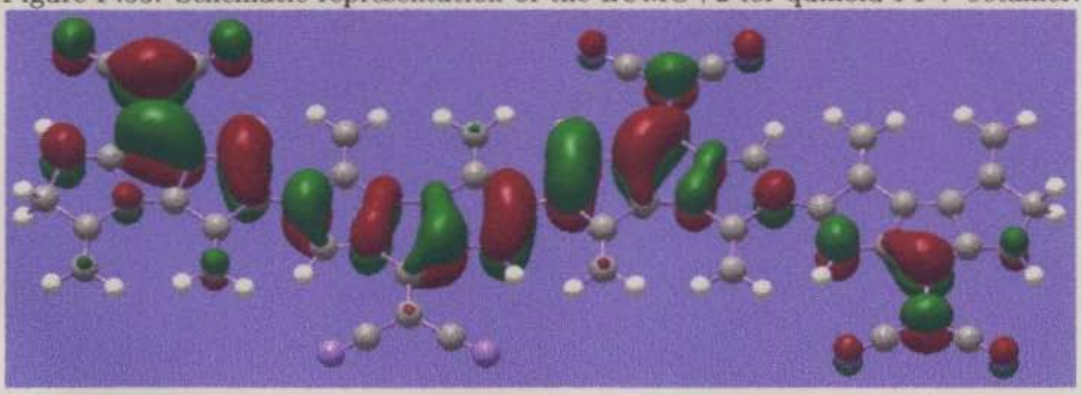

Figure F.54: Schematic representation of the LUMO+2 for PCNFV tetramer.